NORTHWESTERN UNIVERSITY

Studies on the Activation Patterns and the Catalytic Behaviors of Binuclear Organotitanium Complexes towards Olefin Polymerization

A DISSERTATION

SUBMITTED TO THE GRADUATE SCHOOL
IN PARTIAL FULFILLMENT OF THE REQUIREMENTS

for the degree

DOCTOR OF PHILOSOPHY

Field of Chemistry

By

Anna Magdalene Invergo

EVANSTON, ILLINOIS

September 2018

ABSTRACT

Studies on the Activation Patterns and the Catalytic Behaviors of Binuclear Organotitanium Complexes towards Olefin Polymerization

Anna Magdalene Invergo

Bimetallic polymerization catalysis represents a small, though active, area of research due largely to the interesting properties observed in the resulting product polymers, including higher molecular weight, increased comonomer incorporation, and enhanced tacticity. Current work is focused on furthering an understanding of the active catalytic species that give rise to these desirable polymer properties. Presented here are the synthesis and reactivity of two series of bimetallic organotitanium catalysts. The active species of both catalysts are extensively studied, and the catalytic performance is evaluated based on this knowledge of the active species. It will be seen that one catalyst series is comprised of separable diastereomers, which display distinct modes of reactivity with stoichiometric boron-based cocatalysts and produce widely varying polymers depending on stereochemistry of the catalyst and identity of cocatalyst. The second catalyst series, on the other hand, will be seen to rearrange and produce a chemically distinct, yet highly active species upon activation with a boron-based cocatalyst. Thus, though they differ largely in reactivity with activators, both catalyst series highlight the importance of knowing the nature of the active species in order to explain the observed polymerization characteristics.

ACKNOWLEDGEMENTS

I would first like to thank Prof. Tobin Marks for giving me the opportunity to work in his lab and pursue research in a world-class institution. Even with a group as large as his, he has always been willing to meet and discuss my chemistry with me, and I am very grateful for that. I also want to thank my thesis committee members, Prof. Regan Thomson and Prof. Ken Poeppelmeier, for their helpful advice and contributions to my graduate career.

My graduate career would not be where it is without the support, advice, and efforts of my close friend and mentor, Dr. Tracy Lohr. She has been there for me for everything, from advice for the job search to qual paper corrections to preparing very large manuscripts with a fine-toothed comb. It has been such a pleasure to work with someone who values my slow and steady approach to projects, and I cannot thank her enough for everything she has done for me.

I have been fortunate enough to have had some very helpful collaborators on my work while at Northwestern. Dr. Max Delferro and Dr. Shaofeng Liu taught me many of the techniques I now use on a regular basis, for which I am very grateful. I also thank Shaofeng for allowing me to work on and complete his projects, both of which have become the core of my dissertation. I also thank Dr. Alessandro Motta for his computational contributions to my work. A special thank you goes to Dr. Yuyang Wu and Dr. Yongbo Zhang for their patience with my thousands of questions about NMR.

As I begin to thank my labmates, there are three special people who have also served as my collaborators on my projects. Dr. Jenny McInnis taught me a lot about the field of bimetallic polymerization catalysis when I first joined the group and has since provided me with helpful advice and comforting words throughout my job search. Dr. Aidan Mouat has solved countless crystal structures for my projects, and has also kindly endured/fielded endless questions from me

at the bench without hesitation or complaint, for which I am very grateful. Rachel Dicken has also provided crystal structures and data for me, while also proving to be a fantastic friend who is always ready to hang out and eat great food. She is one of the people who made my last year in lab a lot less lonely.

The rest of my labmates in the Marks group have been a spectacular group of people, and they have all made this entire journey easier with their helpfulness, laughter and friendship. I count Dr. Victoria Weidner and Dr. Madelyn Stalzer among my closest friends, and I thank them so much for all the shopping trips, brewery trips, dinners out, coffee breaks, movies, various TV show-watching sessions, and general time spent together. Shanfu Liu has become one of my best friends, and I thank him for the many hours we have spent talking about literally everything, and also for those brunch and ramen trips. Dr. Michael Desanker is also one of my closest friends in lab, and I have him to thank for both solidarity throughout many graduate school milestones, especially the job search, as well as countless hours of entertainment, along with Jake Rothbaum, who has never failed to be enthusiastic for every one of my achievements/life events since he's known me, and with whom I've had fantastic discussions on all things Star Wars and Marvel. Chris Barger, Shengsi "Mike" Liu, Jiaqi Li, Allison Arinaga, and Cole Carter have all been a calm in the relative storm, and I thank all five of them for being great friends and listeners, always willing to talk with me about any topic that popped into my head or to silently make fun of Jake's antics (looking at you, Chris). Dr. Matthias Peter and Dr. Titel Jurca were great friends of mine and were always willing to hang out and partake in discussions about life. I thank Jialong "Bruce" Zhang for our many talks about places we wanted to work and trips we wanted to take. Jiazhen Chen and Dr. Yang Wang have been great friends and very helpful to me with my polymerization work. Very special thanks go to Dr. Yanshan Gao, who has always gone above and beyond in his

willingness to help me with my chemistry issues, as well as giving me ideas for new project directions and talking with me about jobs and life.

I was also fortunate to have two very close friends at Northwestern outside of the A-Team of the Marks Lab. Jennifer Grant showed me so much of what Chicago had to offer, as well as always having a new adventure to share. Weiwei Wang is one of my greatest friends, and has been there with me through every step of the way. She has been my go-to person for everything, from scouting out new cupcake shops to skiing in Wisconsin. She has always been up for any adventure, and I couldn't have asked for a better friend to go through graduate school with.

A special thank you goes to Dr. Christopher Burns, my undergraduate research advisor, for giving me my first experience of working in a real lab, as well as for fostering my love of organometallic chemistry and polymerization catalysis. It is rare to have a professor that works side by side with their students in the lab, and I was fortunate to be able to learn so much from him because of this. I also thank Prof. Christine Rich for always believing in me, and for giving me the opportunity to be a TA as an undergraduate, which tremendously helped to ease my transition into graduate school teaching. I thank Prof. Craig Grapperhaus, Prof. Natali Richter, Prof. John Richardson, Prof. Richard Wittebort, and Prof. Mark Noble for their support and advice throughout my undergraduate career. I also thank my Burns group labmates: Samantha DeWitt, Jessica Ringo, Dr. Ben Moberly, Dr. Abigail Halleron, Yousef Hindi, and Dr. Lindsay Cameron.

A huge thank you goes to my close friends from Kentucky: Charles Spears, Kathryn Cross, Ethan Gibson, Luke South, Dr. Adrienne Childress, Josephine Lee, and Ariel Briggs, who always provided much needed support and much welcomed distraction from lab work during their visits to Chicago or my visits home. Clare Ciriaco will always hold a special place in my heart as a lifelong friend who has been there for me every step of the way.

Among my labmates, the most special to me is Dr. Jeffrey Miles Tan. He was an impressive font of knowledge and was always willing to help me with anything I needed. Then my movie-watching buddy, now my boyfriend of two and a half years, I thank him for those late-night talks about life and for all the things he taught me about chemistry in the early years. His reassurance, dedication and love since then has been unwavering, and I cannot thank him enough.

Finally, the greatest thanks go to my family. I have realized that not everyone is blessed with a family that is as steadfastly loving and supportive as mine is, and I thank God every day for them. I'm so grateful that I got to spend the last nearly five years living near my extended family in Chicago: my grandparents, Ben and Louise; my aunts, Gina and Judy; my uncles Mike and Jim; and my cousins, Mitch, Kelsey, Ethan, Trevor and Luke, and I can't thank them enough for always opening their door to me and providing a place to go whenever I needed it. I thank them, along with my extended family in Kentucky: my grandmother, Brigitte and my uncle Chris, as well as my honorary family: Fr. Jim Sichko and Thereze Sichko, for their steady love and support.

Above all, I thank my sisters, Christine and Emily, and my parents, Ben and Regina. They have celebrated my good times and have encouraged me through the bad. They have been a source of happiness on even the darkest days. I thank my parents especially for going through their own years of post-graduate education, for empathizing with me throughout the process, for being amazing role models, and for encouraging me to follow my dreams from day one. I thank them so much for being the greatest family I could've ever dreamed of or asked for. With you all, the sky is the limit. I love you.

Thanks for everything, y'all.

TABLE OF CONTENTS

ABSTRACT....2
ACKNOWLEDGEMENTS....3
TABLE OF CONTENTS....7
LIST OF SCHEMES....8
LIST OF TABLES....10
LIST OF CHARTS....11
LIST OF FIGURES....12
CHAPTERS

1. **Distinctive Stereochemically Linked Cooperative Effects in Bimetallic Titanium Olefin Polymerization Catalysts**....17
    - Abstract....18
    - Introduction....19
    - Results....22
    - Discussion....45
    - Conclusions....53
    - Experimental Section....54
    - Acknowledgements....98

2. **Polymerization Behavior and Monomer Dependent Reorganization of a Bimetallic Salphen Organotitanium Catalyst**....99
    - Abstract....100
    - Introduction....100
    - Results and Discussion....103
    - Conclusions....113
    - Experimental Section....113
    - Acknowledgements....130

REFERENCES....131

APPENDIX: **Original Research Proposal: Design of a Catalytic Surface as a Fully Immobilized Frustrated Lewis Pair for Organic Transformations**....158
    - Abstract....158
    - Introduction....159
    - Scientific Objectives....160
    - Previous Work....160
    - Proposed Research....162
    - Summary and Conclusions....168
    - References....170

CURRICULUM VITAE....174

LIST OF SCHEMES

Chapter 1

Scheme 1.1. Synthesis of the diastereomeric bimetallic precatalysts ***rac*-3** and ***meso*-3**.....24

Scheme 1.2. Formation of complex ***rac*-4** via thermolysis of complex ***rac*-3**.....27

Scheme 1.3. Proposed activation pathway of ***rac*-3** with $Ph_3C^+B(C_6F_5)_4^-$ to form ***rac*-5** and ***rac*-6**.....30

Scheme 1.4. Activation of complex ***meso*-3** with $Ph_3C^+B(C_6F_5)_4^-$ to form ***meso*-5**.....32

Scheme 1.5. Formation of ***rac*-5-Cl**$_3$ by reaction of ***rac*-5** with CD_2Cl_2.....35

Scheme 1.6. Proposed activation pathway of complex ***rac*-3** with $B(C_6F_5)_3$ to form complex ***rac*-7**.....36

Scheme 1.7. Activation of ***meso*-3** with $B(C_6F_5)_3$ to form complex ***meso*-7**.....36

Scheme 1.8. Proposed cooperative bimetallic scenario for enhanced 1-octene (**A**) and styrene (**B**) enchainment by ***rac*-3** and ***meso*-3** –based catalysts.....46

Scheme 1.9. Proposed scenario for bimetallic precatalyst ***rac*-3** and ***meso*-3** activation and ethylene polymerization propagation.....51

Scheme 1.10. Synthesis of binuclear ligand **1**.....65

Chapter 2

Scheme 2.1. Synthesis of monometallic **1** (A), bimetallic **2** (B), and asymmetric bimetallic **3** (C) salphen catalysts.....104

Scheme 2.2. Proposed formation of charged complex **4**.....107

Scheme 2.3. Proposed monomer-dependent active species in ethylene and 1-hexene homopolymerizations and ethylene + 1-hexene copolymerizations mediated by activating precatalyst **2**.....112

Appendix

Scheme A1. Example of a well-known FLP activating H_2.....158

Scheme A2. Sample preparation of MgO on SiO_2.....162

Scheme A3. (**A**) Proposed synthetic route for siloxyborane to be used in the supporting reaction. (**B**) Retrosynthetic analysis of Piers' reagent.....163

Scheme A4. General procedure for tethering of the siloxyborane to MgO/SiO_2.....164

LIST OF TABLES

Chapter 1

Table 1.1. Ethylene homopolymerization data for catalysts **Ti**$_1$, ***rac*-3**, and ***meso*-3**.....38

Table 1.2. Propylene homopolymerization data for catalysts **Ti**$_1$, ***rac*-3**, and ***meso*-3**.....40

Table 1.3. 1-octene homopolymerization data for catalysts **Ti**$_1$, ***rac*-3**, and ***meso*-3**.....40

Table 1.4. Ethylene/1-octene copolymerization data for catalysts **Ti**$_1$, ***rac*-3**, and ***meso*-3**.....44

Table 1.5. Ethylene/styrene copolymerization data for catalysts **Ti**$_1$, ***rac*-3**, and ***meso*-3**.....44

Table 1.6. Crystal data and structure refinement for ***rac*-2**, ***meso*-2**, ***rac*-3**, ***meso*-3, and *rac*-4**.....94

Table 1.7. Crystal data and structure refinement for ***meso*-5**, ***rac*-5**, ***rac*-5-Cl**, **and *meso*-7**.....95

Chapter 2

Table 2.1. Ethylene Homopolymerization Data for Monometallic and Bimetallic Salphen Catalysts.....109

Table 2.2. Ethylene/1-hexene Copolymerization Data for Monometallic and Bimetallic Salphen Catalysts.....109

Table 2.3. 1-Hexene Homopolymerization Data for Monometallic and Bimetallic Salphen Catalysts.....109

Table 2.4. Crystal data and structure refinement for 3 and 4.....129

LIST OF CHARTS

Chapter 1

Chart 1.1. Selected examples of multimetallic enzymatic (**A**) and abiotic (**B**, **C**) catalysts.....20

Chart 1.2. Dinuclear zirconium (D) and nickel (E) catalysts for olefin polymerization.....20

Chart 1.3. (**A**) Structures of the present diastereomeric bimetallic Ti(IV) catalysts; (**B**) View of bimetallic stereoisomers perpendicular to the Cp ring planes showing nomenclature; (**C**) Structures of the monometallic CGCTi(IV) control olefin polymerization catalysts.....21

Chart 1.4. Rare examples of μ-CH_2, μ-CH_3 bridged binuclear monocationic group 4 complexes.....32

Chapter 2

Chart 2.1. Examples of variable nuclearity polymerization catalysts.....101

LIST OF FIGURES

Chapter 1.

Figure 1.1. ORTEP plot of the molecular structures of bimetallic tetramethyl complexes ***rac*-3** and ***meso*-3**.....25

Figure 1.2. VT ^{1}H NMR spectrum of ***rac*-4** in C_7D_8 from -90 to +100 °C.....27

Figure 1.3. (**A**) ORTEP view of the molecular structure of complex ***rac*-4**. (**B**) Optimized DFT geometry of the ***rac*-4** molecular structure.....29

Figure 1.4. ^{1}H NMR spectra (25 °C) of ***rac*-3** activated with 1 (**A**) or 2 (**B**) equiv. of $Ph_3C^+B(C_6F_5)_4^-$ in C_6D_5Cl, with proposed structures.....32

Figure 1.5. ORTEP view of the molecular structures of ***rac*-5** and ***meso*-5**.....35

Figure 1.6. Optimized DFT computed geometries of the "naked" ***rac*-5** and ***meso*-5** cations...36

Figure 1.7. ORTEP view of the molecular structure of ***meso*-7**.....37

Figure 1.8. ^{13}C NMR spectra (100 MHz, $C_2D_2Cl_4$, 120 °C) of the poly-1-octene samples from Table 1.3, entries 2 and 3.....41

Figure 1.9. Schematic structures of activated group 4 complexes which produce isotactic poly-α-olefins.....46

Figure 1.10. ^{1}H NMR spectrum of **Ti$_1$** in C_6D_6.....66

Figure 1.11. ^{13}C NMR spectrum of **Ti$_1$** in C_6D_6.....66

Figure 1.12. ORTEP view of the molecular structure of ***meso*-2**.....67

Figure 1.13. ORTEP view of the molecular structure of ***rac*-2**.....67

Figure 1.14. ^{1}H NMR spectrum of ***meso*-2** in C_6D_6.....68

Figure 1.15. ^{13}C NMR spectrum of ***meso*-2** in C_6D_6.....68

Figure 1.16. ^{1}H NMR spectrum of ***rac*-2** in C_6D_6.....69

Figure 1.17. ^{13}C NMR spectrum of ***rac*-2** in C_6D_6.....69

Figure 1.18. ^{1}H NMR spectrum of ***rac*-3** in C_6D_6.....70

Figure 1.19. ^{13}C NMR spectrum of ***rac*-3** in C_6D_6.....70

Figure 1.20. ^{1}H NMR spectrum of ***meso*-3** in C_6D_6.....71

Figure 1.21. ^{13}C NMR spectrum of ***meso*-3** in C_6D_6.....71

Figure 1.22. ^{1}H NMR spectrum of ***rac*-4** in C_7D_8.....72

Figure 1.23. ^{13}C NMR spectrum of ***rac*-4** in C_7D_8.....72

Figure 1.24. VT ^{1}H NMR spectrum of ***rac*-4** in C_7D_8 from -90 to 100° C.....73

Figure 1.25. Stack plot of ^{1}H-coupled ^{13}C (**A**) and ^{1}H-decoupled ^{13}C (**B**) NMR spectra of the methylene bridge region of ***rac*-4** in C_7D_8 at -90° C.....73

Figure 1.26. ^{1}H-^{13}C HSQC spectrum of ***rac*-4** in C_7D_8 at -90° C.....74

Figure 1.27. ^{1}H-^{13}C HSQC spectrum of ***rac*-4** in C_7D_8 at 100° C.....74

Figure 1.28. ^{1}H NMR spectrum of ***rac*-5** in C_6D_5Cl.....75

Figure 1.29. ^{13}C NMR spectrum of ***rac*-5** in C_6D_5Cl.....75

Figure 1.30. ORTEP view of the molecular structures of ***rac*-5-Cl$_3$**.....76

Figure 1.31. ^{1}H NMR spectrum of ***rac*-5-Cl$_3$** in CD_2Cl_2.....76

Figure 1.32. ^{13}C NMR spectrum of ***rac*-5-Cl$_3$** in CD_2Cl_2.....77

Figure 1.33. ^{1}H NMR spectrum of ***rac*-6** in C_6D_5Cl.....77

Figure 1.34. ^{13}C NMR spectrum of ***rac*-6** in C_6D_5Cl.....78

Figure 1.35. VT ^{1}H NMR spectra of ***rac*-6** in C_6D_5Cl from -35 to 100° C.....78

Figure 1.36. ^{1}H NMR spectrum of ***meso*-5** in C_6D_5Cl with 1 equiv. of $Ph_3C^+B(C_6F_5)_4^-$.....79

Figure 1.37. ^{13}C NMR spectrum of ***meso*-5** in C_6D_5Cl with 1 equiv. of $Ph_3C^+B(C_6F_5)_4^-$.....79

Figure 1.38. ^{1}H NMR spectrum of ***meso*-5** in C_6D_5Cl with 2 equiv. of $Ph_3C^+B(C_6F_5)_4^-$.....80

Figure 1.39. ^{13}C NMR spectrum of ***meso*-5** in C_6D_5Cl with 2 equiv. of $Ph_3C^+B(C_6F_5)_4^-$.....80

Figure 1.40. VT ^{1}H NMR spectra of ***meso*-5** in CD_2Cl_2 from -90 to 20° C.....81

Figure 1.41. ^{1}H-^{13}C HSQC spectrum of ***meso*-5** in C_6D_5Cl at 20° C.....81

Figure 1.42. ORTEP view of the molecular structure of ***rac*-7**.....82

Figure 1.43. ^{1}H NMR spectrum of ***rac*-7-Cl**$_3$ in CD_2Cl_2.....82

Figure 1.44. ^{13}C NMR spectrum of ***rac*-7-Cl**$_3$ in CD_2Cl_2.....83

Figure 1.45. ^{1}H NMR spectrum of ***meso*-7** in CD_2Cl_2.....83

Figure 1.46. ^{1}H NMR spectrum of ***meso*-7** in C_6D_5Cl.....84

Figure 1.47. ^{13}C NMR spectrum of ***meso*-7** in C_6D_5Cl.....84

Figure 1.48. ^{13}C NMR of polymer generated by 1-octene homopolymerization with ***meso*-3** with $B(C_6F_5)_3$.....87

Figure 1.49. ^{13}C NMR of polymer generated by 1-hexene homopolymerization with ***meso*-3** with $B(C_6F_5)_3$.....87

Figure 1.50. ^{13}C NMR of polymer generated by propylene polymerization with **Ti**$_1$ with $Ph_3C^+B(C_6F_5)_4^-$.....88

Figure 1.51. ^{13}C NMR of polymer generated by propylene polymerization with ***rac*-3** with $Ph_3C^+B(C_6F_5)_4^-$.....88

Figure 1.52. ^{13}C NMR of polymer generated by propylene polymerization with ***meso*-3** with $Ph_3C^+B(C_6F_5)_4^-$.....88

Figure 1.53. ^{13}C NMR of polymer generated by the copolymerization of ethylene and 1-octene with **Ti**$_1$ with $Ph_3C^+B(C_6F_5)_4^-$.....89

Figure 1.54. ^{13}C NMR of polymer generated by the copolymerization of ethylene and 1-octene with ***rac*-3** with $Ph_3C^+B(C_6F_5)_4^-$.....89

Figure 1.55. ^{13}C NMR of polymer generated by the copolymerization of ethylene and 1-octene with ***meso*-5** with $Ph_3C^+B(C_6F_5)_4^-$.....90

Figure 1.56. ^{13}C NMR of polymer generated by the copolymerization of ethylene and styrene with **Ti**$_1$ with $Ph_3C^+B(C_6F_5)_4^-$.....90

Figure 1.57. ^{13}C NMR of polymer generated by the copolymerization of ethylene and styrene with ***rac*-5** with $Ph_3C^+B(C_6F_5)_4^-$.....91

Figure 1.58. ^{13}C NMR of polymer generated by the copolymerization of ethylene and styrene with ***meso*-3** with $Ph_3C^+B(C_6F_5)_4^-$ 91

Figure 1.59. ^{13}C NMR spectra (100 MHz in 1,1,2,2-tetrachloroethane-d_2 at 120 °C) of the poly(ethylene-*co*-styrene) samples.....92

Figure 1.60. DFT optimized structure of ***rac*-6**.....97

Figure 1.61. DFT optimized structures of ***rac*-8** and ***meso*-8**.....97

Chapter 2

Figure 2.1. ^{1}H NMR spectra (500 MHz, C_6D_6, 25° C), of (A) bimetallic complex **2** and (B) bimetallic complex **3**.....104

Figure 2.2. The structure of asymmetric bimetallic complex **3**.....105

Figure 2.3. The structure of polymerization-inactive ion pair **4**.....107

Figure 2.4. ^{1}H NMR spectrum of **1** in C_6D_6.....118

Figure 2.5. ^{13}C NMR spectrum of **1** in C_6D_6.....118

Figure 2.6. COSY spectrum of **1** in C_6D_6.....119

Figure 2.7. HSQC spectrum of **1** in C_6D_6.....119

Figure 2.8. ^{1}H NMR spectrum of **2** in C_6D_6.....120

Figure 2.9. ^{13}C NMR spectrum of **2** in C_6D_6.....120

Figure 2.10. ^{1}H-^{1}H NOESY spectrum of **2** in C_6D_6.....121

Figure 2.11. ^{1}H NMR spectrum of **3** in C_6D_6.....121

Figure 2.12. ^{13}C NMR spectrum of **3** in C_6D_6.....122

Figure 2.13. ^{1}H-^{1}H NOESY spectrum of **3** in C_6D_6.....122

Figure 2.14. ^{1}H NMR spectrum of crude **4** in CD_2Cl_2 at -40 ºC.....123

Figure 2.15. Stacked ^{1}H NMR spectra of **4** (red, bottom) and NMR of **2** activated with 2 equiv. $Ph_3C^+B(C_6F_5)_4^-$ (teal, top), both in CD_2Cl_2 at -40 ºC.....123

Figure 2.16. ^{13}C NMR of polymer generated by ethylene/1-hexene copolymerization with **2+1B**.....125

Figure 2.17. ^{13}C NMR of polymer generated by ethylene/1-hexene copolymerization with **2+2B**.....125

Figure 2.18. ^{13}C NMR of polymer generated by ethylene/1-hexene copolymerization with **Cp*TiMe$_3$**.....126

Figure 2.19. ^{13}C NMR of polymer generated by 1-hexene homopolymerization with **2+2B**.....126

Figure 2.20. ^{13}C NMR of polymer generated by 1-hexene homopolymerization with **Cp*TiMe$_3$**.....127

CHAPTER 1

Distinctive Stereochemically Linked Cooperative Effects in Bimetallic Titanium Olefin Polymerization Catalysts

Adapted from:

Liu, S.; Invergo, A. M.; McInnis, J. P.; Mouat, A. R.; Motta, A.; Lohr, T. L.; Delferro, M.; Marks, T. J. Distinctive Stereochemically Linked Cooperative Effects in Bimetallic Titanium Olefin Polymerization Catalysts. *Organometallics*, **2017**, *36*, 4403-4421

Abstract

The complex (μ-Me_2C-3,3'){(η^5-cyclopentadienyl)[1-Me_2Si-(^{t}BuN)]($TiMe_2$)}$_2$ (**3**) was prepared as a new binuclear catalyst motif for homogeneous olefin polymerization. Complex **3** exists as ***rac*-3** and ***meso*-3** diastereomers which can be separated, and characterized by solution NMR spectroscopy and single crystal X-ray diffraction. While ***meso*-3** has high thermal stability, ***rac*-3** undergoes thermolysis in solution to quantitatively form the dimeric methylidene complex (μ-Me_2C-3,3')){(η^5-cyclopentadienyl)[1-Me_2Si(^{t}BuN)][(μ-CH_2)Ti]}$_2$ (***rac*-4**). Activation of ***rac*-3** and ***meso*-3** with 1 equiv. of $Ph_3C^+B(C_6F_5)_4^-$ yields [(μ-CMe_2-3,3')){(η^5-cyclopentadienyl)[1-Me_2Si(^{t}BuN)]}$_2$(μ-CH_2)(μ-CH_3)Ti_2]$^+B(C_6F_5)_4^-$ (**5**; ***rac*-5** and ***meso*-5**, respectively). Interestingly, ***meso*-5** is stable in the presence of an additional $Ph_3C^+B(C_6F_5)_4^-$equiv., while ***rac*-5** reacts to yield *rac*-[(μ-CMe_2-3,3')){(η^5-cyclopentadienyl)[1-Me_2Si(^{t}BuN)]}$_2$(μ-CH_2)[($TiCH_3$)-(Ti-η^1-Ph_3C)]$^{2+}$ [$B(C_6F_5)_4^-$]$_2$ (***rac*-6**) as indicated by multinuclear NMR spectroscopy and DFT computation. ***Meso*-3** reacts with 2 equiv. $B(C_6F_5)_3$ to yield *meso*-[(μ-CMe_2-3,3')){(η^5-cyclopentadienyl)[1-Me_2Si(^{t}BuN)]}$_2$-(μ-CH_2)(μ-CH_3)Ti_2]$^+MeB(C_6F_5)_3^-$ (***meso*-7**) containing the same ***meso*-5** cation but with a $MeB(C_6F_5)_3^-$counteranion. These findings, along with catalytic results, indicate that ***rac*-3** and ***meso*-3** remain structurally intact during polymerization, consistent with the observed diastereoselectivity effects. Under identical ethylene/1-octene copolymerization conditions, only activated bimetallic ***rac*-3** produces polymer, with ***meso-3*** exhibiting low activity but yielding polymer with a branch density >2x that of the monometallic control [(3-^{t}Bu-C_5H_3)$SiMe_2N^t$Bu]$TiMe_2$ (**Ti$_1$**). In ethylene/styrene copolymerizations, ***rac*-3** produces polymers with 3.1x higher M_n and 2.1x greater styrene incorporation versus **Ti$_1$**, while ***meso*-3** catalyzes only ethylene-free styrene homopolymerization. In 1-octene homopolymerizations, ***meso*-3** + $B(C_6F_5)_3$ (i.e., ***meso*-7**) produces highly *isotactic* poly-1-octene (*mmmm* 91.7%); while ***rac*-3** + $Ph_3C^+B(C_6F_5)_4^-$ (i.e., ***rac*-5**), ***rac*-3** +

$B(C_6F_5)_3$ (i.e., ***rac*-7**) and ***meso*-3** + $Ph_3C^+B(C_6F_5)_4^-$ (i.e., ***meso*-5**) produce only *atactic* poly-1-octene. These bimetallic polymerization catalysts exhibit distinctive cooperative effects influencing product M_n, tacticity, and comonomer selection, demonstrating that binuclear catalyst stereochemical factors are significant.

Introduction

In nature, multinuclear metalloenzyme active sites play key roles in organizing reactive functional groups to achieve enhanced turnover frequencies and product selectivity (Chart 1.1, **A**).[1-7] Inspired by such biocatalysts, research on abiotic multimetallic catalysis (Chart 1.1, **B**, **C**) has focused on mimicking enzymatic function to discover and perfect more efficient catalytic processes.[8-22] As a result, bimetallic complexes have emerged as powerful polymerization catalysts, and metal···metal cooperative effects have been shown to dramatically and instructively impact polymer microstructure (Chart 1.1, **C**).[21, 23-43] For example, bimetallic "constrained geometry catalysts" (**CGC^2-M$_2$, M = Ti, Zr**) exhibit high activities and significant cooperative effects, affording macromolecular products with enhanced M_n and comonomer enchainment densities.[44-51] Subsequent studies have broadened the diversity of bimetallic catalysts to include rigidly constrained phenoxyiminato[52-53] as well as heterobimetallic **Ti-C$_n$-Cr** catalysts (Chart 1.1, **C**).[54-55]

Although bimetallic cooperative effects on product M_n and comonomer enchainment selectivity have been documented with respect to metal identity, supporting ligation, and metal···metal proximity, the effects of catalyst stereochemistry, arising from bimetallic geometries, are virtually unexplored.[30, 42, 56-57] The **CGC^2-Ti$_2$** bimetallic catalyst (Chart 1.1, **C**) exists as mixture of inseparable diastereomers,[44, 46, 49-50] and stereochemical effects on cooperativity in group 4 bimetallic catalysts have barely been investigated.[58] Sita reported tethered mononuclear group 4 complexes that exist in solution as a mixture of *meso* and *racemic* diastereomers (Chart 1.2, **D**).[3g] These catalysts modulate

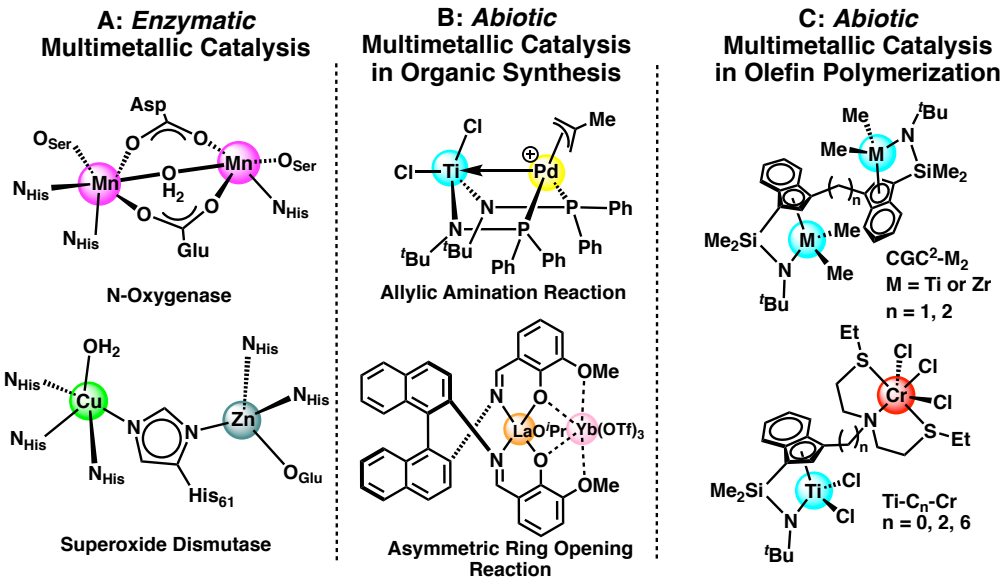

Chart 1.1. Selected examples of multimetallic enzymatic (**A**) and abiotic (**B**, **C**) catalysts.

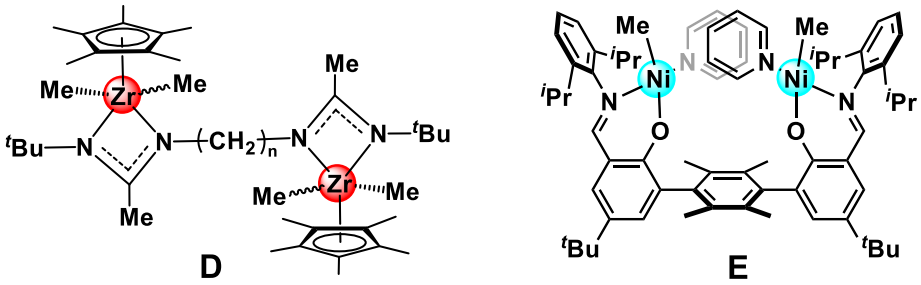

Chart 1.2. Dinuclear zirconium (D) and nickel (E) catalysts for olefin polymerization.

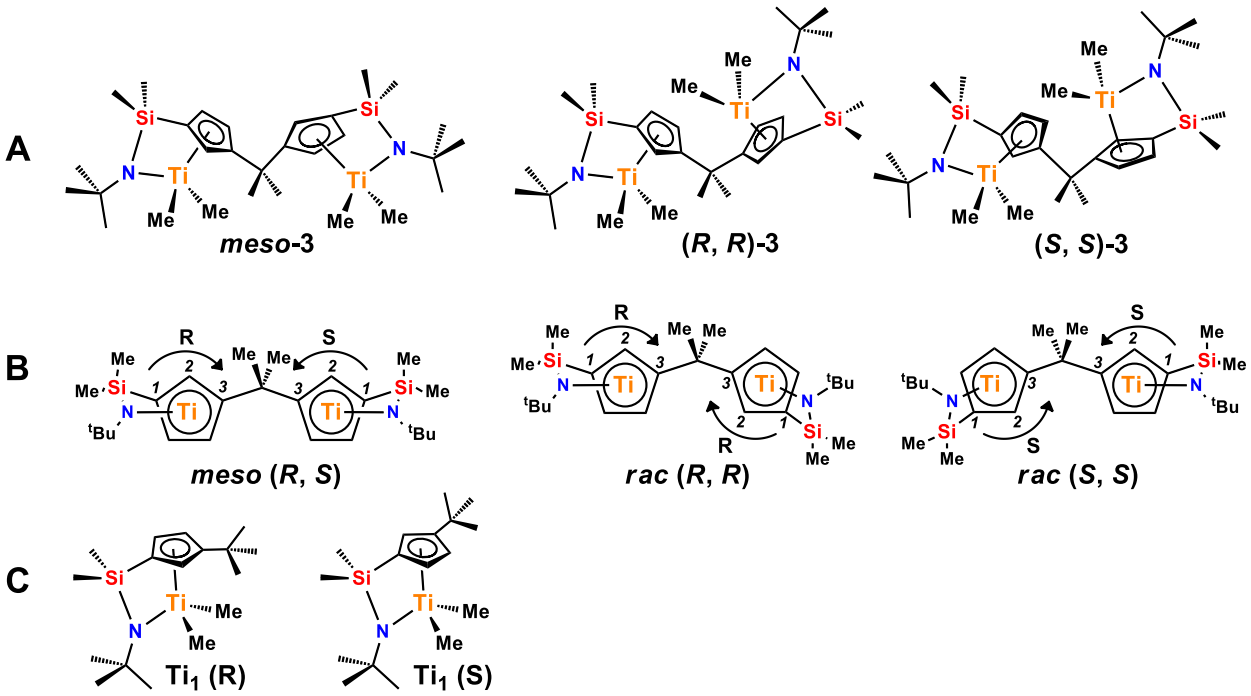

Chart 1.3. (**A**) Structures of the present diastereomeric bimetallic Ti(IV) catalysts; (**B**) View of bimetallic stereoisomers perpendicular to the Cp ring planes showing nomenclature. Substituents on Ti omitted for clarity; (**C**) Structures of the monometallic CGCTi(IV) control olefin polymerization catalysts.

the relative rates of reversible chain transfer to chain propagation in achieving stereoselective, living coordinative chain transfer polymerization to yield isotactic stereo block polypropylenes.[36] Agapie reported bimetallic salicylaldiminato Ni(II) atropisomers in which the *syn*-isomer (Chart 1.2, **E**) exhibits significant polar comonomer enchainment selectivity versus that of both the *anti*-isomer and the monometallic analogue.[59]

Note that structural details concerning the active species in solution-phase mononuclear coordinative polymerization catalysis are sparse and, starting from solid state crystallographic information, are typically inferred from in situ NMR spectroscopic data or connections between catalyst stereochemistry and product microstructure such as tacticity.[50, 60-73] Although extensive discussions of this subject are available and many mononuclear ion-paired catalysts have been characterized in detail, far less structural information is available for multinuclear polymerization catalysts. Here we report a new series of diastereomeric bimetallic Ti constrained geometry catalysts (Chart 1.3) that are characterized by appropriate spectroscopic, analytical, and diffraction techniques. Additionally, we present observations on the activation of these complexes by the cocatalysts/activators $Ph_3C^+B(C_6F_5)_4^-$ and $B(C_6F_5)_3$. The resulting ion pair structures are also characterized by NMR and X-ray diffraction, and their olefin polymerization characteristics are explored, revealing marked bimetallic diastereoselectivity effects.

Results

Synthesis of monometallic complex Ti$_1$. The titanium dichloride [(3-^{t}Bu-C_5H_3)$SiMe_2N^t$Bu]$TiCl_2$ was prepared according to literature procedures.[74] Stirring the dichloride with 2 equiv. of MeLi in diethyl ether followed by filtration and removal of solvent in vacuo yielded the yellow oily product [(3-^{t}Bu-C_5H_3)$SiMe_2N^t$Bu]$TiMe_2$ (**Ti$_1$**)[75] in high yield (83%).

Synthesis of bimetallic complexes. The synthesis of binuclear ligand (μ-CMe_2-3,3')-[1-(Me_2SiNH^tBu)cyclopentadienyl]$_2$ (**1**) is shown in Scheme 1.1.[76,77] Bimetallic precatalyst **3** was prepared via the two-step approach outlined in the Scheme. Bimetallic amido complexes **2** were synthesized via protodeamination of free ligand **1** with excess $Ti(NMe_2)_4$ in refluxing toluene with continuous removal of the $HNMe_2$ byproduct. Product **2** consists of two diastereomers (*SS*, *RR;* ***rac-2***) and (*RS*, *SR;* ***meso-2***) (1:1 ratio) as indicated by ^{1}H NMR spectroscopy (Figures 1.14 and 1.16). In contrast to MBICGC[$Ti(NMe_2)_2$]$_2$ (Chart 1.1, **C**, **CGC**^{2}**-Ti**$_2$, n = 1),[46] the two diastereomers of **2** have substantially different solubility characteristics in pentane. Complex ***meso*-2** is less soluble than ***rac*-2**, enabling selective crystallization and separation of each diastereomer (***meso*-2** at -40 °C, ***rac*-2** at -78 °C). Bimetallic amido complexes ***rac*-2** and ***meso*-2** were characterized by standard spectroscopic and analytical techniques, including X-ray diffraction (Figures 1.12 and 1.13). Reactions of ***rac*-2** and ***meso*-2** with $AlMe_3$ at room temperature in pentane cleanly afford bimetallic tetramethyl complexes ***rac*-3** and ***meso*-3**, respectively (Scheme 1.1). Complexes ***rac*-3** and ***meso*-3** were fully characterized by conventional spectroscopic and analytical techniques. According to ^{1}H NMR spectroscopy (Figures 1.18 and 1.20), ***rac*-3** possesses a symmetric configuration, in which the two methyl groups on the Cp-bridge are magnetically equivalent and give rise to a singlet at δ = 1.84 ppm. In contrast, two singlets are observed for ***meso*-3** at δ = 1.85 and 1.82 ppm, consistent with an asymmetric structure. Single crystals of ***rac*-3** and ***meso*-3** were grown from concentrated pentane solutions at -40 ºC and their molecular structures are shown in Figure 1. Both ***rac*-3** and ***meso*-3** crystallize in triclinic space group *P-1* with Z = 4 and 2, respectively. The sum of the bond angles around N1 in ***rac*-3** and ***meso*-3** are 359.8º and 359.3º respectively, indicating atoms Si1, N1, C8, and Ti1 are essentially coplanar in both complexes. Such geometry suggests a possible π-bonding interaction between the formally d^0 Ti(IV) and the

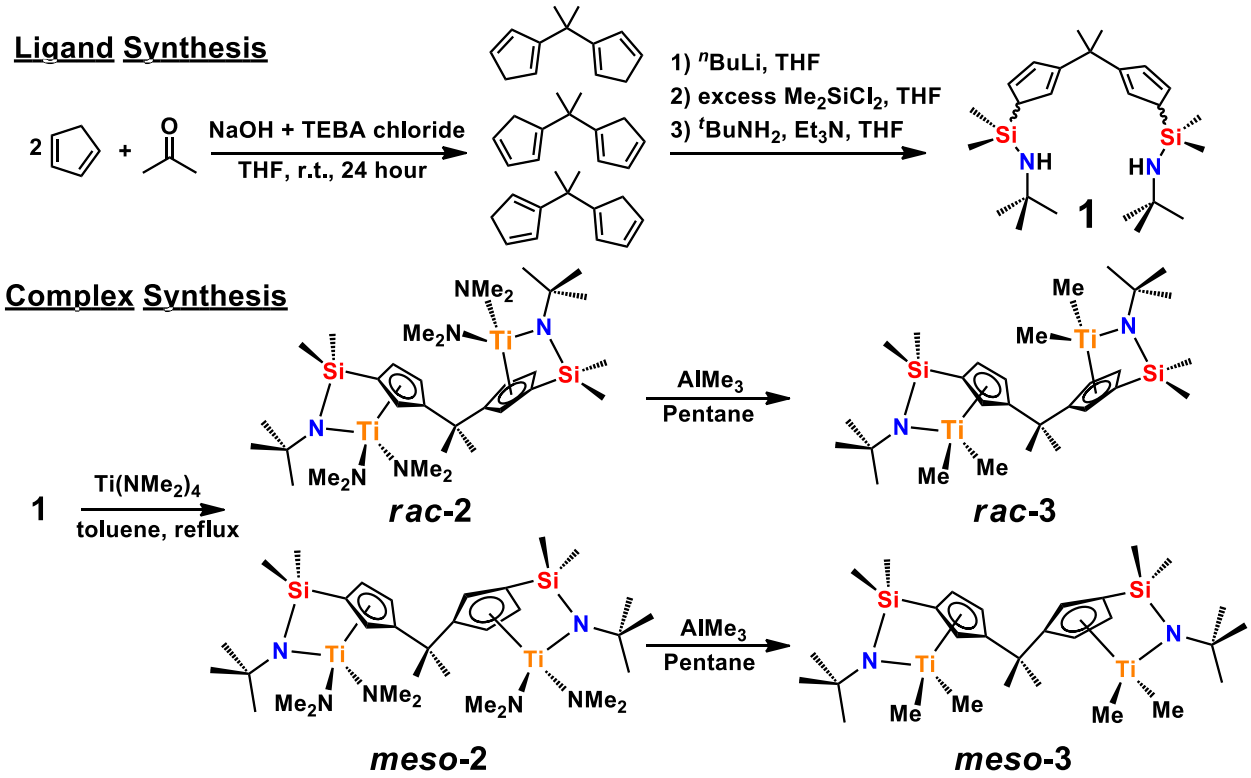

Scheme 1.1. Synthesis of the diastereomeric bimetallic precatalysts ***rac*-3** and ***meso*-3**.

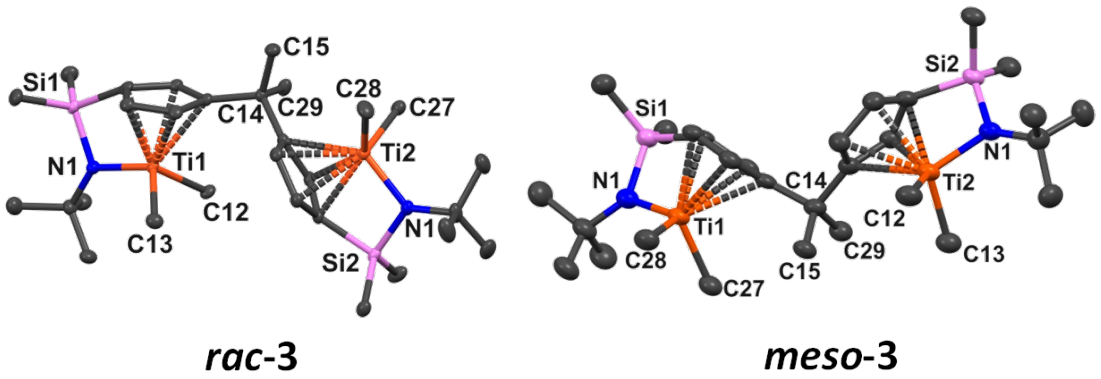

***rac*-3** ***meso*-3**

Figure 1.1. ORTEP plot of the molecular structures of bimetallic tetramethyl complexes ***rac*-3**and ***meso*-3**. Thermal ellipsoids are drawn at the 50% probability level, and H atoms are omitted for clarity. Selected distances (Å) and angles (°) for ***rac*-3**: Ti1-Ti2 6.443 (2), Ti1-Cn1 2.071 (3), Ti2-Cn2 2.075 (4), Ti1-N1 1.937 (5); Cn1-Ti1-N1 108.71 (16), Cn2-Ti2-N2 108.29 (19). Selected distances (Å) and angles (°) for ***meso*-3**: Ti1-Ti2 7.260 (2), Ti1-Cn1 2.076 (2), Ti2-Cn2 2.065 (2), Ti1-N1 1.941 (4); Cn1-Ti1-N1 108.45 (12), Cn2-Ti2-N2 108.86 (15). Ti, orange; C, dark gray; N, blue; Si, pink. Cn is the centroid of the Cp ring.

N atom lone pair.[78-83] The sum of bond angles around the Cp ring carbon atom bound to Si (C1) is 349.4º in ***rac*-3** and 348.6º in ***meso*-3**, indicating that the C1-Si1 bond vector is slightly displaced from the ring plane as a result of the constrained geometry. The Ti1-Cn1 distance (the distance between Ti and centroid of Cp) is 2.071(3) Å in ***rac*-3** and 2.076(2) Å in ***meso*-3**, with the C atoms of the Cp rings having unequal bonding distances to the Ti centers.[84-86] Note that ***rac*-3** has a Ti· · · Ti distance of 6.443(2) Å, while this distance is significantly longer for ***meso*-3** at 7.260(2) Å. This may be a factor influencing cooperative enchainment effects during polymerizations mediated by ***rac*-3** versus ***meso*-3** (*vide infra*).

Thermal properties of *rac*-3 and *meso*-3. Since both NMR data and crystal structure analysis indicate significant geometrical differences between isomeric configurations, differing physical properties and reactivities were expected for ***rac*-3** and ***meso*-3**. VT NMR studies of each isomer show that ***meso*-3** is stable at 100 °C in toluene solution, while ***rac*-3** cleanly undergoes thermolysis to quantitatively form complex ***rac*-4** (Scheme 1.2) with concomitant evolution of methane (assayed by NMR). The ^{1}H NMR spectrum of ***rac*-4** at 25 °C shows a broad, downfield signal corresponding to 4 protons at δ 7.96 ppm (Figure 1.22) coupled to a methylene resonance at δ 227.18 ppm in the ^{13}C NMR spectrum (see ^{1}H-^{13}C HSQC in Figures 1.26 and 1.27).[87] These features suggest, in addition to analytical data and the fact that ~2 equiv. of CH_4 are released in its formation, that the product is the μ-(methylidene)$_2$ dimer ***rac*-4** (Scheme 2).[88] VT ^{1}H NMR, ^{1}H-coupled ^{13}C, and ^{1}H-^{13}C HSQC NMR experiments (Figures 1.2 and 1.24-1.27) indicate that the protons within each methylene group in ***rac*-4** are magnetically non-equivalent at low temperature, appearing as two broadened signals at δ = 10.01 and δ = 6.10 ppm (Figure 1.2, -90 °C). Furthermore, the J_{CH} coupling constants (-90 °C: J_{CH} = 124.6 Hz and J_{CH} = 112.7 Hz; 100 °C: J_{CH} = 120.3 Hz) suggest that the methylene hybridization is intermediate[89] between a sp^3 and sp^2.[90-91] The latter methylidene parameter

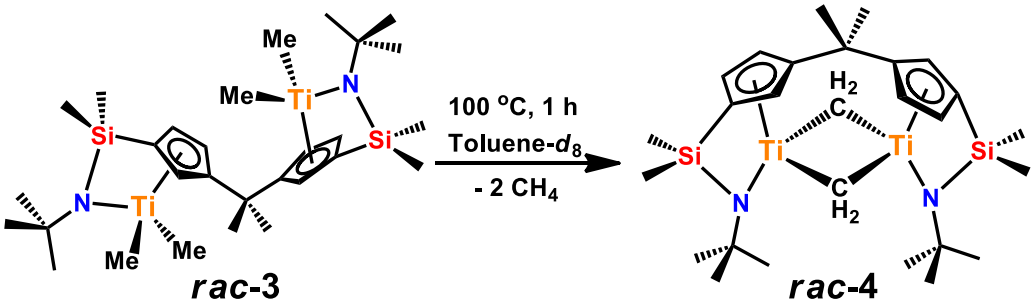

Scheme 1.2. Formation of complex ***rac*-4** via thermolysis of complex ***rac*-3**

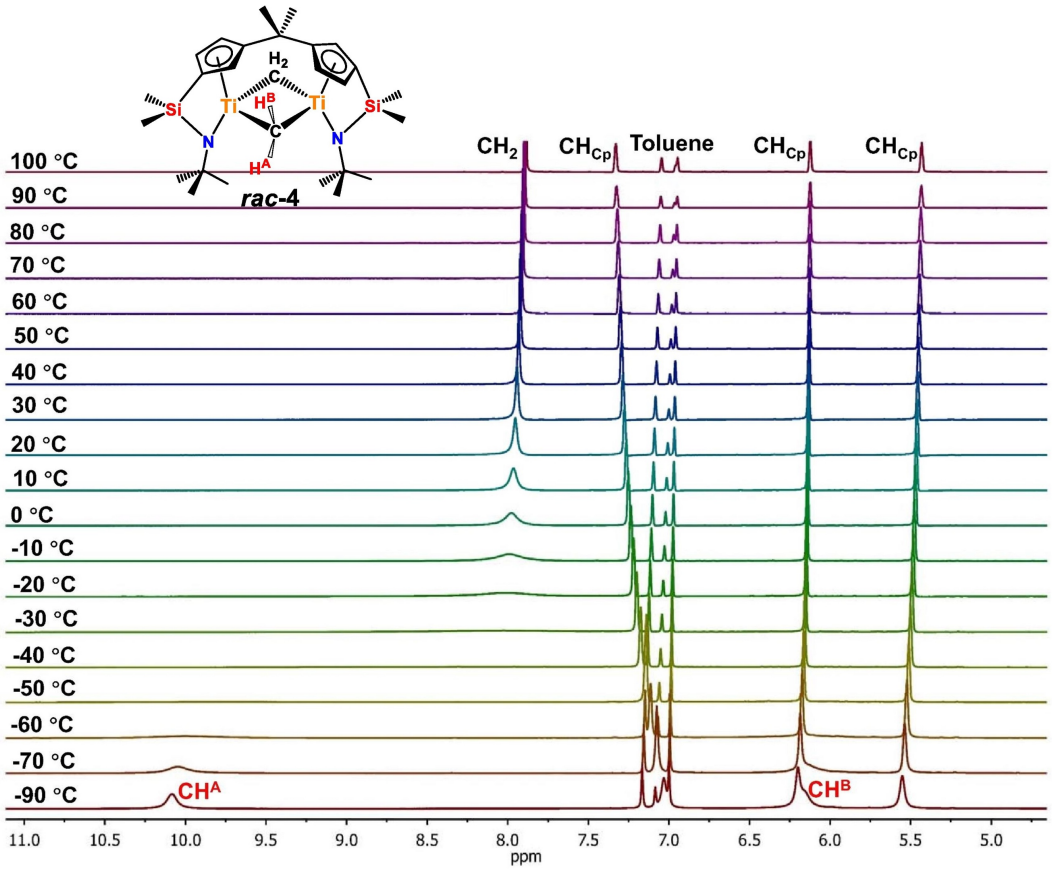

Figure 1.2. Variable-temperature ^{1}H NMR spectrum of ***rac*-4** in C_7D_8 from -90 to +100 °C.

is reminiscent of the Ti=CH_2 species in Tebbe's reagent.[54, 92-97] Red crystals of ***rac*-4** were isolated from a concentrated hexane solution at -40 °C and the molecular structure is shown in Figure 1.3A, confirming ***rac*-4** as a Ti μ-(methylidene)$_2$ dimer. The two Ti centers are pointed towards the "inside" of the molecule, which orients them face-to-face with a very short Ti· · · Ti distance of 2.9975(11) Å, likely due to the methylidene bridges. NBO calculations on the optimized ***rac*-4** structure (Figure 1.3B) indicate that hybridization of the methylene carbon orbitals involved in Ti bonding ranges between $sp^{2.46}$ and $sp^{3.09}$, in good agreement with the experimental NMR data (see more below).

Activation studies of *rac*-3 and *meso*-3 with $Ph_3C^+B(C_6F_5)_4^-$. *Rac*-3 reacts with 1 equiv. of $Ph_3C^+B(C_6F_5)_4^-$ in C_6D_5Cl to release 1 equiv. each of Ph_3CMe and CH_4 while quantitatively yielding monocationic complex ***rac*-5**, consisting of a monocationic ion-pair binuclear species/$B(C_6F_5)_4^-$anion (Scheme 1.3). The ^{1}H NMR spectrum of ***rac*-5** (Figure 1.4A) shows a broad resonance at δ 7.29 ppm integrating as 2 protons, and coupled to a methylene resonance at δ 227.37 ppm in the ^{13}C NMR spectrum, for the bridged methylene (μ-CH_2) group, and a sharp resonance integrating as 3 protons for the bridged methyl (μ-CH_3) group at δ -0.15 ppm (coupled to a resonance at δ 61.89 ppm in the ^{13}C NMR spectrum). In C_6D_5Cl solution, addition of 2 equiv. of $Ph_3C^+B(C_6F_5)_4^-$ to ***rac*-3** produces ***rac*-6** (Scheme 1.3) and CH_4. The ^{1}H NMR spectrum (Figure 1.4B) exhibits a single broadened resonance at δ = 7.77 ppm integrating to 2 protons coupled to a signal at δ 233.43 ppm in the ^{13}C NMR, indicating a μ-CH_2 group similar to that in ***rac*-5**.[98] However, the two Cp rings and the two $Si(CH_3)_2$ groups are magnetically non-equivalent, suggesting that the second equiv. of $Ph_3C^+B(C_6F_5)_4^-$weakly binds to one Ti center, affording an asymmetric molecular structure (*vide infra*). Thus, the singlet at δ = -0.41 ppm (coupled to a signal at δ 67.63 ppm in the

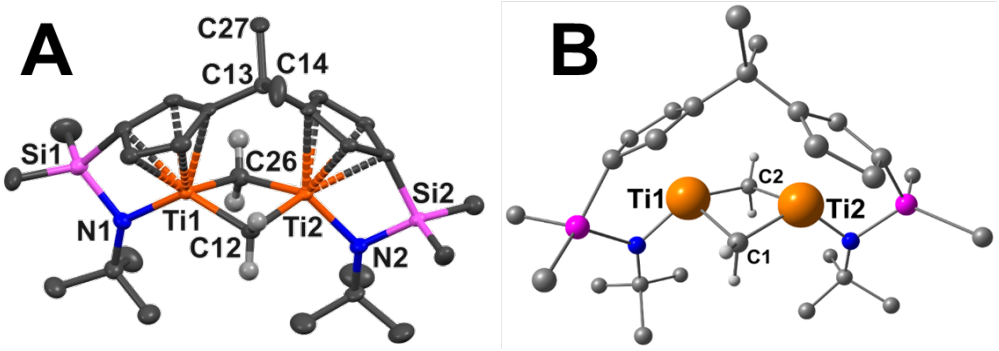

Figure 1.3. (**A**) ORTEP view of the molecular structure of complex ***rac*-4**. Thermal ellipsoids are drawn at the 50% probability level, and H atoms are omitted for clarity, except for the μ-CH_2 groups. Selected distances (Å) and angles (deg): Ti1-Ti2 2.9975 (11), Ti1-Cn1 2.0349 (18), Ti2-Cn2 2.0487 (16), Ti1-N1 1.969 (3), Ti2-N2 1.962 (3), Ti1-C12 2.038 (4), Ti1-C26 2.141 (4), Ti2-C12 2.136 (4), Ti2-C26 2.141 (4); Si1-N1-Ti1 100.99 (14), Si2-N2-Ti2 99.79 (14), Cn1-Ti1-N1 108.14 (10), Cn2-Ti2-N2 108.78 (11). (**B**) Optimized DFT geometry of the ***rac*-4** molecular structure. Ti, orange; C, dark gray; H, light gray; N, blue; Si, pink. Cn represents the centroid of the Cp ring.

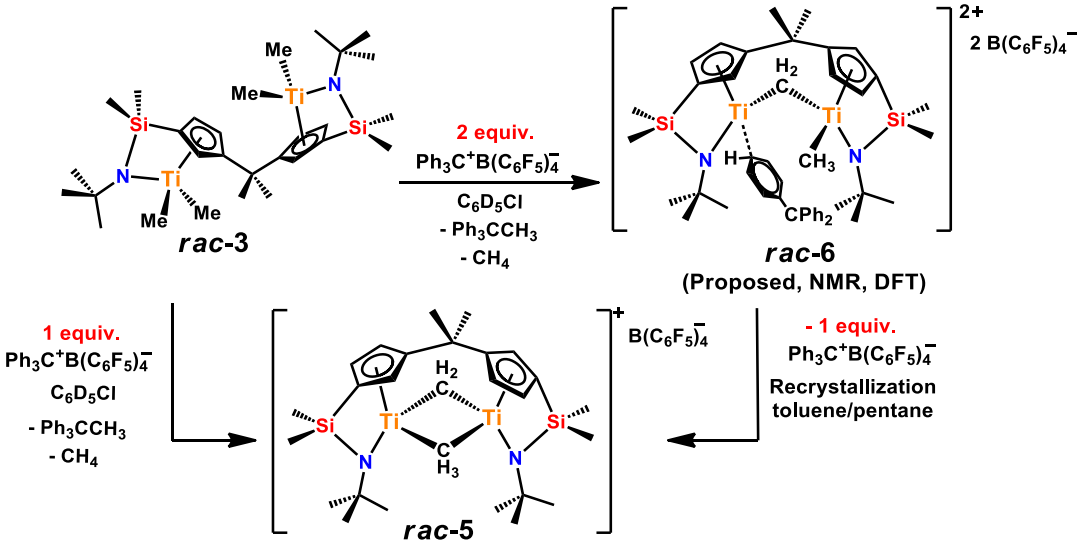

Scheme 1.3. Proposed activation pathway of ***rac*-3** with $Ph_3C^+B(C_6F_5)_4^-$ to form ***rac*-5** and ***rac*-6**.

^{13}C NMR) is assigned to a terminal Ti-CH_3 group. Note that the resonances of the second equiv. of Ph_3C^+ are not detected in the ^{1}H NMR spectrum at room temperature, suggesting possible η^{1+n}-coordination of a tritylphenyl ring to one Ti center, which broadens the resonances.[99] Computational modeling finds a weak Ti···C interaction with the *para* carbon of one trityl ring, resulting in slight elongation of the *para* C-H bonds relative to the other phenyl C-H bonds, 1.10 Å *vs* 1.09 Å respectively (Figure 1.60). High temperature (100 °C) VT-NMR reveals a broad signal at δ = 7.23-7.36 ppm, assigned to a weakly coordinated trityl ring (Figure 1.35). Moreover, recrystallization of ***rac*-6** from toluene yields solid ***rac*-5** with 1 equiv. of $Ph_3C^+B(C_6F_5)_4^-$ remaining in solution. Based on NMR and computation, the structure of ***rac*-6** is suggested to be a μ-CH_2 bridged asymmetric binuclear dication with an additional weak interaction involving the second equiv. of $Ph_3C^+B(C_6F_5)_4^-$ (Scheme 1.3).

In contrast to the above results, when ***meso*-3** is activated with either 1 or 2 equiv. of $Ph_3C^+B(C_6F_5)_4^-$, only ***meso*-5** is formed and quantitatively (Scheme 1.4), as indicated by ^{1}H NMR and ^{13}C NMR (Figures 1.36-1.39). Variable temperature NMR spectroscopy (Figure 1.40), shows the μ-CH_2 protons to be magnetically non-equivalent at -90 °C in CD_2Cl_2 (δ 9.71, 7.68 ppm), with negligible chemical shift variations for other resonances between -90 °C and 20 °C. Red crystals of ***rac*-5** and ***meso*-5** were grown from dilute toluene solutions at -40 °C, and the solid state structures of the μ-CH_2, μ-CH_3 binuclear ***rac*-5** and ***meso*-5** cations are shown in Figure 1.5. The Ti· · · Ti metal distances in ***rac*-5** and ***meso*-5** are 3.000(3) Å and 3.0041(14) Å, respectively, similar to that of ***rac*-4** (2.9975(11) Å). The μ-CH_2 and μ-CH_3 groups are occupationally disordered, and no bridging methyl/methylene group H atoms could be located crystallographically. Bochmann[100] previously provided spectroscopic evidence for the Zr_2 cation, $(CpZr)_2(\mu\text{-}CH_2)(\mu\text{-}CH_3)(\eta^5\text{:}\eta^5\text{-}C_{10}H_8)^+B(C_6F_5)_4^-$, Sita[55] reported the crystal structure of dizirconium

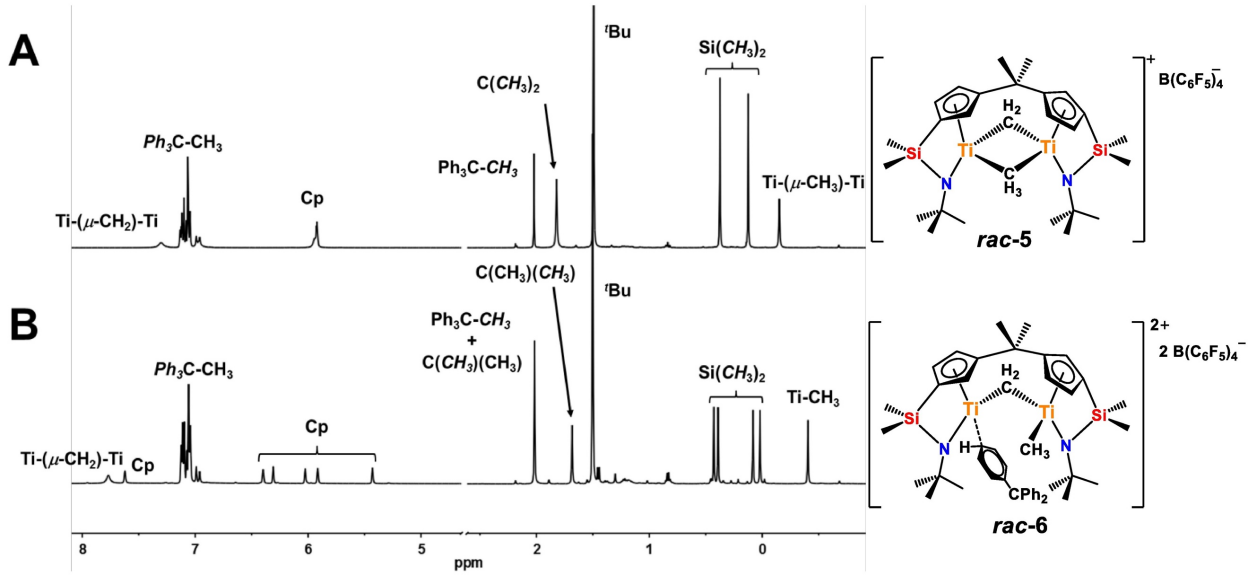

Figure 1.4. ^{1}H NMR spectra (25 °C) of ***rac*-3** activated with 1 (**A**) or 2 (**B**) equiv. of $Ph_3C^+B(C_6F_5)_4^-$ in C_6D_6Cl, with proposed structures.

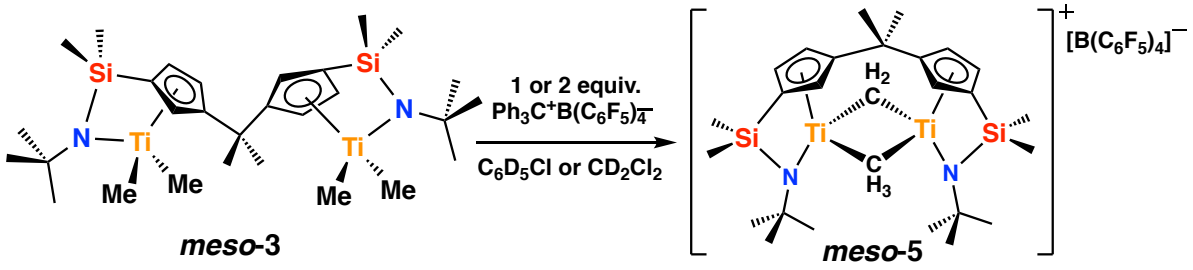

Scheme 1.4. Activation of complex ***meso*-3** with $Ph_3C^+B(C_6F_5)_4^-$ to form ***meso*-5**.

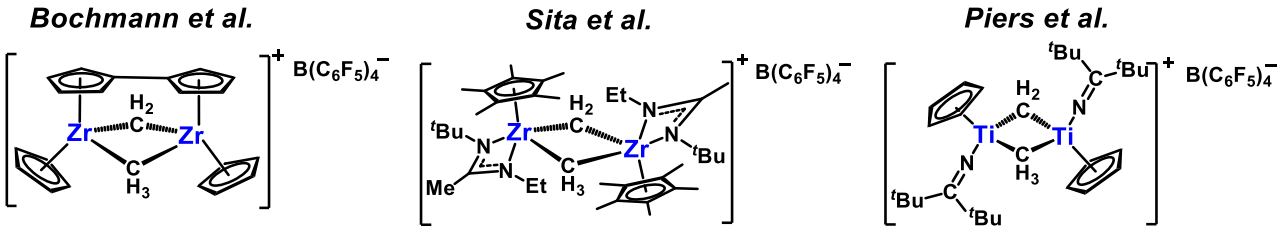

Chart 1.4. Rare examples of μ-CH_2, μ-CH_3 bridged binuclear monocationic group 4 complexes.

$[Cp^*_2Zr_2\{N(^tBu)C(Me)N(Et)\}_2(\mu\text{-}CH_2)(\mu\text{-}CH_3)]^+B(C_6F_5)_4^-$, and Piers[101] described methane loss from a cationic μ-CH_3 dimer formed via trityl borate activation to form $[CpTiN{=}C(^tBu)_2]_2(\mu\text{-}CH_2)(\mu\text{-}CH_3)^+B(C_6F_5)_4^-$ (Chart 1.4). Therefore, while there is some structural precedent, ***rac*-5** and ***meso*-5** represent two of the very few examples of μ-CH_2, μ-CH_3 binuclear monocationic Ti complexes. Note also that ***meso*-5** is relatively stable in polar solvents such as CD_2Cl_2 over the course of hours, while ***rac*-5** quickly activates CD_2Cl_2[102-107] under identical conditions to form binuclear μ-Cl monocationic trichloride ***rac*-5-Cl$_3$**, as confirmed by NMR and X-ray analysis (Scheme 1.5 and Figures 1.30-1.32).

DFT calculations were next performed to analyze the electronic structures of ***meso*-5** and ***rac*-5**. In this comparative analysis, the "naked cation approach" was adopted as a first level of approximation, neglecting cocatalyst/counteranion effects. The computed structure of ***meso*-5** features C_s symmetry with a mirror plane bisecting the Ti-Ti vector and containing bridging carbons atoms C1 and C2 (Figure 1.6). Negligible differences are observed in the Ti-CH_3 and -CH_2 distances (Ti1-C1 vs Ti2-C1 and Ti1-C2 vs Ti2-C2, Table S52). This is consistent with the metrical parameters found experimentally in the solid state structure of ***meso*-5** (Figure 1.5). Comparable positive charges are also found on Ti1 (0.446 D) and Ti2 (0.438 D), indicating symmetric charge delocalization on the two Ti centers. In contrast, ***rac*-5** is less symmetrical (C_1) as a result of the different Ti-CH_3 (C1) and Ti-CH_2 (C2) interactions. These different interactions find counterparts in the different Ti1-C1 and Ti2-C1 as well as Ti1-C2 and Ti2-C2 bond distances in ***rac*-5** (Figure 1.6). Thus, Ti1-C1 is 0.11(2) Å shorter than Ti2-C1, whereas Ti1-C2 is 0.04(2) Å longer than Ti2-C2. This asymmetry is also detected in the diffraction-derived solid state structure of ***rac*-5** (Figure 1.5). Moreover, the evaluated NBO charge distribution on the two Ti centers shows that

greater positive charge is located on Ti2 as a result of the asymmetry in electronic distribution (Ti1 = 0.390 D, Ti2 = 0.464 D).

Activation studies of *rac*-3 and *meso*-3 with $B(C_6F_5)_3$. ***Rac*-3** reacts with 2 equiv. of $B(C_6F_5)_3$ in toluene to yield ion-pair ***rac*-7** with release of 1 equiv. of CH_4 (Scheme 1.6, Figure 1.42). Yellow crystals of ***rac*-7** were grown from dilute toluene solutions at -40 °C. Unfortunately, refinement to a suitable resolution is precluded by the twinned nature of the crystals. Nevertheless, the connectivity of the weakly bound methylborate anions is evident (Figure 1.42).[46, 50, 108-113] ^1H and ^{13}C NMR analysis of ***rac*-7** in CD_2Cl_2 shows no Ti-*Me* resonance and implies that ***rac*-7** activates CD_2Cl_2 to selectively afford ***rac*-7-Cl$_3$**, which is structurally very similar to ***rac*-5-Cl$_3$** but with a $MeB(C_6F_5)_4^-$ counteranion (Scheme 1.6, Figures 1.31 and 1.32 versus 1.43 and 1.44).

In contrast to the above results, ^1H NMR and ^{13}C NMR spectra indicate that reacting ***meso*-3** with 2 equiv. of $B(C_6F_5)_3$ quantitatively yields ***meso*-7** (Scheme 1.7, Figures 1.45-1.47) which is stable in chlorinated solvents (C_6D_5Cl for days, CD_2Cl_2 for hours). Red crystals of ***meso*-7** were grown from dilute toluene solution at -40 °C, and the solid state structure of μ-CH_2, μ-CH_3 binuclear ***meso*-7** is shown in Figure 1.7. Note that the cation of ***meso*-7** is identical to that of ***meso*-5**, and the structures of both were confirmed by X-ray diffraction (Figures 1.5, 1.7) and NMR (Figures 1.36-1.39, 1.45-1.47). ***Meso*-5** and ***meso*-7** only differ in counteranion: a free $B(C_6F_5)_4^-$ anion in the former and a free $MeB(C_6F_5)_3^-$ anion in the latter, with a broad ^1H NMR B-*Me* resonance at $\delta = 0.47$ ppm integrating as 3 protons.

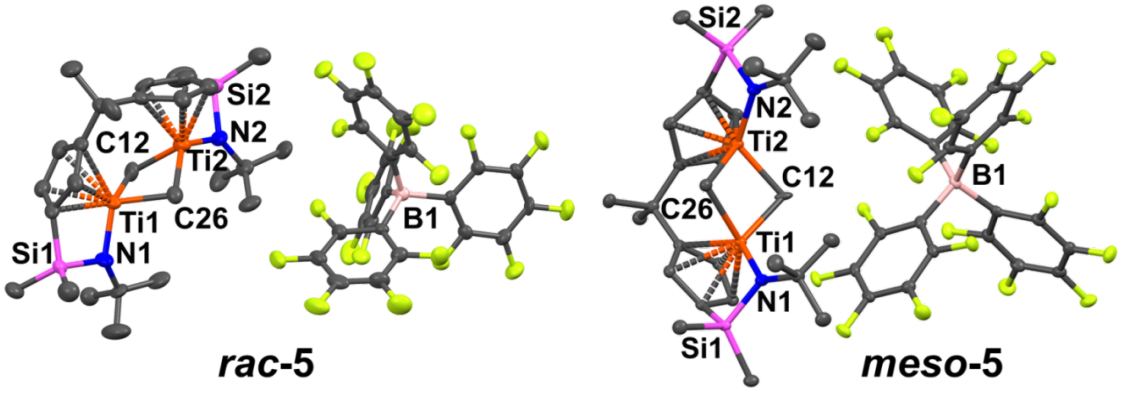

Figure 1.5. ORTEP view of the molecular structures of ***rac*-5** and ***meso*-5**. Ellipsoids enclose 50% of the electronic density and H atoms are omitted for clarity. Selected distances (Å) and angles (deg) in ***rac*-5**: Ti1-Ti2 3.000 (3), Ti1-Cn1 2.026 (5), Ti2-Cn2 2.049 (4), Ti1-C12 2.088 (8), Ti1-C26 2.182 (10), Ti2-C12 2.178 (9), Ti2-C26 2.196 (9); Cn1-Ti1-N1 108.8 (3), Cn2-Ti2-N2 108.6 (2). Selected distances (Å) and angles (deg) in ***meso*-5**: Ti1-Ti2 3.0058 (13), Ti1-Cn1 2.0306 (13), Ti2-Cn2 2.0192 (13), Ti1-C12 2.090 (2), Ti1-C26 2.269 (3), Ti2-C12 2.108 (3), Ti2-C26 2.255 (2); Cn1-Ti1-N1 109.20 (6), Cn2-Ti2-N2 108.78 (8). Ti, orange; C, dark gray; N, blue; Si, pink; F, yellow-green; B, light pink. Cn represents the centroid of the Cp ring.

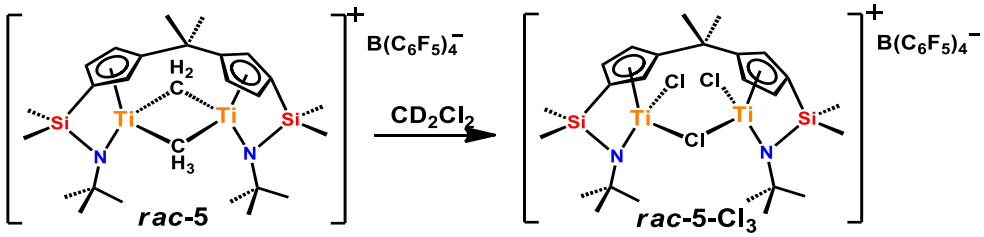

Scheme 1.5. Formation of ***rac*-5-Cl**$_3$ by reaction of ***rac*-5** with CD_2Cl_2.

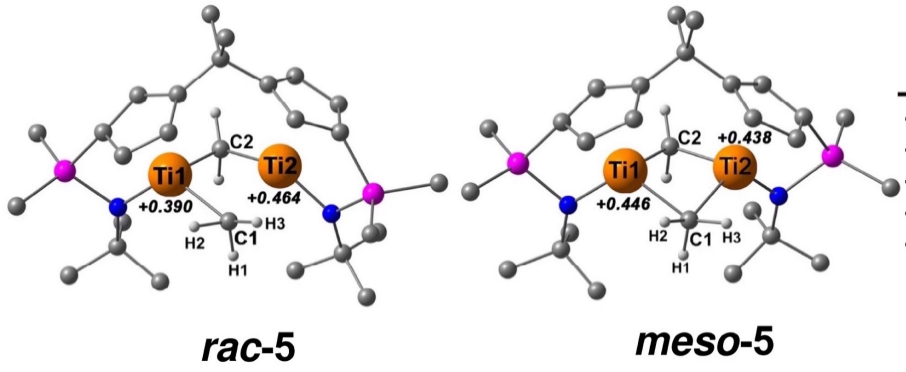

	rac-5	meso-5
Ti1-Ti2	3.01	3.03
Ti1-C1	2.21	2.25
Ti1-C2	2.08	2.06
Ti2-C1	2.32	2.25
Ti2-C2	2.04	2.06

Figure 1.6. Optimized DFT computed geometries of the "naked" ***rac*-5** and ***meso*-5** cations.

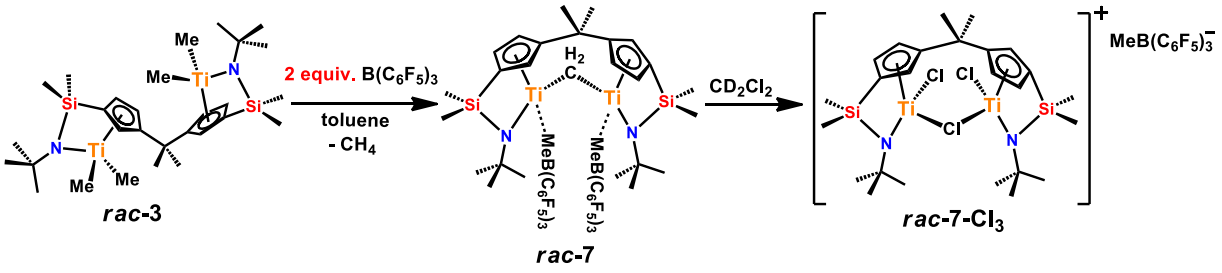

Scheme 1.6. Proposed activation pathway of complex ***rac*-3** with $B(C_6F_5)_3$ to form complex ***rac*-7**.

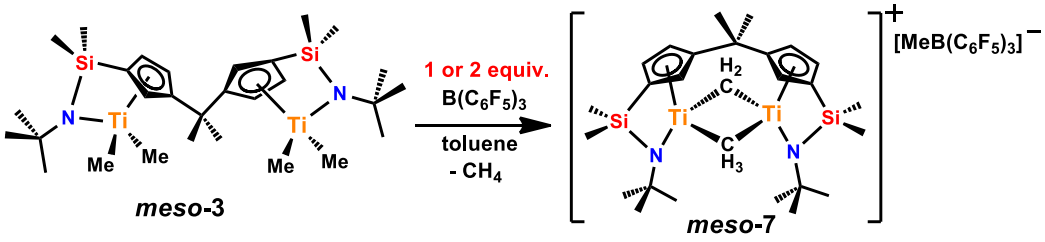

Scheme 1.7. Activation of ***meso*-3** with $B(C_6F_5)_3$ to form complex ***meso*-7**.

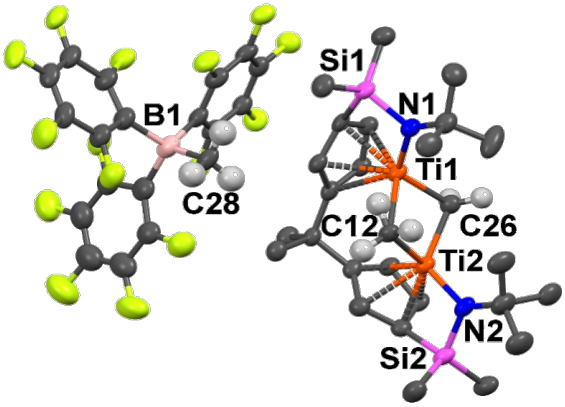

Figure 1.7. ORTEP view of the molecular structure of ***meso*-7** (ellipsoids enclose 50% electronic density; H atoms are omitted for clarity, except for the μ-CH_2, μ-CH_3 and B-CH_3 groups). Selected distances (Å) and angles (deg) in ***meso*-7**: Ti1-Ti2 2.9871 (18), Ti1-N1 1.924 (6), Ti2-N2 1.914 (5), Ti1-Cn1 2.019 (3), Ti2-Cn2 2.021 (4), Ti1-C12 2.234 (6), Ti1-C26 2.071 (6), Ti2-C12 2.227 (6), Ti2-C26 2.077 (6); Cn1-Ti1-N1 109.38 (18), Cn2-Ti2-N2 109.7 (2). Ti, orange; C, dark gray; H, light gray; N, blue; Si, pink; F, yellow-green; B, light pink. Cn represents the centroid of the Cp ring.

Table 1.1. Ethylene homopolymerization data for catalysts **Ti**$_1$, ***rac*-3**, and ***meso*-3**.[a]

Entry	Catalyst	Equiv. of $Ph_3C^+B(C_6F_5)_4^-$	Polymer (g)	Activity[b] (PE)	M_n[c] (kg·mol^{-1})	$Đ$[c]
1	**Ti**$_1$	1.2	1.66	4980	67	2.7
2	***rac*-3**	1.0	0.04	120	93	5.5
3	***rac*-3**	2.4	0.56	1680	299	1.9
4	***meso*-3**	1.0	trace	-	-	-
5	***meso*-3**	2.4	0.04	120	258	2.8

[a]Polymerization conditions: [catalyst] = 10 μmol **Ti**$_1$; 5 μmol ***rac*-3**; 5 μmol ***meso*-3**; 50 mL toluene, at 25 °C, and under constant 1 atm of ethylene pressure for 2 min. Entries performed in duplicate. [b]kg (polymer)·mol^{-1}(Ti)·h^{-1}·atm^{-1}. [c]GPC vs polystyrene standards in (kg·mol^{-1}).

Catalytic Olefin Polymerization

Ethylene, propylene, and 1-octene homopolymerizations. Ethylene, propylene, and 1-octene homopolymerizations were carried out under rigorously anhydrous/anaerobic conditions with attention to exotherm and mass transfer effects.[114-115] Data are presented in Tables 1.1, 1.2, and 1.3. Monometallic catalyst [(3-^{t}Bu-C_5H_3)$SiMe_2N^t$Bu]$TiMe_2$ (**Ti$_1$**) was used as a control. For all polymerizations, except ***rac-3*** + 1 equiv. $Ph_3C^+B(C_6F_5)_4^-$, the monomodal gel-permeation chromatography (GPC) traces and product $Đ$ values are consistent with single-site processes.[116-118] In agreement with the catalyst structural data, the unique properties of each bimetallic diastereomer are readily apparent. When activated with 1 equiv. of $Ph_3C^+B(C_6F_5)_4^-$ per Ti, ***rac*-3** is far more active for ethylene homopolymerizations than ***meso*-3**, which only produces small quantities of polymer (Table 1.1, entries 3 and 5). In contrast, **Ti$_1$** produces significantly more polymer than either of the binuclear catalysts under identical reaction conditions (Table 1.1, entry 1). The reduced activity in both bimetallic systems likely reflects increased steric bulk around the Ti centers.[119] Note that ~4.5x greater M_n is achieved with ***rac*-3** vs. **Ti$_1$** under identical polymerization conditions (Table 1.1 entries 2 and 3 vs 1). Experiments with 0.5 equiv. of co-catalyst $Ph_3C^+B(C_6F_5)_4^-$ per Ti show that ***meso*-3** is almost completely inactive under these conditions, while ***rac*-3** produces far less polymer than when both metals are activated (Table 1.1, entries 2 vs 3), suggesting the necessity of the second borate equivalent and activation at both metal centers to achieve appreciable activity under these conditions (*vide infra*).

Propylene and 1-octene homopolymerization data with Ti : cocatalyst ratios of 1:1 equivalents are presented in Tables 1.2 and 1.3. Note that ***rac*-3** again is more active than ***meso*-3**, but less active than monometallic **Ti$_1$**. All of the present polypropylene products are atactic as judged by ^{13}C NMR spectroscopy[120-122] (Figures 1.50-1.52) and readily soluble in ether, hydrocarbons, and

Table 1.2. Propylene homopolymerization data for catalysts **Ti$_1$**, ***rac*-3**, and ***meso*-3**.[a]

Entry	Catal.	Cocatalyst	Polymer (g)	Activity[b]	*mmmm* (%)[c]	M_n[d] (kg·mol^{-1})	$Đ$[d]
1	**Ti$_1$**	$Ph_3C^+B(C_6F_5)_4^-$	9.81	3270	atactic	20.9	2.4
2	***rac*-3**	$Ph_3C^+B(C_6F_5)_4^-$	1.85	616	atactic	47.8	2.0
3	***meso*-3**	$Ph_3C^+B(C_6F_5)_4^-$	0.61	203	atactic	47.1	2.1

[a]Polymerization conditions: [catalyst] = 10 μmol **Ti$_1$**; 5 μmol ***rac*-3**; 5 μmol ***meso*-3**; activator ratio of $Ph_3C^+B(C_6F_5)_4^-$/Ti = 1.2; 1 atm of propylene pressure for 20 min in 50 mL toluene at 25 °C. Entries performed in duplicate. [b]kg (polymer)·mol^{-1} (Ti)·h^{-1}·atm^{-1}. [c]By ^{13}C NMR.[123-124] [d]GPC vs polystyrene in (kg·mol^{-1}).

Table 1.3. 1-octene homopolymerization data for catalysts **Ti$_1$**, ***rac*-3**, and ***meso*-3**.[a]

Entry	Catal.	Cocatalyst	Polymer (g)	Activity[b]	*mmmm* (%)[c]	M_n[d] (kg·mol^{-1})	$Đ$[d]
1	**Ti$_1$**	$B(C_6F_5)_3$	1.43	5.95	36.2	14.2	1.9
2	***rac*-3**	$B(C_6F_5)_3$	0.03	0.125	40.8	70.4	1.8
3	***meso*-3**	$B(C_6F_5)_3$	0.02	0.083	91.7	26.1	1.1
4	**Ti$_1$**	$Ph_3C^+B(C_6F_5)_4^-$	3.30	13.75	34.4	1.57	1.3
5	***rac*-3**	$Ph_3C^+B(C_6F_5)_4^-$	1.89	7.87	39.5	3.68	2.1
6	***meso*-3**	$Ph_3C^+B(C_6F_5)_4^-$	1.07	4.45	35.2	3.22	1.4

[a]Polymerization conditions: [catalyst] = 10 μmol **Ti$_1$**; 5 μmol ***rac*-3**; 5 μmol ***meso*-3**; activator ratio of $B(C_6F_5)_3$ or $Ph_3C^+B(C_6F_5)_4^-$/Ti = 1.2; 5.60 g of 1-octene for 24 h in 20 mL toluene, at 25 °C. Entries performed in duplicate. [b]kg (polymer)·mol^{-1} (Ti)·h^{-1}·atm^{-1}. [c]By ^{13}C NMR.[123-124] [d]GPC vs polystyrene in (kg·mol^{-1}).

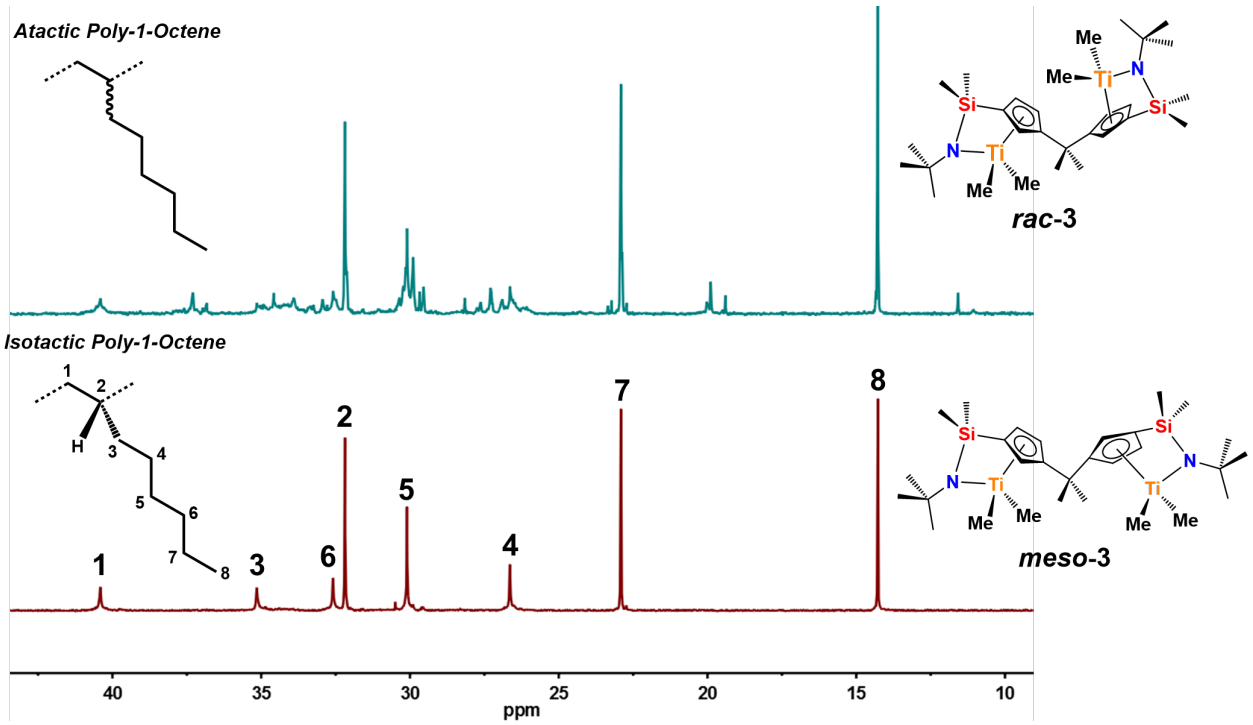

Figure 1.8. ^{13}C NMR spectra (100 MHz, $C_2D_2Cl_4$, 120 °C) of the poly-1-octene samples from Table 1.3, entries 2 and 3, showing the tacticity sensitivity to the indicated activated precatalysts.

chlorinated solvents, although solubility falls with increasing M_n.[125, 126] Similar to ethylene polymerization, the polypropylenes produced by bimetallic ***rac*-3** and ***meso*-3** have significantly higher M_ns (~2.2×) than those produced by monometallic **Ti$_1$**.[127] Recall that ***meso*-3** activated by $Ph_3C^+B(C_6F_5)_4^-$ and $B(C_6F_5)_3$ yields ***meso*-5** and ***meso*-7**, containing the same cation but different counteranions, $B(C_6F_5)_4^-$ and $MeB(C_6F_5)_3^-$, respectively. The results of the 1-octene homopolymerization experiments (Table 1.3, entries 1-6) reveal striking catalyst and cocatalyst-dependent product tacticity control, indicating that cation - cocatalyst counteranion interactions significantly affect enchainment activity and selectivity.[68, 118, 128] Note that ***rac*-3** with either $Ph_3C^+B(C_6F_5)_4^-$ or $B(C_6F_5)_3$ exhibits higher activity than ***meso*-3** under identical conditions. Note also that only ***meso*-3** activated by $B(C_6F_5)_3$ produces highly isotactic poly-1-octene with 91.7% *mmmm* (Figure 1.8), while **Ti$_1$** and ***rac*-3** with $B(C_6F_5)_3$ or $Ph_3C^+B(C_6F_5)_4^-$, as well as ***meso*-3** with $Ph_3C^+B(C_6F_5)_4^-$, yield poly-1-octenes with only 30-40% *mmmm*.[124] The poly-1-octenes produced with $B(C_6F_5)_3$ as cocatalyst have much higher M_ns than those produced with $Ph_3C^+B(C_6F_5)_4^-$. With the same cocatalyst, both bimetallic ***rac*-3** and ***meso*-3** form higher M_n polymers than the **Ti$_1$** control.

Ethylene/1-octene copolymerization. Ethylene + 1-octene copolymerization data are presented in entries 1, 3 and 5 of Table 1.4 with Ti : cocatalyst ratios of 1:1 equivalents. Bimetallic catalyst ***rac*-3** displays 1.9x greater activity for ethylene/1-octene copolymerization versus the analogous ethylene homopolymerization (Table 1.4 entry 3 vs. Table 1.1 entry 3), indicating an uncommonly encountered "comonomer effect".[58, 129-132] Note that the exact opposite trend is observed for ***meso*-3** (Table 1.4 entry 5 vs Table 1.1 entry 5). Once again, ***rac*-3** is the more active bimetallic catalyst, producing ethylene/1-octene copolymers with ~36x greater activity than ***meso*-3** (Table 1.4 entries 3 vs 5). ***Rac*-3** and ***meso*-3** also produce polymer with more than double the enchainment of 1-octene (7.0 and 7.1 % respectively) than achieved by **Ti$_1$**. In both cases, the presence of the second

metal center may play the role of a multi-centered bonding "α-olefin trap"[30] to enhance comonomer enchainment selectivity vs. monometallic **Ti**$_1$ (*vide infra*). Interestingly, ***rac*-3** and **Ti**$_1$ produce copolymers of comparable M_n, while ***meso*-3** produces a copolymer that has a M_n 1.6x *lower* than **Ti**$_1$. Once again, these results reveal markedly different catalytic performances for the two bimetallic diastereomers. To complement the ethylene homopolymerization studies, control experiments were performed in which polymerizations were conducted with only 0.5 equiv. $Ph_3C^+B(C_6F_5)_4^-$ per Ti. Both ***rac*-3** and ***meso*-3** display vanishingly low activities, with ***rac*-3** producing only a few mg of polymer and ***meso*-3** producing almost no polymer (Table 1.4, entries 2 and 4), again highlighting the significance of the second co-catalyst equiv. in promoting appreciable polymerization activity.

Ethylene/styrene copolymerization. Under identical reaction conditions, bimetallic ***rac*-3** incorporates styrene in compositions as high as 63.0%, which is 2.1x higher than the enchainment achieved by monometallic **Ti**$_1$ (Table 1.5 entries 2-4). In the ^{13}C NMR of the poly(ethylene-*co*-styrene) (Figure S50),[125, 136-140] the resonances centered at δ = 25.5, 27.7, 29.8, 36.9, and 46.0 ppm in the aliphatic region can be assigned to $S_{\beta\beta}$, $S_{\beta\delta}$, $S_{\gamma\delta}$, $S_{\alpha\gamma}$ + $S_{\alpha\delta}$ and $T_{\delta\delta}$ positions, respectively, corresponding to SES, SEE, SEE_nS, SES + SEE, and E_nSE_n (n≥ 1) sequences.[140] The signals observed at δ = 146.4 and 125.7 ppm in the aromatic region are assigned to the *ipso* and *para* carbons of the phenyl ring attached to the copolymer backbone, respectively. Thus, all evidence indicates that the polymers produced by **Ti**$_1$ and ***rac*-3** are exclusively poly(ethylene-*co*-styrene) copolymers. However, the ^{13}C NMR spectrum (Figure 1.58) of polymer obtained by ***meso*-3** (Table 1.5, entry 4) mainly exhibits a single broad resonance at δ = 41-45 ppm, attributable to *atactic* polystyrene.[141] The absence of other resonances indicates that the polymerization product is not a

Table 1.4. Ethylene/1-octene copolymerization data for catalysts **Ti$_1$**, ***rac*-3**, and ***meso*-3**.[a]

Entry	Catalyst	*t* (min)	PE (g)	Activity[c] (PE)	Comonomer Incorp. (%)[d]	M_n[e] (kg·mol^{-1})	$Đ$[e]
1	**Ti$_1$**	1	1.66	9970	3.2	111	2.0
2[b]	***rac*-3**	2	trace	-	-	-	-
3	***rac*-3**	2	1.09	3270	7.0	124	1.9
4[b]	***meso*-3**	2	trace	-	-	-	-
5	***meso*-3**	2	0.03	90	7.1	69	1.7

[a]Polymerization conditions: [catalyst] = 10 μmol **Ti$_1$**; 5 μmol ***rac*-3**; 5 μmol ***meso*-3**; activator ratio of $Ph_3C^+B(C_6F_5)_4^-$/Ti = 1.2; 0.064 M 1-octene in 50 mL toluene, at 25 °C, and under constant 1 atm of ethylene pressure. Entries performed in duplicate.[b]Polymerization conditions: [catalyst] = 5 μmol ***rac*-3**; 5 μmol ***meso*-3**; activator ratio of $Ph_3C^+B(C_6F_5)_4^-$/Ti = 0.5; 0.064 M 1-octene in 50 mL toluene, at 25 °C, and under constant 1 atm of ethylene pressure. Entries performed in duplicate. [c]kg (PE)·mol^{-1}(Ti)·h^{-1}·atm^{-1}. [d]By ^{1}H NMR and ^{13}C NMR.[133-135] [e]GPC vs polystyrene standards in (kg/mol).

Table 1.5. Ethylene/styrene copolymerization data for catalysts **Ti$_1$**, ***rac*-3**, and ***meso*-3**.[a]

Entry	Catalyst	*t* (min)	PE (g)	Activity[c] (PE)	Comonomer Incorp. (%)[d]	M_n[e] (kg·mol^{-1})	$Đ$[e]
1[b]	**$Ph_3C^+B(C_6F_5)_4^-$**	60	0.67	67	polystyrene	3.5	2.0
2	**Ti$_1$**	10	13.30	7980	30.1	3.4	2.0
3	***rac*-3**	10	3.50	2100	63.0	10.5	1.7
4	***meso*-3**	10	8.50	5100	polystyrene	2.2	2.7

[a]Polymerization conditions: [catalyst] = 10 μmol **Ti$_1$**; 5 μmol ***rac*-3**; 5 μmol ***meso*-3**; activator ratio of $Ph_3C^+B(C_6F_5)_4^-$/Ti = 1.2; 1.75 M styrene in 50 mL toluene, at 25 °C, and under constant 1 atm of ethylene pressure. Entries performed in duplicate.[b]Polymerization conditions: 1.45 M styrene in 50 mL toluene, at 25 °C, and under constant 1 atm of ethylene pressure. Entries performed in duplicate. [c]kg (PE)·mol^{-1}(Ti)·h^{-1}·atm^{-1}. [d]By ^{1}H NMR and ^{13}C NMR.[133-135] [e]GPC vs polystyrene standards in (kg/mol).

true coordination copolymerization product, but rather an *atactic* polystyrene homopolymer. A control experiment indicates that $Ph_3C^+B(C_6F_5)_4^-$ alone is also active, presumably via a cationic styrene homopolymerization mechanism (Table 1.5, entry 1), although with lower activity and producing a higher M_n polymer than the ***meso*-3**/ $Ph_3C^+B(C_6F_5)_4^-$ system (Table 1.5, entry 4). Purely ***meso*-3**/$Ph_3C^+B(C_6F_5)_4^-$ (***meso*-5**) mediated cationic polymerization is likely the reason for the activity observed using ***meso*-3**, since the results stand in contrast to the results for the other homo- and copolymerizations that show ***rac*-3** exhibits higher activity.

Discussion

Ethylene, Propylene, and 1-octene homopolymerization. For all three monomers, homopolymerization experiments with $Ph_3C^+B(C_6F_5)_4^-$ -activated ***rac*-3** and ***meso*-3** (Ti : cocatalyst = 1:1 equivalents) reveal that ***rac*-3** is the more active of the present bimetallic catalysts, while monometallic **Ti**$_1$ is significantly more active than both bimetallics but produces lower M_n polymers. Such activity differences likely reflect increased steric congestion around the catalytic center as evidenced by the corresponding structural data (Figures 1.1, 1.3, 1.5-1.7).[119] Furthermore, the variations in activity between propylene and 1-octene homopolymerizations can be partially explained by differences in monomer solubility in toluene at 25 °C ([propylene = 0.83 M at 1.0 atm system pressure;[66, 142] [1-octene] = 1.0 M). For single-site polymerizations, M_n values typically scale as the net rate of chain propagation divided by the net rate of all competing chain termination processes.[117] In view of the present lower bimetallic versus monometallic catalytic activities, the relative chain termination rates of the bimetallic species must be substantially lower to explain the increased M_n values. This suggests that the second proximate metal center in the bimetallic catalysts may interact with the growing polymer chains, probably via an agostic interaction (see

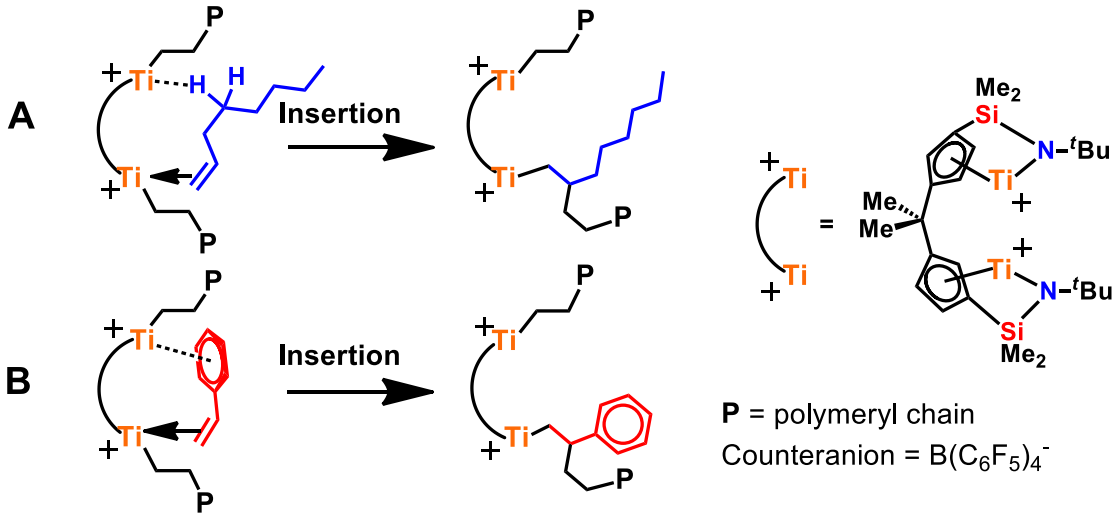

Scheme 1.8. Proposed cooperative bimetallic scenario for enhanced 1-octene (**A**) and styrene (**B**) enchainment by ***rac*-3** and ***meso*-3** –based catalysts.

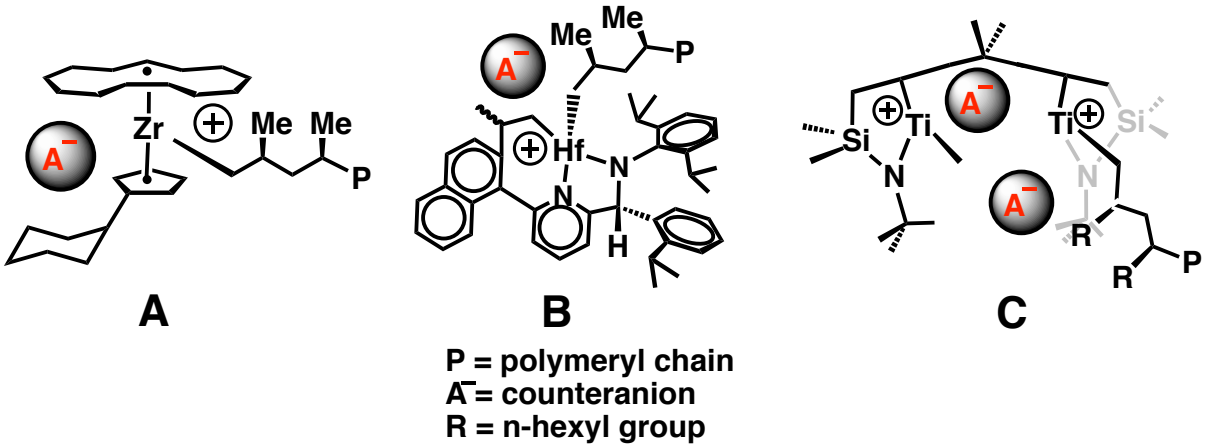

Figure 1.9. Schematic structures of activated group 4 complexes which produce isotactic poly-α-olefins.

Scheme 1.8), to stabilize the propagating chain and enhance comonomer selectivity while suppressing chain transfer and termination processes.[42143]

According to the catalyst NMR, X-ray diffraction, DFT computational, and polymerization data, ***meso*-7** (i.e., ***meso*-3 +** 1 $B(C_6F_5)_3$) is an approximately C_s-symmetric cation (Figure 1.7), which, when activated with a second $B(C_6F_5)_3$ equivalent (see Figure 1.42) exhibits remarkably high isoselectivity for 1-octene polymerization (Table 1.3). In contrast, ***meso*-5** (i.e., ***meso*-3 +** $Ph_3C^+B(C_6F_5)_4^-$) with the same cation as ***meso*-7** produces only marginally isotactic poly-1-octene or polypropylene upon activation with a second $Ph_3C^+B(C_6F_5)_4^-$ equivalent. Proceeding via mechanisms that are generally well-understood for mononuclear catalysts,[144] optimized group 4 single-site C_s-symmetric catalysts typically polymerize α-olefins in a syndiospecific fashion,[66, 145-149] while optimized group 4 single-site C_2-symmetric[150] and C_1-symmetric[151-160] catalysts typically afford isotactic poly-α-olefins. In the present CGC-based catalytic systems, note that the mononuclear **Ti**$_1$ ancillary ligation (Chart 1.3) does not offer the large stereodifferentiating bulk typical of high-tacticity-selective group 4 metallocene[161-164] and pyridylamido[165-167] catalysts (Figures 1.9A, B, respectively). Indeed, activated **Ti**$_1$ yields atactic polypropylene and marginally isotactic poly-1-octene (Table 1.3), with the latter relatively insensitive to the cocatalyst. In the case of suitably activated binuclear catalysts, note that both ***rac*-3** and ***meso*-3** afford atactic polypropylene (Table 1.2, entries 2 and 3) and marginally isotactic poly-1-octene for both cocatalysts (Table 1.3, entries 2, 5, 6). The only exception is ***meso*-3** + 2 $B(C_6F_5)_3$ which yields an impressive *mmmm* = 91.7%.[168]

Regarding mechanism, few studies have been reported on tacticity induction in binuclear group 4 polymerization catalysts.[24, 58] While ***meso*-3** activated by two equivalents of $B(C_6F_5)_3$ may be approximately C_2-symmetric (see Figure 1.42 for the ***rac*-3** analogue), it is probably simplest to consider the individual Ti centers as independent polymer-generators, and each is expected to have

approximate C_1 local symmetry, with the second metal center acting as a bulky ring substituent (Figure 1.9C). While, as noted above, C_1-symmetric complexes can afford poly-α-olefins with high isotacticity, this does not fully explain why ***meso*-7** produces highly isotactic poly(1-octene) while all the other binuclear catalyst/cocatalyst combinations, ostensibly C_1-symmetric at Ti, are far less selective. It is possible that the tighter ion-pairing[169-170] in ***meso*-7** afforded by $MeB(C_6F_5)_3^-$ (which could influence the kinetics of site epimerization),[66, 156, 161, 171-174] combined with the steric influence of the nearby second metal center and supporting ligation, selectively forces monomer approach/chain growth from a particular orientation.[165, 171, 175] This suggests, therefore, that the polymerization may proceed via an isospecific backskip mechanism[161, 176] in which monomer insertion orients the growing polymer towards the more hindered side of the catalyst. In the case of ***meso*-7**, this would presumably involve positioning of the polymeryl chain towards the second metal center and remaining ligand (Figure 1.9C). Prior to the next insertion, the steric hindrance forces a site epimerization process to re-position the polymer chain away from the other metal center, and repeated insertion/epimerization eventually yields highly isotactic polymer.[161]

Ethylene + 1-octene and styrene copolymerization. The present ethylene + 1-octene copolymerization data (Table 1.4) indicate that, compared to typical monometallic polymerizations at typically low catalyst concentrations (10^{-4}-10^{-8} M), the enforced proximity of two catalytic centers in ***rac*-3** and ***meso*-3** affords significantly greater comonomer enchainment versus **Ti**$_1$. It is likely that coordination/activation of the 1-octene at one cationic metal center is facilitated/stabilized by a secondary, possibly agostic interaction with the second proximate cationic metal center, which is likely to enhance the probability of subsequent enchainment or re-enchainment after chain transfer (Scheme 1.8A). Note that ***rac*-3** exhibits significantly higher activity and produces much larger M_n product than ***meso*-3**, suggesting enhanced metal···metal

cooperativity in ***rac*-3**. This is noteworthy since ***rac*-3** exhibits higher activity for copolymerizations versus ethylene homopolymerization, while ***meso*-3** trends exactly the opposite. From the single-crystal structures of ***rac*-3** and ***meso*-3** (Figure 1.1), the Ti···Ti distance in ***rac*-3** (6.443(2) Å) is ~0.82 Å shorter than that in ***meso*-3** (7.260(2) Å). Furthermore, the single-crystal data (Figure 1.5) and NMR studies of ***rac*-5** and ***meso*-5** indicate that ***rac*-5** is probably more strained and is more reactive than ***meso*-5**. Therefore, the combined shorter accessible metal···metal distance in ***rac*-3** and the asymmetric, more reactive structure of ***rac*-5** may more effectively stabilize the proximate growing polymer chain via agostic interactions (Scheme 1.8A), which would also suppress the rates of chain transfer and termination relative to ***meso*-3**.[43] Note that in previous bimetallic **CGC-Ti**$_2$ catalysts (Chart 1.1, **C**) significant α-olefin comonomer enchainment selectivity is also observed versus analogous monometallic CGC catalysts,[50] but is lower as compared to the present bimetallic system under similar polymerization conditions.

The emergence of single-site olefin polymerization catalysis has stimulated renewed interest in ethylene-styrene copolymers due to their impressive viscoelastic behavior, mechanical properties, and compatibilities with a wide range of other macromolecular materials, reflecting the aromatic functionality embedded in the polyethylene backbone.[125, 137, 177-178] Nevertheless, conventional single-site catalysts have rarely achieved styrene incorporation greater than 50 mol%, regardless of the styrene/ethylene feed ratio.[138-139, 179-180] Previously, we reported that bimetallic **CGC-Ti**$_2$ not only exhibits far greater activity for styrene homopolymerizations with an unusual 1,2-enchainment regiochemistry[181-183] (up to ~50%) than the corresponding monometallic analogue, but also installs styrene in ethylene/styrene copolymerizations with broadly tunable styrene content.[44, 49] The present ethylene + styrene copolymerization data indicate that the polymers produced by **Ti**$_2$ and ***rac*-3** are exclusively poly(ethylene-*co*-styrene) copolymers, while under identical conditions ***meso*-3** only

produces atactic styrene homopolymer (Figures 1.58 and 1.59). The analysis of chain-ends of homopolymers produced by ***meso*-3**/borate indicates propagation occurs through both 1,2-insertion and 2,1-insertion pathways. The ratio of 1,2-insertion/2,1-insertion can be evaluated from ^{13}C NMR (Figure 1.54), where the signal at δ 22.10 ppm is assignable to 1,2-insertion and the signal at δ 22.08 ppm to 2,1-insertion. This result is similar as our previous report where styrene 1,2-insertion competes with 2,1-insertion to a significant degree in bimetallic CGC catalysts (up to 50%).[49] For ethylene polymerization, monomer coordination/activation at the cationic metal center in the presence of the counteranion is usually the rate-limiting step for each ethylene insertion,[184-186] while for styrene polymerization, the proposed rate limiting-step is insertion of the vinylic fragment of the π-coordinated styrene into the metal-polymeryl bond (Scheme 1.8B).[187] Theoretical[188-190] and experimental[191] studies of ethylene/styrene copolymerization suggest that while ethylene has a lower binding energy than styrene, styrene has a significantly higher insertion barrier. As noted above and evident in Tables 1.1 – 1.3 (except Table 1.5 entry 3 vs. 4), ***rac*-5** is catalytically more active but less stable than ***meso*-5**. The present catalyst activity/reactivity trends qualitatively correlate with X-ray diffraction analyses which reveal substantial differences in ***rac*-5** and ***meso*-5** $\cdots B(C_6F_5)_4^-$ ion-pairing (Figure 1.5). The distances between the borate B atom and the two Ti centers in ***rac*-5** are 7.297(11) Å and 6.365(10) Å, while ***meso*-5** contains more symmetrical/tighter ion-pairing with 7.184(3) Å and 6.938(3) Å for the corresponding distances.

Catalytic center proximity and conformational effects: precatalyst activation and proposed catalytic mechanism. The aforementioned data show that activated bimetallic CGC catalysts ***rac*-3** and ***meso*-3** exhibit distinctive cooperative enchainment effects in terms of product M_n and comonomer selectivity versus the monometallic control **Ti**$_1$. Specifically, ***rac*-3** is more active for both homo- and copolymerizations than ***meso*-3**. A reasonable, DFT-based scenario for ethylene

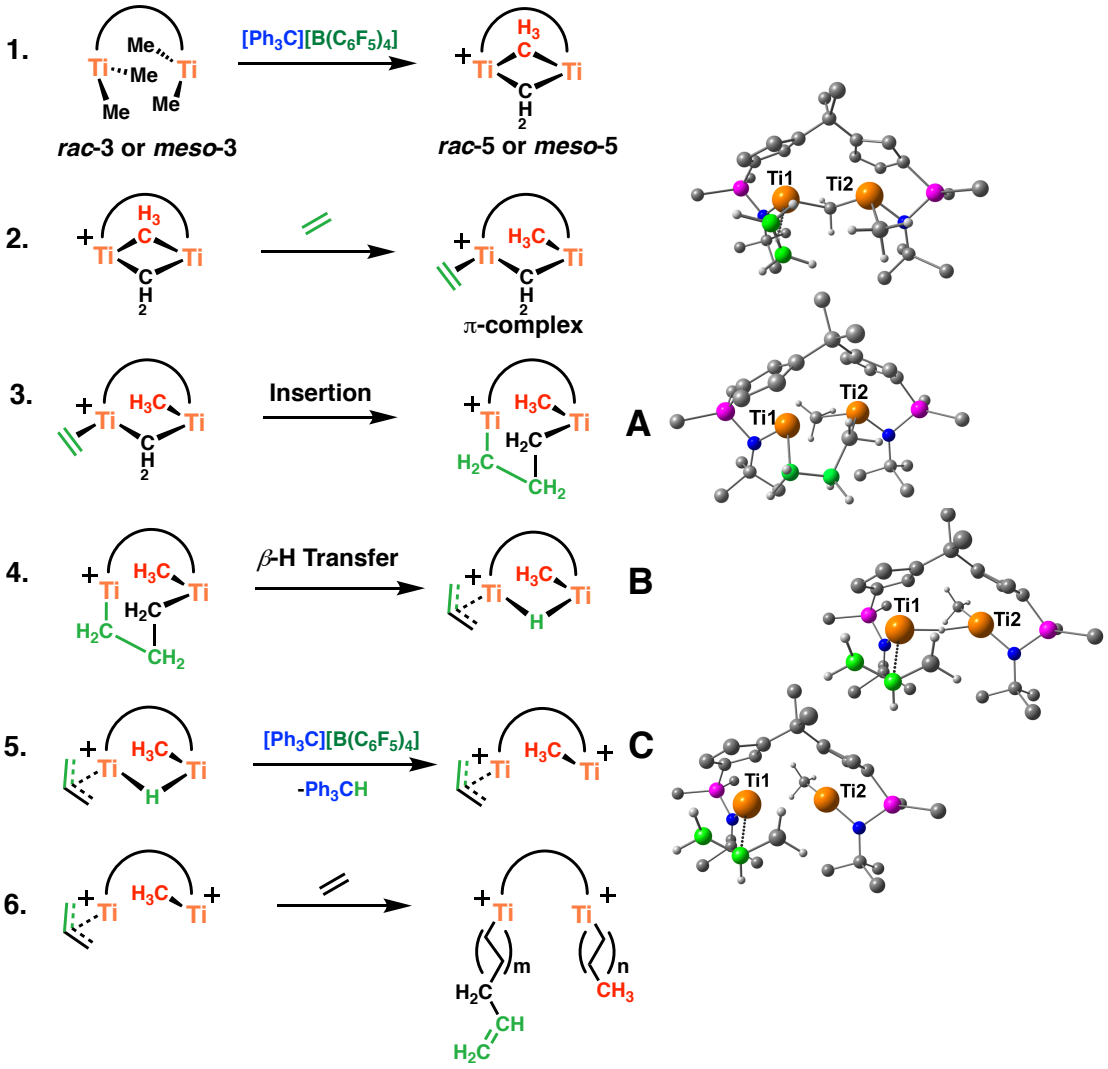

Scheme 1.9. Proposed scenario for bimetallic precatalyst ***rac*-3** and ***meso*-3** activation and ethylene polymerization propagation; optimized geometry structures (*rac* only) of "naked" cations (pictured top to bottom): π-complex, structures **A**, **B**, and **C**.

polymerization by ***rac*-3** and ***meso*-3** activated by $Ph_3C^+B(C_6F_5)_4^-$ is depicted in Scheme 1.9. ***Rac*-3** and ***meso*-3** activated by 1 equiv. of $Ph_3C^+B(C_6F_5)_4^-$ yield ***rac*-5** and ***meso*-5** (Schemes 1.3, 1.4). The solution stable species ***rac*-6** (***rac*-3** + 2 equiv. of $Ph_3C^+B(C_6F_5)_4^-$; see Figure 1.4) is found to be too sterically hindered for ethylene coordination/activation; however, exchange of the coordinated trityl moiety for ethylene to reform ***rac*-5** is exothermic by ~ 10 kcal/mol, arguing that ***rac*-5** can initiate polymerization. ***Rac*-5** and ***meso*-5** are μ-CH_2, μ-CH_3 binuclear monocationic Ti complexes, which bind one ethylene molecule to one cationic Ti center (π-complex; ΔE = +1.0 kcal/mol), followed by insertion into the presumably strained Ti-CH_2 bond (intermediate **A**; *rac* isomer, ΔE = -13.2 kcal/mol). Interestingly, the DFT calculations suggest that ethylene insertion into the Ti-CH_3 bond of these species is not favored. In fact, any attempts to induce olefin insertion by forcing the approach of ethylene into the Ti1-CH_3 bond leads to methane release and the formation of bridging complexes ***rac*-8** and ***meso*-8** (Figure 1.61), in which the methyl ligand is replaced by a vinyl group (Ti1-CH=CH_2) and an interaction is formed between the double bond of the vinyl fragment and the Ti2 center. These complexes are inactive for further ethylene coordination/activation or insertion. Intermediate **A** evolves via β-H elimination from the 1,3-μ^2-propylene group to more stable structure **B** (*rac* isomer ΔE = -16.1kcal/mol) with a μ^2-H bridge, methyl displacement toward to the Ti2 center, and a new allylic fragment[192-193] at Ti2.[194] A similar Ti_2 complex, reminiscent of intermediate **B**, was observed experimentally by Cuenca *et al*.[195] DFT yields similar results for ***meso*-5**, however intermediates **A** and **B** are far less stable than ***rac*-5** (**ΔE** = -1.7 kcal/mol and -2.5 kcal/mol for **A** and **B**, respectively). In the presence of a second $Ph_3C^+B(C_6F_5)_4^-$ equiv., structure **B** can be re-activated by abstraction of either the Ti-CH_3 or μ^2-H bridging group to yield dicationic complex **C**, which is active for chain propagation.[196]

Computationally, H abstraction is favored over CH_3 abstraction by ~6 kcal/mol. In the absence of a second $Ph_3C^+B(C_6F_5)_4^-$equiv., monocationic intermediate **B** is found to coordinate ethylene with ΔE = 2.5 and 12.3 kcal/mol for the ***rac-5*** and ***meso-5*** diastereomers, respectively. This agrees with the ethylene polymerization results where only 1 equiv. of cocatalyst + the *meso* diastereomer results yields negligible polymer production in comparison to the *rac* diastereomer (Tables 1.1-1.3). Polymerization by monocationic bimetallic complexes in the presence of 1 equiv. of $Ph_3C^+B(C_6F_5)_4^-$ is considered a minor participant based on the high *Đ*'s obtained, and the much lower (or lack of) activity observed for monocationic polymerizations.

The results of this study argue that the present Ti_2 bimetallic catalysts are activated in a way that is quite distinct from their monometallic counterpart, in agreement with the different catalytic performances. For the two bimetallic catalyst diastereomers, at least three intermediates exist during polymerization; their stability as well as kinetics and energetics depend significantly on conformation, where in general the *rac* intermediates are lower in energy. This leads to different diastereomeric active species with markedly varying activities, comonomer selectivities, as well as polymer product molecular weights and tacticities.

Conclusions

We report here the synthesis, isolation, and detailed experimental/theoretical characterization of two bimetallic Ti constrained geometry diastereomers, ***rac*-3** and ***meso*-3**, and their olefin polymerization properties. ***Rac*-3** undergoes clean thermolysis to yield a dimeric μ^2-CH_2 complex ***rac*-4**, while ***meso*-3** is stable under these conditions. Activation of ***rac*-3** and ***meso*-3** with 1 equiv. of $Ph_3C^+B(C_6F_5)_4^-$ affords ***rac*-5** and ***meso*-5**, which are monocationic binuclear μ^2-CH_2, μ^2-CH_3 Ti complexes. An additional equiv. of $Ph_3C^+B(C_6F_5)_4^-$weakly interacts with ***rac*-5** and forms aryl-

coordinated ion pair ***rac*-6**, while ***meso*-5** is unreactive under these conditions. ***Meso*-3** reacts with 2 equiv. of $B(C_6F_5)_3$ to form ***meso*-7**, which contains the same cation as ***meso*-5** but with a $MeB(C_6F_5)_3^-$ anion instead of $B(C_6F_5)_4^-$. ***Rac*-3** reacts with 2 equiv. of $B(C_6F_5)_3$ to form the ion pair ***rac*-7**, which contains two weak Ti· · · $MeB(C_6F_5)_3$ interactions, and decomposes in CD_2Cl_2 to form ***rac*-7-Cl**$_3$. Compared to the monometallic control **Ti**$_1$, ***rac*-3** activated with 2 equiv. of $Ph_3C^+B(C_6F_5)_4^-$ exhibits distinctive olefin polymerization cooperative effects in terms of enhanced product molecular mass and comonomer enchainment selectivity. Furthermore, the ***rac*-3**-derived catalyst is more active for both of homo- and copolymerizations than similarly activated ***meso*-3**, arguing that very diastereomerically distinct active species are operative during polymerization, and that the polymerization activity, enchainment selectivity, isoselectivity, product molecular mass, and catalyst stability vary dramatically with the bimetallic catalyst conformation. This study, through NMR spectroscopy, X-ray diffraction, and DFT calculation, provides a better understanding of both the activation processes and the ion-paired nature of the active species in bimetallic catalyst-mediated coordinative olefin polymerization. The results argue that conformationally distinct bimetallic single-site polymerization catalysts can provide unusual cooperative enchainment pathways and the potential for creating new macromolecular architectures that conventional monometallic catalysts cannot offer.

Experimental Section

Materials and Methods. All manipulations of air-sensitive materials were performed with rigorous exclusion of O_2 and moisture in oven-dried Schlenk-type glassware on a dual manifold Schlenk line, interfaced to a high-vacuum line (10^{-6} Torr), or in a N_2-filled Mbraun glove box with a high-capacity recirculator (<1 ppm O_2). Argon and N_2 (Airgas, pre-purified grade) was purified by passage through a supported MnO oxygen-removal column and an activated Davison 4A

molecular sieve column. Ethylene (Airgas) was purified by passage through an oxygen/moisture trap (Matheson, model MTRP-0042-XX). Diethyl ether and tetrahydrofuran were distilled over Na/benzophenone ketyl. Hydrocarbon solvents (*n*-pentane and toluene) were dried using activated alumina columns according to the method described by Grubbs[197] and were additionally vacuum-transferred from Na/K alloy immediately before vacuum line manipulations. All solvents for high-vacuum line manipulations were stored in *vacuo* over Na/K alloy in Teflon-valve sealed bulbs. Benzene-d_6 and Toluene-d_8 (Cambridge Isotope Laboratories, 99+ atom % D) were stored over Na/K alloy in *vacuo* and vacuum transferred immediately prior to use. Chlorobenzene-d_5 and dichloromethane-d_2 were dried by CaH_2 and stored over activated Davison 4A molecular sieves. All other deuterated solvents were used as received (Cambridge Isotope Laboratories, 99+ atom %D). Other non-halogenated solvents were dried over Na/K alloy, and halogenated solvents were distilled from CaH_2 and stored over activated Davison 4A molecular sieves. The reagents dicyclopentadiene, iodoethane, Me_2SiCl_2, *tert*-butylamine, $Ti(NMe_2)_4$, Me_3SiCl, trimethylaluminum (2 M in hexanes), acetone, benzyltriethylammonium chloride (TEBA chloride), NaOH, and *n*-butyllithium (2.5 M in hexanes) were purchased from Sigma-Aldrich and used as received. Triphenylcarbenium tetrakis(pentafluorophenyl)borate, $Ph_3C^+B(C_6F_5)_4^-$ (**B**$_1$), was a generous gift from Albemarle Corporation (Baton Rouge, LA), and purified by recrystallization from CH_2Cl_2/pentane. The complex [(3-^{t}Bu-C_5H_3)$SiMe_2N^t$Bu]$TiCl_2$ was prepared according to literature procedures.[74]

Physical and Analytical Measurements. NMR spectra were recorded on Agilent F500 (DDR2, FT, 500 MHz, ^{1}H; 125 MHz, ^{13}C; 470 MHz, ^{19}F; 160 MHz, ^{11}B), Varian UNITYInova-500 (FT, 500 MHz, ^{1}H; 125 MHz, ^{13}C), Agilent Au400 (DDR2, FT, 400 MHz, ^{1}H; 100 MHz, ^{13}C), Hg400 (400 MHz, 1H; 100 MHz, ^{13}C) or Bruker Avance III 500 (direct cryoprobe, 500 MHz, ^{1}H; 125 MHz, ^{13}C)

instruments. Chemical shifts for ^{1}H and ^{13}C spectra were referenced using internal solvent resonances and are reported relative to tetramethylsilane (TMS). NMR experiments on air-sensitive samples were conducted in Teflon valve-sealed sample tubes (J.Young). Elemental analyses were performed by Midwest Microlab, Indianapolis, Indiana for % C, N, and H. ^{1}H and ^{13}C NMR assays of polymer microstructure were conducted in 1,1,2,2-tetrachloroethane-d_2 at 120 ºC with a delay time (d_1) = 10 seconds. Signals were assigned according to the literature for these polymers.[123-124, 133-135] Gel permeation chromatography (GPC) was carried out in 1,2,4-trichlorobenzene (stabilized with 125 ppm BHT) at 150 °C on a Polymer Laboratories GPC-220 instrument equipped with a set of three Agilent PLgel 10 μm mixed-B LS columns with differential refractive index and viscosity detectors. Molecular weights were determined through universal calibration relative to polystyrene standards.

Synthesis of [(3-^{t}Bu-C$_5$H$_3$)SiMe$_2$N^{t}Bu]TiMe$_2$ (Ti$_1$).[12] [(3-^{t}Bu-C$_5$H$_3$)SiMe$_2$N^{t}Bu]TiCl$_2$ (0.368 g, 1.00 mmol) was dissolved with 30 mL Et$_2$O in a 100 mL reaction flask. A solution of MeLi (2.00 mmol, 1.25 mL, 1.6 M in ethyl ether) was added by syringe at room temperature. The yellow solution turned cloudy immediately after the addition. The solution was stirred at room temperature for another 2 h. All the volatiles were next removed in vacuum, and the residue was extracted with 20 mL pentane. LiCl was removed by filtration. The filtrate was collected and all the volatiles were then removed in vacuum to give the yellow oily product (0.271 g, 0.83 mmol, 83%). ^{1}H NMR (500 MHz, C$_6$D$_6$): δ = 6.76 (t, J = 2.5 Hz, 1 H, Cp), 5.87 (d, J = 2.5 Hz, 2 H, Cp), 1.55 (s, 9 H, CpCMe_3), 1.30 (s, 9 H, NCMe_3), 0.81 (s, 3 H, TiMe), 0.71 (s, 3 H, TiMe), 0.32 (s, 3 H, SiMe), 0.29 (s, 3 H, SiMe) ppm. ^{13}C NMR (125 MHz, C$_6$D$_6$) δ = 150.35 (s, Cp), 124.32 (s, Cp), 120.04 (s, Cp), 116.15 (s, Cp), 102.64 (s, Cp), 59.28 (s, Me$_3$*C*N), 51.70 (s, TiMe), 51.53 (s, TiMe), 34.69 (s, NCMe_3), 33.69 (s, Cp*C*Me$_3$), 31.45 (s, CpCMe_3), 1.65 (s, SiMe), 1.08 (s, SiMe) ppm.

Synthesis of Dicyclopentadienyldimethylmethane. 13.2 g (200 mmol) of freshly distilled cyclopentadiene was added to a cooled (0 ºC) mixture of 20 g of NaOH and 1.0 g of TEBA chloridein 200 mL of THF. Acetone (5.8 g, 100 mmol) was added followed by 1 h of vigorous stirring at 0 ºC. The resulting mixture was allowed to warm gradually to room temperature and then stirred for another 24 h. The solution was next decanted from the solid residue and the volatile components were removed *in vacuo*. The residue was dissolved in Et_2O and washed until the aqueous washings were neutral. The organic layer was separated and dried over Na_2SO_4, filtered, and the volatile components were removed *in vacuo*. The resulting oil was distilled and the fraction boiling at 54-55 ºC (0.1 Torr) was collected (10.0 g, yield 59.2%). Spectroscopic and analytical data are consistent with the literature[576] and are as follows (three isomers). ^{1}H NMR (500 MHz, $CDCl_3$) δ = 6.46-6.36 + 6.27-6.18 + 6.05-6.01 (m, 6 H, Cp), 2.98-2.96 + 2.85-2.83 (m, 4H, CH_2 of Cp), 1.46 + 1.45 + 1.44 (s, 6 H, CMe_2) ppm. ^{13}C NMR (125 MHz, $CDCl_3$) δ = 158.01 (Cp), 157.08 (Cp), 155.57 (Cp), 154.59 (Cp), 133.51 (Cp), 133.44 (Cp), 133.28 (Cp), 133.24 (Cp), 131.92 (Cp), 131.14 (Cp), 131.02 (Cp), 125.26 (Cp), 124.81 (Cp), 123.96 (Cp), 123.26 (Cp), 41.03 + 40.97 + 40.79 + 40.71 (CH_2 of Cp), 38.73 + 37.87 + 36.99 (*C*Me_2), 29.32 + 28.51 + 27.56 (C*Me*$_2$) ppm.

Synthesis of (μ-CMe_2-3,3')[1-(Me_2SiNH^tBu)cyclopentadienyl]$_2$(1). A 16.0 mL sample of ^{n}BuLi (2.5 M in hexanes; 40.0 mmol) was added dropwise at -78 ºC to a solution of 3.44 g of dicyclopentadienyldimethylmethane (20.0 mmol) in THF (100 mL). At the end of the addition, the reaction mixture was allowed to warm to room temperature and stirred for 12 h. Next, the Li salt suspension was slowly added to a THF solution of dichlorodimethylsilane (30 mL, 248 mmol) at room temperature. After stirring for 12 h, all the volatiles were removed under vacuum and the residue was dissolved in 100 mL of THF. To this THF solution, ^{t}BuNH$_2$ (10 mL, 95.2 mmol) was added by syringe with stirring. The solution was stirred at room temperature overnight. Volatiles

were then removed under vacuum and the product extracted with 100 mL pentane. A yellow oily product (three isomers in ratio of 4/1/1, 7.93 g, 18.4 mmol, 92.0% yield) was obtained after filtration and removal of the solvent *in vacuo*. Major product of ^{1}H NMR (500 MHz, C_6D_6) δ: = 6.72-6.67 (m, 2 H, Cp), 6.52-6.47 (m, 2 H, Cp), 6.30-6.25 (m, 2 H, Cp), 3.34 (s, 2 H, CH of Cp), 1.60, (s, 6 H, $C(CH_3)_2$), 1.07 (s, 18 H, $C(CH_3)_3$), 0.04 (s, 6 H, $SiCH_3$), 0.01 (s, 6 H, $SiCH_3$) ppm. Major product of ^{13}C NMR (125 MHz, C_6D_6) δ = 154.40 (s, 2 C, Cp), 134.23 (s, 2 CH, Cp), 131.85 (s, 2 CH, Cp), 125.59 (s, 2 CH, Cp), 52.80 (s, 2 CH, Cp), 49.50 (s, 2 C, Me_3C), 37.62 (s, 1 C, CMe_2), 33.92 (s, 6 CH_3, CMe_3), 29.38 (s, 2 CH_3, CMe_2), 0.63 (s, 2 CH_3, SiMe), 0.32 (s, 2 CH_3, SiMe) ppm. ESI ($[M + H]^+$): m/z = 431.42.

Synthesis of *rac*-(μ-CMe_2-3,3')\{(η^5-cyclopentadienyl)[1-Me_2Si(^{t}BuN)][Ti(NMe_2)$_2$]\}$_2$ (*rac*-2) and *meso*-(μ-CMe_2-3,3')\{(η^5-cyclopentadienyl)[1-Me_2Si(^{t}BuN)][Ti(NMe_2)$_2$]\}$_2$ (*meso*-2). The ligand **1** (4.31 g, 10.0 mmol) was dissolved with 50 mL dry toluene in a 100 mL reaction flask. $Ti(NMe_2)_4$ (6.72 g, 30.0 mmol) was then added at room temperature. The resulting solution was refluxed at 120 ºC for 2 days with slow but constant N_2 flow to remove evolved $HNMe_2$. Then all the volatiles were removed under vacuum, and the residue was dissolved in 50 mL pentane and kept at -40 ºC for 2 h to afford one isomer ***meso*-2** as orange-red blocky crystals (3.07 g, 4.40 mmol, 44.0% yield). ^{1}H NMR of ***meso*-2** (500 MHz, C_6D_6) δ = 6.29 (dd, J = 3.0 Hz, J = 2.0 Hz, 2 H, Cp), 6.08 (t, J = 2.1 Hz, 2 H, Cp), 6.02 (dd, J = 3.0 Hz, J = 2.1 Hz, 2 H, Cp), 3.11 (s, 12 H, $TiNMe_2$), 2.99 (s, 6 H, $TiNMe_2$), 1.70 (s, 3 H, CCH_3Me), 1.64 (s, 3 H, $CMeCH_3$), 1.37 (s, 18 H, Me_3C), 0.62 (s, 6 H, SiMe), 0.56 (s, 6 H, SiMe) ppm. ^{13}C NMR (125 MHz, C_6D_6) δ = 148.21 (s, Cp), 118.24 (s, Cp), 116.67 (s, Cp), 112.82 (s, Cp), 103.98 (s, Cp), 60.85 (s, Me_3C), 50.18 (s, $TiNMe_2$), 49.62 (s, $TiNMe_2$), 38.57 (s, CMe_2), 34.60 (s, CMe_3), 30.77 (s, CCH_3Me), 30.45 (s, $CMeCH_3$), 2.31 (s, SiMe), 2.07 (s, SiMe) ppm. Anal. Calcd for $C_{33}H_{66}N_6Si_2Ti_2$: C, 56.72; H, 9.52; N, 12.03. Found: C, 56.59;

H, 9.39; N, 11.98. The above pentane filtrate was concentrated to 20 mL and kept at -78 ºC for 1 h to give the other isomer ***rac*-2** as yellow-orange crystals (2.10 g, 2.10 mmol, 30.0% yield). ^{1}H NMR of ***rac*-2** (500 MHz, C_6D_6) δ = 6.16 (dd, J = 3.1 Hz, J = 2.0 Hz, 2 H, Cp), 6.07 (t, J = 2.1 Hz, 2 H, Cp), 5.88 (dd, J = 3.0 Hz, J = 2.2 Hz, 2 H, Cp), 3.05 (s, 12 H, $TiNMe_2$), 2.89 (s, 6 H, $TiNMe_2$), 1.65 (s, 6 H, CMe_2), 1.33 (s, 18 H, Me_3C), 0.60 (s, 6 H, SiMe), 0.51 (s, 6 H, SiMe) ppm. ^{13}C NMR (125 MHz, C_6D_6) δ = 148.27 (s, Cp), 118.77 (s, Cp), 116.72 (s, Cp), 111.76 (s, Cp), 103.76 (s, Cp), 60.70 (s, $Me_3\mathit{C}$), 50.01 (s, $TiNMe_2$), 49.43 (s, $TiNMe_2$), 37.87 (s, $\mathit{C}Me_2$), 34.59 (s, $C\mathit{Me}_3$), 28.62 (s, CMe_2), 2.40 (s, SiMe), 2.11 (s, SiMe) ppm. Anal. Calcd for $C_{33}H_{66}N_6Si_2Ti_2$: C, 56.72; H, 9.52; N, 12.03. Found: C, 56.57; H, 9.50; N, 12.02.

Synthesis of *rac*-(μ-CMe_2-3,3')\{(η^5-cyclopentadienyl)[1-Me_2Si(^{t}BuN)]($TiMe_2$)\}$_2$ (*rac*-3). *Rac*-2 (0.349 g, 0.500 mmol) was suspended in 50 mL pentane in a 100 mL reaction flask. A solution of $AlMe_3$ (2.5 mL, 2.0 M in hexanes) was added slowly by syringe at room temperature. The solution first turned deep red and then cloudy during the addition. The solution was stirred at room temperature for five days. All the volatiles were then removed in vacuum, and the dark yellow solid product was purified by recrystallization from pentane at -40 ºC. Yield, 0.265 g (0.456 mmol, 91.3% yield). ^{1}H NMR of ***rac*-3** (500 MHz, C_6D_6) δ = 6.92 (dd, J = 3.0 Hz, J = 1.9 Hz, 2 H, Cp), 6.01 (t, J = 2.1 Hz, 2 H, Cp), 5.84 (dd, J = 3.0 Hz, J = 2.2 Hz, 2 H, Cp), 1.84 (s, 6 H, CMe_2), 1.54 (s, 18 H, Me_3C), 0.90 (s, 6 H, TiMe), 0.69 (s, 6 H, TiMe), 0.30 (s, 12 H, SiMe) ppm. ^{13}C NMR (125 MHz, C_6D_6) δ = 148.75 (s, Cp), 124.12 (s, Cp), 121.07 (s, Cp), 115.79 (s, Cp), 102.68 (s, Cp), 59.21 (s, $Me_3\mathit{C}$), 52.16 (s, TiMe), 52.02 (s, TiMe), 38.84 (s, $\mathit{C}Me_2$),, 34.42 (s, $C\mathit{Me}_3$), 27.62 (s, $C\mathit{Me}_2$), 1.32 (s, SiMe), 0.78 (s, SiMe) ppm. Anal. Calcd for $C_{29}H_{54}N_2Si_2Ti_2$: C, 59.78; H, 9.34; N, 4.81. Found: C, 59.58; H, 9.26; N, 4.71.

Synthesis of *meso*-(μ-CMe_2-3,3')\{(η^5-cyclopentadienyl)[1-$Me_2Si(^tBuN)$][$TiMe_2$)\}$_2$ (*meso*-3). ***Meso*-2** (0.349 g, 0.500 mmol) was suspended in 50 mL pentane in a 100 mL reaction flask. A solution of $AlMe_3$ (2.5 mL, 2.0 M in hexanes) was added slowly by syringe at room temperature. The solution first turned deep red and then cloudy during the addition. The solution was stirred at room temperature for five days. All the volatiles were then removed in vacuum, and the dark yellow solid product was purified by recrystallization from pentane at -40 ºC. Yield, 0.250 g (0.431 mmol, 86.1% yield). ^{1}H NMR of ***meso*-3** (500 MHz, C_6D_6) δ = 6.93 (dd, J = 3.0 Hz, J = 1.9 Hz, 2 H, Cp), 5.96 (t, J = 2.1 Hz, 2 H, Cp), 5.84 (t, J = 2.6 Hz, 2 H, Cp), 1.85 (s, 3 H, CCH_3Me), 1.82 (s, 3 H, CMeCH_3), 1.54 (s, 18 H, Me_3C), 0.90 (s, 6 H, TiMe), 0.73 (s, 6 H, TiMe), 0.29 (s, 6 H, SiMe), 0.26 (s, 6 H, SiMe) ppm. ^{13}C NMR (125 MHz, C_6D_6) δ = 148.72 (s, Cp), 123.84 (s, Cp), 120.94 (s, Cp), 116.69 (s, Cp), 102.87 (s, Cp), 59.24 (s, Me_3C), 52.32 (s, TiMe), 51.89 (s, TiMe), 39.27 (s, CMe$_2$), 34.40 (s, CMe_3), 29.91 (s, CCH_3Me), 27.87 (s, CMeCH_3), 1.30 (s, SiMe), 0.73 (s, SiMe) ppm. Anal. Calcd for $C_{29}H_{54}N_2Si_2Ti_2$: C, 59.78; H, 9.34; N, 4.81. Found: C, 59.63; H, 9.21; N, 4.65.

Synthesis of (μ-CMe_2-3,3')\{(η^5-cyclopentadienyl)[1-$Me_2Si(^tBuN)$][(μ-CH_2)Ti]\}$_2$ (*rac*-4). *Rac*-3 (0.058 g, 0.100 mmol) was dissolved in 2 mL toluene in a 10 mL reaction flask and stirred at 100 ºC for 1 h under nitrogen. All the volatiles were then removed in vacuum. The residue was dissolved in 5 mL pentane and kept at -40 ºC to give red needle crystals (0.050 g, 0.091 mmol, 91.0%). ^{1}H NMR of ***rac*-4** (500 MHz, C_7D_8) δ = 7.96 (s, 4 H, μ-CH_2), 7.29 (dd, J = 3.2 Hz, J = 1.9 Hz, 2 H, Cp), 6.14 (t, J = 2.0 Hz, 2 H, Cp), 5.46 (dd, J = 3.2 Hz, J = 2.2 Hz, 2 H, Cp), 2.17 (s, 6 H, CMe_2), 1.98 (s, 18 H, Me_3C), 0.28 (s, 6 H, SiMe), -0.02 (s, 6 H, SiMe) ppm. ^{13}C NMR (125 MHz, C_7D_8) δ = 227.18 (s, Ti-CH_2), 145.55 (s, Cp), 124.85 (s, Cp), 119.86 (s, Cp), 113.12 (s, Cp), 107.80 (s, Cp), 58.10 (s, Me_3C), 38.01 (s, CMe$_2$), 35.80 (s, CMe_3), 32.44 (s, CMe_2), 2.70 (s, SiMe), 1.02 (s,

SiMe) ppm. Anal. Calcd for $C_{27}H_{46}N_2Si_2Ti_2$: C, 58.90; H, 8.42; N, 5.09. Found: C, 58.76; H, 8.37; N, 4.97.

NMR study of *rac*-[(μ-CMe$_2$-3,3')\{(η^5-cyclopentadienyl)[1-Me$_2$Si(^{t}BuN)]\}$_2$-(μ-CH$_2$)(μ-CH$_3$)Ti$_2$]$^+$[B(C$_6$F$_5$)$_4$]$^-$ (*rac*-5). In the glove box, ***rac*-3** (0.058 g, 0.10 mmol) and $Ph_3C^+B(C_6F_5)_4^-$ (0.092 g, 0.10 mmol) in a 1:1 molar ratio were loaded into a J. Young NMR tube. The sealed tube was then removed from the glovebox, attached to the vacuum line, and cooled to -78 °C, and C_6D_5Cl was immediately transferred in. The sample was shaken vigorously and transferred directly to the NMR spectrometer. ^{1}H NMR of ***rac*-5** (500 MHz, C_6D_5Cl) δ = 7.29 (br, 2 H, μ-CH_2), 6.97 (m, 2 H, Cp), 5.94 (m, 2 H, Cp), 5.92 (m, 2 H, Cp), 1.82 (s, 6 H, CMe_2), 1.49 (s, 18 H, Me_3C), 0.37 (s, 6 H, SiMe), 0.12 (s, 6 H, SiMe), -0.15 (s, 3 H, μ-CH_3) ppm. ^{13}C NMR (125 MHz, C_6D_5Cl) δ = 227.37 (br, μ-CH_2), 148.92 (s, Cp), 128.39 (s, Cp, overlapped by solvent and assigned by HSQC), 122.90 (s, Cp), 117.81 (s, Cp), 112.78 (s, Cp), 63.02 (s, Me_3C), 61.89 (br, μ-CH_3), 37.59 (s, CMe_2), 33.71 (s, CMe_3), 31.30 (s, CMe_2), 0.67 (s, SiMe), -0.65 (s, SiMe) ppm. The resonances of the free anion $[B(C_6F_5)_4]^-$ and byproduct Ph_3CMe are not included in the ^{1}H NMR and ^{13}C NMR data here. ^{19}F NMR (470 MHz, C_6D_5Cl) δ = -131.58 (q, J = 10.8 Hz, 8 F), -162.26 (t, J = 20.4 Hz, 4 F), -166.04 (t, J = 19.0 Hz, 8 F) ppm. ^{11}B NMR (160 MHz, C_6D_5Cl) δ = -15.99 (s) ppm.

NMR study of *rac*-[(μ-CMe$_2$-3,3')\{(η^5-cyclopentadienyl)[1-Me$_2$Si(^{t}BuN)]\}$_2$-(μ-Cl)(TiCl)$_2$]$^+$[B(C$_6$F$_5$)$_4$]$^-$ (*rac*-5-Cl$_3$) in CD$_2$Cl$_2$. In the glove box, ***rac*-3** (0.058 g, 0.10 mmol) and $Ph_3C^+B(C_6F_5)_4^-$ (0.184 g, 0.20 mmol) in a 1:2 molar ratio were loaded into a J. Young NMR tube. The sealed tube was then removed from the glovebox, attached to the vacuum line, and cooled to -78 °C, and CD_2Cl_2 was immediately transferred in. The sample was shaken vigorously, kept at room temperature for 3 h, and transferred to the NMR spectrometer. ^{1}H NMR of ***rac*-5-Cl$_3$** (500 MHz, CD_2Cl_2) δ = 7.47 (dd, J_1 = 2.9 Hz, J_2 = 2.4 Hz, 2 H, Cp), 6.70 (d, J = 2.3 Hz, 2 H, Cp), 5.60

(d, J = 2.8 Hz, 2 H, Cp), 1.70 (s, 6 H, CMe_2), 1.46 (s, 18 H, Me_3C), 0.82 (s, 6 H, SiMe), 0.76 (s, 6 H, SiMe) ppm. ^{13}C NMR (125 MHz, CD_2Cl_2) δ = 154.97 (s, Cp), 132.69 (s, Cp), 127.95 (s, Cp), 127.20 (s, Cp), 113.71 (s, Cp), 69.41 (s, Me_3C), 40.26 (s, CMe_2), 32.72 (s, CMe_2), 32.58 (s, CMe_3), -0.03 (s, SiMe), -0.81 (s, SiMe) ppm. The resonances of the free anion $[B(C_6F_5)_4]^-$ and byproduct Ph_3CMe and 1 equiv. of unreacted $Ph_3C^+B(C_6F_5)_4^-$ are not included in the ^{1}H NMR and ^{13}C NMR data here. ^{19}F NMR (470 MHz, CD_2Cl_2) δ = -133.06 (q, J = 10.8 Hz, 8 F), -163.63 (t, J = 20.4 Hz, 4 F), -167.48 (t, J = 19.0 Hz, 8 F) ppm. ^{11}B NMR (160 MHz, CD_2Cl_2) δ = -16.70 (s) ppm.

NMR study of *rac*-[(μ-CMe_2-3,3')\{(η^5-cyclopentadienyl)[1-Me_2Si(^{t}BuN)]\}$_2$- (μ-CH_2)[(TiCH_3)-(Ti-η^1-Ph_3C)]$^{2+}$[$B(C_6F_5)_4$]$_2^-$ (*rac*-6). In the glove box, ***rac*-3** (0.058 g, 0.10 mmol) and $Ph_3C^+B(C_6F_5)_4^-$ (0.184 g, 0.20 mmol) in a 1:2 molar ratio were loaded into a J. Young NMR tube. The sealed tube was then removed from the glovebox, attached to the vacuum line, and cooled to -78 °C, and C_6D_5Cl was immediately transferred in. The sample was shaken vigorously and transferred directly to the NMR spectrometer. ^{1}H NMR of ***rac*-6** (500 MHz, C_6D_5Cl) δ = 7.77 (br, 2 H, μ-CH_2), 7.62 (m, 1 H, Cp), 6.40 (m, 1 H, Cp), 6.31 (m, 1 H, Cp), 6.03 (m, 1 H, Cp), 5.91 (m, 1 H, Cp), 5.43 (m, 1 H, Cp), 2.02 (s, 3 H, C*Me*Me, overlapped by Ph_3CMe and assigned by HSQC), 1.68 (s, 3 H, CMe*Me*), 1.50 (s, 18 H, Me_3C), 0.43 (s, 3 H, SiMe), 0.39 (s, 3 H, SiMe), 0.08 (s, 3 H, SiMe), 0.02 (s, 3 H, SiMe), -0.41 (s, 3 H, Ti-CH_3) ppm. ^{13}C NMR (125 MHz, C_6D_5Cl) δ = 233.43 (s, μ-CH_2), 149.47 (s, Cp), 148.13 (s, Cp), 133.16 (s, Cp), 127.74 (s, Cp), 124.53 (s, Cp), 122.32 (s, , Cp), 117.76 (s, Cp), 117.46 (s, Cp), 116.74 (s, , Cp), 133.16 (s, Cp), 112.21 (s, Cp), 67.63 (s, Ti-CH_3), 63.56 (s, Me_3C), 63.43 (s, Me_3C), 37.50 (s, CMe_2), 33.90 (s, CMe_3), 33.44 (s, CMe_3), 31.34 (s, C*Me*Me), 30.26 (s, CMe*Me*), 0.84 (s, , SiMe), 0.76 (s, SiMe), -0.70 (s, SiMe), -1.19 (s, SiMe) ppm. The resonances of the free anion $[B(C_6F_5)_4]^-$ and byproduct Ph_3CMe are not listed in ^{1}H NMR and

^{13}C NMR. ^{19}F NMR (470 MHz, C_6D_5Cl) δ = -131.68 (q, J = 10.8 Hz, 8 F), -162.25 (t, J = 20.4 Hz, 4 F), -166.09 (t, J = 19.0 Hz, 8 F) ppm. ^{11}B NMR (160 MHz, C_6D_5Cl) δ = -16.04 (s) ppm.

NMR study of *meso*-[(μ-CMe$_2$-3,3')\{(η^5-cyclopentadienyl)[1-Me$_2$Si(^{t}BuN)]\}$_2$-(μ-CH$_2$)(μ-CH$_3$)Ti$_2$]$^+$[B(C$_6$F$_5$)$_4$]$^-$ (*meso*-5). In the glove box, ***meso*-3** (0.058 g, 0.10 mmol) and $Ph_3C^+B(C_6F_5)_4^-$ (0.092 g, 0.10 mmol) in a 1:1 molar ratio were loaded into a J. Young NMR tube. The sealed tube was then removed from the glovebox, attached to the vacuum line, and cooled to -78 °C, and CD_2Cl_2 was immediately transferred in. The sample was shaken vigorously and transferred directly to the NMR spectrometer. ^{1}H NMR of ***meso*-5** (500 MHz, CD_2Cl_2) δ = 8.80 (s, 2 H, μ-CH_2), 8.65 (dd, J = 3.2 Hz, J = 2.0 Hz, 2 H, Cp), 6.39 (t, J = 2.8 Hz, 2 H, Cp), 5.55 (t, J = 2.2 Hz, 2 H, Cp), 2.09 (s, 3 H, C*Me*Me), 1.75 (s, 18 H, Me_3C), 1.66 (s, 6 H, CMe*Me*), 0.67 (s, 6 H, SiMe), 0.43 (s, 6 H, SiMe), -0.04 (s, 3H, μ-CH_3) ppm. ^{13}C NMR (125 MHz, CD_2Cl_2) δ = 253.14 (s, μ-CH_2), 148.51 (s, Cp) , 133.25 (s, Cp), 125.80 (s, Cp), 118.92 (s, Cp), 109.73 (s, Cp), 64.20 (s, Me_3C), 63.04 (s, μ-CH_3), 38.94 (s, CMe$_2$), 36.42 (s, C*Me*Me), 34.96 (s, C*Me*$_3$), 25.66 (s, CMe*Me*), 0.99 (s, SiMe), 0.37 (s, SiMe) ppm. The resonances of the free anion $[B(C_6F_5)_4]^-$ and byproduct Ph_3CMe are not listed in ^{1}H NMR and ^{13}C NMR data here. ^{19}F NMR (470 MHz, CD_2Cl_2) δ = -132.98 (d, J = 18.1 Hz, 16 F), -163.56 (t, J = 20.4 Hz, 8 F), -167.40 (t, J = 19.1 Hz, 16 F) ppm. ^{11}B NMR (160 MHz, CD_2Cl_2) δ = -16.68 (s) ppm.

NMR Study of *rac*-[(μ-CMe$_2$-3,3')\{(η^5-cyclopentadienyl)[1-Me$_2$Si(^{t}BuN)]\}$_2$ (μ-CH$_2$)[TiMe···B(C$_6$F$_5$)$_3$]$_2$] (*rac*-7) and *rac*-[(μ-CMe$_2$-3,3')\{(η^5-cyclopentadienyl)-[1-Me$_2$Si(^{t}BuN)]\}$_2$(μ-Cl)(TiCl)$_2$]$^+$[MeB(C$_6$F$_5$)$_3$]$^-$ (*rac*-7-Cl$_3$) in CD_2Cl_2. In the glove box, ***rac*-3** (0.058 g, 0.10 mmol) and $B(C_6F_5)_3$ (0.103 g, 0.20 mmol) in a 1:2 molar ratio were loaded into a small vial, and at room temperature toluene was added. After 1h, the vial was place in fridge at -40 °C overnigh and yellow crystals were obtained after removing the solution. The crystals were no longer soluble

in C_6D_6 or C_7D_8 and no helpful NMR data were recorded. The yellow crystals were characterized by X-ray diffraction (see Supporting Information, Figure S33). The yellow crystals ***rac*-7** were dissolved in CD_2Cl_2, and the sample was shaken vigorously, kept at room temperature for 3 h, and transferred to the NMR spectrometer. ^{1}H NMR of ***rac*-7-Cl**$_3$ (500 MHz, CD_2Cl_2) δ = 7.47 (dd, J_1 = 2.9 Hz, J_2 = 2.4 Hz, 2 H, Cp), 6.70 (d, J = 2.3 Hz, 2 H, Cp), 5.60 (d, J = 2.8 Hz, 2 H, Cp), 1.70 (s, 6 H, CMe_2), 1.47 (s, 18 H, Me_3C), 0.82 (s, 6 H, SiMe), 0.76 (s, 6 H, SiMe) ppm. ^{13}C NMR (125 MHz, CD_2Cl_2) δ = 154.99 (s, Cp), 132.69 (s, Cp), 127.97 (s, Cp), 127.20 (s, Cp), 113.70 (s, Cp), 69.36 (s, Me_3C), 40.26 (s, CMe_2), 32.67 (s, CMe_2), 32.55 (s, CMe_3), -0.08 (s, SiMe), -0.86 (s, SiMe) ppm. These ^{1}H and ^{13}C NMR spectra are the same as those of ***rac*-5-Cl**$_3$. The resonances of the free $[MeB(C_6F_5)_3]^-$ anion are not listed in ^{1}H NMR and ^{13}C NMR data here. ^{19}F NMR (470 MHz, CD_2Cl_2) δ = -128.13 (dd, J = 22.2, 8.4 Hz), -133.09 (d, J = 23.8 Hz), -143.81 (td, J = 20.4, 9.8 Hz), -161.00 (dq, J = 23.0, 9.6 Hz), -165.32 (t, J = 20.4 Hz), -167.86 (t, J = 22.1 Hz) ppm.

NMR study of *meso*-[(μ-CMe_2-3,3')\{(η^5-cyclopentadienyl)[1-Me_2Si(^{t}BuN)]\}$_2$-(μ-CH_2) (μ-CH_3)Ti_2]$^+$[$MeB(C_6F_5)_3$]$^-$ (*meso*-7). In the glove box, ***meso*-3** (0.058 g, 0.10 mmol) and $B(C_6F_5)_3$ (0.051 g, 0.10 mmol) in a 1:1 molar ratio were loaded into a J. Young NMR tube. The sealed tube was then removed from the glovebox, attached to the vacuum line, and cooled to -78 °C, and CD_2Cl_2 or C_6D_5Cl was immediately transferred in. The sample was shaken vigorously and transferred directly to the NMR spectrometer. ^{1}H NMR of ***meso*-5** (500 MHz, CD_2Cl_2) δ = 8.81 (s, 2 H, μ-CH_2), 8.65 (dd, J = 3.2 Hz, J = 2.0 Hz, 2 H, Cp), 6.39 (t, J = 2.8 Hz, 2 H, Cp), 5.56 (t, J = 2.2 Hz, 2 H, Cp), 2.09 (s, 3 H, C*Me*Me), 1.75 (s, 18 H, Me_3C), 1.66 (s, 6 H, CMe*Me*), 0.67 (s, 6 H, SiMe), 0.43 (s, 6 H, SiMe), -0.02 (s, 3H, μ-CH_3) ppm. This ^{1}H NMR spectrum is essentially identical to that of ***meso*-5**. ^{13}C NMR (125 MHz, C_6D_5Cl) δ = 253.14 (s, μ-CH_2), 148.51 (s, Cp) , 133.25 (s, Cp), 125.80 (s, Cp), 118.92 (s, Cp), 109.73 (s, Cp), 64.20 (s, Me_3C), 63.04 (s, μ-CH_3),

38.94 (s, *C*Me$_2$), 36.42 (s, C*Me*Me), 34.96 (s, C*Me*$_3$), 25.66 (s, CMe*Me*), 0.99 (s, SiMe), 0.37 (s, SiMe) ppm. The resonances of the free [MeB(C_6F_5)$_3$] anion are not listed in the ^{1}H NMR and ^{13}C NMR data here. ^{19}F NMR (470 MHz, C_6D_5Cl) δ = -131.65 (m), -164.13 (t, J = 20.7 Hz), -166.56 (m) ppm. ^{11}B NMR (160 MHz, C_6D_5Cl) δ = -14.29 (s) ppm.

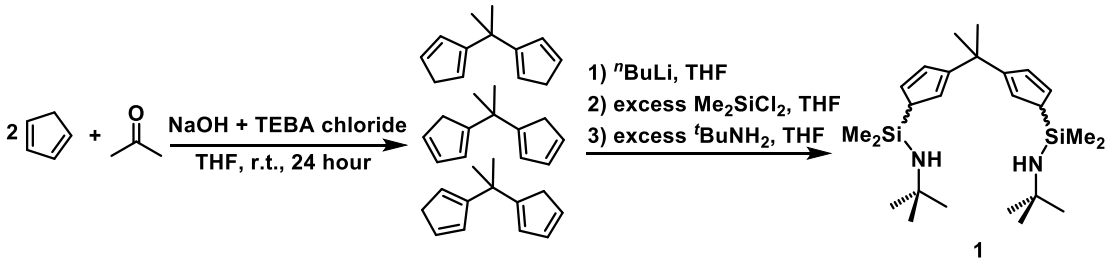

Scheme 1.10. Synthesis of the binuclear ligand **1**.

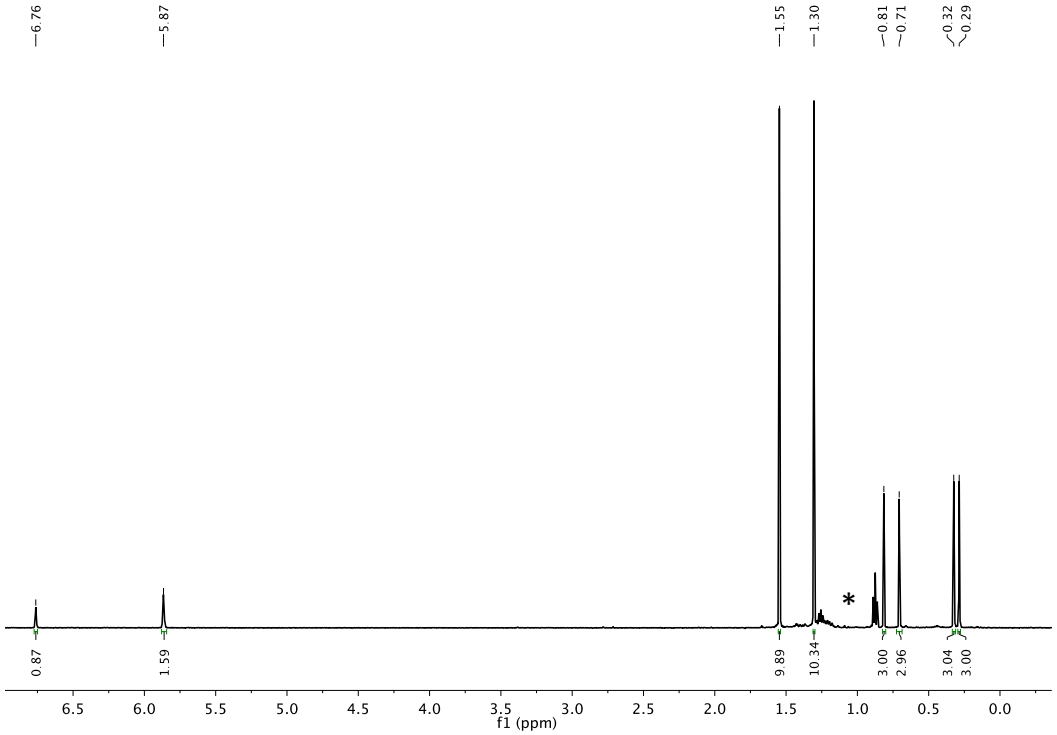

Figure 1.10. ^{1}H NMR spectrum of **Ti**$_{1}$ in C_6D_6. [*Additional peaks caused by pentane.]

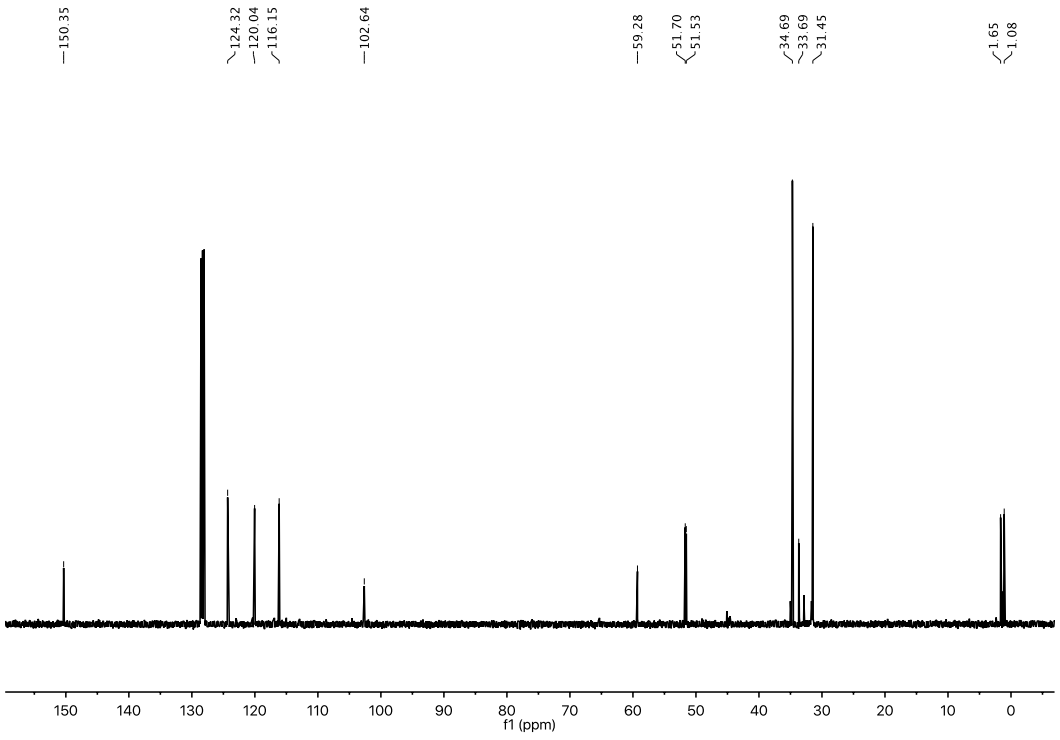

Figure 1.11. ^{13}C NMR spectrum of **Ti**$_{1}$ in C_6D_6.

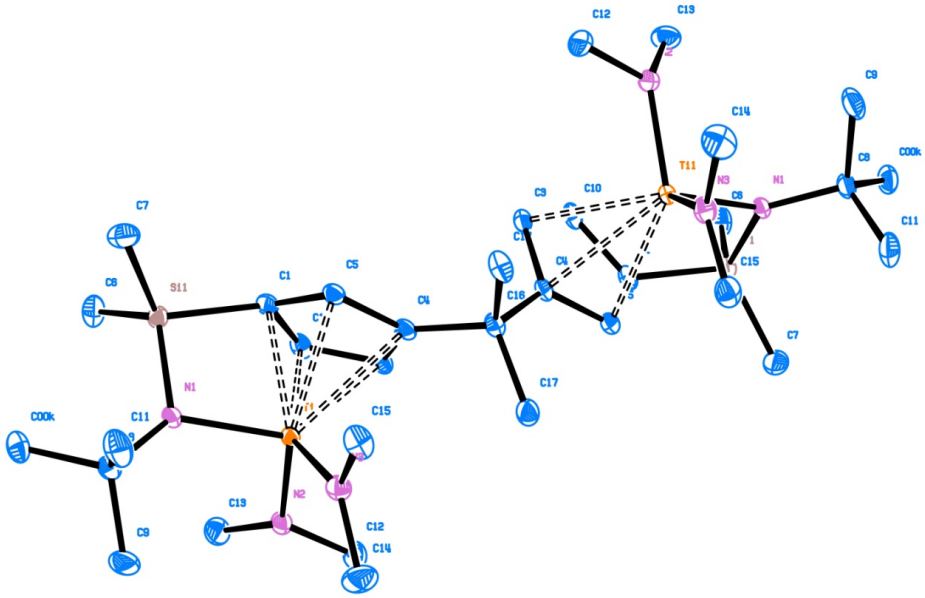

Figure 1.12. ORTEP view of the molecular structure of ***meso*-2** (ellipsoids enclose 50% electronic density; H atoms are omitted for clarity).

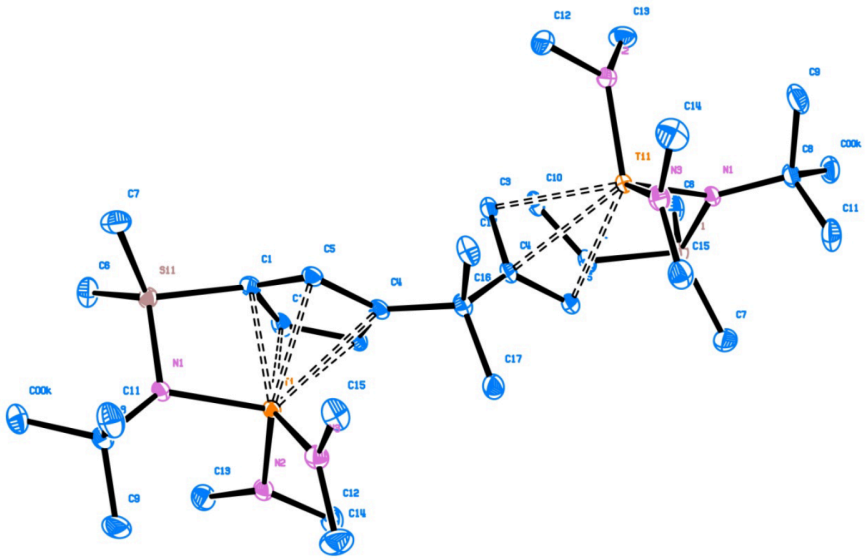

Figure 1.13. ORTEP view of the molecular structure of ***rac*-2** (ellipsoids enclose 50% electronic density; H atoms are omitted for clarity).

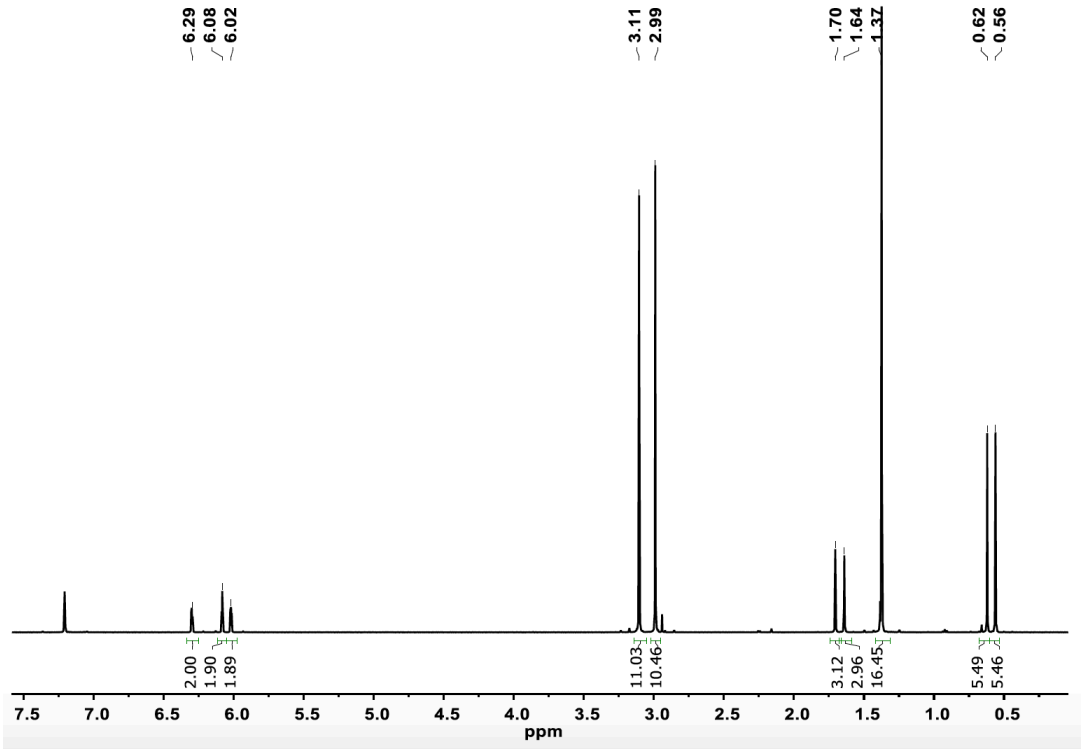

Figure 1.14. ^{1}H NMR spectrum of ***meso*-2** in C_6D_6.

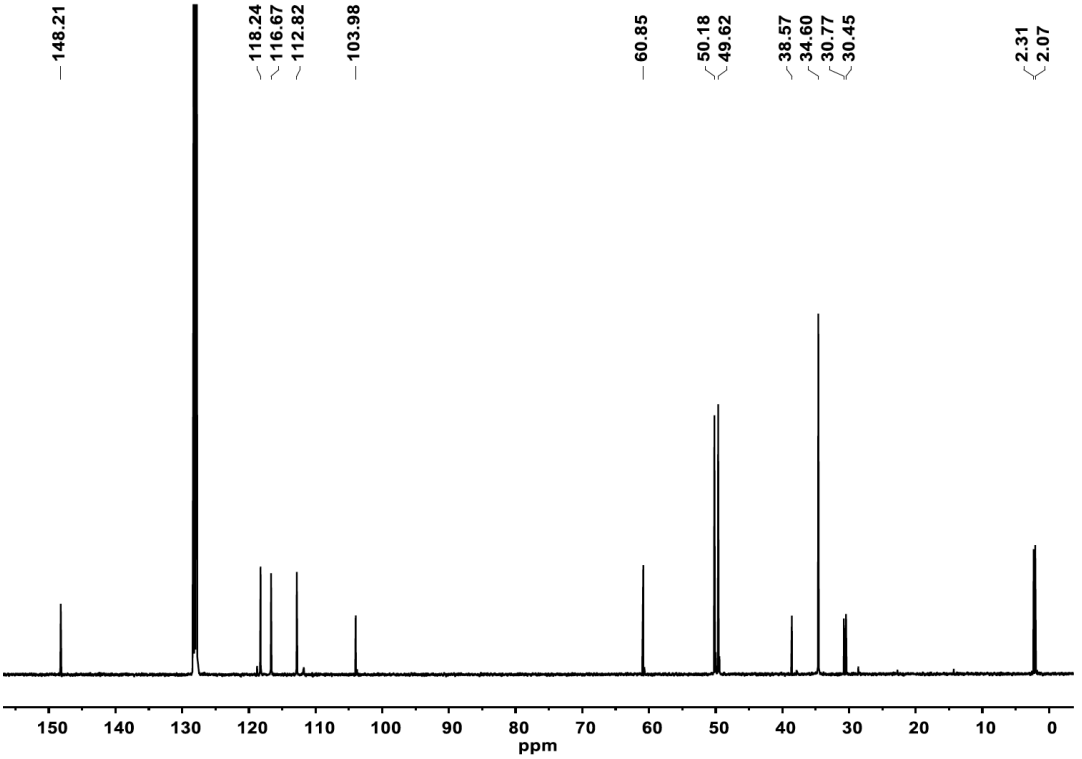

Figure 1.15. ^{13}C NMR spectrum of ***meso*-2** in C_6D_6.

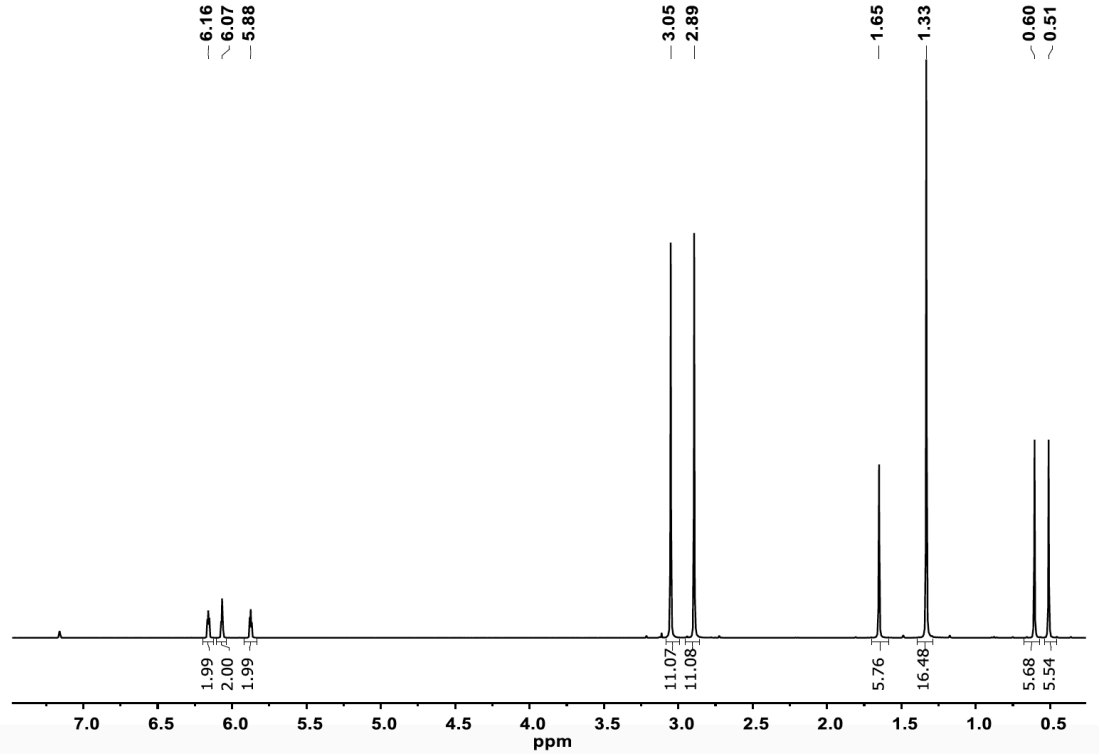

Figure 1.16. ^{1}H NMR spectrum of ***rac*-2** in C_6D_6.

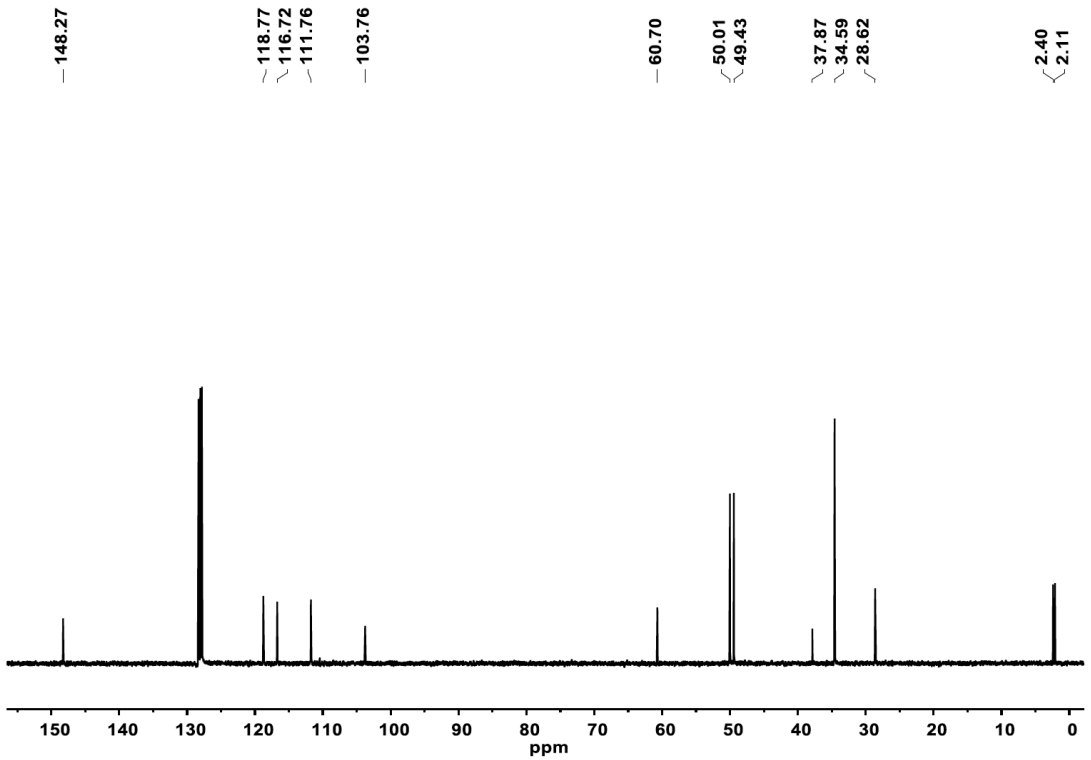

Figure 1.17. ^{13}C NMR spectrum of ***rac*-2** in C_6D_6.

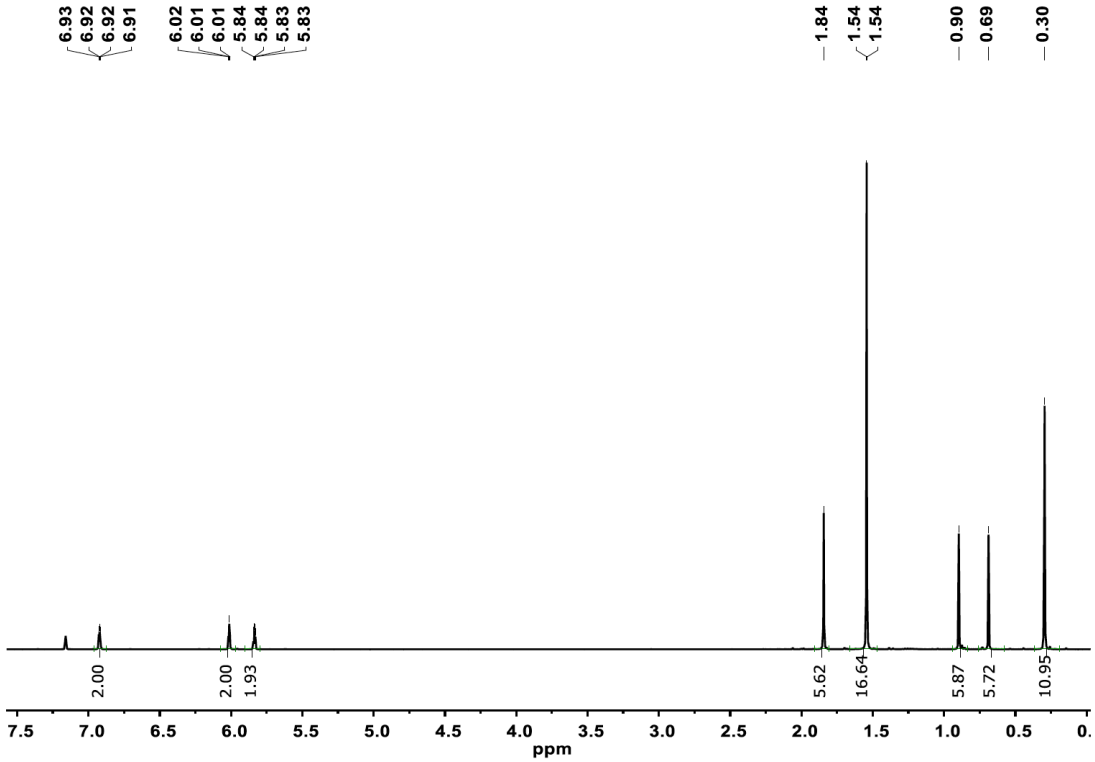

Figure 1.18. ^{1}H NMR spectrum of ***rac*-3** in C_6D_6.

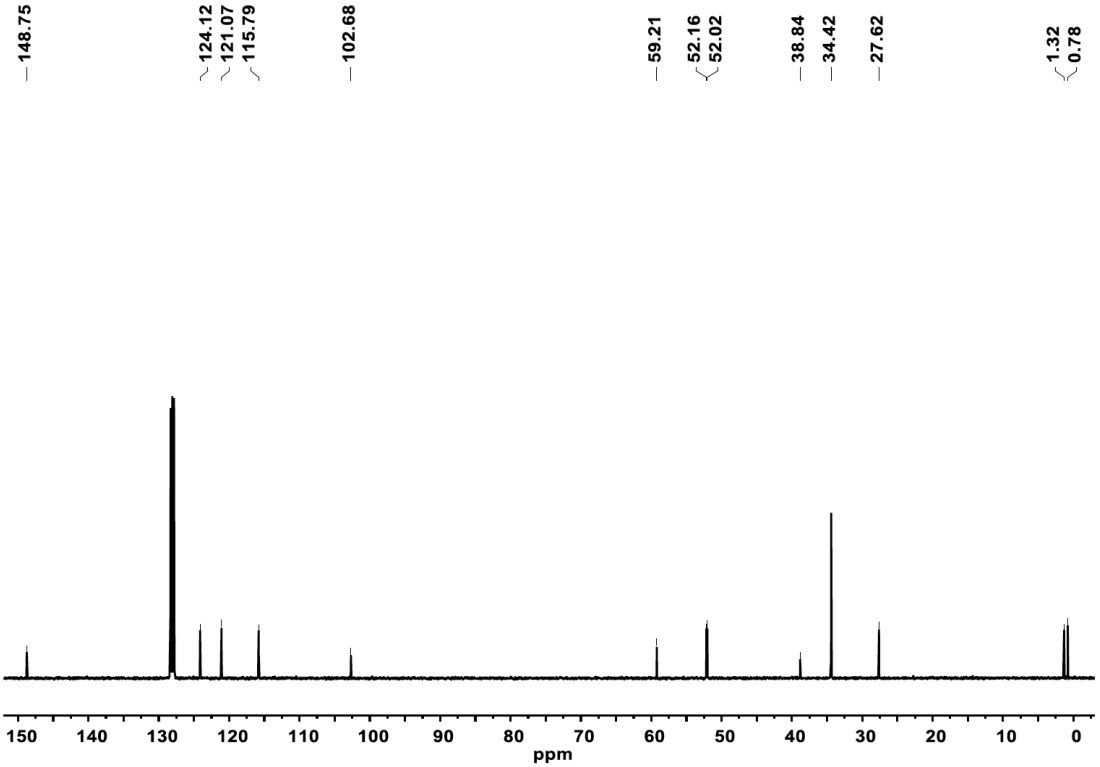

Figure 1.19. ^{13}C NMR spectrum of ***rac*-3** in C_6D_6.

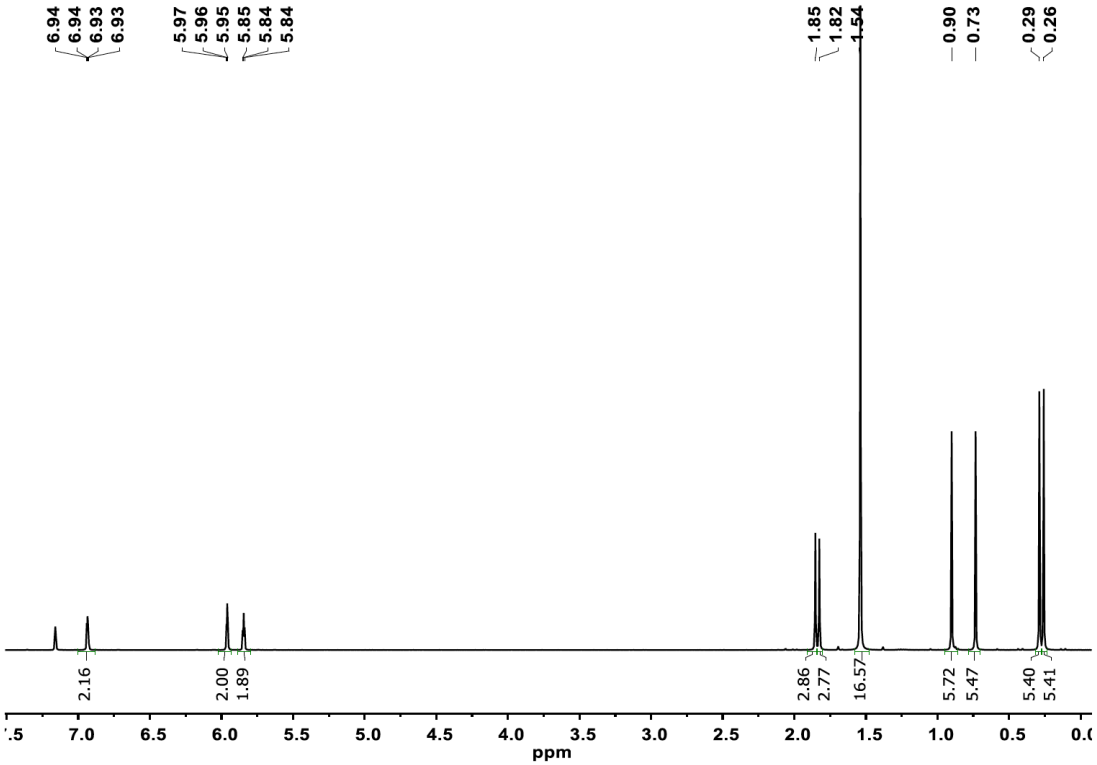

Figure 1.20. ^{1}H NMR spectrum of ***meso*-3** in C_6D_6.

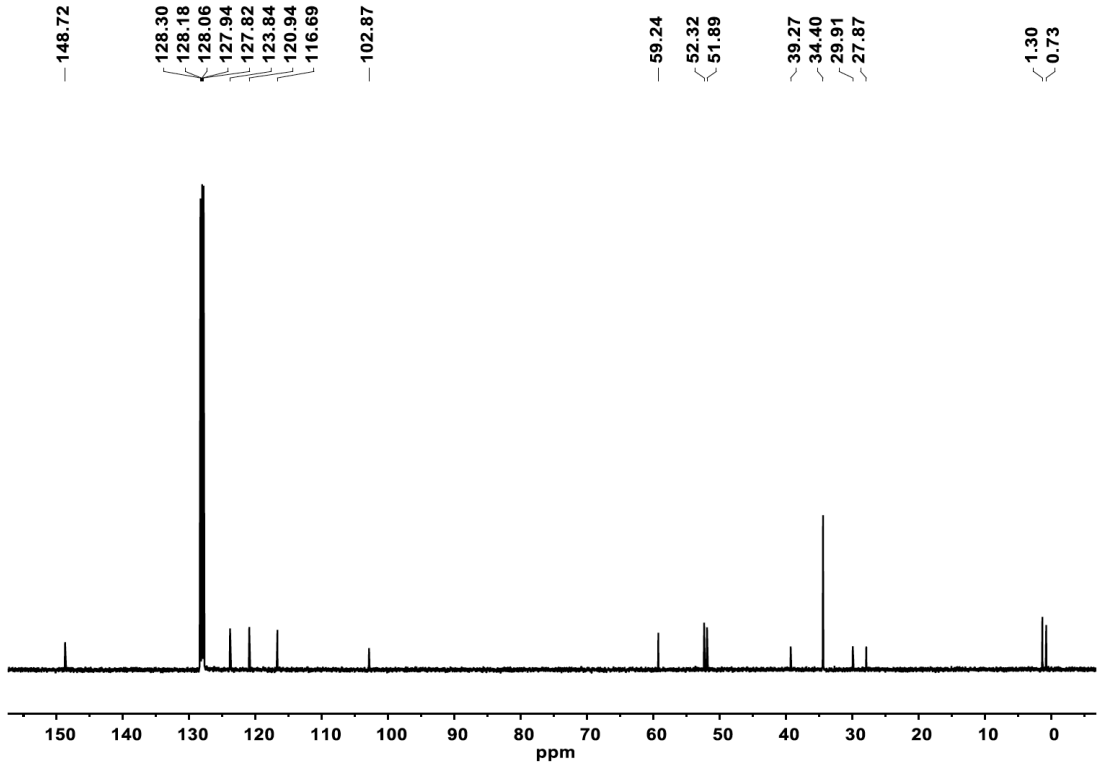

Figure 1.21. ^{13}C NMR spectrum of ***meso*-3** in C_6D_6.

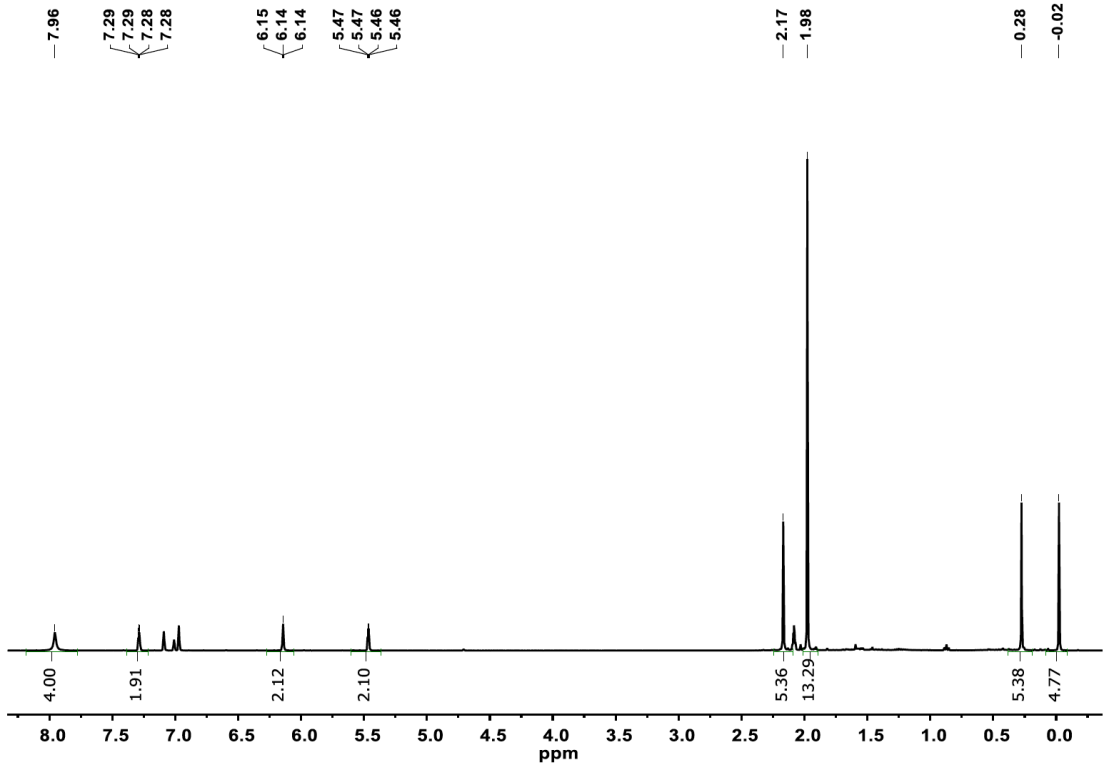

Figure 1.22. ^{1}H NMR spectrum of ***rac*-4** in C_7D_8.

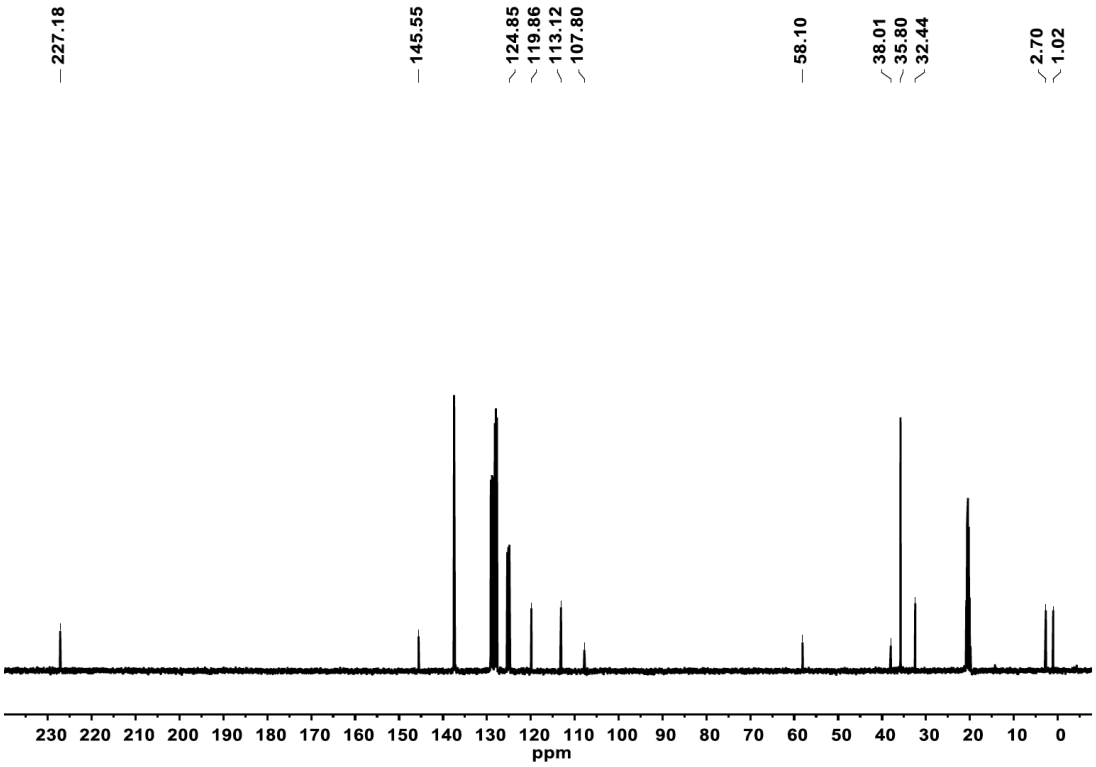

Figure 1.23. ^{13}C NMR spectrum of ***rac*-4** in C_7D_8.

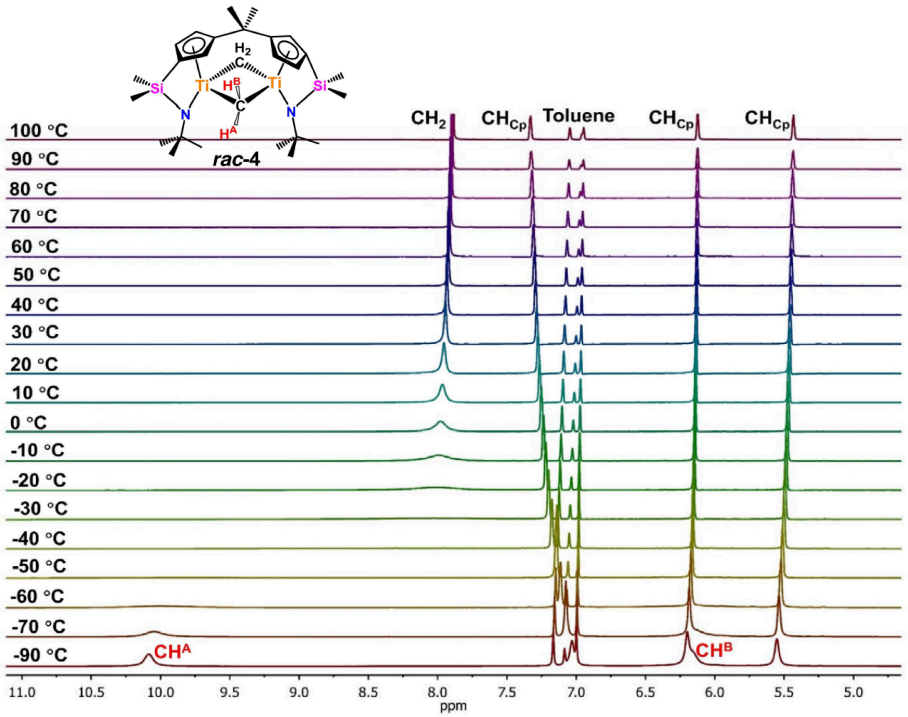

Figure 1.24. VT ^{1}H NMR spectrum of ***rac*-4** in C_7D_8 from -90 to 100° C.

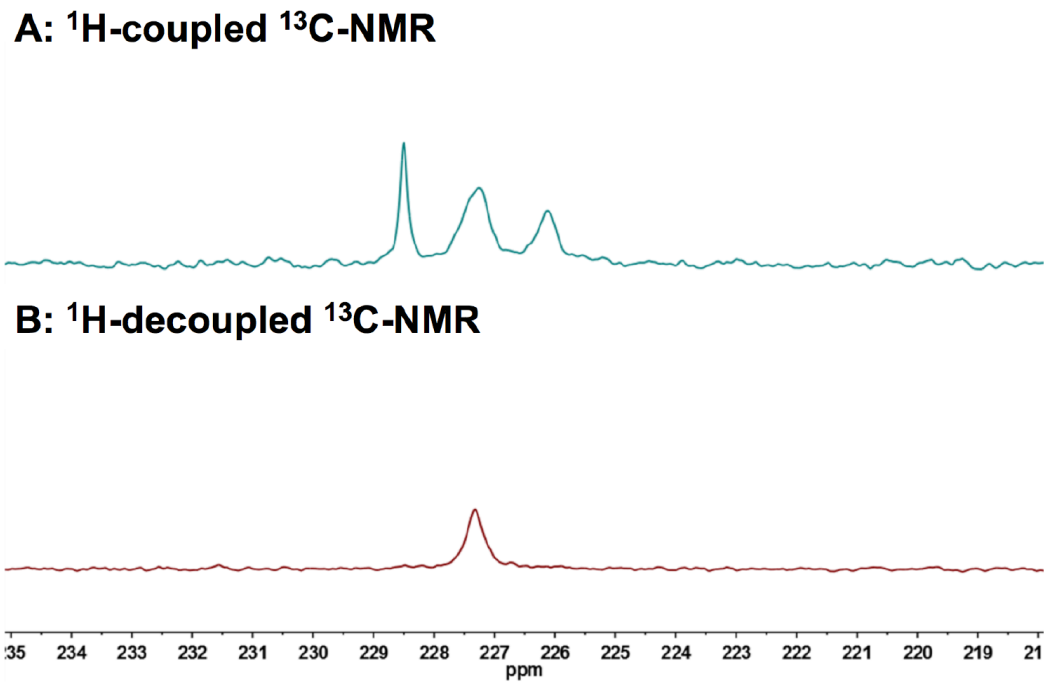

Figure 1.25. Stack plot of ^{1}H-coupled ^{13}C (**A**) and ^{1}H-decoupled ^{13}C (**B**) NMR spectra of the methylene bridge region of ***rac*-4** in C_7D_8 at -90° C.

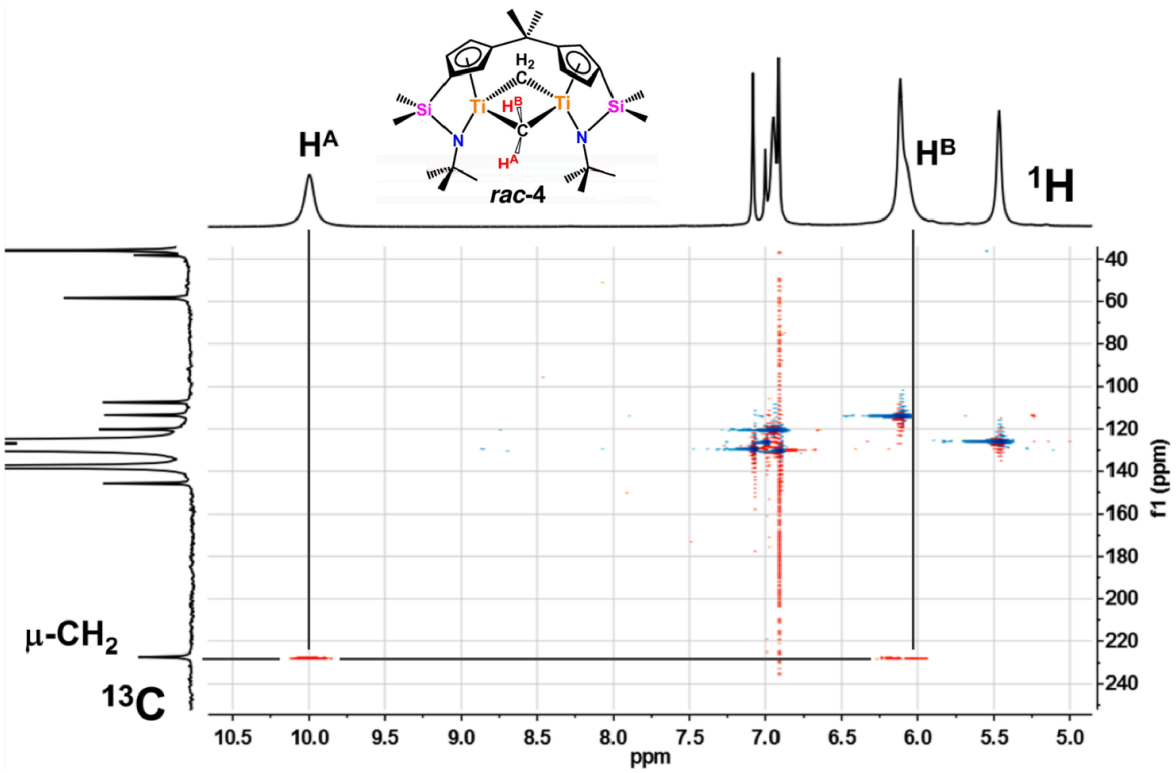

Figure 1.26. ^{1}H-^{13}C HSQC spectrum of ***rac*-4** in C_7D_8 at -90° C.

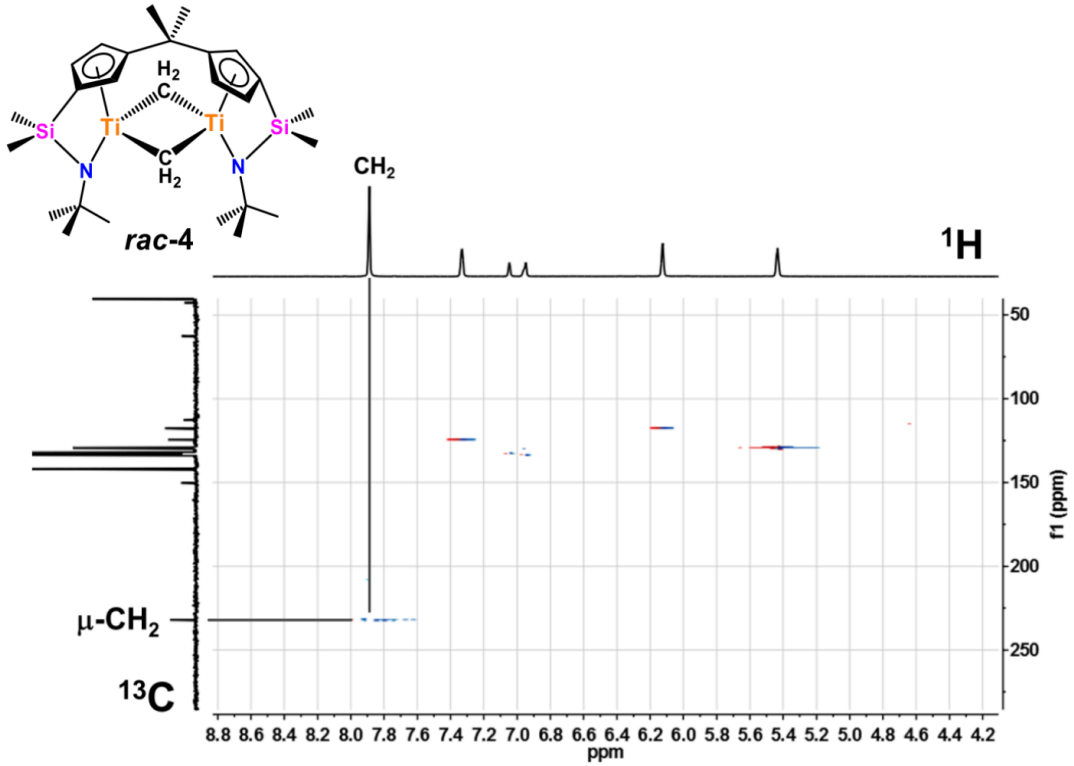

Figure 1.27. ^{1}H-^{13}C HSQC spectrum of ***rac*-4** in C_7D_8 at 100° C.

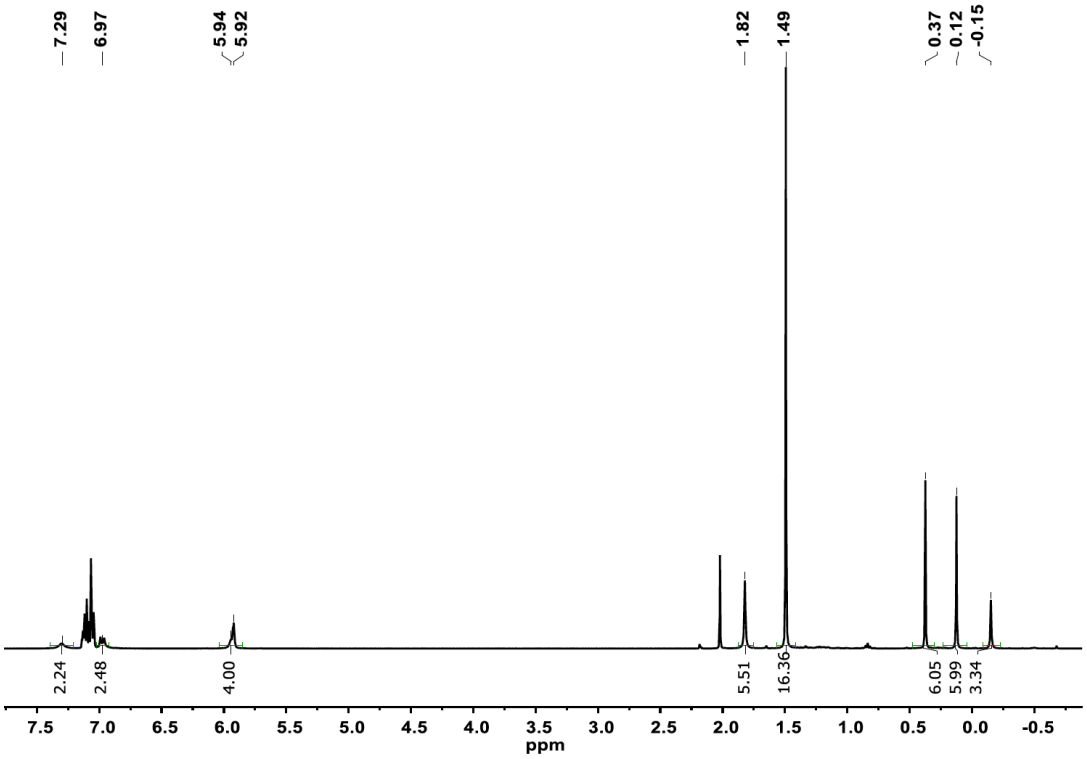

Figure 1.28. ^{1}H NMR spectrum of ***rac*-5** in C_6D_5Cl.

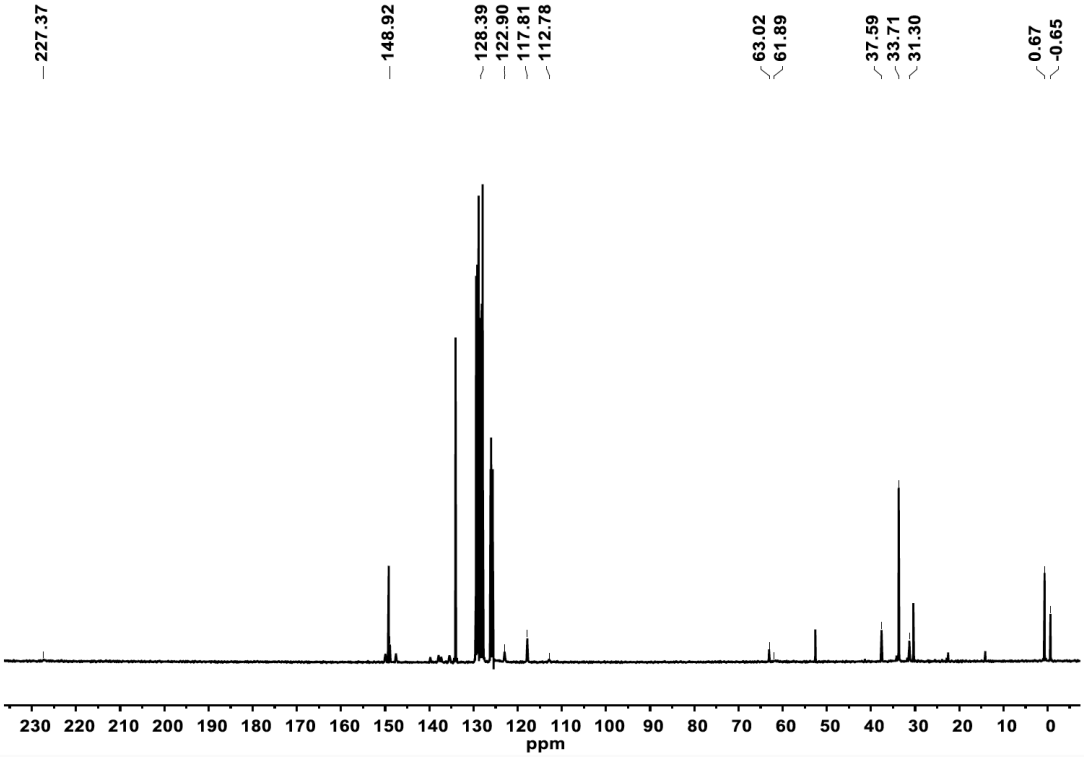

Figure 1.29. ^{13}C NMR spectrum of ***rac*-5** in C_6D_5Cl.

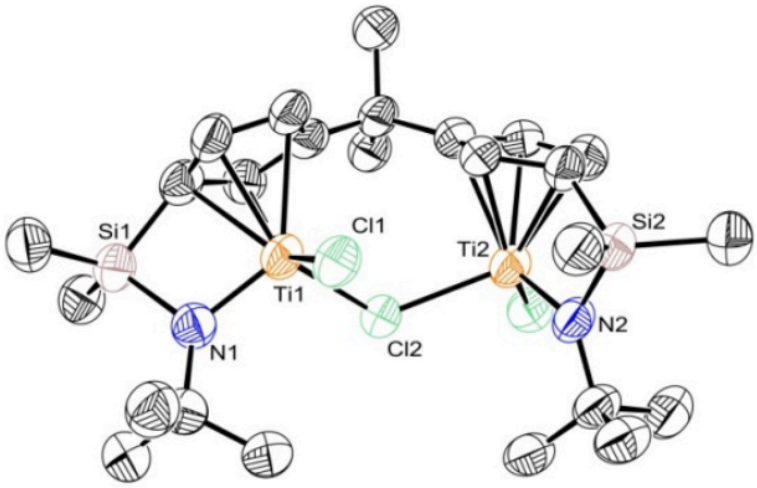

Figure 1.30. ORTEP view of the molecular structures of ***rac*-5-Cl**$_2$ (ellipsoids enclose 50% electronic density; H atoms and $[B(C_6F_5)_4]^-$ anions are omitted for clarity).

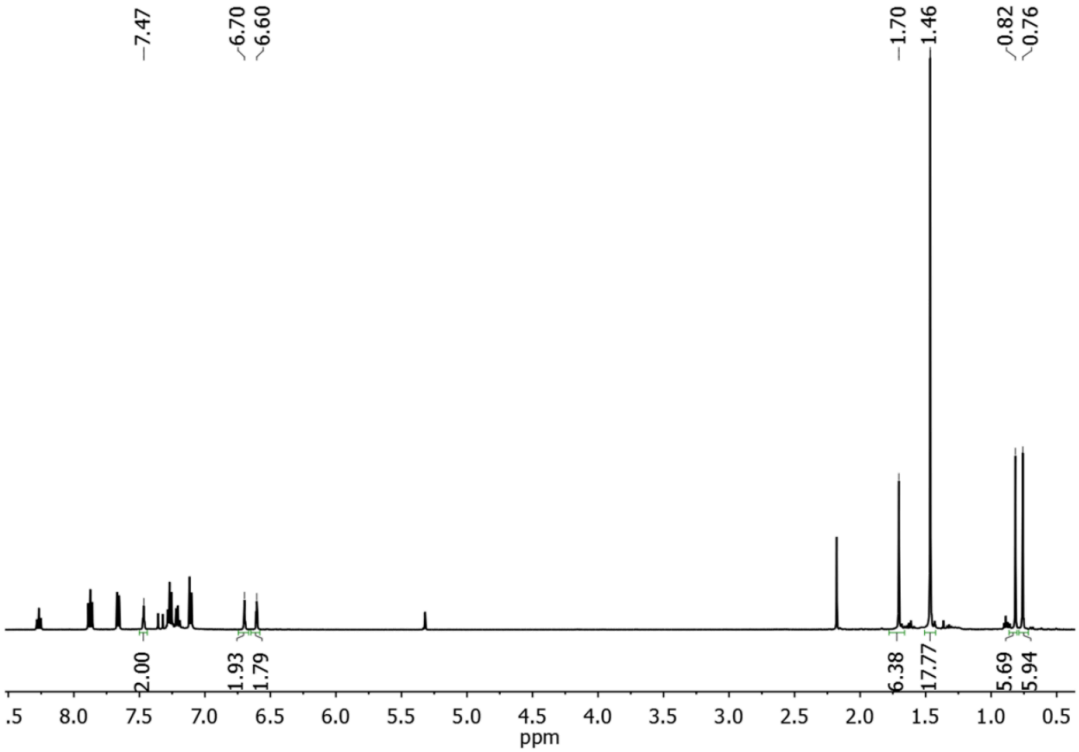

Figure 1.31. ^{1}H NMR spectrum of ***rac*-5-Cl**$_2$ in CD_2Cl_2.

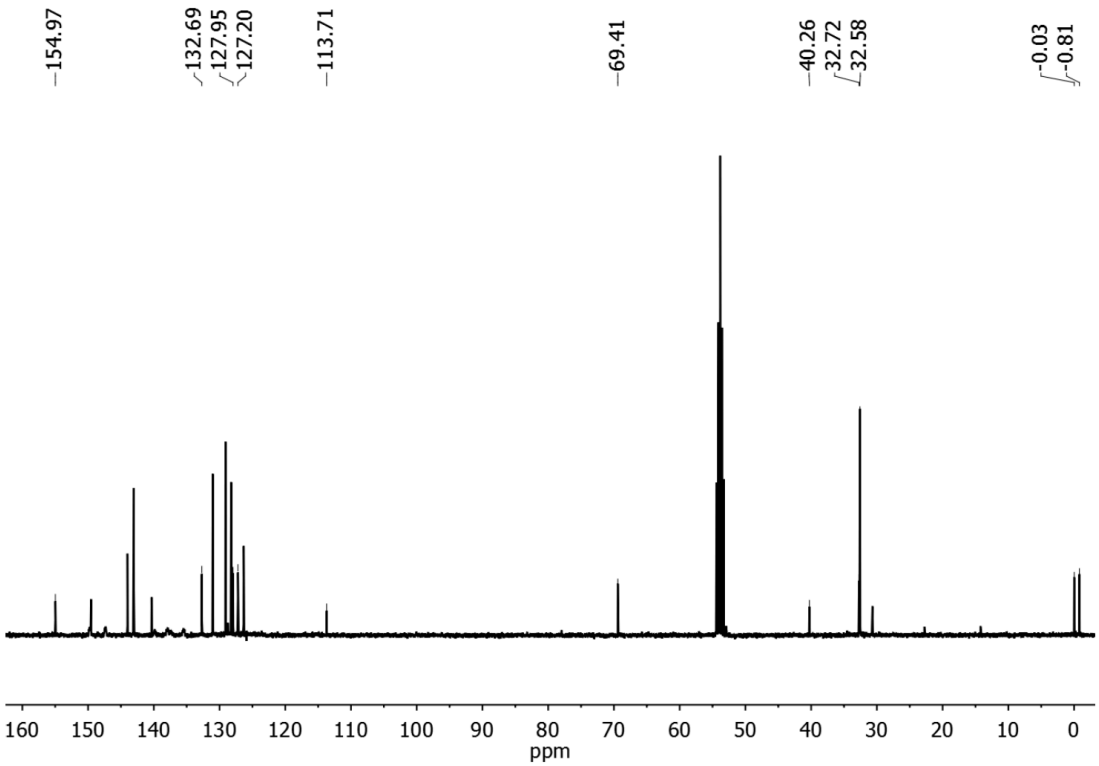

Figure 1.32. ^{13}C NMR spectrum of ***rac*-5-Cl**$_3$ in CD_2Cl_2.

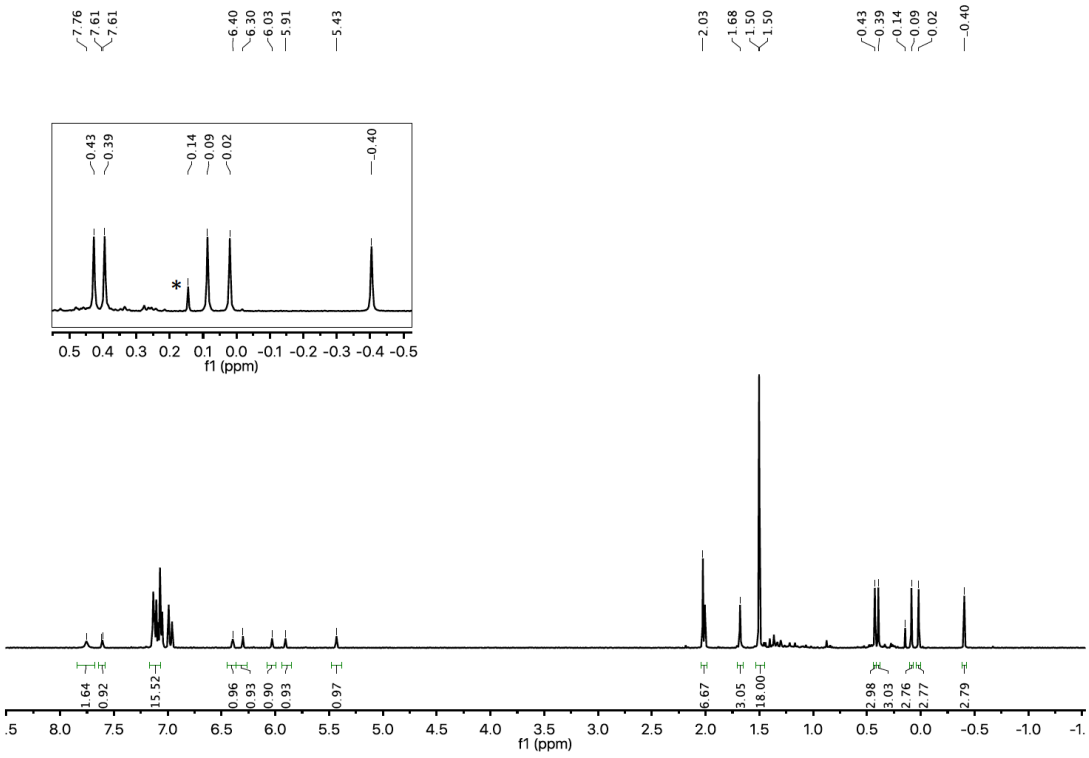

Figure 1.33. ^{1}H NMR spectrum of ***rac*-6** in C_6D_5Cl [* indicates peak from CH_4 release).

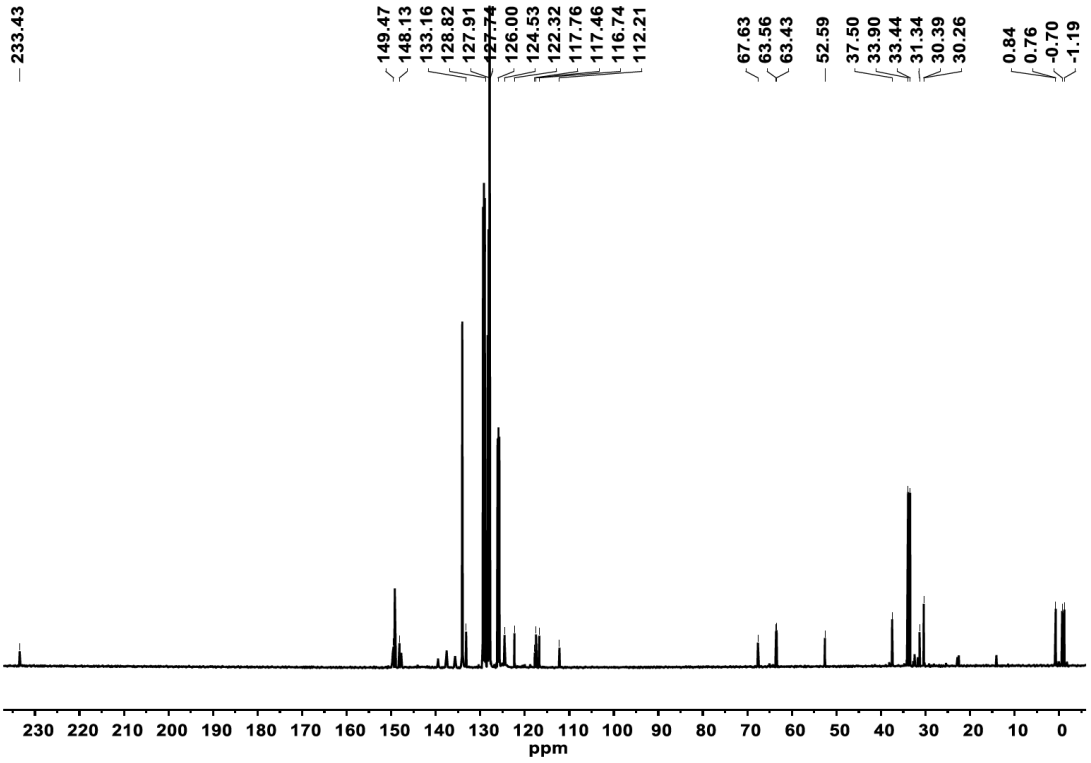

Figure 1.34. ^{13}C NMR spectrum of ***rac*-6** in C_6D_5Cl.

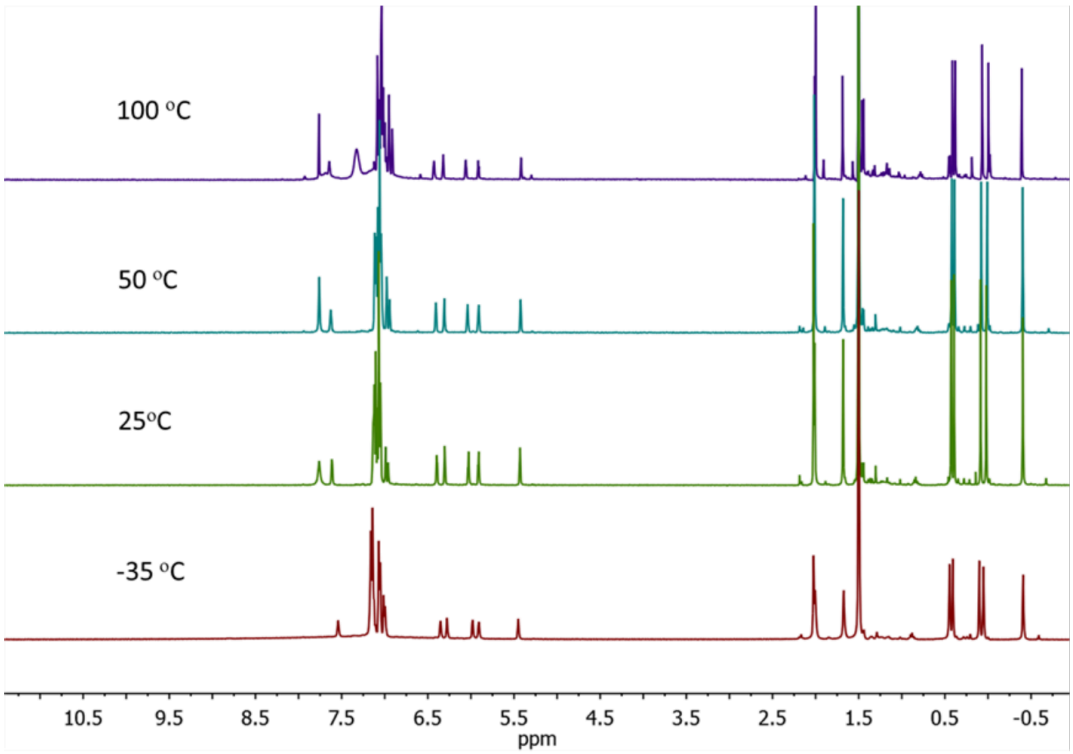

Figure 1.35. VT ^{1}H NMR spectra of ***rac*-6** in C_6D_5Cl from -35 to 100° C.

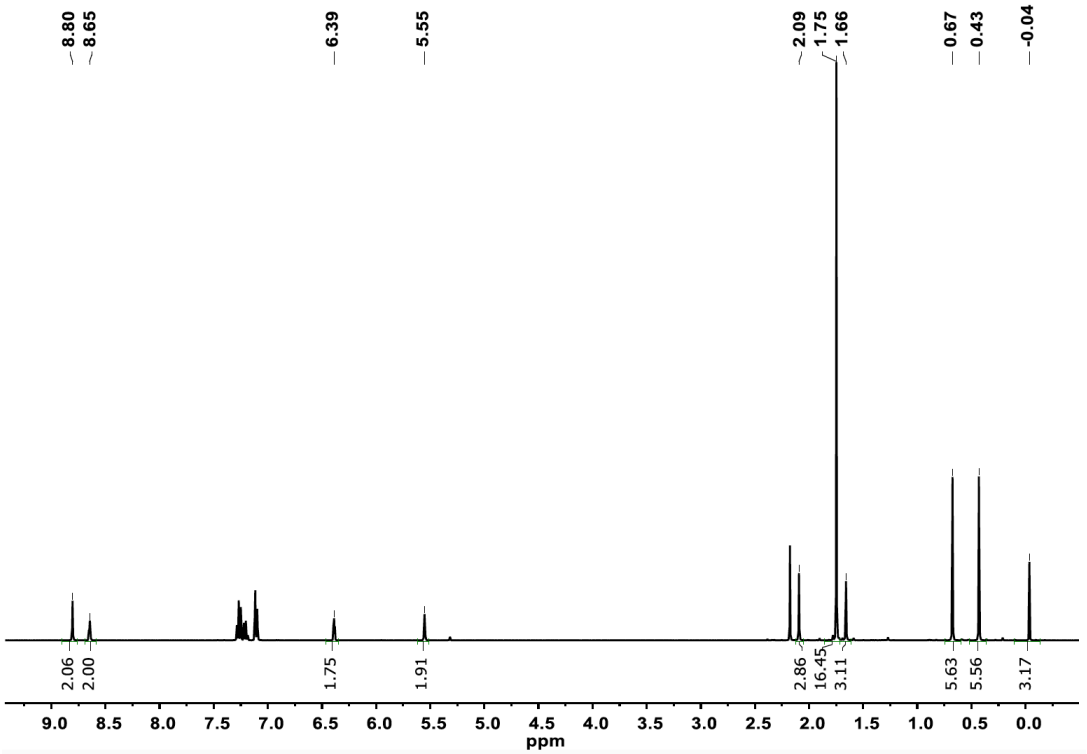

Figure 1.36. ^{1}H NMR spectrum of ***meso*-5** in C_6D_5Cl with 1 equiv. of $Ph_3C^+B(C_6F_5)_4^-$.

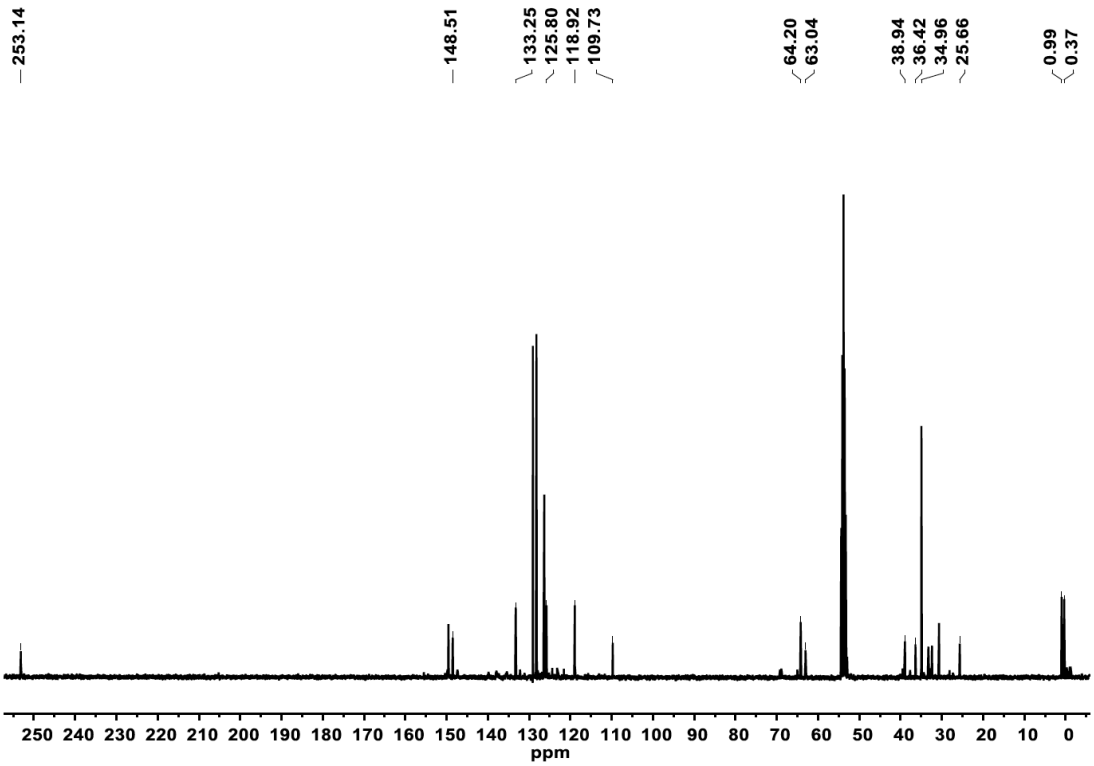

Figure 1.37. ^{13}C NMR spectrum of ***meso*-5** in C_6D_5Cl with 1 equiv. of $Ph_3C^+B(C_6F_5)_4^-$.

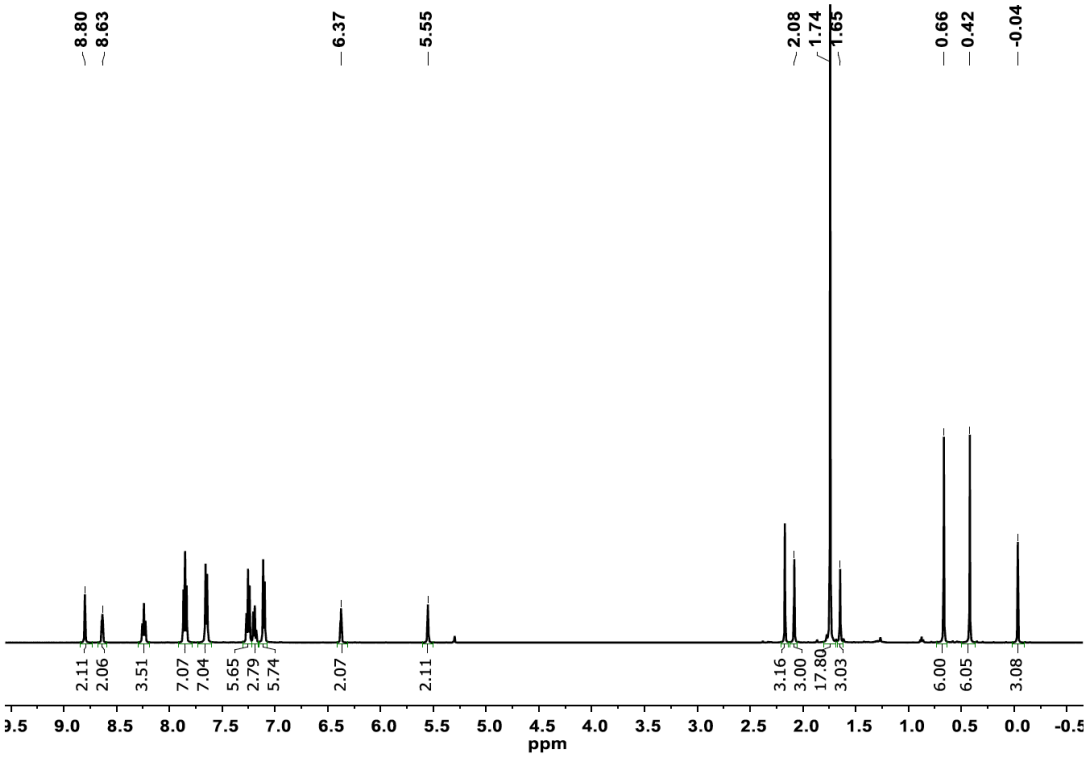

Figure 1.38. ^{1}H NMR spectrum of ***meso*-5** in C_6D_5Cl with 2 equiv. of $Ph_3C^+B(C_6F_5)_4^-$.

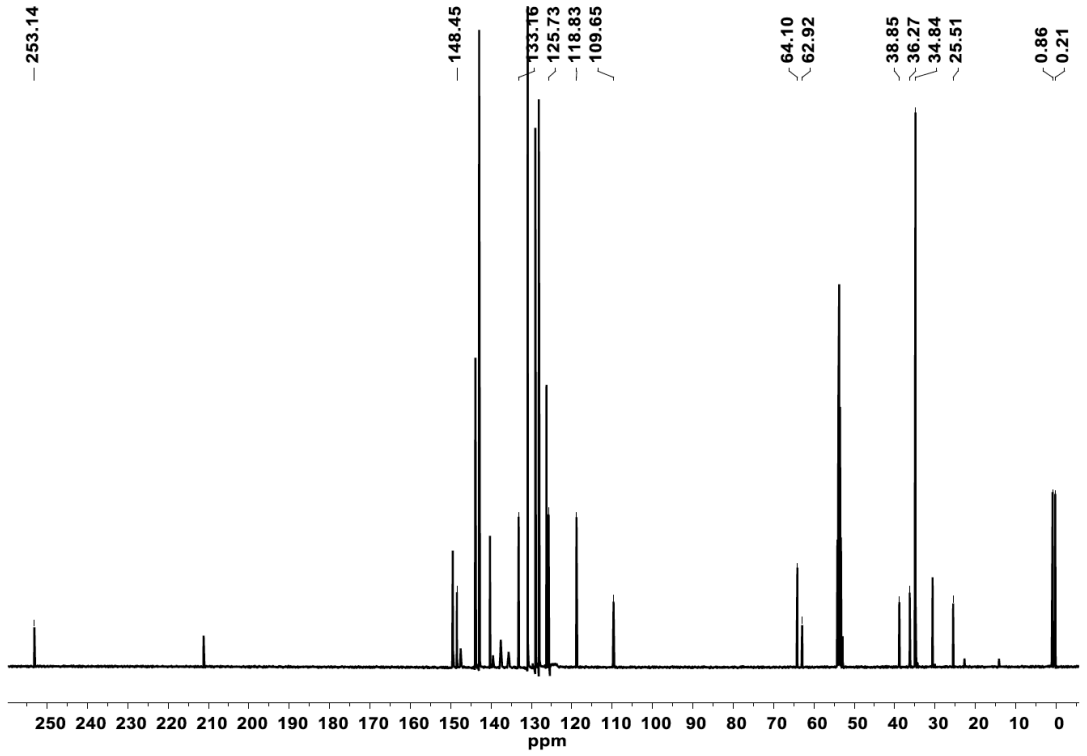

Figure 1.39. ^{13}C NMR spectrum of ***meso*-5** in C_6D_5Cl with 2 equiv. of $Ph_3C^+B(C_6F_5)_4^-$.

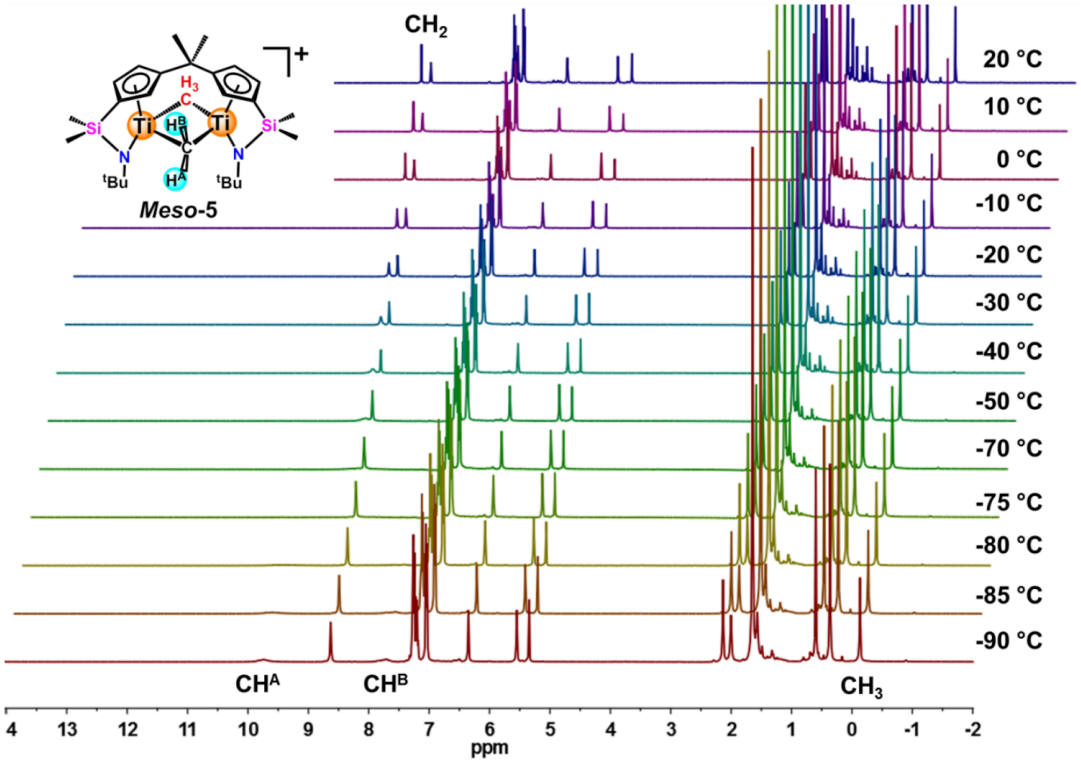

Figure 1.40. VT ^{1}H NMR spectra of ***meso*-5** in CD_2Cl_2 from -90 to 20° C.

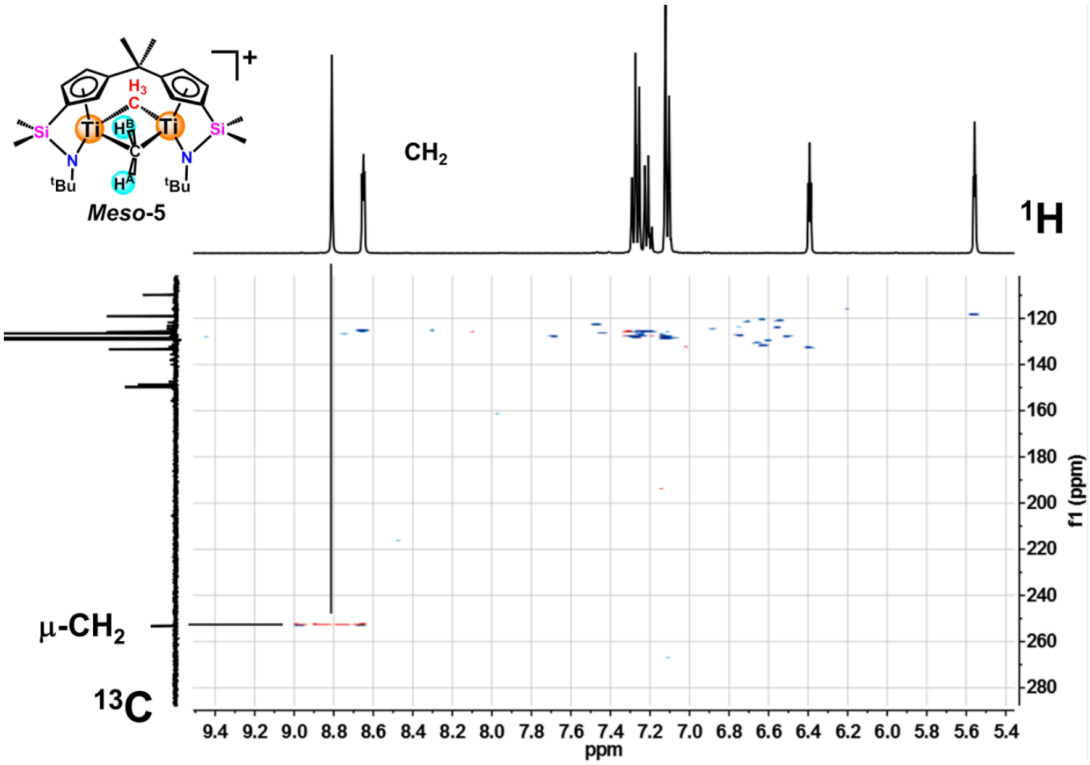

Figure 1.41. ^{1}H-^{13}C HSQC spectrum of ***meso*-5** in C_6D_5Cl at 20° C.

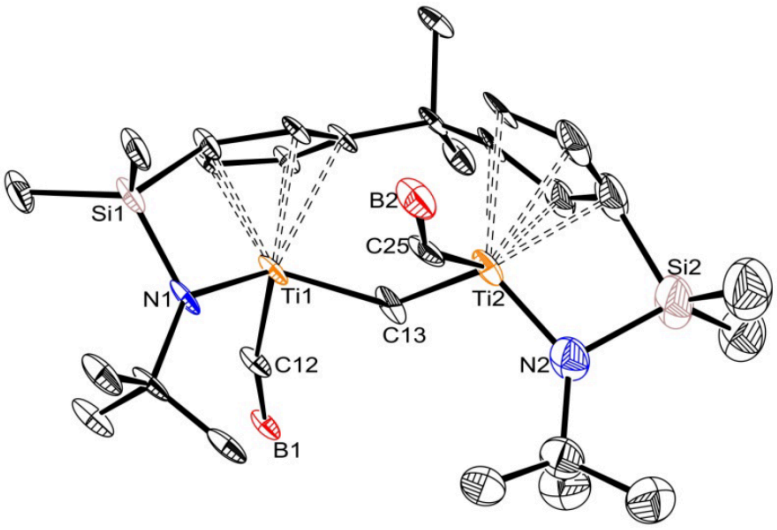

Figure 1.42. ORTEP view of the molecular structure of ***rac*-7** (ellipsoids enclose 50% electronic density; H atoms and six C_6F_5 on boranes are omitted for clarity).

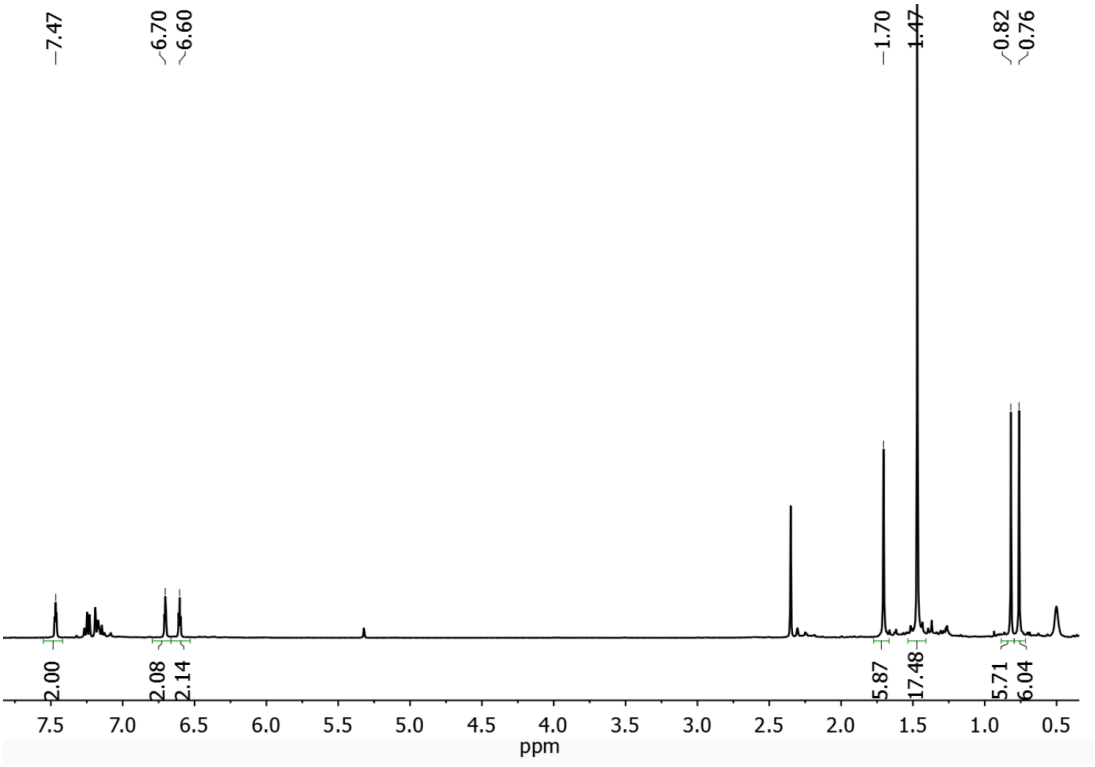

Figure 1.43. ^{1}H NMR spectrum of ***rac*-7-Cl**$_3$ in CD_2Cl_2.

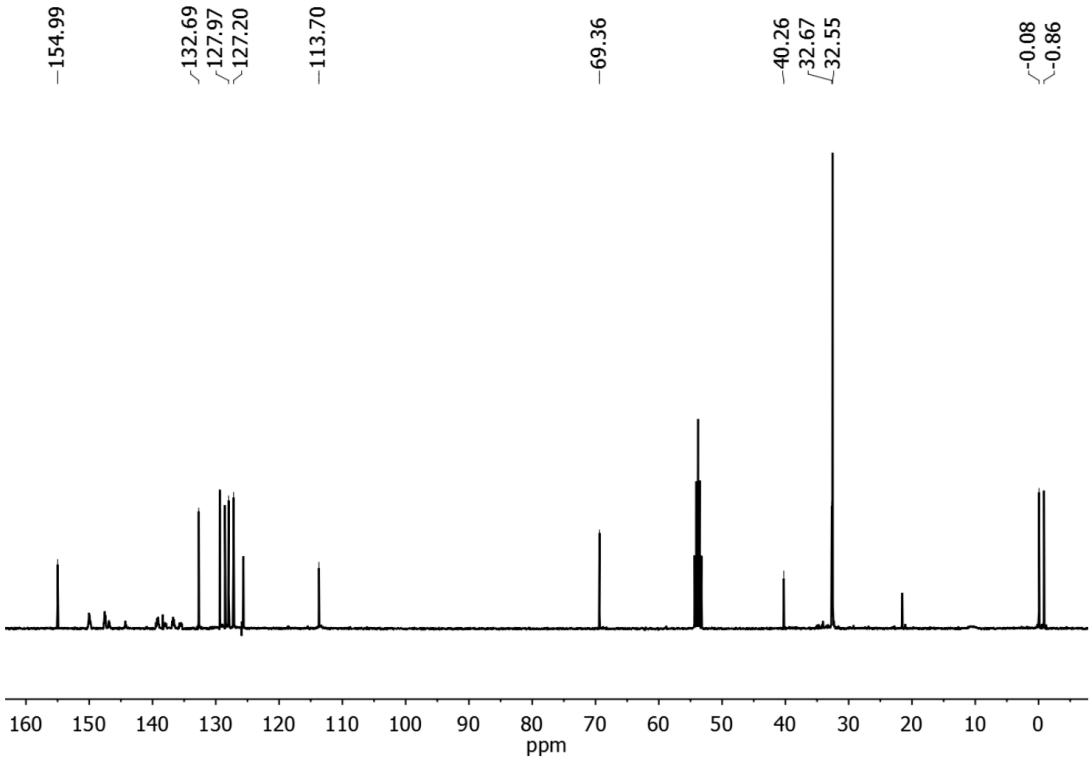

Figure 1.44. ^{13}C NMR spectrum of ***rac*-7-Cl**$_3$ in CD_2Cl_2.

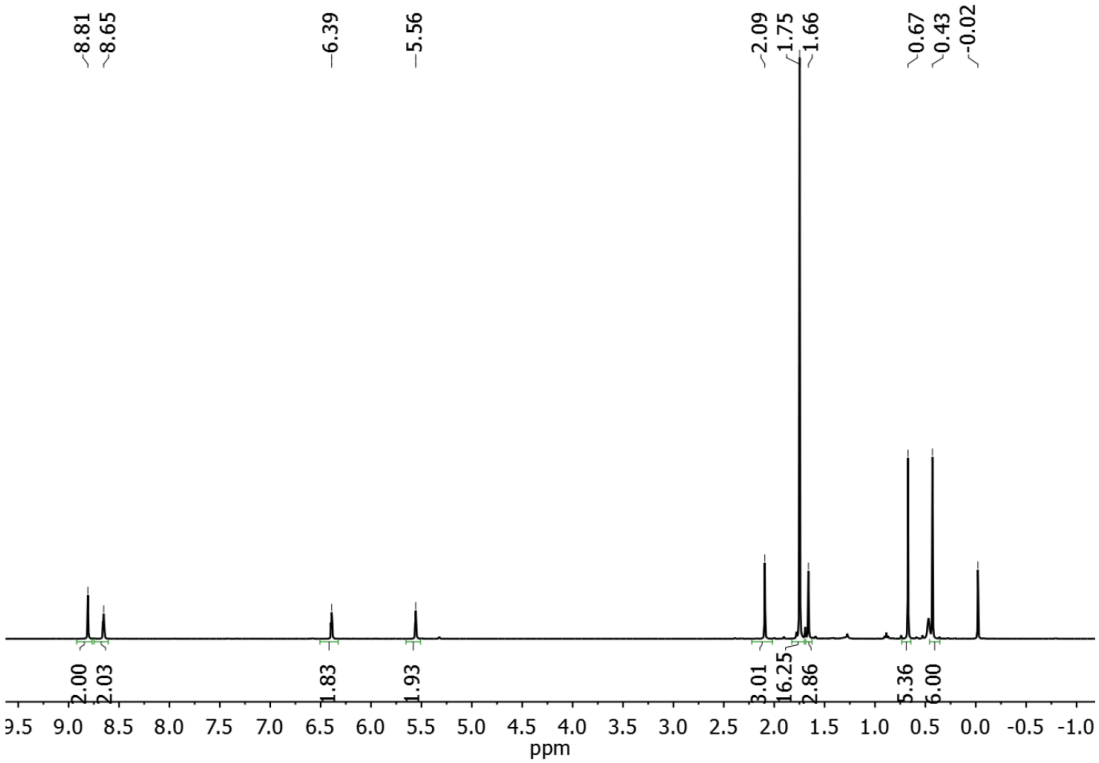

Figure 1.45. ^{1}H NMR spectrum of ***meso*-7** in CD_2Cl_2.

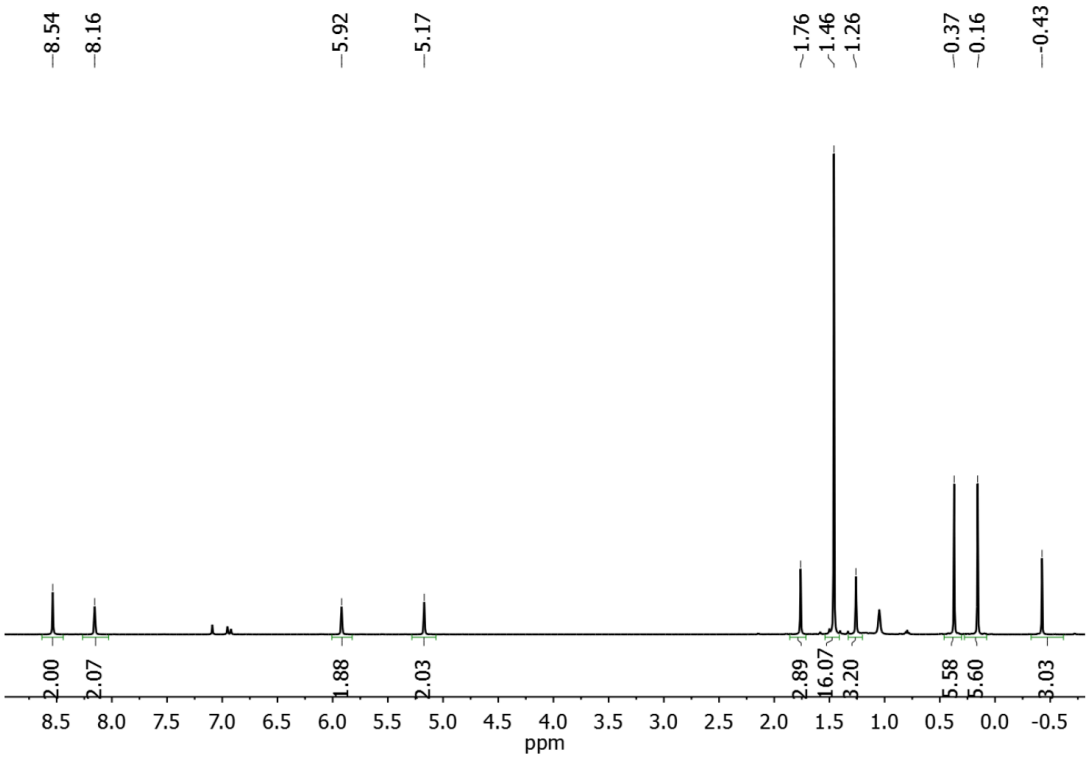

Figure 1.46. ^{1}H NMR spectrum of ***meso*-7** in C_6D_5Cl.

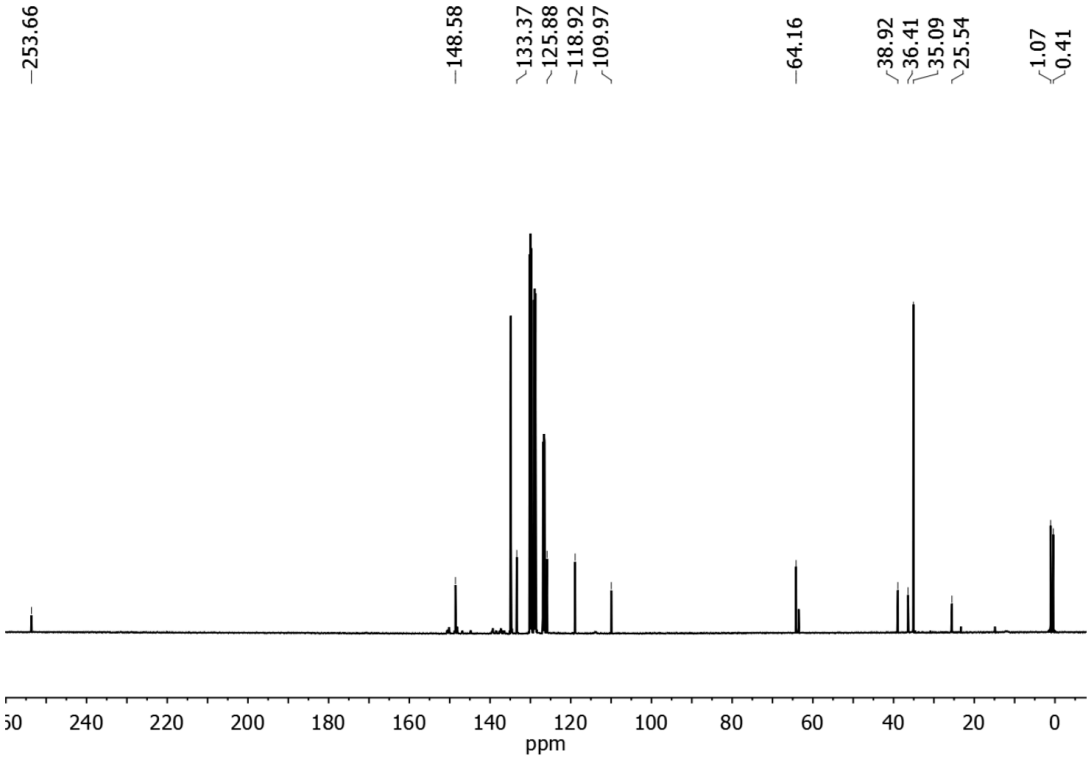

Figure 1.47. ^{13}C NMR spectrum of ***meso*-7** in C_6D_5Cl.

General procedure for ethylene or propylene homopolymerization. In the glove box, a 350 mL oven-dried heavy walled glass reactor equipped with stir bar was loaded with 10 μmol metal catalyst ([Catalyst] = 10 μmol of **Ti**; 5 μmol of ***rac*-3**; 5 μmol of ***meso*-3**), 1.2 equivalents of $B(C_6F_5)_3$ or $Ph_3C^+B(C_6F_5)_4^-$ per Ti metal equivalent, and 50 mL toluene. The glass reactor was then interfaced to a high pressure line and the solution was degassed by freeze-pump-thaw cycles. The solution was then brought to room temperature using an external water bath. The reactor was then charged with 1 atm of ethylene or propene. After desired reaction time, the reactor was vented and 5 mL of acidified methanol was syringed in. The contents of the polymerization vessel were poured into a large volume of methanol, and the polymer flakes precipitated out. The resulting polymer was filtered off, washed with methanol, and then dried under vacuum overnight.

General procedure for 1-octene homopolymerizations. In the glove box, an oven-dried 350 mL heavy walled glass reactor equipped with stir bar was loaded 5.60 g 1-octene and 20 mL toluene. In a separate vial, 5 μmol metal catalyst ([Catalyst] = 10 μmol of **Ti**; 5 μmol of ***rac*-3**; 5 μmol of ***meso*-3**) and 1.2 equivalents of $B(C_6F_5)_3$ or $Ph_3C^+B(C_6F_5)_4^-$ per Ti metal equivalent were dissolved in 1 mL toluene. The glass reactor was then interfaced to a high pressure line and the solution was degassed by freeze-pump-thaw cycles. The solution was then brought to room temperature using an external water bath. The catalyst/cocatalyst solution was syringed in under argon. After desired time, the reactor was vented and 5 mL of acidified methanol was syringed in. The contents of the polymerization vessel were poured into a large volume of methanol, and the polymer precipitated out. The resulting polymer was isolated by decanting the solvent, and was then washed with methanol and dried under vacuum overnight.

General procedure for ethylene/α-olefin copolymerizations. In the glove box, a 350 mL oven-dried heavy walled glass reactor equipped with stir bar was loaded with the desired amount of

comonomer and 50 mL toluene. In a separate vial, 5 μmol metal catalyst ([Catalyst] = 10 μmol of **Ti**$_1$; 5 μmol of ***rac*-3**; 5 μmol of ***meso*-3**) and 1.2 equivalents of $Ph_3C^+B(C_6F_5)_4^-$ per Ti metal equivalent were dissolved in 1 mL toluene. The glass reactor was then interfaced to a high pressure line and the solution was degassed by freeze-pump-thaw cycles. The solution was then brought to room temperature using an external water bath. The reactor was then charged with 1 atm of ethylene and the catalyst/cocatalyst solution was syringed in. After desired time, the reactor was vented and 5 mL of acidified methanol was syringed in. The contents of the polymerization vessel were poured into a large volume of methanol, and the polymer flakes precipitated out. The resulting polymer was filtered off, washed with methanol, and then dried under vacuum overnight.

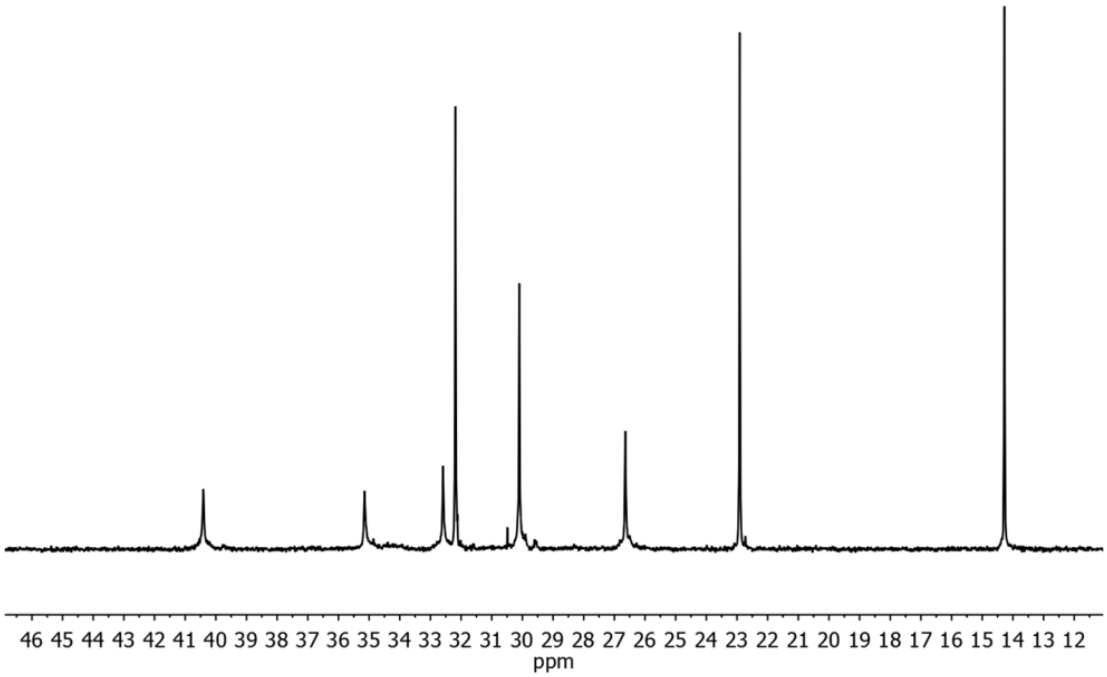

Figure 1.48. ^{13}C NMR of polymer generated by 1-octene homopolymerization with ***meso*-3** with $B(C_6F_5)_3$ (Table 1.3, entry 3, 100 MHz in 1,1,2,2 tetrachloroethane-d_2 at 120 °C).

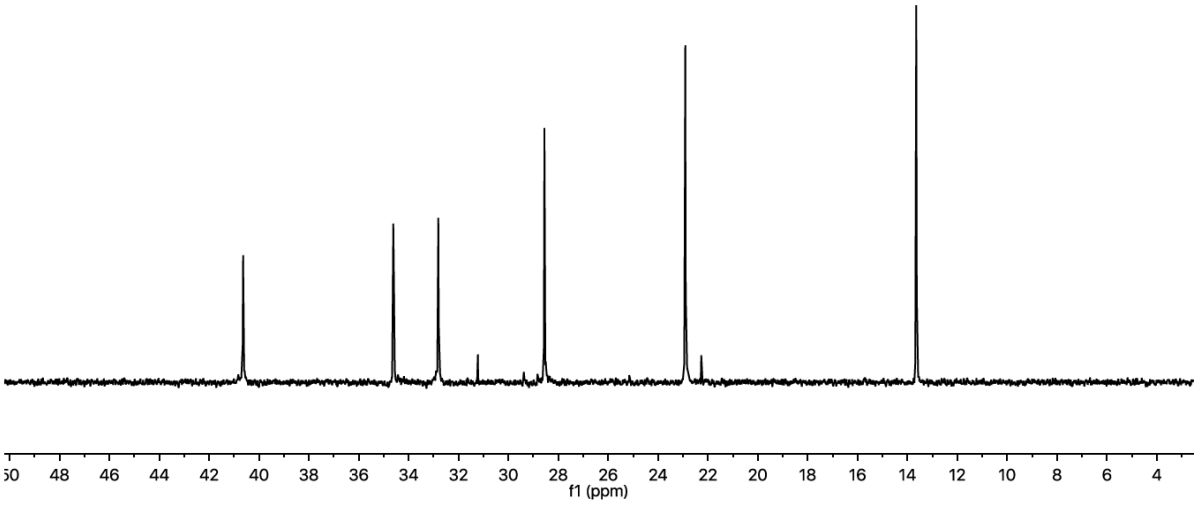

Figure 1.49. ^{13}C NMR of polymer generated by 1-hexene homopolymerization with ***meso*-3** with $B(C_6F_5)_3$ (100 MHz in 1,1,2,2 tetrachloroethane-d_2 at 120 °C).

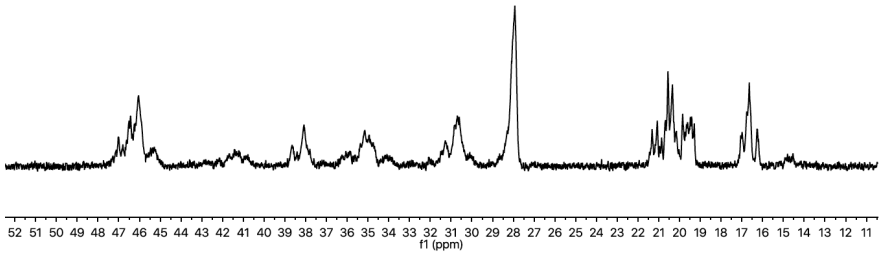

Figure 1.50. ^{13}C NMR of polymer generated by propylene polymerization with **Ti**$_1$ with $Ph_3C^+B(C_6F_5)_4^-$ (Table 1.2 entry 1, 100 MHz in 1,1,2,2-tetrachloroethane-d_2 at 120 °C).

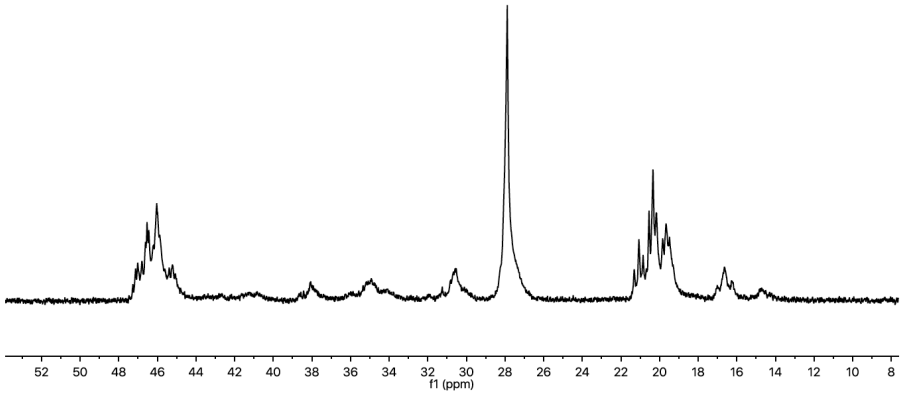

Figure 1.51. ^{13}C NMR of polymer generated by propylene polymerization with ***rac*-3** with $Ph_3C^+B(C_6F_5)_4^-$ (Table 1.2 entry 2, 100 MHz in 1,1,2,2-tetrachloroethane-d_2 at 120 °C).

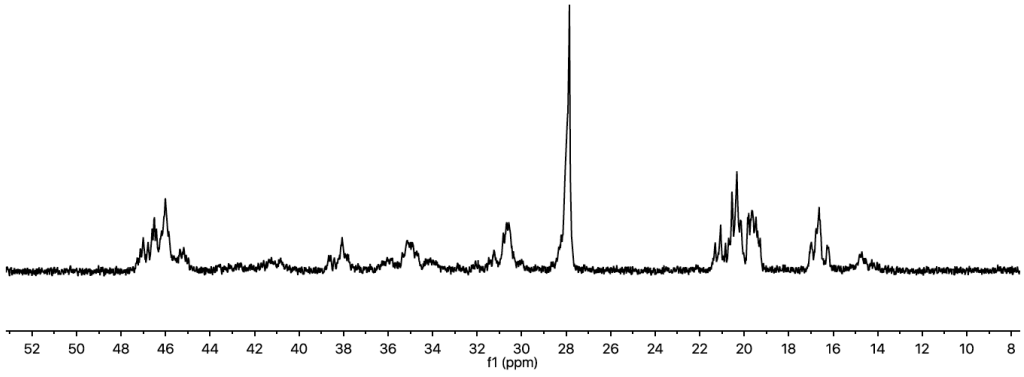

Figure 1.52. ^{13}C NMR of polymer generated by propylene polymerization with ***meso*-3** with $Ph_3C^+B(C_6F_5)_4^-$ (Table 1.2 entry 3, 100 MHz in 1,1,2,2-tetrachloroethane-d_2 at 120 °C).

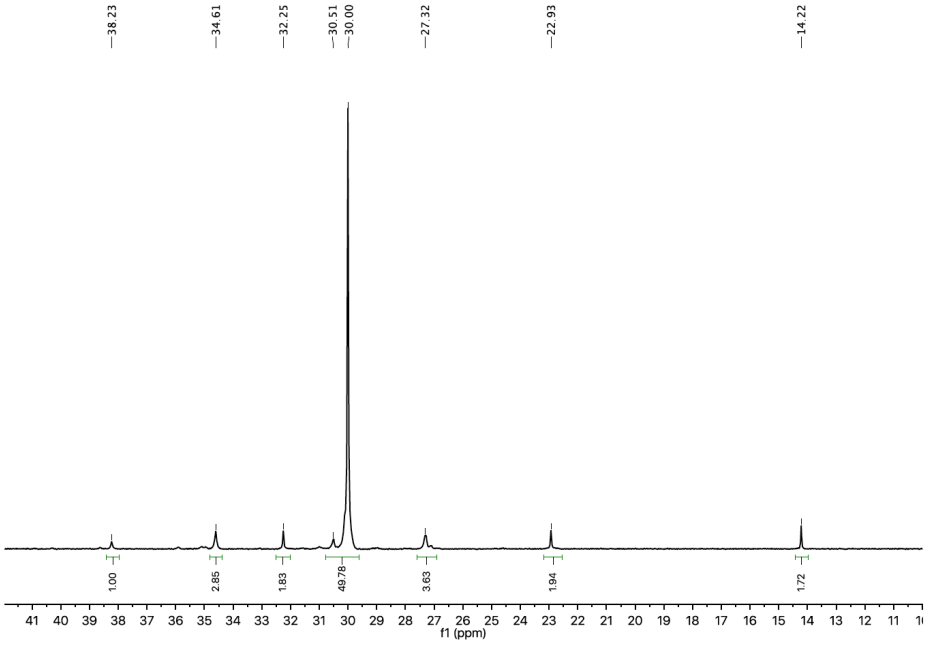

Figure 1.53. ^{13}C NMR of polymer generated by the copolymerization of ethylene and 1-octene with **Ti**$_1$ with $Ph_3C^+B(C_6F_5)_4^-$ (Table 1.4 entry 1, 100 MHz in 1,1,2,2-tetrachloroethane-d_2 at 120 °C).

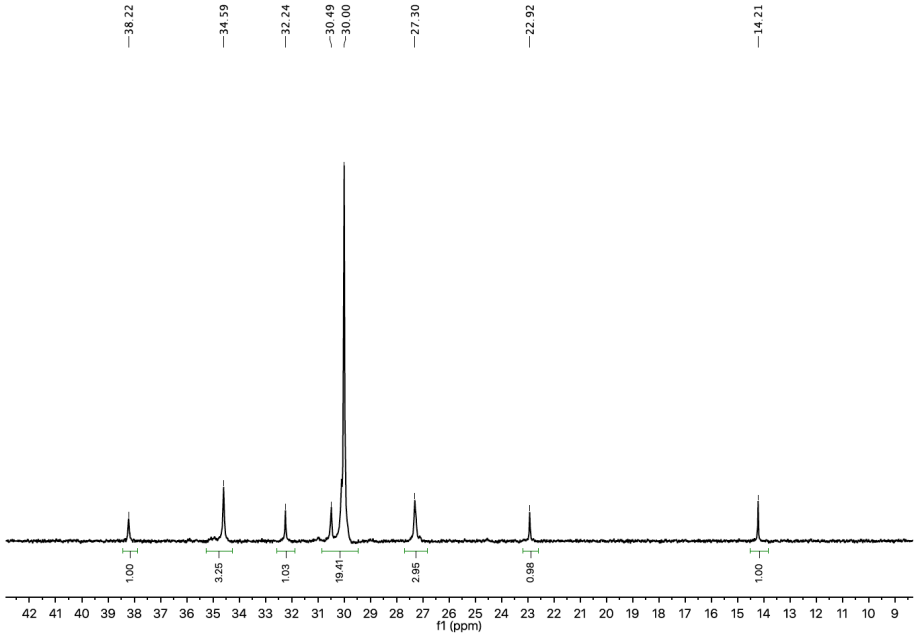

Figure 1.54. ^{13}C NMR of polymer generated by the copolymerization of ethylene and 1-octene with ***rac*-3** with $Ph_3C^+B(C_6F_5)_4^-$ (Table 1.4 entry 3, 100 MHz in 1,1,2,2-tetrachloroethane-d_2 at 120 °C).

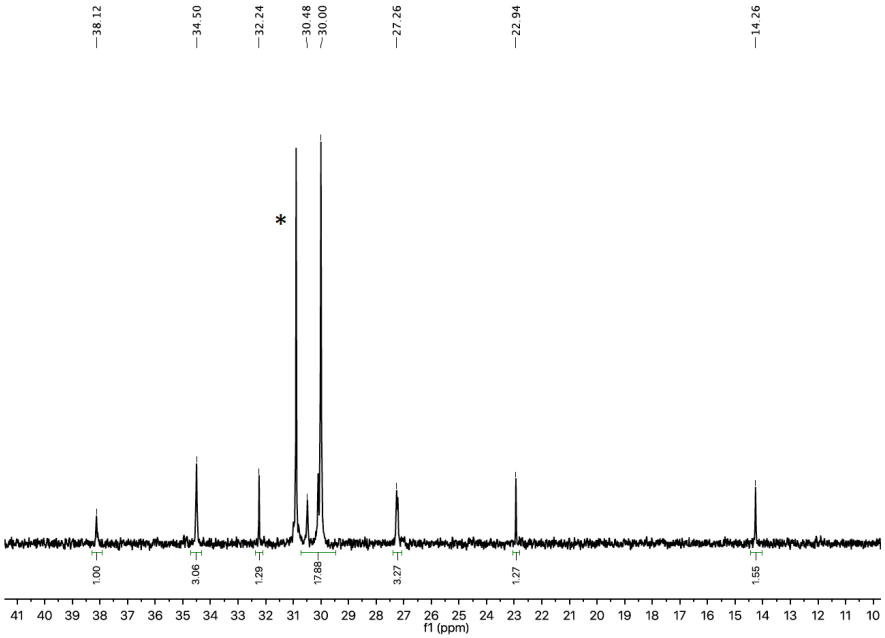

Figure 1.55. ^{13}C NMR of polymer generated by the copolymerization of ethylene and 1-octene with ***meso*-5** with $Ph_3C^+B(C_6F_5)_4^-$ (Table 1.4 entry 5, 100 MHz in 1,1,2,2-tetrachloroethane-d_2 at 120 °C). [*Additional peak caused by acetone.]

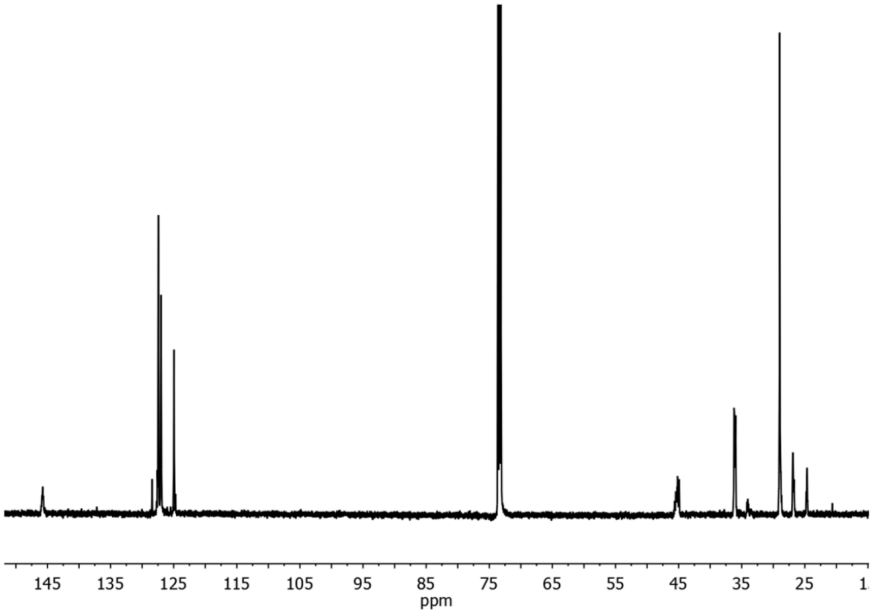

Figure 1.56. ^{13}C NMR of polymer generated by the copolymerization of ethylene and styrene with **Ti**$_1$ with $Ph_3C^+B(C_6F_5)_4^-$ (Table 1.5 entry 2, 100 MHz in 1,1,2,2-tetrachloroethane-d_2 at 120 °C).

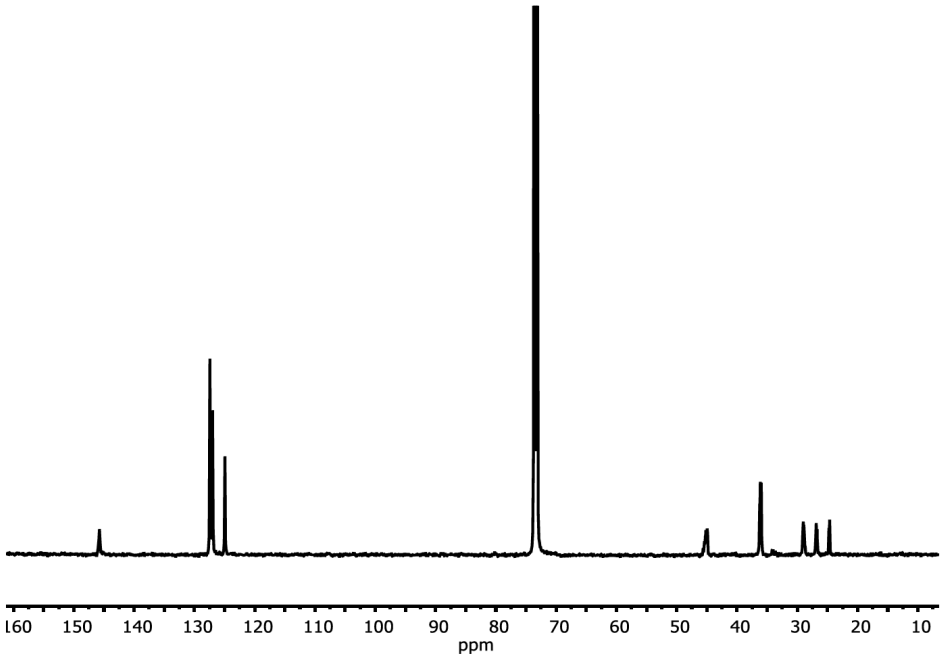

Figure 1.57. ^{13}C NMR of polymer generated by the copolymerization of ethylene and styrene with ***rac*-5** with $Ph_3C^+B(C_6F_5)_4^-$ (Table 1.5 entry 3, 100 MHz in 1,1,2,2-tetrachloroethane-d_2 at 120 °C).

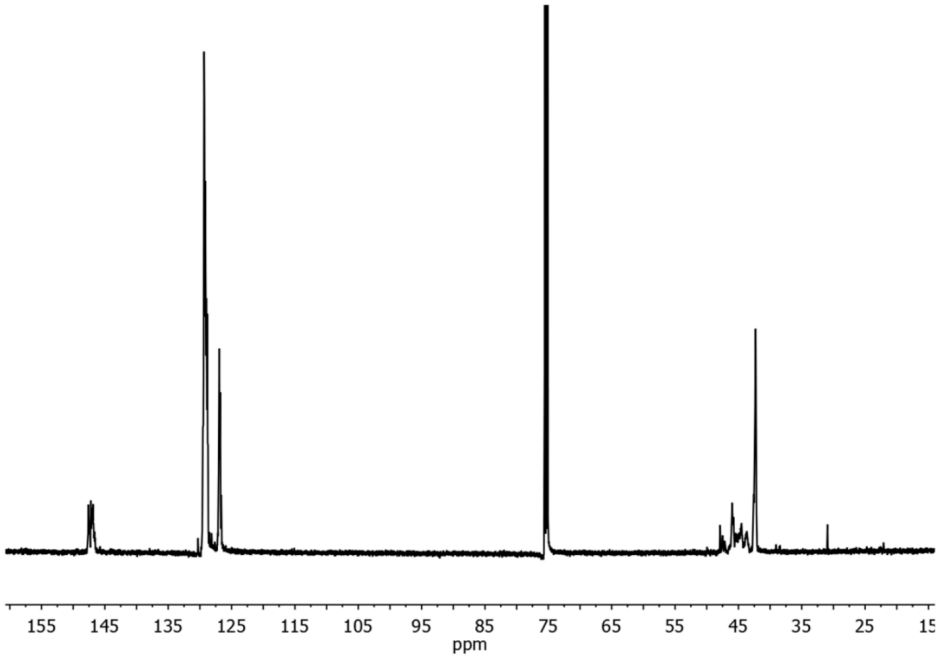

Figure 1.58. ^{13}C NMR of polymer generated by the copolymerization of ethylene and styrene with ***meso*-3** with $Ph_3C^+B(C_6F_5)_4^-$ (Table 1.5 entry 4, 100 MHz in 1,1,2,2-tetrachloroethane-d_2 at 120 °C).

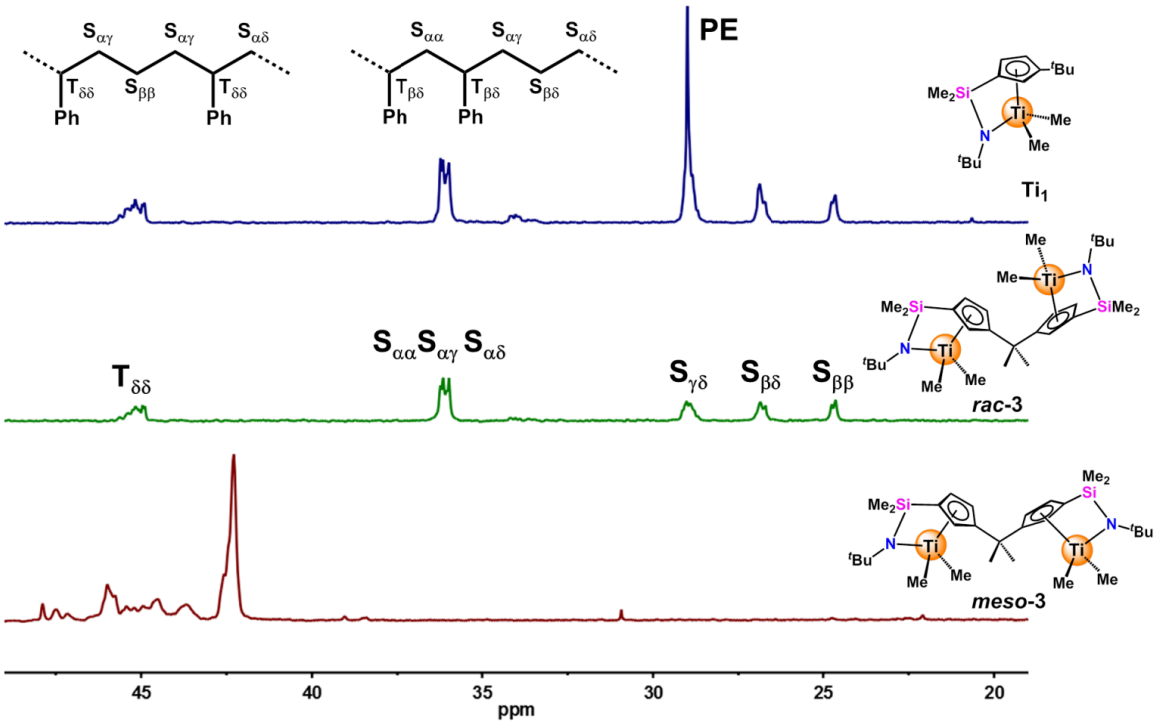

Figure 1.59. ^{13}C NMR spectra (100 MHz in 1,1,2,2-tetrachloroethane-d_2 at 120 °C) of the poly(ethylene-*co*-styrene) samples from Table 1.5, entries 2-4.

X-ray Data Collection, Structure Solution, and Refinement. Single crystals of ***meso*-2**, ***rac*-2**, ***meso*-5**, ***rac*-5** and ***meso*-7** were crystallized from toluene at -40 °C, ***rac*-3**, ***rac*-4** and ***meso*-3** were crystallized from pentanes at -40 °C, ***rac*-5-Cl**$_3$ was crystallized from CH_2Cl_2/toluene/pentane. Crystals were mounted in inert oil in glovebox, and transferred to the cold gas stream of a Bruker Kappa APEX CCD area detector equipped with a CuK_α microsource with Quazar optics or a MoK_α source with crd mx optics. The crystal was maintained at 100.01 K during data collection. Crystallographic and experimental details of the structure determination are summarized in Table S1. Molecular structure plots of ***rac*-2**, ***meso*-2**, ***rac*-3**, ***meso*-3**, ***rac*-4**, ***meso*-5**, ***rac*-5**, ***rac*-5-Cl**$_3$ and ***meso*-7** are depicted in Figure 1A, 1B, 3A, 5A, 5B, 7, 8 and S1, S4, and bonds and angles are shown in Table S2-S19. An empirical correction for absorption was made. Using Olex2,[198] the structure was solved with the XS[199] structure solution program using Patterson Method and refined with the ShelXL refinement package using full-matrix least-squares procedures (based on F_o^2) first with isotropic thermal parameters and then with anisotropic thermal parameters in the last cycles of refinement for all the non-hydrogen atoms. The hydrogen atoms were introduced into the geometrically calculated positions and refined riding on the corresponding parent atoms. Similar distances were refined for the disordered carbon and sulfur atoms. Rigid bond restraints were imposed on the displacement parameters as well as restraints on similar amplitudes separated by less than 1.7 Å on the disordered methyl group. Group anisotropic displacement parameters were refined for the remaining disordered atoms.

Table 1.6. Crystal data and structure refinement for ***rac*-2**, ***meso*-2**, ***rac*-3**, ***meso*-3, and *rac*-4**

Complexes	***rac*-2**	***meso*-2**	***rac*-3**	***meso*-3**	***rac*-4**
Empirical formula	$C_{33}H_{66}N_6Si_2Ti_2$	$C_{33}H_{66}N_6Si_2Ti_2$	$C_{29}H_{54}N_2Si_2Ti_2$	$C_{29}H_{54}N_2Si_2Ti_2$	$C_{27}H_{46}N_2Si_2Ti_2$
Formula weight	698.89	698.89	582.72	582.72	550.64
Temperature / K	100.07	100.0	100.0	100.0	99.99
Crystal system	monoclinic	orthorhombic	triclinic	triclinic	Triclinic
Space group	C2/c	Pbcn	P-1	P-1	P-1
a / Å	30.358(6)	23.9269(4)	12.895(3)	6.7655(14)	13.3885(7)
b / Å	8.8407(18)	16.5580(3)	15.661(3)	14.973(3)	14.2509(7)
c / Å	17.003(3)	19.6377(4)	17.229(3)	16.877(3)	15.9419(8)
α/°	90	90	73.24(3)	74.86(3)	101.559(3)
β/°	121.86(3)	90	79.09(3)	79.12(3)	92.474(3)
γ/°	90	90	79.33(3)	85.35(3)	94.551(3)
Volume / Å^3	3875.9(17)	7780.1(2)	3239.6(13)	1619.8(6)	2965.2(3)
Z	4	8	4	2	4
ϱ_{calc} / mg mm^{-3}	1.198	1.193	1.195	1.195	1.233
μ / mm^{-1}	0.503	0.502	0.586	0.586	5.469
F(000)	1512.0	3024.0	1256.0	628.0	1176.0
2Θ range for data collection	4.87 to 52.734°	4.684 to 52.744°	2.494 to 52.82°	3.286 to 44.07°	5.668 to 122.646°
Index ranges	-19 ≤ h ≤ 37, -11 ≤ k ≤ 11, -20 ≤ l ≤ 20	-29 ≤ h ≤ 29, -20 ≤ k ≤ 20, -24 ≤ l ≤ 24	-15 ≤ h ≤ 16, -18 ≤ k ≤ 19, 0 ≤ l ≤ 21	-6 ≤ h ≤ 7, -14 ≤ k ≤ 15, 0 ≤ l ≤ 17	-14 ≤ h ≤ 15, -16 ≤ k ≤ 16, -17 ≤ l ≤ 18
Reflections collected	6518	44093	13192	3919	22146
Independent reflections	3685	7960	13192	3919	9013
Data/restraints/parameters	3685/82/205	7960/0/408	13192/888/665	3919/360/334	9013/828/641
Goodness-of-fit on F^2	1.053	1.041	1.073	1.072	1.048
Final R indexes [I>2σ (I)]	R_1 = 0.0390, wR_2 = 0.1026	R_1 = 0.0355, wR_2 = 0.0926	R_1 = 0.0749, wR_2 = 0.1678	R_1 = 0.0623, wR_2 = 0.1689	R_1 = 0.0577, wR_2 = 0.1464
Final R indexes [all data]	R_1 = 0.0457, wR_2 = 0.1062	R_1 = 0.0488, wR_2 = 0.0970	R_1 = 0.1103, wR_2 = 0.1896	R_1 = 0.0726, wR_2 = 0.1793	R_1 = 0.0710, wR_2 = 0.1565
Largest diff. peak/hole / e Å^{-3}	0.49/-0.77	0.40/-0.88	0.85/-0.63	0.87/-0.59	2.86/-0.43

$R_1 = ||F_o| - |F_c|| / \Sigma |F_o|$; $wR_2 = [\sum [w(F_o^2 - F_c^2)^2] / \sum [w(F_o^2)^2]]$.

Table 1.7. Crystal data and structure refinement for ***meso*-5**, ***rac*-5**, ***rac*-5-Cl$_3$ and *meso*-7.**

Complexes	***rac*-5**	***rac*-5-Cl$_3$**	***meso-5***	***meso-7***
Empirical formula	$C_{51}H_{47}BF_{20}N_2Si_2Ti_2$	$C_{49}H_{42}BCl_3F_{20}N_2Si_2Ti_2$	$C_{51}H_{47}BF_{20}N_2Si_2Ti_2$	$C_{52}H_{52.5}BF_{15}N_3Si_2Ti_2$
Formula weight	1230.69	1307.98	1230.69	1167.26
Temperature / K	100.0	100.0	100.0	100.0
Crystal system	triclinic	triclinic	monoclinic	triclinic
Space group	P-1	P-1	I2/a	P-1
a / Å	11.9472(5)	11.321(2)	43.260(9)	11.824(2)
b / Å	14.2295(7)	12.804(3)	11.917(2)	13.888(3)
c / Å	17.3352(8)	19.584(4)	44.131(9)	16.917(3)
α/°	69.845(3)	76.43(3)	90	96.58(3)
β/°	86.819(3)	86.19(3)	111.89(3)	106.48(3)
γ/°	73.322(3)	79.42(3)	90	95.63(3)
Volume / Å^3	2647.1(2)	2711.8(10)	21110(8)	2621.3(10)
Z	2	2	16	2
ϱ_{calc} / mg mm^{-3}	1.544	1.602	1.548	1.479
μ / mm^{-1}	3.982	0.593	0.457	0.443
F(000)	1248.0	1316.0	9968.0	1195.0
2Θ range for data collection	7.172 to 108.61°	3.322 to 41.708°	1.988 to 49.442°	2.538 to 48.272°
Index ranges	-12 ≤ h ≤ 12, -14 ≤ k ≤ 14, -17 ≤ l ≤ 18	-11 ≤ h ≤ 11, -12 ≤ k ≤ 12, 0 ≤ l ≤ 19	-50 ≤ h ≤ 47, 0 ≤ k ≤ 14, 0 ≤ l ≤ 51	-13 ≤ h ≤ 12, -15 ≤ k ≤ 15, 0 ≤ l ≤ 19
Reflections collected	14208	5676	17715	8127
Independent reflections	5866	5676	17715	8127
Data/restraints/parameters	5866/735/761	5676/735/726	17715/1449/1431	8127/686/733
Goodness-of-fit on F	1.015	1.064	1.107	1.026
Final R indexes [I>2σ (I)]	R_1 = 0.0710, wR_2 = 0.1648	R_1 = 0.0733, wR_2 = 0.1775	R_1 = 0.0356, wR_2 = 0.0906	R_1 = 0.0725, wR_2 = 0.1655
Final R indexes [all data]	R_1 = 0.1277, wR_2 = 0.1963	R_1 = 0.1113, wR_2 = 0.2053	R_1 = 0.0386, wR_2 = 0.0921	R_1 = 0.1474, wR_2 = 0.2001
Largest diff. peak/hole / e Å^{-3}	1.70/-0.72	0.66/-0.42	0.64/-0.68	0.75/-0.62

$R_1 = ||F_o| - |F_c|| / \Sigma |F_o|$; $wR_2 = [\sum [w(F_o^2 - F_c^2)^2] / \sum [w(F_o^2)^2]]$.

Computational details. Calculations were performed adopting the PBE formalism for both exchange and correlation functionals.[200] The effective core potential of Hay and Wadt (LANL2DZ)[201] which explicitly treats 3s, 3p, 4s, and 3d electrons was employed for the Ti atoms. The standard all-electron 6-31G** basis was used for all remaining atoms.[202] Molecular geometry optimizations of stationary points were carried out without symmetry constraints and used analytical gradient techniques. In the present modeling, the effect of the solvent and counteranions were omitted in calculations due to the size of the catalytic system. Optimization was performed using NWCHEM[203] code on Linux cluster systems. NBO analysis[204] was evaluated using Gaussian 09 code.[205]

Table 1.8. Geometrical parameters (Å and deg) of the ***rac*-4**, the naked cation ***meso*-5** and ***rac*-5** optimized structures.

	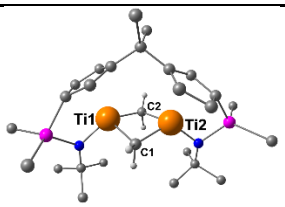 ***rac*-4**	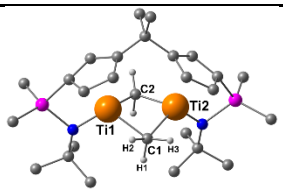 ***meso*-5**	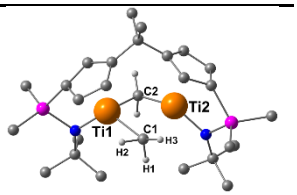 ***rac*-5**
Ti1-Ti2	3.01	3.03	3.01
Ti1-C1	2.12	2.25	2.21
Ti2-C1	2.05	2.25	2.32
Ti1-C2	2.04	2.06	2.08
Ti2-C2	2.14	2.06	2.04
C1-H2		1.12	1.12
C1-H3		1.12	1.11
Ti1-C1-H2		78.9	71.4
Ti2-C1-H3		78.2	86.6
$Ti1\text{-}C1\text{-}(C1H_2)_{plane}$	53.2		
$Ti2\text{-}C1\text{-}(C1H_2)_{plane}$	42.5		
$Ti1\text{-}C2\text{-}(C2H_2)_{plane}$	40.1	48.8	53.6
$Ti2\text{-}C2\text{-}(C2H_2)_{plane}$	56.9	51.5	44.5

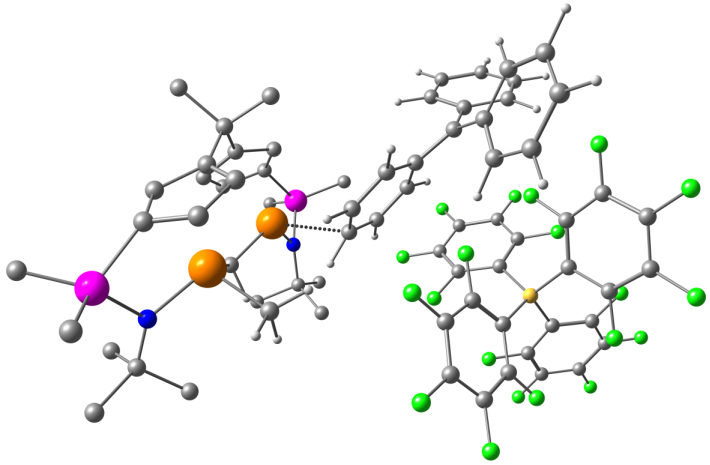

Figure 1.60. DFT optimized structure of ***rac*-6**. Ti, orange; Si, pink; N, blue; C, gray.

A η^1-coordination of the phenyl group if CPh3+ to the Ti was found. The coordination is evidenced by a slight C-H elongation compared to the other phenyl C-H bonds (1.10 Å *vs* 1.09 Å). Moreover, the involved C-H bond lies out of the phenyl ring plane of about 15°.

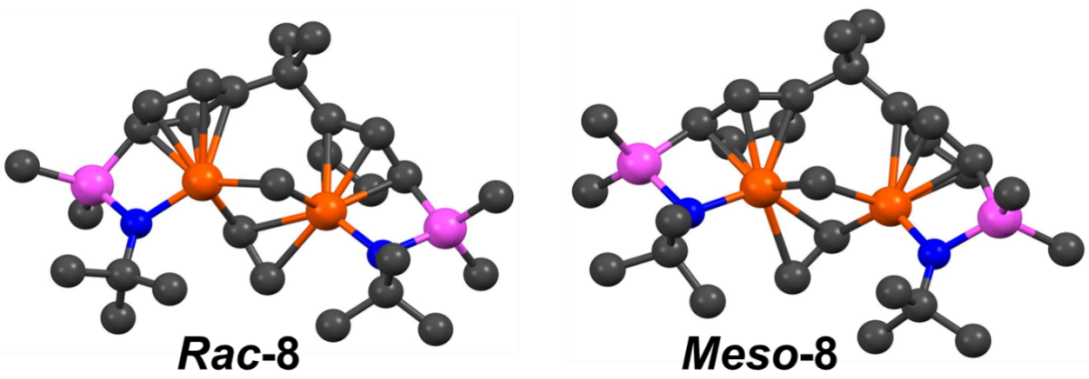

Figure 1.61. DFT optimized structures of ***rac*-8** and ***meso*-8**. Ti, orange; Si, pink; N, blue; C, dark grey.

Acknowledgements

This material is based upon work supported by the U.S. Department of Energy, Office of Science, Office of Basic Energy Sciences under Award Number DOE DE-FG02-03-ER154757 for C-C bond-forming catalysis and by NSF CHE-1464488 for cooperative catalyst design whose support is gratefully acknowledged. The purchase of the NMR instrumentation at IMSERC at Northwestern University was supported by NSF (CHE-1048773). Computational resources supporting this work were provided by the Northwestern University Quest High Performance Computing cluster and CINECA award N. HP10CBHAYD 2014 under the ISCRA initiative. We also thank Albemarle Corp. for the generous gifts of $Ph_3C^+B(C_6F_5)_4^-$ and $B(C_6F_5)_3$.

CHAPTER 2

Polymerization Behavior and Monomer-Dependent Reorganization of a Bimetallic Salphen Organotitanium Catalyst

Adapted from:

Invergo, A. M.; Liu, S.; Dicken, R. D.; Mouat, A. R.; Delferro, M.; Lohr, T. L.; Marks, T. J. How Close is too Close? Polymerization Behavior and Monomer Dependent Reorganization of a Bimetallic Salphen Organotitanium Catalyst. *Organometallics*, **2018**, *Submitted*.

Abstract

The binuclear salphen Ti polymerization catalyst *N*,*N*'-1,2-phenylene-[salicylideneaminatoTi(Cp*)Me_2]$_2$ (**2**) is synthesized by reaction of salphen-H_2 with Cp*$TiMe_3$. Mononuclear [*N*-(2,6-diisopropyl)phenyl(salicylideneaminato)]-Ti(Cp*)Me_2 (**1**) serves as a control. Activation studies with cocatalyst $Ph_3C^+B(C_6F_5)_4^-$ yield the cationic polymerization-inactive complex [*N*,*N*'-1,2-phenylene(salicylideneaminato)Ti(Cp*)]$^+B(C_6F_5)_4^-$ (**4**) and polymerization-active Cp*$TiMe_2^+B(C_6F_5)_4^-$. Polymerization studies comparing **2** with **Cp*TiMe$_3$** suggest that within the catalytic timeframe, while **2** retains bimetallic character under both ambient conditions and under an ethylene atmosphere, it rapidly decomposes to **4** and Cp*$TiMe_2^+$ in the presence of 1-hexene. These monomer dependent reorganization results highlight the importance of olefin polymerization activation mechanistic studies while providing insight for improved bimetallic catalyst design.

Introduction

In optimum scenarios for enzyme catalysis, proximate multi-center active site – substrate interactions play an essential role in turnover frequency and selective activation/conversion of otherwise challenging substrates.[1-6] This is due to high local reagent concentrations, conformational control, and preorganization of reactive species.[7,8] Using these biocatalysts as a conceptual model, intensive efforts have been devoted to mimicking enzymatic function to discover unique and/or more efficient abiotic catalytic processes.[9-19]

In the area of homogeneous olefin polymerization catalysis, bimetallic assemblies have been shown to exhibit distinctive metal···metal cooperative effects compared with their monometallic analogues in terms of how various monomers are enchained.[20-23] In previous work

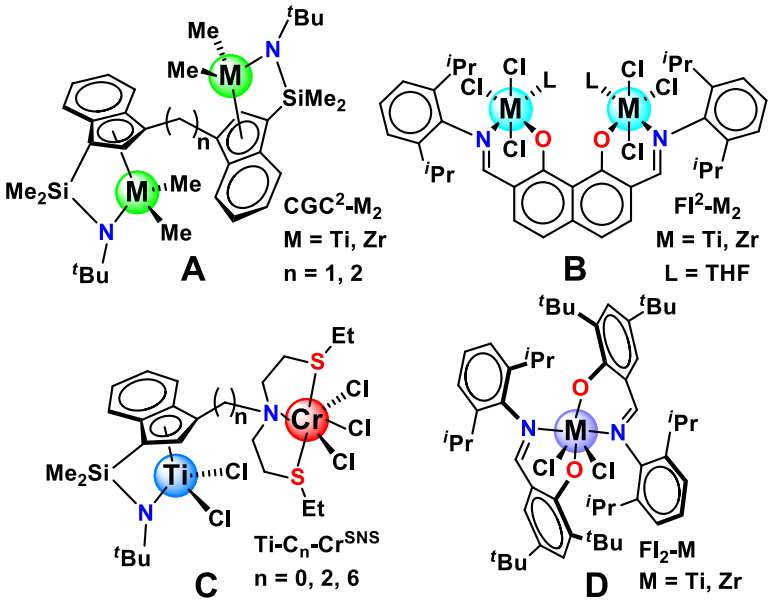

Chart 2.1. Examples of variable nuclearity polymerization catalysts.

involving group IV metal centers, we identified these cooperative effects in covalently linked homobimetallic constrained geometry (**C_n-CGC^2-M_2**, M = Ti, Zr; n = 1, 2; Chart 2.1, A),[24-29] phenoxy-imine (**FI^2-M_2**, M = Ti, Zr; Chart 2.1, B),[30,31] pyridylamido (M = Hf),[32,33] and heterobimetallic **Ti-C_n-Cr** (n = 0, 2, 6; Chart 2.1, C) polymerization catalysts.[34,35] The bimetallic centers exhibit pronounced nuclearity effects such as enhanced product polymer branching, tacticity,[36,37] a-olefin comonomer enchainment selectivity,[38,39] and higher M_n/M_w vs their mononuclear counterparts. Qualitatively, we have observed that the magnitude of these cooperative effects scales inversely with metal···metal distance, thus resulting in a push to design bimetallic catalysts with shorter intermetallic separation. However, despite these unusual and potentially useful effects, binuclear catalysts often exhibit lower activity than related mononuclear catalysts, often ascribed to steric congestion arising from the proximal bimetallic ligand scaffold and second metal, which inhibits access to the catalytic centers.[21,30,34,35] Naturally, the intriguing question arises as to whether it would be possible to synthesize a bimetallic catalyst that could enhance desirable polymer properties while still maintaining a significant level of activity relative to a monometallic control. Phenoxy-imine (FI) ligand-based catalysts (Chart 2.1, D) have demonstrated exceptionally high activities for ethylene polymerizations,[40] and the readily tunable nature of the FI ligand platform makes it a promising candidate for achieving cooperative effects as well as high activity in a bimetallic catalyst.

In past studies of bimetallic FI-like catalysts, moderately enhanced cooperative effects versus mononuclear controls were observed along with a significant fall in catalytic activity.[30] Thus, **FI^2-M_2** (M = Ti; Chart 2.1, B) exhibits an activity 1000x lower than **FI^2-M** (M = Ti; Chart 2.1, D)[40] under identical reaction conditions, which can be attributed to inhibition by the strongly bound THF ligands at each metal.[30] In marked contrast, catalysts combining both FI ligands with a Cp-

type moiety at the same metal center exhibit high polymerization activity with the production of high molecular mass polymers.[41-44] Here we report the synthesis, activation pathway, and polymerization characteristics of a bimetallic half-FI, half metallocene complex utilizing the salphen ligand and $Ti(Cp^*)Me_2$ moieties, where ligand re-organization, and subsequent polymerization activity, is highly dependent on the olefin monomer.

Results and Discussion

Ti complexes **1** and **2** were synthesized via the straightforward methodology outlined in Scheme 1. Thus, dropwise addition of a pentane solution of *N*-(salicylidene)-2,6-diisopropylaniline[45] to a pentane solution of Cp^*TiMe_3[46] at room temperature affords the monometallic complex **1** (Scheme 2.1A) in 78% yield with evolution of methane. Upon dropwise addition of salphen ligand to a solution of Cp^*TiMe_3 in toluene at room temperature, bimetallic complex **2** is formed rapidly in 84% yield, accompanied by evolution of methane (Scheme 2.1B). Note however that bimetallic complex **2** undergoes subsequent migratory methyl rearrangement[47] to generate asymmetric bimetallic complex **3** in solution for over the course of 48 hours (Scheme 2.1C).

Complexes **1-3** were characterized by standard analytical and spectroscopic techniques. ^1H NMR spectra (Figure 2.1) indicate that a room temperature complex **2** displays two magnetically equivalent Cp^*TiMe_2 (δ = 1.69 ppm for TiCp*, 0.70 ppm for TiMe) moieties, suggesting possible fluxional behavior in solution at 25°C. Based on 2D NOESY experiments, we believe the imino N atoms are bound to the Ti centers, due to an observed interaction between the Ti-*Me* and the C*H*=N protons. In contrast, complex **3** has non-equivalent Cp*Ti centers, with Cp* resonances at δ = 1.89 and 1.65 ppm, as well as TiMe resonances at δ = 1.46 and 0.87 ppm. The solid-state structure of **3**

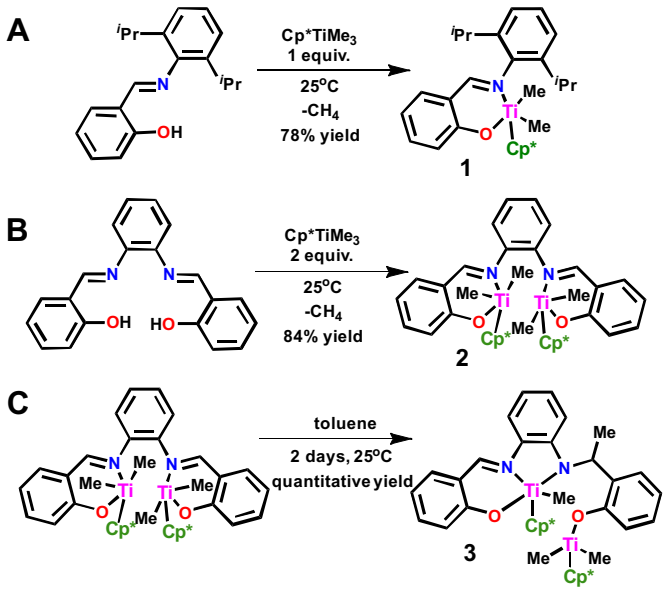

Scheme 2.1. Synthesis of monometallic **1** (A), bimetallic **2** (B), and asymmetric bimetallic **3** (C) salphen catalysts.

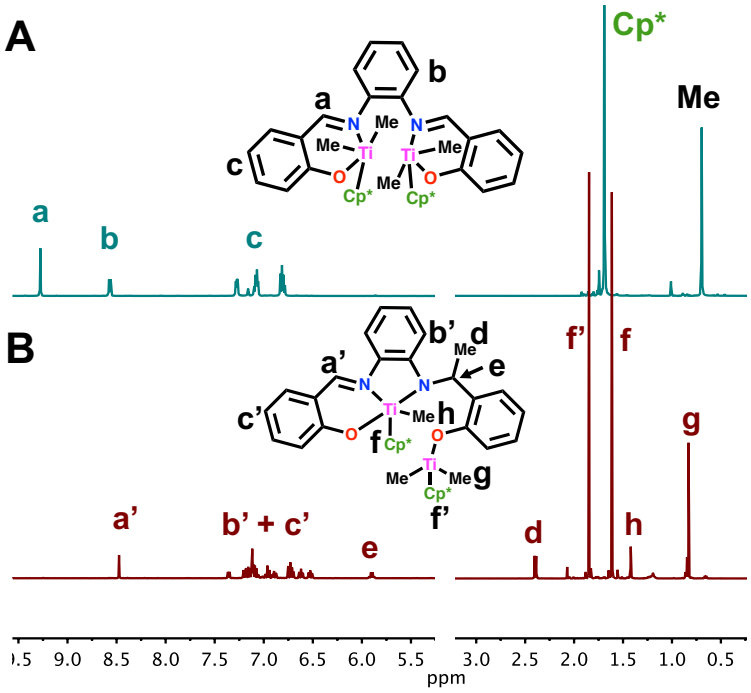

Figure 2.1. ^{1}H NMR spectra (500 MHz, C_6D_6, 25° C), of (A) bimetallic complex **2** and (B) bimetallic complex **3**.

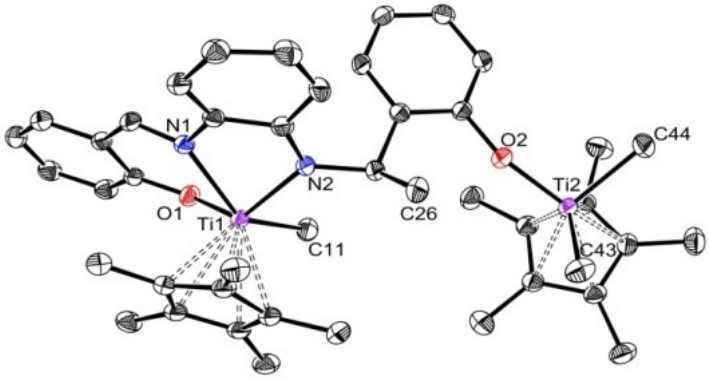

Figure 2.2. The structure of asymmetric bimetallic complex **3**. Thermal ellipsoids are drawn at the 50% probability level. Hydrogen atoms and two toluene molecules are omitted for clarity. Selected bond distances (Å): Ti1-C11, 2.167(2), Ti1-N2, 2.069(2), Ti2-C43, 2.102(3), Ti2-C44, 2.103(2).

reveals one five-coordinate and one four-coordinate Cp*Ti center (Figure 2.2). Note that in complex **3**, the methyl migration[48-50] from Ti to the imino carbon affords a new stereogenic center. However, there is no evidence from either ^{1}H NMR or ^{1}H-^{1}H NOESY spectroscopy for the formation of more than one diastereomer; therefore, the rearrangement of **2** leads quantitatively to diastereomerically pure **3**.

Due to the reactive nature of the Ti-Me bonds, activation of precatalyst **2** was studied using two equiv. of borate cocatalyst $Ph_3C^+B(C_6F_5)_4^-$. The activated species initially yielded complex NMR spectra in a variety of solvents at 25°C, suggesting the presence of one or more unstable reactive species. Insoluble crystals grow within several hours from a solution of borate and the precatalyst **2** in C_6D_6 and proved to be suitable for X-ray diffraction, which positively identified complex **4** as a structure generated during the activation process (Scheme 2.2). One Ti is bound by the salphen ligand in a tetradentate fashion while also retaining its ancillary Cp* ligand (Figure 2.3). This charged complex is paired with a borate counteranion and is inactive towards polymerization.

A plausible scenario is that $Cp^*TiMe_2^+$ $B(C_6F_5)_4^-$ moiety is eliminated with concomitant formation of salt **4** (Scheme 2). This $Cp^*TiMe_2^+$ species is known to be a highly active olefin polymerization catalyst and to afford complex ^{1}H NMR spectra due to the instability at room temperature.[51] A low temperature (-40°C) ^{1}H NMR study of the activation of 2 with 2 equiv. of $Ph_3C^+B(C_6F_5)_4^-$ in CD_2Cl_2, while yielding very complex spectra, does display a characteristic Ti-*Me* resonance at -0.22 ppm, which can be assigned to an organotitanium species. There are several examples of olefin polymerization precatalyst activation resulting in the formation of a separate, modified active species,[52,53] but to our knowledge, this is the first bimetallic complex that rearranges upon activation with a boron-based cocatalyst to release another completely distinct yet highly active polymerization catalyst. Furthermore, this complex proves to be highly instructive for future

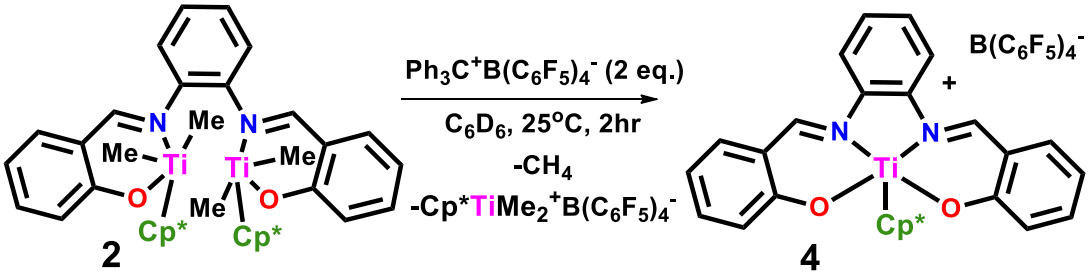

Scheme 2.2. Proposed formation of charged complex **4** by activation of bimetallic complex **2** with 2 equiv. $Ph_3C^+B(C_6F_5)_4^-$.

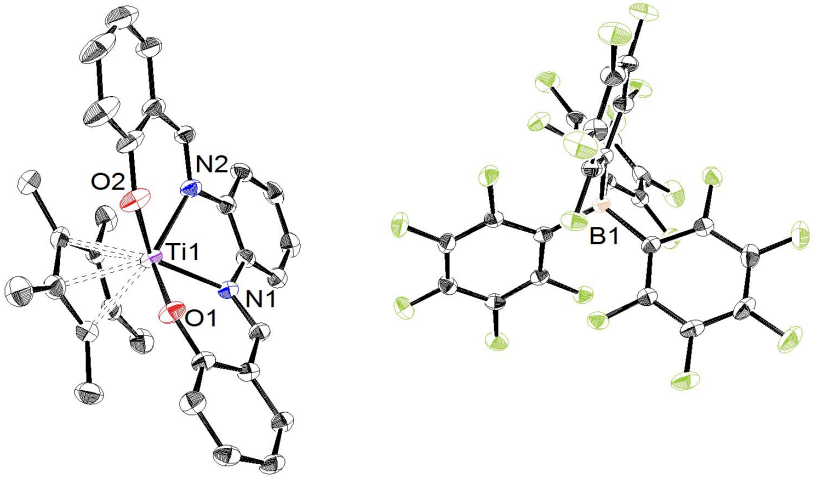

Figure 2.3. The structure of polymerization-inactive ion pair **4** generated during activation of **2** with 2 equivalents of $Ph_3C^+B(C_6F_5)_4^-$. Thermal ellipsoids are drawn at the 50% probability level. Hydrogen atoms are omitted for clarity. Selected bond distances (Å): Ti-O1, 1.8760(15), Ti-O2, 1.8843(16), Ti-N1, 2.1637(17), Ti-N2, 2.1676(19).

bimetallic catalyst design. While metal-metal proximity is undoubtedly a highly desirable characteristic, the present activation studies of **2** indicate that there may be a limit to how short an ideal metal-metal distance should be.

Because significant amounts of complex **4** do not appear to form until ~2 hours after activation of **2** (Scheme 2.2), the reactivity of complex **2** was further probed in polymerization experiments. Possible cooperative effects in ethylene and 1-hexene copolymerizations were investigated under rigorously anhydrous and anaerobic conditions, with attention paid to minimizing exotherm and mass transfer effects.[21,34,35,54] The presence of **3** was not observed within the timescale of the polymerization experiments (2-10 min). Activity differences between complex **2** activated with 1 (**2 + 1 B**) and 2 (**2 + 2 B**) equiv. of $Ph_3C^+B(C_6F_5)_4^-$ were investigated in all polymerizations. To determine whether $Cp^*TiMe_2^+$ $B(C_6F_5)_4^-$ species contributes to the observed polymerization behavior, additional experiments were also conducted under identical conditions using **Cp*TiMe$_3$** activated with 1 equiv. of $Ph_3C^+B(C_6F_5)_4^-$. These studies utilized 5 μmol of **Cp*TiMe$_3$** to mimic the release of one active Ti from **2**, run with 10 μmol Ti in polymerizations. Test polymerizations utilizing 5 μmol of crude **4** yielded no polymer, and experiments using 5 μmol each of **Cp*TiMe$_3$** and complex **4** gave the same results as **Cp*TiMe$_3$** alone, confirming that **4** is not active and exerts no influence over the observed catalytic behavior.

As can be seen in Table 2.1, broad, monomodal *Đ* values are obtained for the ethylene homopolymers produced by all catalysts, particularly for **Cp*TiMe$_3$** and monometallic **1**. The unstable catalyst formed by **Cp*TiMe$_3$** activation at room temperature is likely responsible for the broad dispersity value observed. Additionally, the rapid formation of polyethylene by **Cp*TiMe$_3$** and **2** greatly impedes reactor stirring. Mass-transfer limitations are known to result in broad *Đ* values, which may partially account for the obtained dispersities.[55] In the case of **1**, this effect is

Table 2.1. Ethylene Homopolymerization Data for Monometallic and Bimetallic Salphen Catalysts[a]

Entry	Catalyst	Equiv. of Cocatalyst	Polymer (g)	Activity[b] (PE)	M_n[c] (kg·mol^{-1})	$Đ$[c]
1	**1**	1.2	0.010	12.1	44.3	10.1
2	**2**	1.0	0.369	1107	110	9.1
3	**2**	2.4	0.253	759	177	8.2
4	**Cp*TiMe$_3$**	1.2	0.339	2043	89.4	16.6
5[d]	**FI^2-Ti$_2$**	2.4	0.083	8.3	66.1	4.5

[a]Polymerization conditions: [catalyst] = 5 μmol of **2**; 10 μmol of **1**; 5 μmol of **Cp*TiMe$_3$**; 48 mL toluene, 2 mL of fluorobenzene for catalyst/cocatalyst injection, at 25 °C, under constant 1 atm ethylene for 2 min. Entries performed in duplicate. [b]kg (PE)·mol^{-1} (Ti)·h^{-1}·atm^{-1}; [c]By GPC vs. polystyrene standards. [d]Results from reference.[30]

Table 2.2. Ethylene/1-hexene Copolymerization Data for Monometallic and Bimetallic Salphen Catalysts.[a]

Entry	Catalyst	Equiv. of Cocatalyst	PE (g)	Activity[b] (PE)	Comonomer Incorp. (%)[c]	M_n[d] (kg·mol^{-1})	$Đ$[d]
1	**1**	1.2	trace	-	-	-	-
2	**2**	1.0	0.498	1494	17.5	78.3	2.3
3	**2**	2.4	1.278	3834	18.2	98.3	3.7
4	**Cp*TiMe$_3$**	1.2	1.391	8346	16.5	97.5	4.1
5[e]	**FI^2-Ti$_2$**	2.4	0.045	4.5	9.4	19.4	3.9

[a]Polymerization conditions: [catalyst] = 5 μmol of **2**; 10 μmol of **1**; 5 μmol of **Cp*TiMe$_3$**; 0.1 M 1-hexene, 48 mL toluene, 2 mL of fluorobenzene for catalyst/cocatalyst injection, at 25 °C, under constant 1 atm ethylene for 2 min. Entries performed in duplicate. [b]kg (PE)·mol^{-1} (Ti)·h^{-1}·atm^{-1}; [c]By ^{13}C NMR.[56-58] [d]By GPC vs. polystyrene standards. [e]Results from reference.[30]

Table 2.3. 1-Hexene Homopolymerization Data for Monometallic and Bimetallic Salphen Catalysts.[a]

Entry	Catalyst	Equiv. of Cocatalyst	PE (g)	Activity[b] (PE)	% *mmmm*[c]	M_n[d] (kg·mol^{-1})	$Đ$[d]
1	**1**	1.2	trace	-	-	-	-
2	**2**	1.0	trace	-	-	-	-
3	**2**	2.4	0.377	226	13.9	7.19	3.5
4	**Cp*TiMe$_3$**	1.2	0.307	368	12.2	6.48	2.5

[a]Polymerization conditions: [catalyst]: 5 μmol of **2**; 10 μmol of **1**; 5 μmol of **Cp*TiMe$_3$**; 1.0 M 1-hexene, 23 mL toluene, 2 mL fluorobenzene for catalyst/cocatalyst addition, at 25 °C, for 10 min under static argon, no ethylene. Entries performed in duplicate. [b]kg (PE)·mol^{-1} (Ti)·h^{-1}·atm^{-1}; [c]By ^{13}C NMR.[59,60] [d]By GPC vs. polystyrene standards.

occasionally encountered in polymerizations catalyzed by mono-[41,44] or bis-FI-ligated group IV catalysts[61] and in multinuclear mixed ligand systems,[62] and is thought to reflect the fluxional nature of these complexes in solution.[63]

Note also that bimetallic **2**, activated with either 1.0 or 2.4 equiv. of the borate cocatalyst, produces similar amounts of polyolefin as that produced by **Cp*TiMe$_3$**. However, compared to **Cp*TiMe$_3$**, **2 + 2 B** produces polymer with nearly double the M_n, which suggests some level of bimetallic character under these polymerization conditions, as the higher M_n values suggest some cooperation between proximate metal centers.[22] As M_n values are known to scale as the net rate of chain propagation increases relative to all chain transfer/termination mechanism rates,[64] this may well indicate the presence of a second proximal active metal center stabilizing the growing polymer chain via agostic interactions with polymer C-H bonds, thereby suppressing chain termination relative to **2 + 1 B** and **Cp*TiMe$_3$**.[65] This suggests that the second equivalent of borate, along with the presence of ethylene, may help stabilize a bimetallic structure, at least during the timespan of the polymerization. Polymerizations conducted with **2 + 2 B** under 5 atm ethylene pressure for a duration of 1 min and otherwise identical conditions to those presented in Table 2.1 yield 0.265 g polyethylene with M_n = 135 kg/mol and $Đ$ = 10.1. This M_n is lower than that achieved by the same catalyst under 1 atm ethylene. The reason for this decrease is unclear, and could be attributed to either 1) the rapid formation of ethylene, which coats the catalyst and prevents further reaction, or to 2) the possibility that the bimetallic species rearranges under the higher monomer pressure to produce **Cp*TiMe$_3$** as an active species instead. The high M_n values of all polyolefin products precluded end group analysis via NMR. It is notable that bimetallic **2** produces polymers with higher M_n and at a higher level of activity than does **FI^2-Ti$_2$**.[30,31]

The monomodal GPC traces and the narrower *Đ* data obtained for the ethylene + 1-hexene copolymerizations, as well as for the sequential 1-hexene homopolymerizations (*vide infra*), are consistent with single-site processes (Table 2.2, entries 1-4).[64,66-68] It is worth noting that, apart from monometallic **1**, which displays vanishingly low activity for copolymerization, all the polymerization activities are higher than those for the ethylene homopolymerizations, which may indicate a significant "comonomer effect" (Table 2.1, entries 2-4 vs Table 2.2, entries 2-4).[37,69-72] Interestingly, the catalytic behavior for bimetallic **2** begins to mirror that of **Cp*TiMe$_3$** much more closely under copolymerization conditions. **Cp*TiMe$_3$** and bimetallic **2 + 2 B** produce very similar amounts of polymer, both more than double that produced by **2 + 1 B**. The comonomer selectivity of **2** in both activation scenarios is essentially equal to that of **Cp*TiMe$_3$** (18.2 vs 16.5%, respectively). Furthermore, bimetallic **2** and **Cp*TiMe$_3$** also produce polymers with nearly identical M_n values (98.3 vs 97.5 kg·mol^{-1}, respectively). These polymerization results suggest that in the presence of 1-hexene, the decomposition of bimetallic **2** to inactive complex **4** and $Cp^*TiMe_2^+B(C_6F_5)_4^-$ may occur much more rapidly than under either ambient or ethylene homopolymerization conditions.

To further pursue this hypothesis, the activity of the Ti salphen complexes towards 1-hexene homopolymerizations was investigated, with the results shown in Table 2.3 (entries 1-4). Again, bimetallic **2 + 2 B** and **Cp*TiMe$_3$** produce comparable amounts of polymer, while bimetallic **2 + 1 B** produces trace polymer and **1** is completely inactive within the time span of the polymerization. Importantly, the polymers produced by **2 + 2 B** and **Cp*TiMe$_3$** display very similar M_n values (7.19 vs 6.48 kg·mol^{-1} respectively), and the poly(1-hexene)s produced by both catalysts display a similar degree of atacticity by ^{12}C NMR.[59,60]

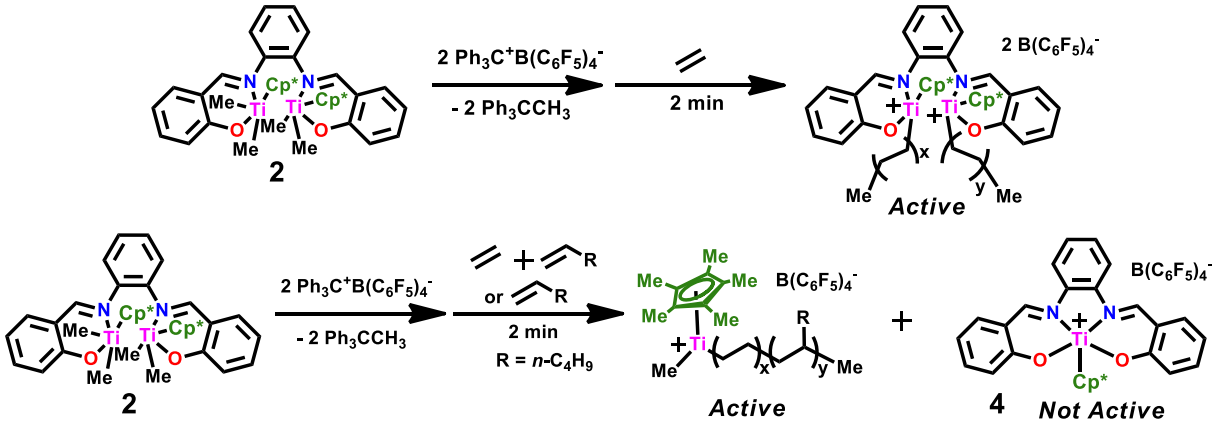

Scheme 2.3. Proposed monomer-dependent active species in ethylene and 1-hexene homopolymerizations and ethylene + 1-hexene copolymerizations mediated by activating precatalyst **2**.

Conclusions

In summary, the efficient synthesis and characterization of novel symmetrical bimetallic half-Fi, half-metallocene Ti-Me complex **2**, along with corresponding monometallic complex **1**, are reported. In solution, bimetallic **2** slowly rearranges to more stable asymmetric bimetallic complex **3** via methyl migration from Ti to the imino carbon. Considering the timescale of the polymerization experiments, this species is not considered to significantly influence the activity of **2** nor contribute to the observed polymerization characteristics. Bimetallic complex **2** decomposes in the presence of borate activator $Ph_3C^+B(C_6F_5)_4^-$ to produce polymerization-inactive complex **4** and, presumably, $Cp^*TiMe_2^+B(C_6F_5)_4^-$, which is polymerization-active. Polymerizations comparing bimetallic **2** with **Cp*TiMe$_3$** were carried out. The results suggest that, while the "bimetallic character" of **2** appears to persist for the duration of the ethylene homopolymerizations, $Cp^*TiMe_2^+B(C_6F_5)_4^-$ is the dominant active species in the presence of 1-hexene (Scheme 2.3). These findings indicate that there is to some degree a limit to the benefits of closer metal-metal distances in bimetallic olefin polymerization and serves as a reminder of the importance of undertaking detailed activation studies.

Experimental Section

Materials and Methods. All manipulations of air-sensitive materials were performed with rigorous exclusion of O_2 and moisture in oven-dried Schlenk-type glassware on a dual manifold Schlenk line, interfaced to a high-vacuum line (10^{-6} Torr), or in a Ar-filled MBraun glove box with a high-capacity recirculator (<1 ppm O_2). Argon (Airgas, pre-purified grade) was purified by passage through a supported MnO oxygen-removal column and an activated Davison 4A molecular sieve column. Ethylene (Airgas) was purified by passage through an oxygen/moisture trap (Matheson, model MTRP-0042-XX). Diethyl ether and tetrahydrofuran were distilled from

Na/benzophenone ketyl. Hydrocarbon solvents (*n*-pentane and toluene) were dried using activated alumina columns using the Grubbs method[73] and were additionally vacuum-transferred from Na/K alloy immediately before vacuum line manipulations. All solvents for high-vacuum line manipulations were stored in *vacuo* over Na/K alloy in Teflon-valve sealed bulbs. Benzene-d_6 and toluene-d_8 (Cambridge Isotope Laboratories, 99+ atom % D) were stored over Na/K alloy in *vacuo* and vacuum transferred immediately prior to use. All other deuterated solvents were used as received (Cambridge Isotope Laboratories, 99+ atom %D). Other non-halogenated solvents were dried over Na/K alloy, and halogenated solvents were distilled from CaH_2. The reagents salicylaldehyde, 2,6-diispropylaniline and *N*,*N*-bis(salicylidene)-1,2-phenylenediamine were purchased from Sigma-Aldrich and used as received. *N*-(salicylidene)-2,6-diisopropylaniline[45] and pentamethylcyclopentadienyltitanium(IV) trimethyl (Cp^*TiMe_3)[46] were prepared according to literature procedures. Trityl tetrakis(pentafluorophenyl)borate, $Ph_3C^+B(C_6F_5)_4^-$ (**B**), was a generous gift from Boulder Scientific Company (Mead, CO) and was used as received.

Physical and Analytical Measurements. NMR spectra were recorded on Agilent F500 (DDR2, FT, 500 MHz, ^{1}H; 125 MHz, ^{13}C), Varian UNITYInova-500 (FT, 500 MHz, ^{1}H; 125 MHz, ^{13}C) or Hg400 (400 MHz, ^{1}H; 100 MHz, ^{13}C) instruments. Chemical shifts for ^{1}H and ^{13}C spectra were referenced using internal solvent resonances and are reported relative to tetramethylsilane (TMS). NMR experiments on air-sensitive samples were conducted in Teflon valve-sealed sample tubes (J.Young). Elemental analyses were performed by Midwest Microlab, Indianapolis, Indiana for % C, N, and H.^{13}C NMR assays of polymer microstructure were conducted in 1,1,2,2-tetrachloroethane-d_2 at 120 ºC with a delay time (d_1) = 10 sec. Signals were assigned according to the literature for these polymers.[56-60,74] Gel permeation chromatography (GPC) was carried out in 1,2,4-trichlorobenzene (stabilized with 125 ppm of BHT) at 150 ºC on a Polymer Laboratories 220

instrument equipped with a set of three PLgel 10 μm mixed-B columns with differential refractive index and viscosity detectors. Data reported were determined through Universal Calibration relative to polystyrene standards.

Synthesis of Monometallic *N*-(2,6-diisopropyl)phenyl(salicylideneiminato) pentamethylcyclopentadienyltitanium Dimethyl (1). A 10 mL pentane solution of *N*-(salicylidene)-2,6-diisopropylaniline (0.281 g, 1.00 mmol) was added to 10 mL of a pentane solution of Cp*$TiMe_3$ (0.228 g, 1.00 mmol). After 1 h, the solvent was removed under vacuum at room temperature, and the resulting yellow oil was triturated several times with pentane to eventually yield a dark yellow solid. (0.382 g, 0.775 mmol, 77.5% yield). ^{1}H NMR (400 MHz, C_6D_6) δ: 9.00 (s, 1 H, CH=N), 8.64 (dd, J = 6.0 Hz, 1.2 Hz, 1 H, phenyl), 7.18-7.14 (m, 3 H, phenyl), 7.10-7.06 (m, 1 H, phenyl), 6.93-6.88 (m, 1 H, phenyl), 6.77-6.69 (dd, J = 6.4 Hz, 0.8 Hz, 1 H, phenyl), 3.28 (septet, J = 5.6 Hz, 2 H, C*H*$(CH_3)_2$), 1.63 (s, 15 H, *Me*$_5$Cp), 1.24 (d, J = 5.6 Hz, 12 H, CH(*CH*$_3$)$_2$), 0.63 (s, 6 H, Ti-Me). ^{13}C NMR (100 MHz, C_6D_6) δ: 164.76 (CH, CH=N), 157.77 (C, phenyl), 150.47 (C, phenyl), 137.29 (C, phenyl), 132.49 (CH, phenyl), 127.25 (C, phenyl), 125.82 (C, phenyl), 124.06 (CH, phenyl), 122.88 (C, Cp), 122.67 (CH, phenyl), 121.75 (CH, phenyl), 121.38 (CH, phenyl), 56.03 (CH_3, Ti-Me), 28.05 (CH, ^{i}Pr), 23.20 (CH_3, ^{i}Pr), 11.07 (CH_3, Me_5Cp). Anal. Calcd for $C_{31}H_{43}NOTi$: C, 75.44; H, 8.78; N, 2.84. Found: C, 72.78; H, 8.16; N, 2.27. (Accurate EA not achieved due to either catalyst decomposition or incomplete combustion despite added combustion aids.)

Synthesis of Symmetric bimetallic *N,N′* -1,2-phenylenebis(salicylideneiminato) pentamethylcyclopentadienyltitanium tetramethyl (2). A 10 mL toluene solution of *N,N*-bis(salicylidene)-1,2-phenylenediamine (0.316 g, 1.00 mmol) was added dropwise to a 10 mL toluene solution of Cp*$TiMe_3$ (0.456 g, 2.00 mmol) at room temperature. After stirring for 1 h, the

solvent was removed under vacuum at room temperature, and the product was extracted with *n*-hexane. The filtrate was then concentrated and a reddish solid was obtained at -40 ºC (0.620 g, 0.838 mmol, 83.8% yield). ^{1}H NMR (500 MHz, C_6D_6) δ: 9.28 (s, 2 H, CH=N), 8.58 (dd, J = 7.8 Hz, 1.8 Hz, 2 H, phenyl), 7.28 (dd, J = 5.8 Hz, 3.5 Hz, 2 H, phenyl), 7.12-7.03 (m, 4 H, phenyl), 6.86-6.76 (m, 4 H, phenyl), 1.69 (s, 30 H, Me_5Cp), 0.70 (s, 12 H, Ti-Me). ^{13}C NMR (125 MHz, C_6D_6) δ: 165.12 (C, phenyl), 157.65 (CH, CH=N), 146.80 (C, phenyl), 132.53 (CH, phenyl), 128.43 (CH, phenyl), 127.15 (C, phenyl), 126.27 (CH, phenyl), 123.04 (C, Cp), 121.71 (CH, phenyl), 121.65 (CH, phenyl), 120.82 (CH, phenyl), 56.06 (CH_3, Ti-Me), 11.57 (CH_3, Me_5Cp). Anal. Calcd for $C_{44}H_{56}N_2O_2Ti_2$: C, 71.35; H, 7.62; N, 3.78. Found: C, 70.98; H, 7.33; N, 3.90.

Synthesis of Asymmetric bimetallic *N,N′* -1,2-phenylenebis(salicylideneiminato)pentamethylcyclopentadienyltitanium trimethyl (3). Recrystallization of **2** from toluene over 2 days gave **3** as dark red crystals via methyl migration. ^{1}H NMR (500 MHz, C_6D_6) δ: 8.51 (s, 1 H, CH=N), 7.40 (d, J = 8.1 Hz, 1 H, phenyl), 7.24-7.18 (m, 3 H, phenyl),7.15-7.10 (m, 2 H, phenyl), 7.00 (t, J = 8.8 Hz, 1 H, phenyl), 6.93 (td, J = 7.6 Hz, 1.6 Hz, 1 H, phenyl), 6.78 (dd, J = 8.0 Hz, 1.2 Hz, 1 H, phenyl), 6.75 (t, J = 7.6 Hz, 1 H, phenyl), 6.66 (t, J = 7.6 Hz, 1 H, phenyl), 6.57 (td, J = 7.6 Hz, 1.2 Hz, 1 H, phenyl), 5.94 (q, J = 6.8 Hz, 1 H, CH_3CHN), 2.44 (d, J = 6.8 Hz, 3 H, CH_3CHN), 1.89 (s, 15H, Me_5Cp), 1.65 (s, 15H, Me_5Cp), 1.46 (s, 3 H, Ti-Me), 0.87 (s, 6 H, Ti-Me). ^{13}C NMR (125 MHz, C_6D_6) δ: 166.40 (C, phenyl), 161.82 (C, phenyl), 156.00 (CH, CH=N), 155.39 (C, phenyl), 137.52 (CH, phenyl), 135.03 (C, phenyl), 133.16 (CH, phenyl), 128.53 (CH, phenyl), 128.30 (CH, phenyl, overlapped by solvent and assigned by ^{13}C-^{1}H HSQC), 127.97 (CH, phenyl), 126.86 (CH, phenyl), 124.68 (C, Me_5Cp), 122.78 (C, Me_5Cp), 122.39 (C, phenyl), 121.44 (CH, phenyl), 121.15 (CH, phenyl), 120.94(C, phenyl), 117.99 (CH, phenyl), 117.55 (CH, phenyl), 115.66 (CH, phenyl), 114.37 (CH, phenyl), 64.05

(CH_3, Ti-Me), 56.64 (CH_3, CH_3*C*HN), 55.76 (CH_3, Ti-Me), 54.89 (CH_3, Ti-Me), 24.34 (CH_3, *C*H_3CHN), 11.88 (CH3, *Me*$_5$Cp), 11.79 (CH3, *Me*$_5$Cp). Anal. Calcd for $C_{44}H_{56}N_2O_2Ti_2$: C, 71.35; H, 7.62; N, 3.78. Found: C, 71.14; H, 7.46; N, 3.63.

Synthesis of crude *N,N′*-1,2-phenylenebis(salicylideneiminato)pentamethylcyclopentadienyltitanium tetrakis(pentafluorophenyl) borate (4). 10 μmol of **2** and 20 μmol of $Ph_3C^+B(C_6F_5)_4^-$ were combined in a vial in a glovebox. 5 mL of benzene was added to the vial, which was lightly shaken to dissolve all components. The vial was capped and allowed to sit at room temperature in the glove box for 24 hrs. Following the 24 hr period, dark red crystals had grown out of a yellow solution. The yellow solution was removed, and the crystals were washed with toluene and pentane. The vial containing the crystals was then placed in a Schlenk flask and dried under high vacuum at room temperature for 24 hrs. ^{1}H NMR (400 MHz, CD_2Cl_2) δ: 9.28 (s, 2 H, C*H*=N), 7.99-7.97 (m, *J* = 8 Hz, 4 Hz, 2 H, phenyl), 7.89-7.87 (m, *J* = 8 Hz, 2 H, phenyl), 7.83-7.79 (m, *J* = 8 Hz, 4 Hz, 2 H, phenyl), 7.72-7.69 (m, *J* = 8 Hz, 4 Hz, 2 H, phenyl), 7.34-7.29 (m, 4 H, phenyl), 1.59 (s, 15 H, *Me*$_5$Cp).

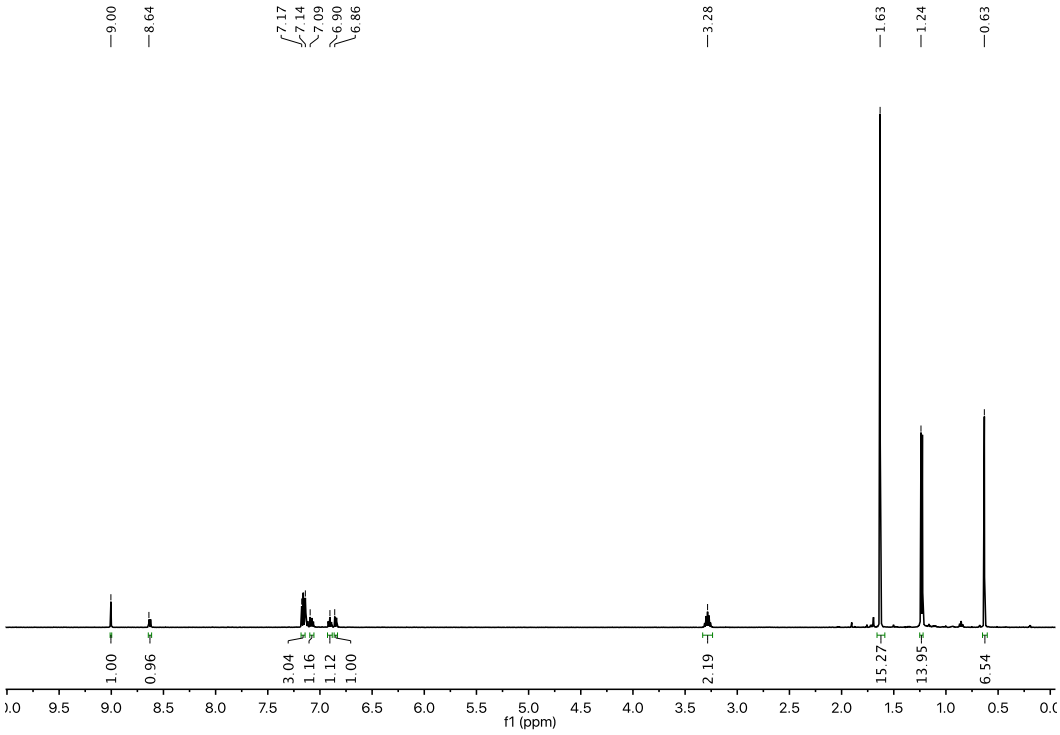

Figure 2.4. ^{1}H NMR spectrum of **1** in C_6D_6.

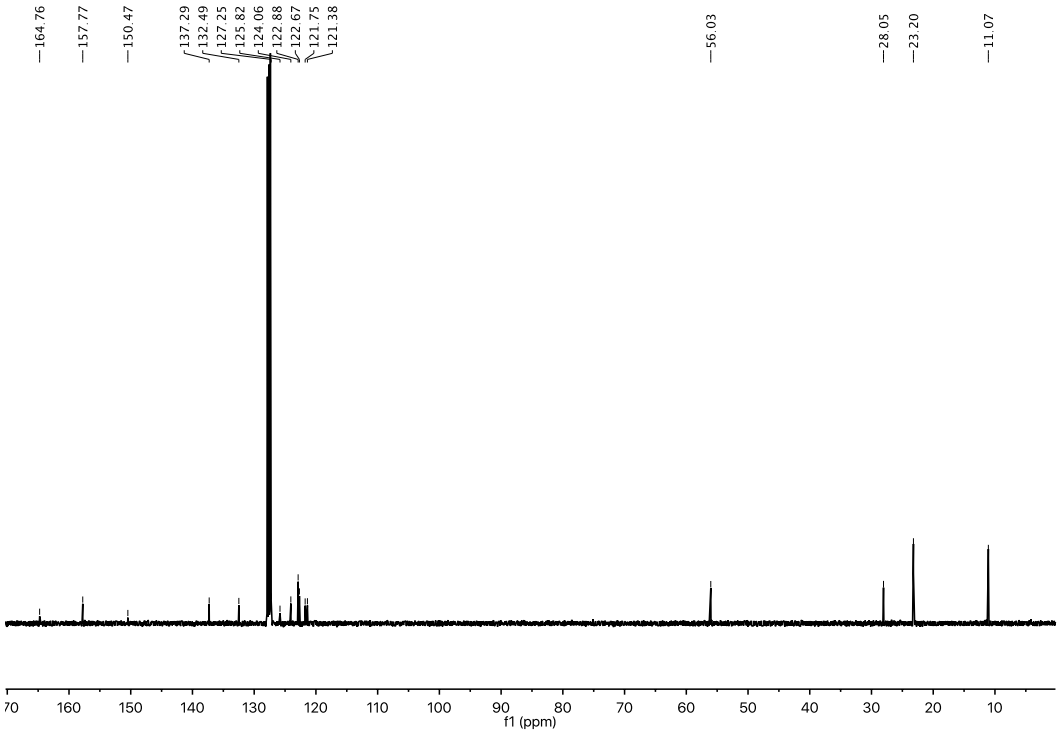

Figure 2.5. ^{13}C NMR spectrum of **1** in C_6D_6.

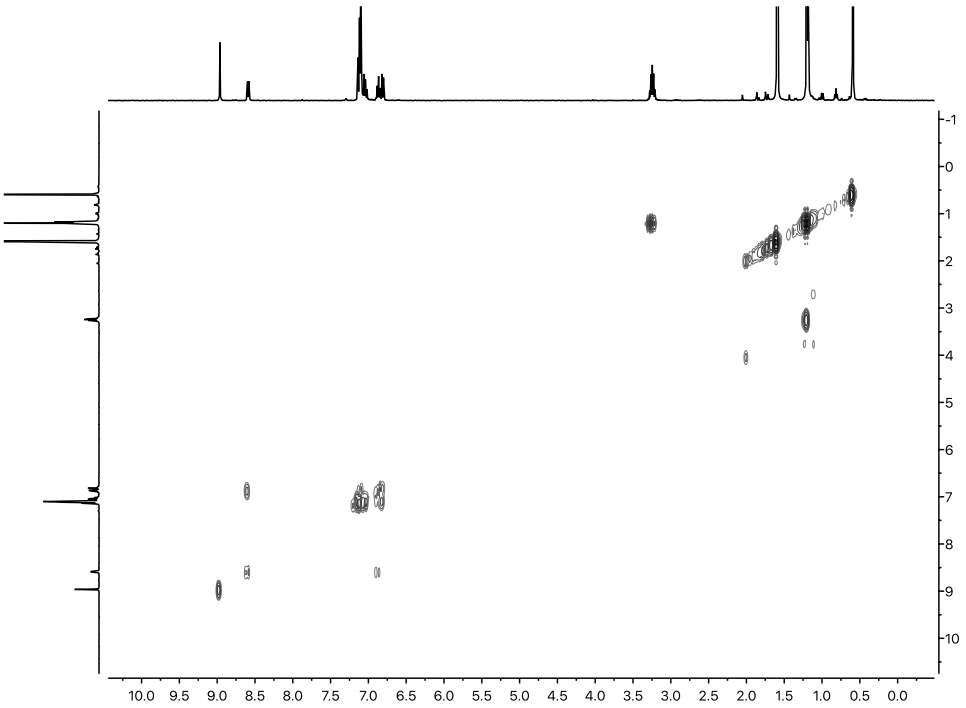

Figure 2.6. COSY spectrum of **1** in C_6D_6.

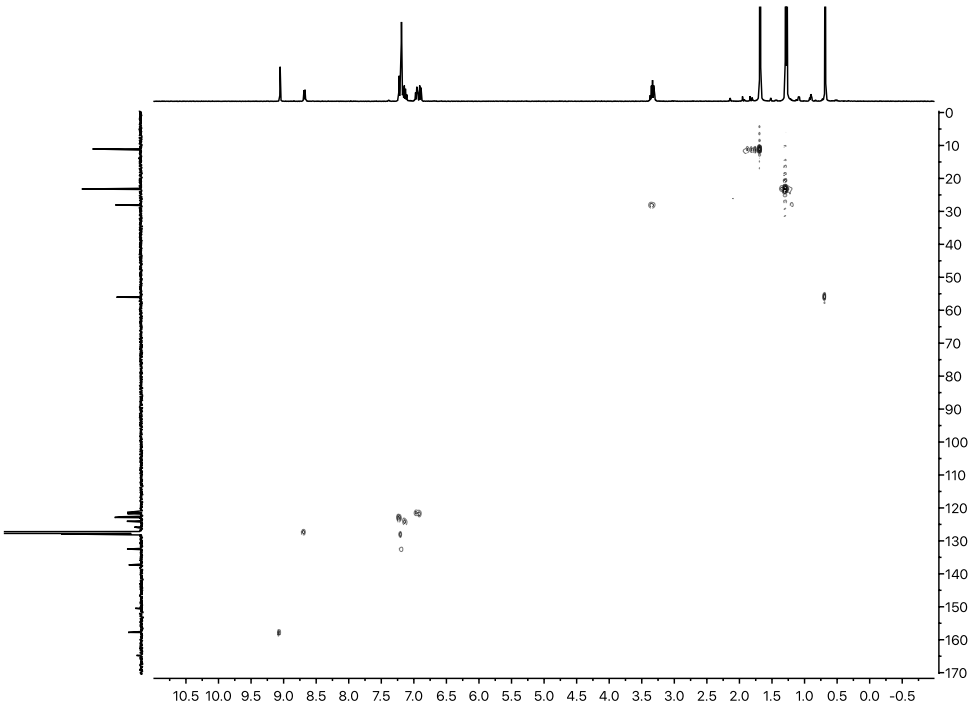

Figure 2.7. HSQC spectrum of **1** in C_6D_6.

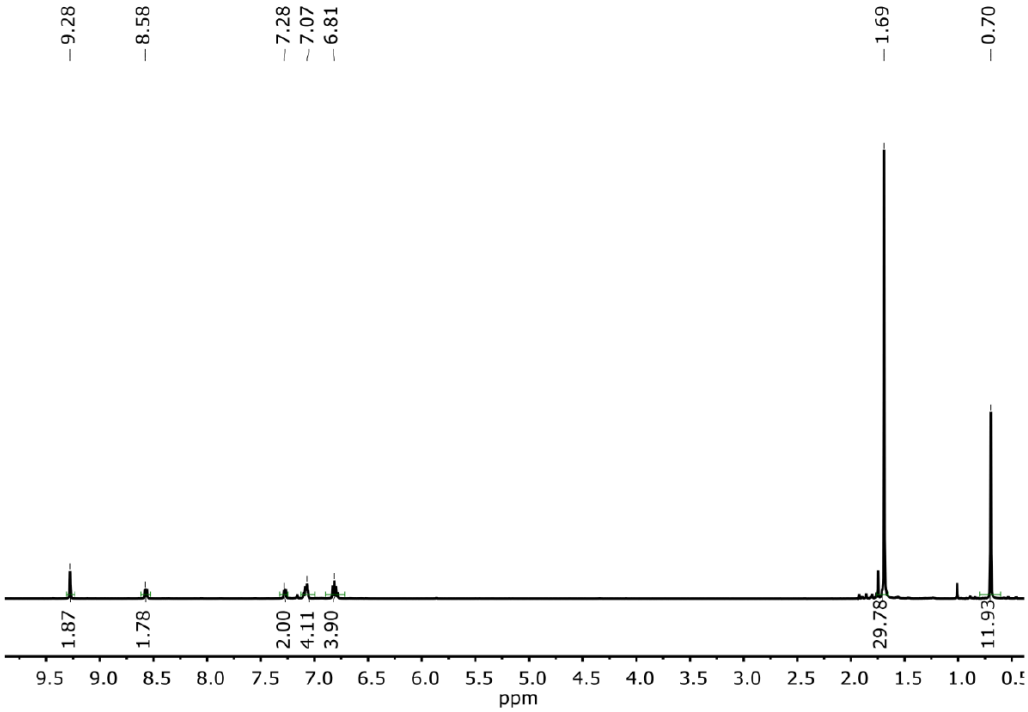

Figure 2.8. ^{1}H NMR spectrum of **2** in C_6D_6.

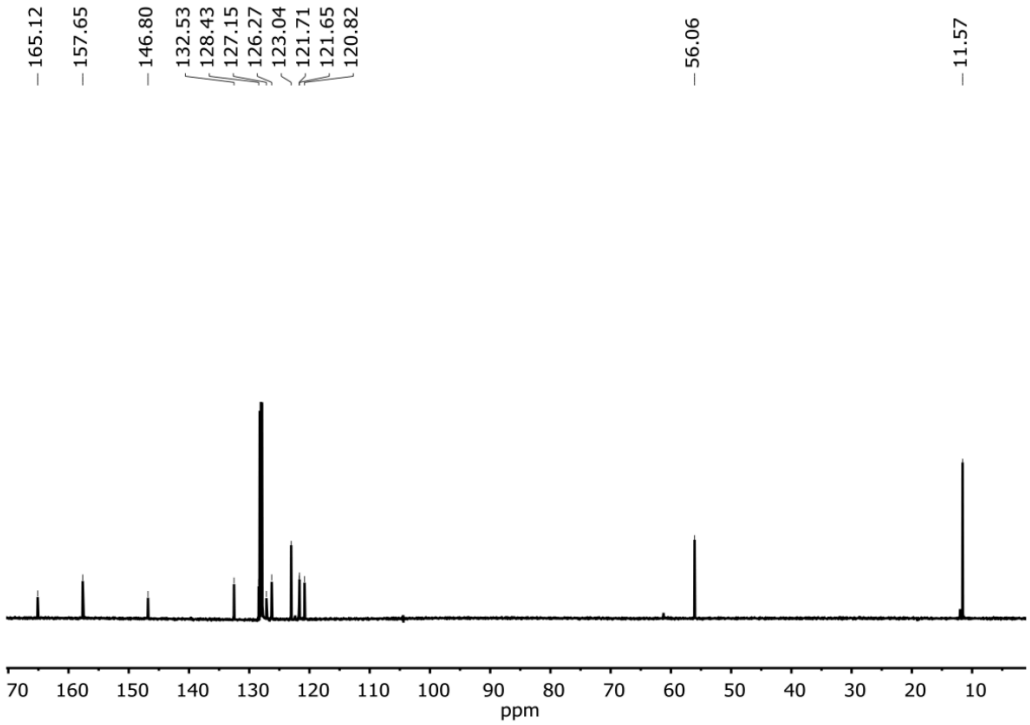

Figure 2.9. ^{13}C NMR spectrum of **2** in C_6D_6.

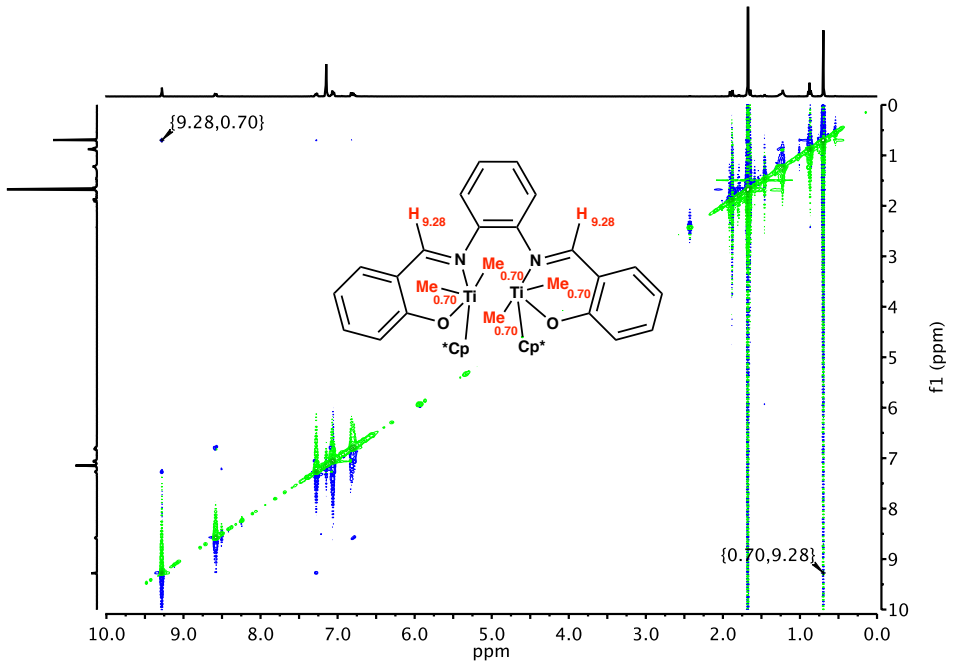

Figure 2.10. ^{1}H-^{1}H NOESY spectrum of **2** in C_6D_6.

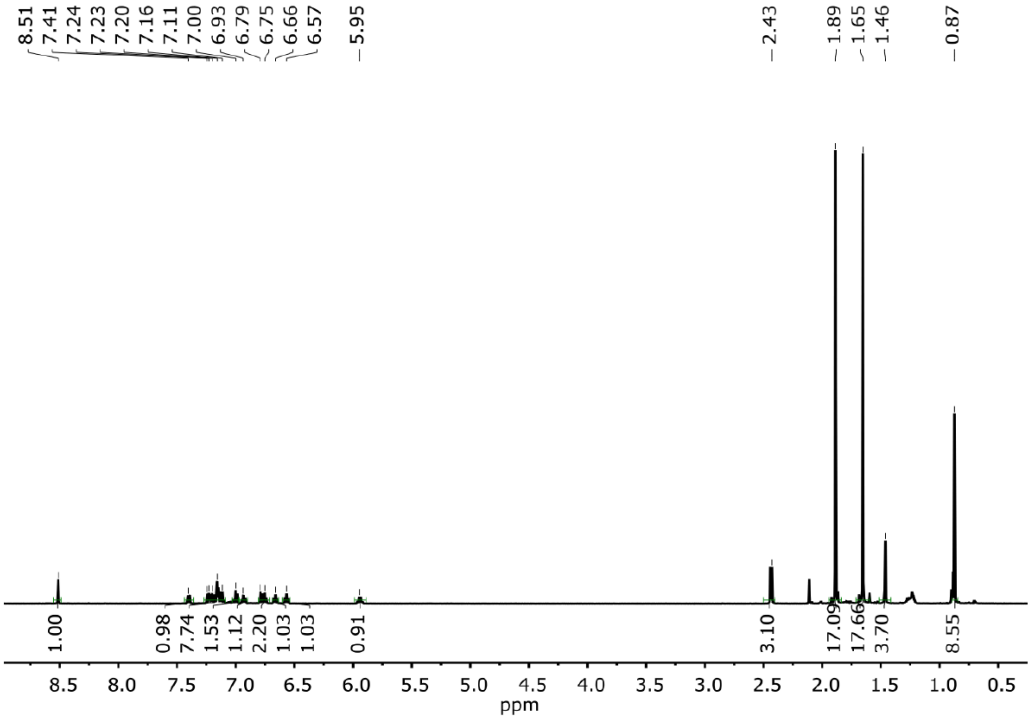

Figure 2.11. ^{1}H NMR spectrum of **3** in C_6D_6.

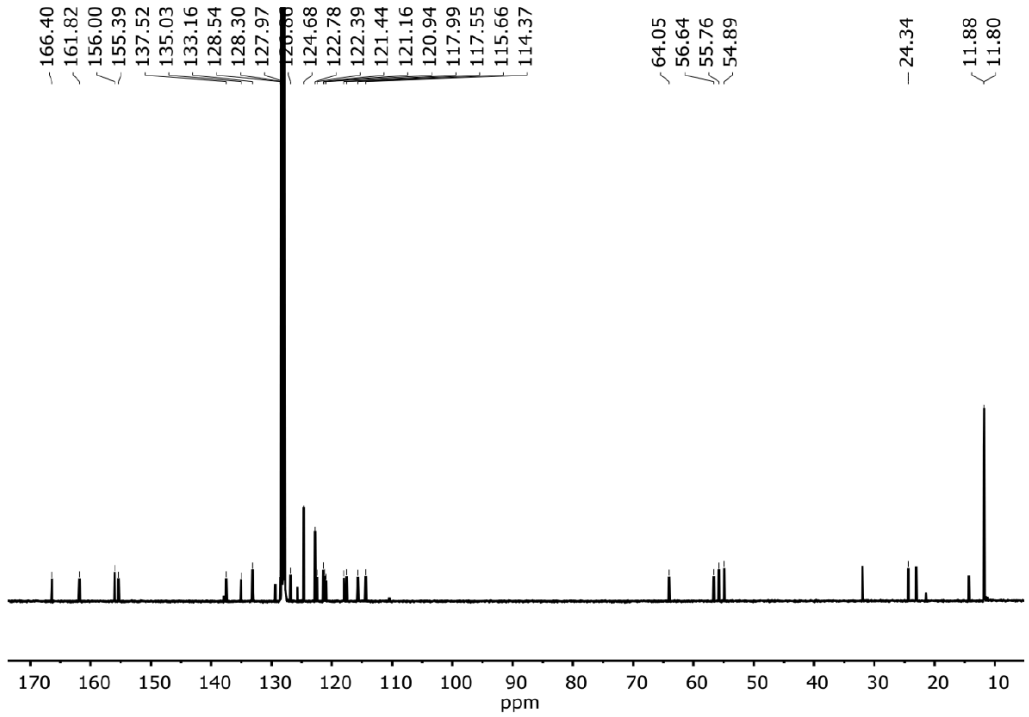

Figure 2.12. ^{13}C NMR spectrum of **3** in C_6D_6.

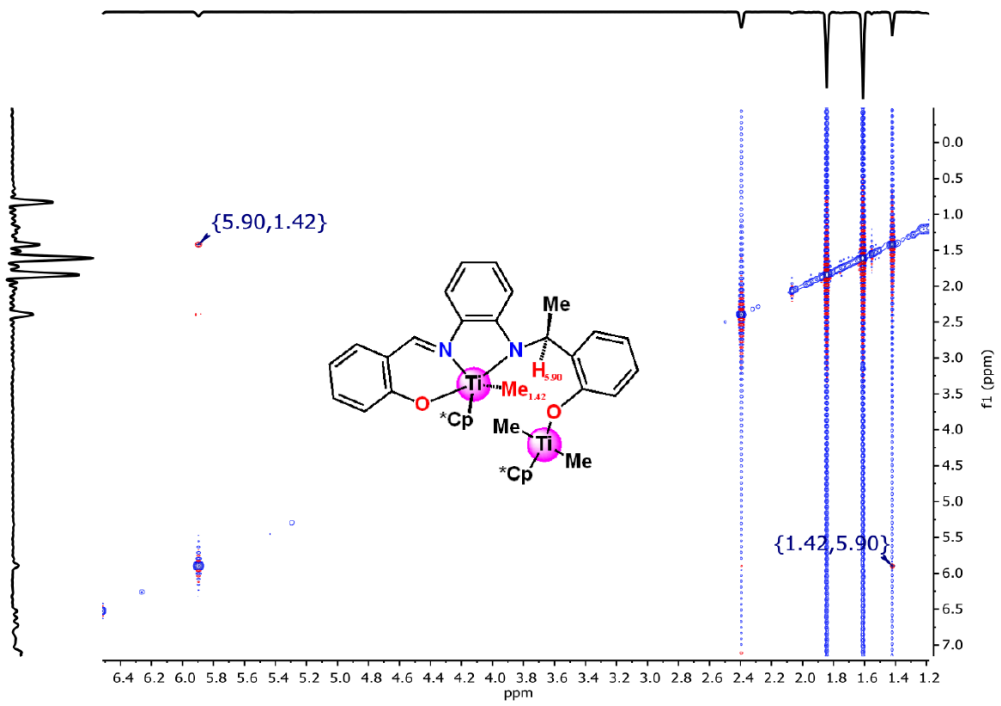

Figure 2.13. ^{1}H-^{1}H NOESY spectrum of **3** in C_6D_6.

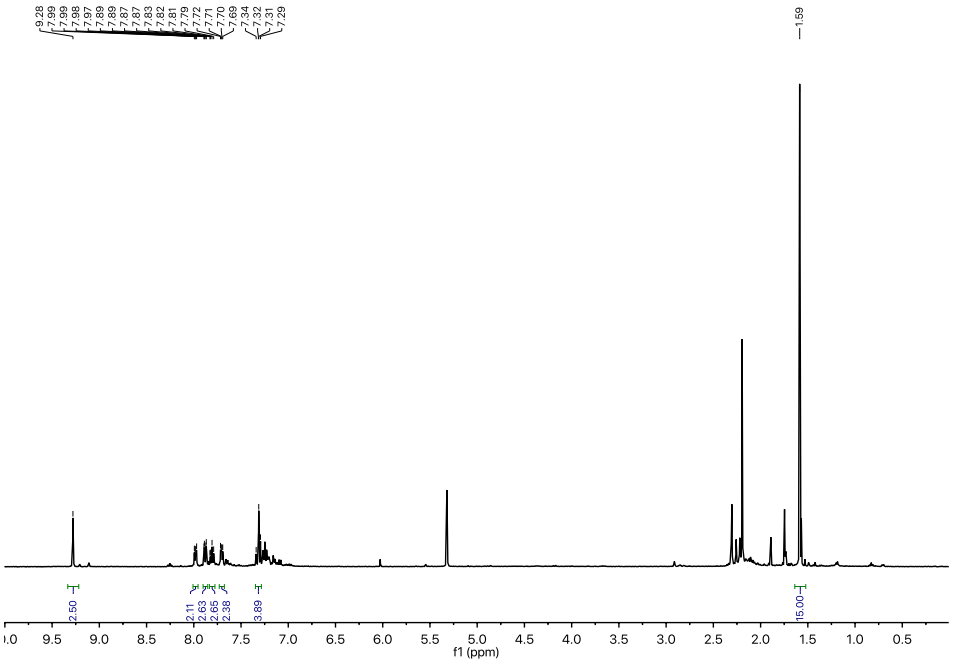

Figure 2.14. ^{1}H NMR spectrum of crude **4** in CD_2Cl_2 at -40 ºC.

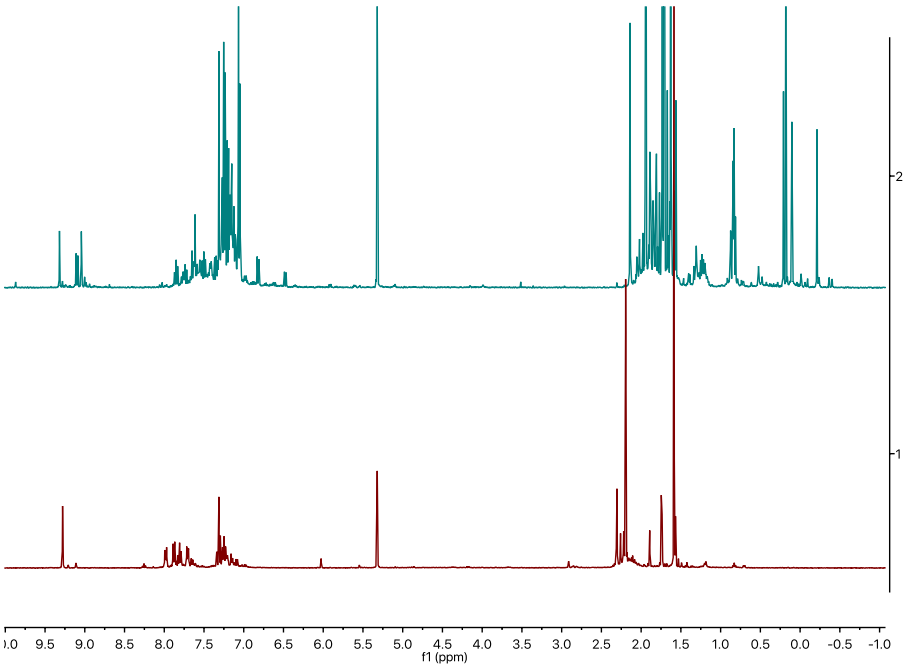

Figure 2.15. Stacked ^{1}H NMR spectra of **4** (red, bottom) and NMR of **2** activated with 2 equiv. $Ph_3C^+B(C_6F_5)_4^-$ (teal, top), both in CD_2Cl_2 at -40 ºC.

General procedure for ethylene homo- and copolymerizations. In the glove box, a 350 mL heavy walled glass reactor equipped with stir bar was loaded with 48 mL toluene (and desired amount of 1-hexene for copolymerizations). In a separate vial, metal catalyst ([Catalyst] = 10 μmol of **1**; 5 μmol of **2**; 5 μmol of **Cp*TiMe$_3$**) and either 1.0 or 2.4 equivalents of [Ph_3C][$B(C_6F_5)_4$] per **2**, or 1.2 equivalents of $Ph_3C^+B(C_6F_5)_4^-$ per **1** and **Cp*TiMe$_3$**, were dissolved in 2 mL of fluorobenzene. The glass reactor was then interfaced to a high-pressure line and the solution was degassed by freeze-pump-thaw cycles. The solution was then brought to room temperature using a water bath. The reactor was then charged with 1 atm of ethylene and the catalyst/cocatalyst solution was syringed in. After 2 min, the reactor was vented and 5 mL of acidified methanol was syringed in. The contents of the polymerization vessel were poured into a large volume of methanol, and the polymer flakes precipitated out. The resulting polymer was filtered off, washed with methanol, and then dried under vacuum overnight.

General Procedures for 1-hexene homopolymerizations. In the glove box, a 250 mL round bottom flask equipped with stir bar was loaded with 23 mL toluene and desired amount of 1-hexene. In a separate vial, metal catalyst ([Catalyst] = 10 μmol of **1**; 5 μmol of **2**; 5 μmol of **Cp*TiMe$_3$**) and either 1.0 or 2.4 equivalents of $Ph_3C^+B(C_6F_5)_4^-$ per **2**, or 1.2 equivalents of $Ph_3C^+B(C_6F_5)_4^-$ per **1** and **Cp*TiMe$_3$**, were dissolved in 2 mL of fluorobenzene. The catalyst/cocatalyst solution was added to the flask. The flask was sealed with a rubber septum, removed from the glovebox, and allowed to stir under static argon for a total of 10 minutes at ambient temperature. After 10 minutes, the flask was opened to air and 200 mL of acidified methanol was added. Polymer precipitated as a gel and was stirred overnight. Methanol was decanted and polymer was transferred with hexanes to a tared flask. Solvent was removed under vacuum and polymer was dried under vacuum overnight.

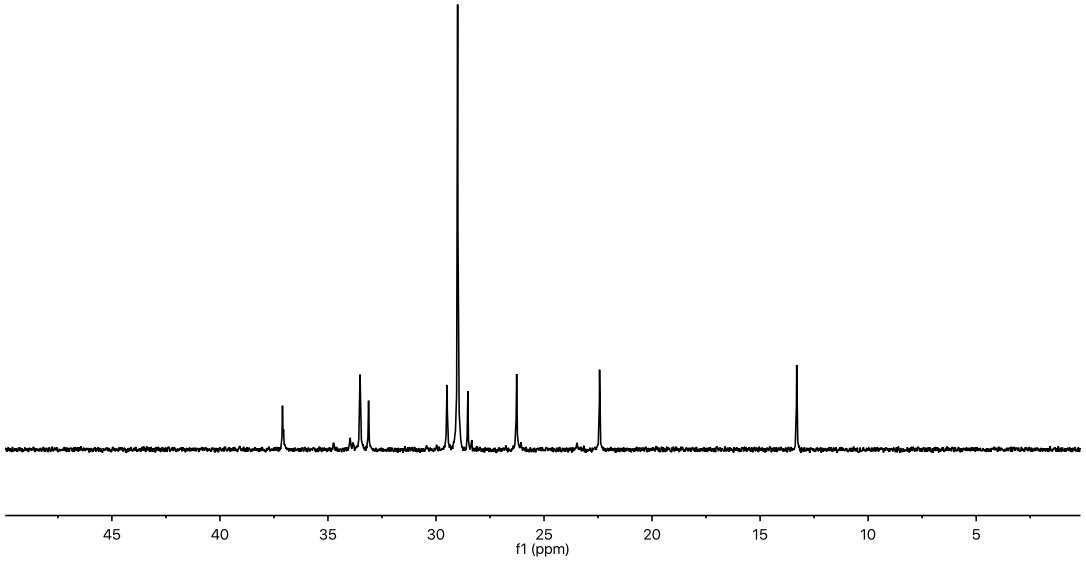

Figure 2.16. ^{13}C NMR of polymer generated by ethylene/1-hexene copolymerization with **2+1B** (Table 2.2 entry 2, 100 MHz in 1,1,2,2 tetrachloroethane-d_2 at 120 °C).

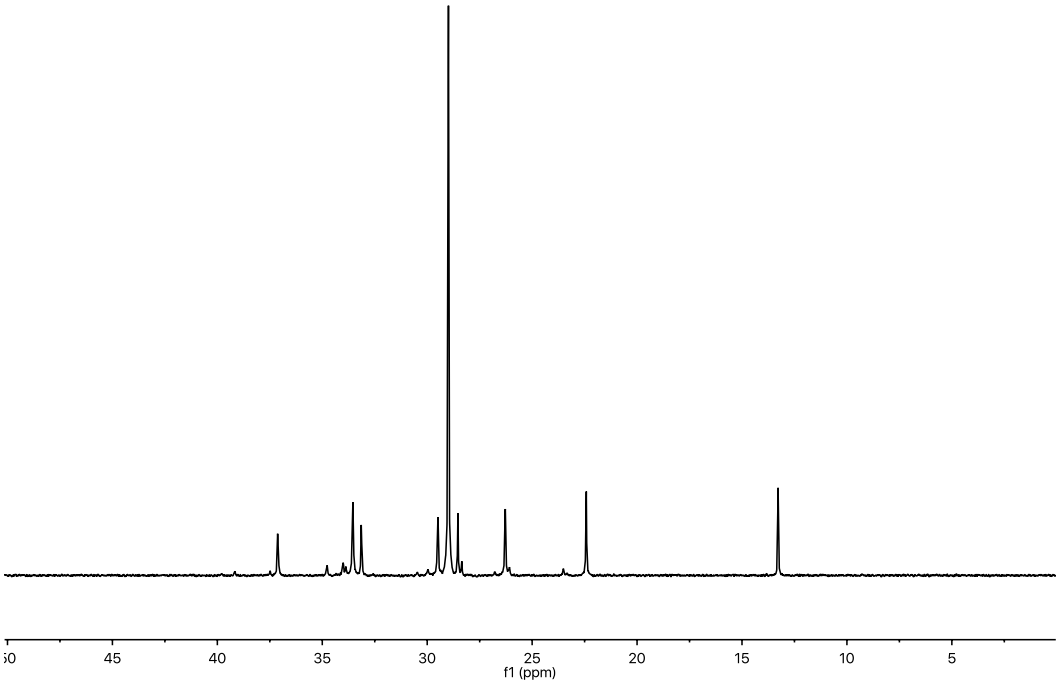

Figure 2.17. ^{13}C NMR of polymer generated by ethylene/1-hexene copolymerization with **2+2B** (Table 2.2 entry 3, 100 MHz in 1,1,2,2 tetrachloroethane-d_2 at 120 °C).

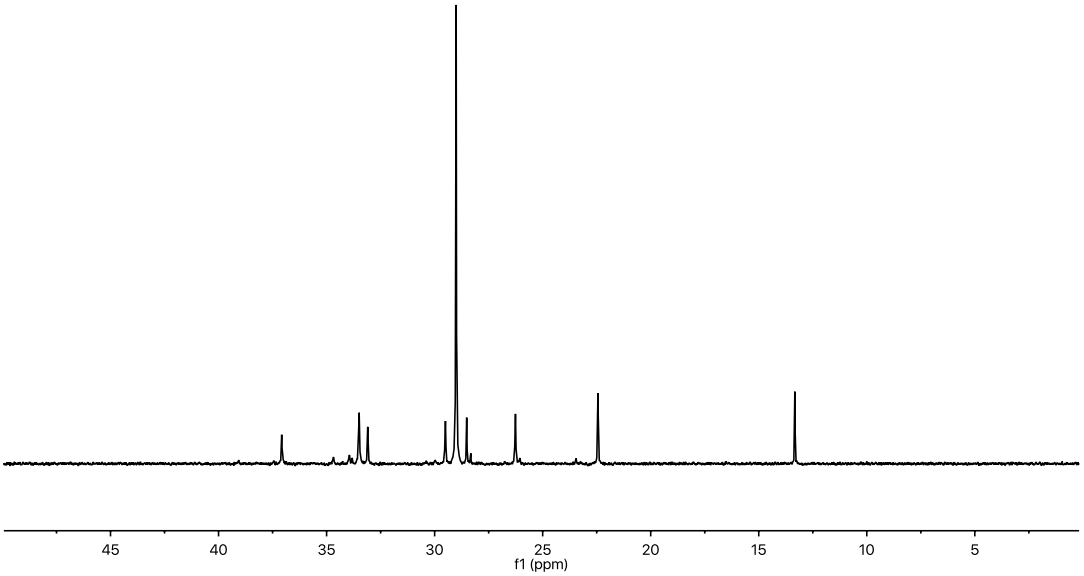

Figure 2.18. ^{13}C NMR of polymer generated by ethylene/1-hexene copolymerization with **Cp*TiMe$_3$** (Table 2.2 entry 4, 100 MHz in 1,1,2,2 tetrachloroethane-d_2 at 120 °C).

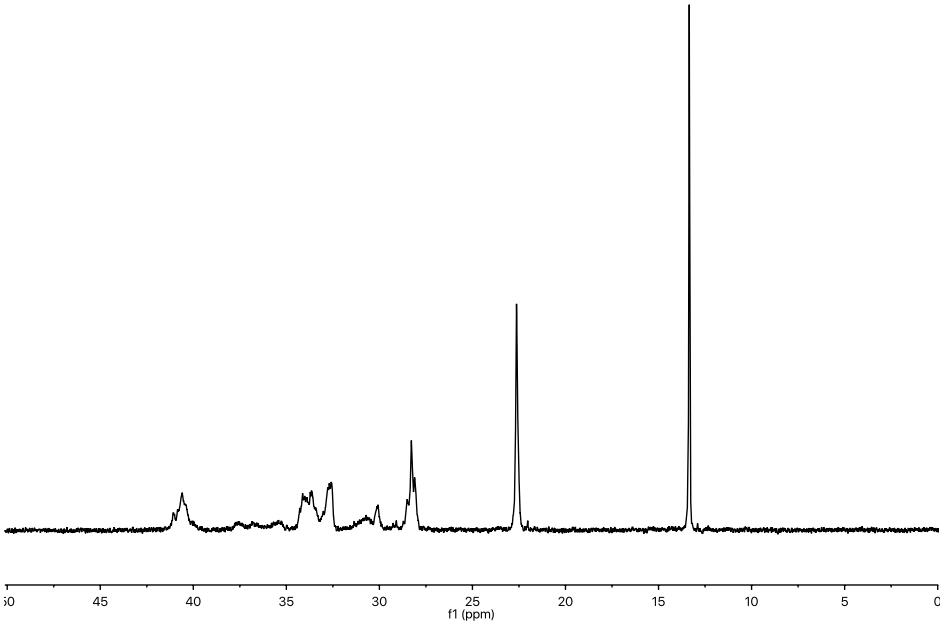

Figure 2.19. ^{13}C NMR of polymer generated by 1-hexene homopolymerization with **2+2B** (Table 2.3 entry 3, 100 MHz in 1,1,2,2 tetrachloroethane-d_2 at 120 °C).

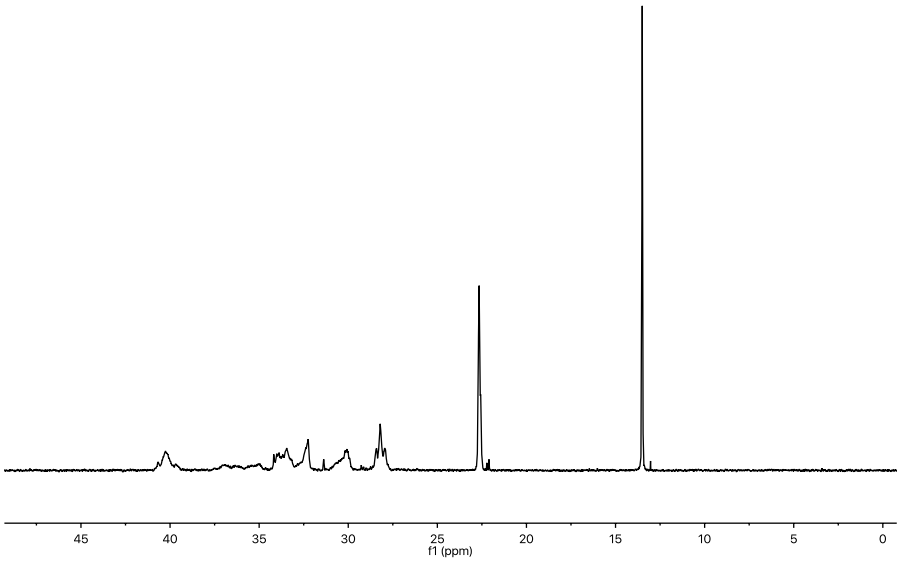

Figure 2.20. ^{13}C NMR of polymer generated by 1-hexene homopolymerization with **Cp*TiMe$_3$** (Table 2.3 entry 4, 100 MHz in 1,1,2,2-tetrachloroethane-d_2 at 120 °C).

X-ray data collection, structure solution, and refinement.

Single crystals of **3** were crystallized from hexane and hexane/toluene, mounted in inert oil, and transferred to the cold gas stream of a Bruker Kappa APEX CCD area detector equipped with a CuK_{α} microsource with Quazar optics. Crystallographic and experimental details of the structure determination are summarized in Table S1. The crystal was maintained at 100.01 K during data collection. An empirical correction for absorption was made.[75] Using Olex2,[76] the structure was solved with the XS[77] structure solution program using Patterson Method and refined with the ShelXL refinement package[78] using full-matrix least-squares procedures (based on F_o^2) first with isotropic thermal parameters and then with anisotropic thermal parameters in the last cycles of refinement for all the non-hydrogen atoms. The hydrogen atoms were introduced into the geometrically calculated positions and refined riding on the corresponding parent atoms. Similar distances were refined for the disordered carbon atoms. Rigid bond restraints were imposed on the displacement parameters as well as restraints on similar amplitudes separated by less than 1.7 Ang. on the disordered methyl group. Group anisotropic displacement parameters were refined for the remaining disordered atoms.

Single crystals of **4** were crystallized from benzene-d_6. A suitable crystal was selected and mounted at 100 K on a brass tip in air-free Paratone-N on a 'Bruker APEX-II CCD' diffractometer. The crystal was kept at 99.99 K during data collection. Using Olex2,[S6] the structure was solved with the XS [2] structure solution program using Direct Methods and refined with the XL[S7] refinement package using Least Squares minimization.

Table 2.4. Crystal data and structure refinement for 3 and 4.

Complex	**3**·2C_7H_8	**4**
Empirical formula	$C_{44}H_{56}N_2O_2Ti_2$·2C_7H_8	$C_{54}H_{29}BF_{20}N_2O_2Ti$
Formula weight	924.97	1176.50
Temperature / K	99.98	99.99
Crystal system	triclinic	triclinic
Space group	P-1	P-1
a / Å, b / Å, c / Å	11.2663(3), 13.0764(4), 18.5004(6)	12.9991(7), 13.3403(7), 15.2032(7)
α/°, β/°, γ/°	109.233(2), 104.076(2), 91.920(2)	66.663(2), 76.222(2), 89.611(3)
Volume / Å^3	2476.86(13)	2339.7(2)
Z	2	2
ϱ_{calc} / mg mm^{-3}	1.240	1.670
μ / mm^{-1}	3.070	2.712
F(000)	988.0	1182.0
Crystal size / mm^3	0.224 × 0.183 × 0.005	0.206 × 0.137 × 0.048
2Θ range for data collection	5.254 to 127.306°	7.252 to 136.382°
Index ranges	-13 ≤ h ≤ 9, -15 ≤ k ≤ 14, -9 ≤ l ≤ 21	-15 ≤ h ≤ 14, -15 ≤ k ≤ 16, -18 ≤ l ≤ 18
Reflections collected	13227	19108
Independent reflections	7888[R(int) = 0.101]	8255[R(int) = 0.0305]
Data/restraints/parameters	7888/0/593	8162/0/837
Goodness-of-fit on F^2	1.019	1.018
Final R indexes [I>2σ (I)]	R_1 = 0.0443, wR_2 = 0.1118	R_1 = 0.0379, wR_2 = 0.0994
Final R indexes [all data]	R_1 = 0.0565, wR_2 = 0.1207	R_1 = 0.0458, wR_2 = 0.1051
Largest diff. peak/hole / e Å^{-3}	0.60/-0.40	0.43/-0.50

$R1 = ||F_o| - |F_c|| / \Sigma |F_o|$; $wR2 = [\sum [w(F_o^2 - F_c^2)^2] / \sum [w(F_o^2)^2]]$.

Acknowledgement

Financial support by DOE (Grant 86ER13511, supported catalysts and models thereof), NSF (Grant CHE-1464488, cooperative effects in multimetallic catalysis), and the Chemical Sciences, Geosciences and Biosciences Division, U.S. Department of Energy through grant DEFG02-03ER15457 to the Institute of Catalysis in Energy Processes (ICEP; supported catalysts and models thereof) at Northwestern University is gratefully acknowledged. Purchases of the NMR instrumentation at the IMSERC at Northwestern U. was supported by NSF (Grant CHE-1048773). We also thank Boulder Scientific Company for the generous gift of $Ph_3C^+B(C_6F_5)_4^-$.

References

Chapter 1.

1. Ginsbach, J. W.; Kieber-Emmons, M. T.; Nomoto, R.; Noguchi, A.; Ohnishi, Y.; Solomon, E. I., Structure/function correlations among coupled binuclear copper proteins through spectroscopic and reactivity studies of NspF. *Proc. Natl. Acad. Sci. U. S. A.* **2012,** *109*, 10793-10797.

2. Schenk, G.; Mitic, N.; Gahan, L. R.; Ollis, D. L.; McGeary, R. P.; Guddat, L. W., Binuclear Metallohydrolases: Complex Mechanistic Strategies for a Simple Chemical Reaction. *Acc. Chem. Res.* **2012,** *45*, 1593-1603.

3. Haak, R. M.; Wezenberg, S. J.; Kleij, A. W., Cooperative multimetallic catalysis using metallosalens. *Chem. Commun.* **2010,** *46*, 2713-2723.

4. Chen, S.-L.; Marino, T.; Fang, W.-H.; Russo, N.; Himo, F., Peptide Hydrolysis by the Binuclear Zinc Enzyme Aminopeptidase from Aeromonas proteolytica: A Density Functional Theory Study. *J. Phys. Chem. B* **2008,** *112*, 2494-2500.

5. Schwartz, J. K.; Liu, X. S.; Tosha, T.; Theil, E. C.; Solomon, E. I., Spectroscopic Definition of the Ferroxidase Site in M Ferritin: Comparison of Binuclear Substrate vs. Cofactor Active Sites. *J. Am. Chem. Soc.* **2008,** *130*, 9441-9450.

6. Hadler, K. S.; Tanifum, E. A.; Yip, S. H.-C.; Mitic, N.; Guddat, L. W.; Jackson, C. J.; Gahan, L. R.; Nguyen, K.; Carr, P. D.; Ollis, D. L.; Hengge, A. C.; Larrabee, J. A.; Schenk, G., Substrate-Promoted Formation of a Catalytically Competent Binuclear Center and Regulation of Reactivity in a Glycerophosphodiesterase from Enterobacter aerogenes. *J. Am. Chem. Soc.* **2008,** *130*, 14129-14138.

7. Mitić, N.; Smith, S. J.; Neves, A.; Guddat, L. W.; Gahan, L. R.; Schenk, G., The catalytic mechanisms of binuclear metallohydrolases. *Chem. Rev.* **2006,** *106*, 3338-3363.

8. Goulas, K. A.; Sreekumar, S.; Song, Y.; Kharidehal, P.; Gunbas, G.; Dietrich, P. J.; Johnson, G. R.; Wang, Y. C.; Grippo, A. M.; Grabow, L. C.; Gokhale, A. A.; Toste, F. D., Synergistic Effects in Bimetallic Palladium–Copper Catalysts Improve Selectivity in Oxygenate Coupling Reactions. *J. Am. Chem. Soc.* **2016,** *138*, 6805-6812.

9. Buchwalter, P.; Rosé, J.; Braunstein, P., Multimetallic Catalysis Based on Heterometallic Complexes and Clusters. *Chem. Rev.* **2015,** *115*, 28-126.

10. Gnanamani, M. K.; Jacobs, G.; Hamdeh, H. H.; Shafer, W. D.; Liu, F.; Hopps, S. D.; Thomas, G. A.; Davis, B. H., Hydrogenation of Carbon Dioxide over Co–Fe Bimetallic Catalysts. *ACS Catal.* **2016**, *6*, 913-927.

11. Walker, W. K.; Kay, B. M.; Michaelis, S. A.; Anderson, D. L.; Smith, S. J.; Ess, D. H.; Michaelis, D. J., Origin of Fast Catalysis in Allylic Amination Reactions Catalyzed by Pd-Ti Heterobimetallic Complexes. *J. Am. Chem. Soc.* **2015,** *137*, 7371-7378.

12. Matsunaga, S.; Shibasaki, M., Recent advances in cooperative bimetallic asymmetric catalysis: dinuclear Schiff base complexes. *Chem. Commun.* **2014,** *50*, 1044-1057.

13. Edwards, J. K.; Freakley, S. J.; Carley, A. F.; Kiely, C. J.; Hutchings, G. J., Strategies for Designing Supported Gold–Palladium Bimetallic Catalysts for the Direct Synthesis of Hydrogen Peroxide. *Acc. Chem. Res.* **2014,** *47*, 845-854.

14. Mata, J. A.; Hahn, F. E.; Peris, E., Heterometallic complexes, tandem catalysis and catalytic cooperativity. *Chem. Sci.* **2014,** *5*, 1723-1732.

15. Anand, M.; Sunoj, R. B.; Schaefer, H. F., Non-innocent Additives in a Palladium(II)-Catalyzed C–H Bond Activation Reaction: Insights into Multimetallic Active Catalysts. *J. Am. Chem. Soc.* **2014,** *136*, 5535-5538.

16. Hetterscheid, D. G. H.; Chikkali, S. H.; de Bruin, B.; Reek, J. N. H., Binuclear Cooperative Catalysts for the Hydrogenation and Hydroformylation of Olefins. *ChemCatChem* **2013,** *5*, 2785-2793.

17. Ogo, S.; Ichikawa, K.; Kishima, T.; Matsumoto, T.; Nakai, H.; Kusaka, K.; Ohhara, T., A Functional [NiFe]Hydrogenase Mimic That Catalyzes Electron and Hydride Transfer from H2. *Science* **2013,** *339*, 682-684.

18. Tsui, E. Y.; Tran, R.; Yano, J.; Agapie, T., Redox-inactive metals modulate the reduction potential in heterometallic manganese-oxido clusters. *Nat. Chem.* **2013,** *5*, 293-299.

19. Tsui, E. Y.; Kanady, J. S.; Agapie, T., Synthetic Cluster Models of Biological and Heterogeneous Manganese Catalysts for O2 Evolution. *Inorg. Chem.* **2013,** *52*, 13833-13848.

20. Shima, T.; Hu, S.; Luo, G.; Kang, X.; Luo, Y.; Hou, Z., Dinitrogen Cleavage and Hydrogenation by a Trinuclear Titanium Polyhydride Complex. *Science* **2013,** *340*, 1549-1552.

21. Ahmed, S. M.; Poater, A.; Childers, M. I.; Widger, P. C. B.; LaPointe, A. M.; Lobkovsky, E. B.; Coates, G. W.; Cavallo, L., Enantioselective Polymerization of Epoxides Using Biaryl-Linked Bimetallic Cobalt Catalysts: A Mechanistic Study. *J. Am. Chem. Soc.* **2013,** *135*, 18901-18911.

22. Park, J.; Hong, S., Cooperative bimetallic catalysis in asymmetric transformations. *Chem. Soc. Rev.* **2012,** *41*, 6931-6943.

23. Gao, Y.; Chen, X.; Zhang, J.; Chen, J.; Lohr, T. L.; Marks, T. J., Catalyst Nuclearity Effects on Stereo- and Regioinduction in Pyridylamidohafnium-Catalyzed Propylene and 1-Octene Polymerizations. *Macromolecules* **2018,** *51*, 2401-2410.

24. Sampson, J.; Choi, G.; Akhtar, M. N.; Jaseer, E. A.; Theravalappil, R.; Al-Muallem, H. A.; Agapie, T., Olefin Polymerization by Dinuclear Zirconium Catalysts Based on Rigid Teraryl Frameworks: Effects on Tacticity and Copolymerization Behavior. *Organometallics* **2017,** *36*, 1915-1928.

25. Chen, J.; Gao, Y.; Wang, B.; Lohr, T. L.; Marks, T. J., Scandium-Catalyzed Self-Assisted Polar Co-monomer Enchainment in Ethylene Polymerization. *Angew. Chem. Intl. Ed.* **2017,** *56*, 15964-15968.

26. Chen, J.; Gao, Y.; Xiong, S.; Delferro, M.; Lohr, T. L.; Marks, T. J., Metal and Counteranion Nuclearity Effects in Organoscandium-Catalyzed Isoprene Polymerization and Copolymerization. *ACS Catal.* **2017**, *7*, 5214-5219.

27. Mu, H.; Pan, L.; Song, D.; Li, Y., Neutral Nickel Catalysts for Olefin Homo- and Copolymerization: Relationships between Catalyst Structures and Catalytic Properties. *Chem. Rev.* **2015,** *115*, 12091-12137.

28. Shu, D.; Mouat, A. R.; Stephenson, C. J.; Invergo, A. M.; Delferro, M.; Marks, T. J., Ligand-unsymmetrical phenoxyiminato dinickel catalyst for high molecular weight long-chain branched polyethylenes. *ACS Macro Lett.* **2015,** *4*, 1297-1301.

29. Gao, Y.; Mouat, A. R.; Motta, A.; Macchioni, A.; Zuccaccia, C.; Delferro, M.; Marks, T. J., Pyridylamido Bi-Hafnium Olefin Polymerization Catalysis: Conformationally Supported Hf···Hf Enchainment Cooperativity. *ACS Catal.* **2015,** *5*, 5272-5282.

30. McInnis, J. P.; Delferro, M.; Marks, T. J., Multinuclear Group 4 Catalysis: Olefin Polymerization Pathways Modified by Strong Metal–Metal Cooperative Effects. *Acc. Chem. Res.* **2014,** *47*, 2545-2557.

31. Xing, Q.; Zhao, T.; Du, S.; Yang, W.; Liang, T.; Redshaw, C.; Sun, W.-H., Biphenyl-Bridged 6-(1-Aryliminoethyl)-2-iminopyridylcobalt Complexes: Synthesis, Characterization, and Ethylene Polymerization Behavior. *Organometallics* **2014,** *33*, 1382-1388.

32. Takeuchi, D.; Takano, S.; Takeuchi, Y.; Osakada, K., Ethylene Polymerization at High Temperatures Catalyzed by Double-Decker-Type Dinuclear Iron and Cobalt Complexes: Dimer Effect on Stability of the Catalyst and Polydispersity of the Product. *Organometallics* **2014,** *33*, 5316-5323.

33. Takano, S.; Takeuchi, D.; Osakada, K.; Akamatsu, N.; Shishido, A., Dipalladium Catalyst for Olefin Polymerization: Introduction of Acrylate Units into the Main Chain of Branched Polyethylene. *Angew. Chem., Int. Ed.* **2014,** *53*, 9246-9250.

34. Liu, J.; Bao, Y.-Y.; Liu, Y.; Ren, W.-M.; Lu, X.-B., Binuclear chromium-salan complex catalyzed alternating copolymerization of epoxides and cyclic anhydrides. *Polym. Chem.* **2013,** *4*, 1439-1444.

35. Han, H.-L.; Liu, Y.; Liu, J.-Y.; Nomura, K.; Li, Y.-S., Synthesis of binuclear phenoxyimino organoaluminum complexes and their use as the catalyst precursors for efficient ring-opening polymerisation of ε-caprolactone. *Dalton Trans.* **2013,** *42*, 12346-12353.

36. Wei, J.; Hwang, W.; Zhang, W.; Sita, L. R., Dinuclear Bis-Propagators for the Stereoselective Living Coordinative Chain Transfer Polymerization of Propene. *J. Am. Chem. Soc.* **2013,** *135*, 2132-2135.

37. Takeuchi, D.; Chiba, Y.; Takano, S.; Osakada, K., Double-Decker-Type Dinuclear Nickel Catalyst for Olefin Polymerization: Efficient Incorporation of Functional Co-monomers. *Angew. Chem., Int. Ed.* **2013,** *52*, 12536-12540.

38. Han, S.; Yao, E.; Qin, W.; Zhang, S.; Ma, Y., Binuclear Heteroligated Titanium Catalyst Based on Phenoxyimine Ligands: Synthesis, Characterization, and Ethylene (Co)polymerization. *Macromolecules* **2012,** *45*, 4054-4059.

39. Radlauer, M. R.; Day, M. W.; Agapie, T., Bimetallic Effects on Ethylene Polymerization in the Presence of Amines: Inhibition of the Deactivation by Lewis Bases. *J. Am. Chem. Soc.* **2012,** *134*, 1478-1481.

40. Delferro, M.; Marks, T. J., Multinuclear Olefin Polymerization Catalysts. *Chem. Rev.* **2011,** *111*, 2450-2485.

41. Thomas, R. M.; Widger, P. C. B.; Ahmed, S. M.; Jeske, R. C.; Hirahata, W.; Lobkovsky, E. B.; Coates, G. W., Enantioselective Epoxide Polymerization Using a Bimetallic Cobalt Catalyst. *J. Am. Chem. Soc.* **2010,** *132*, 16520-16525.

42. Motta, A.; Fragala, I. L.; Marks, T. J., Proximity and Cooperativity Effects in Binuclear d(0) Olefin Polymerization Catalysis. Theoretical Analysis of Structure and Reaction Mechanism. *J. Am. Chem. Soc.* **2009,** *131*, 3974-3984.

43. Li, H.; Marks, T. J., Nuclearity and cooperativity effects in binuclear catalysts and cocatalysts for olefin polymerization. *Proc. Natl. Acad. Sci. U. S. A.* **2006,** *103*, 15295-15302.

44. Guo, N.; Stern, C. L.; Marks, T. J., Bimetallic effects in homopolymerization of styrene and copolymerization of ethylene and styrenic comonomers: Scope, kinetics, and mechanism. *J. Am. Chem. Soc.* **2008,** *130*, 2246-2261.

45. Li, H.; Stern, C. L.; Marks, T. J., Significant proximity and cocatalyst effects in binuclear catalysis for olefin polymerization. *Macromolecules* **2005,** *38*, 9015-9027.

46. Li, H.; Li, L.; Schwartz, D. J.; Metz, M. V.; Marks, T. J.; Liable-Sands, L.; Rheingold, A. L., Coordination copolymerization of severely encumbered isoalkenes with ethylene: Enhanced enchainment mediated by binuclear catalysts and cocatalysts. *J. Am. Chem. Soc.* **2005,** *127*, 14756-14768.

47. Wang, J.; Li, H.; Guo, N.; Li, L.; Stern, C. L.; Marks, T. J., Covalently linked heterobimetallic catalysis for olefin polymerization. *Organometallics* **2004,** *23*, 5112-5114.

48. Li, H.; Li, L.; Marks, T. J., Polynuclear olefin polymerization catalysis: Proximity and cocatalyst effects lead to significantly increased polyethylene molecular weight and comonomer enchainment levels. *Angew. Chem., Int. Ed.* **2004,** *43*, 4937-4940.

49. Guo, N.; Li, L.; Marks, T. J., Bimetallic catalysis for styrene homopolymerization and ethylene-styrene copolymerization. Exceptional comonomer selectivity and insertion regiochemistry. *J. Am. Chem. Soc.* **2004,** *126*, 6542-6543.

50. Li, H.; Li, L.; Marks, T. J.; Liable-Sands, L.; Rheingold, A. L., Catalyst/cocatalyst nuclearity effects in single-site olefin polymerization. Significantly enhanced 1-octene and isobutene comonomer enchainment in ethylene polymerizations mediated by binuclear catalysts and cocatalysts. *J. Am. Chem. Soc.* **2003,** *125*, 10788-10789.

51. Li, L.; Metz, M. V.; Li, H.; Chen, M.-C.; Marks, T. J.; Liable-Sands, L.; Rheingold, A. L., Catalyst/Cocatalyst Nuclearity Effects in Single-Site Polymerization. Enhanced Polyethylene Branching and α-Olefin Comonomer Enchainment in Polymerizations Mediated by Binuclear Catalysts and Cocatalysts via a New Enchainment Pathway. *J. Am. Chem. Soc.* **2002,** *124*, 12725-12741.

52. Salata, M. R.; Marks, T. J., Catalyst Nuclearity Effects in Olefin Polymerization. Enhanced Activity and Comonomer Enchainment in Ethylene + Olefin Copolymerizations Mediated by Bimetallic Group 4 Phenoxyiminato Catalysts. *Macromolecules* **2009,** *42*, 1920-1933.

53. Salata, M. R.; Marks, T. J., Synthesis, Characterization, and Marked Polymerization Selectivity Characteristics of Binuclear Phenoxyiminato Organozirconium Catalysts. *J. Am. Chem. Soc.* **2008,** *130*, 12-13.

54. Kamitani, M.; Pinter, B.; Chen, C.-H.; Pink, M.; Mindiola, D. J., Mononuclear and Terminal Zirconium and Hafnium Methylidenes. *Angew. Chem. Intl. Ed.* **2014,** *53*, 10913-10915.

55. Keaton, R. J.; Jayaratne, K. C.; Fettinger, J. C.; Sita, L. R., Structural Characterization of Zirconium Cations Derived from a Living Ziegler–Natta Polymerization System: New Insights Regarding Propagation and Termination Pathways for Homogeneous Catalysts. *J. Am. Chem. Soc.* **2000,** *122*, 12909-12910.

56. Delferro, M.; Marks, T. J., Multinuclear Olefin Polymerization Catalysts. *Chem. Rev.* **2011,** *111*, 2450-2485.

57. Li, H.; Marks, T. J., Nuclearity and cooperativity effects in binuclear catalysts and cocatalysts for olefin polymerization. *Proc. Natl. Acad. Sci. U.S.A.* **2006,** *103*, 15295-15302.

58. Radlauer, M. R.; Agapie, T., Bimetallic Zirconium Amine Bis(phenolate) Polymerization Catalysts: Enhanced Activity and Tacticity Control for Polyolefin Synthesis. *Organometallics* **2014,** *33*, 3247-3250.

59. Radlauer, M. R.; Buckley, A. K.; Henling, L. M.; Agapie, T., Bimetallic Coordination Insertion Polymerization of Unprotected Polar Monomers: Copolymerization of Amino Olefins and Ethylene by Dinickel Bisphenoxyiminato Catalysts. *J. Am. Chem. Soc.* **2013,** *135*, 3784-3787.

60. Zuccaccia, C.; Macchioni, A.; Busico, V.; Cipullo, R.; Talarico, G.; Alfano, F.; Boone, H. W.; Frazier, K. A.; Hustad, P. D.; Stevens, J. C.; Vosejpka, P. C.; Abboud, K. A., Intra- and Intermolecular NMR Studies on the Activation of Arylcyclometallated Hafnium Pyridyl-Amido Olefin Polymerization Precatalysts. *J. Am. Chem. Soc.* **2008,** *130*, 10354-10368.

61. Bouwkamp, M. W.; Budzelaar, P. H. M.; Gercama, J.; Del Hierro Morales, I.; de Wolf, J.; Meetsma, A.; Troyanov, S. I.; Teuben, J. H.; Hessen, B., Naked (C5Me5)2M Cations (M = Sc, Ti, and V) and Their Fluoroarene Complexes. *J. Am. Chem. Soc.* **2005,** *127*, 14310-14319.

62. Wu, F.; Jordan, R. F., Sigma-Bond Metathesis Reactions of Zirconocene Alkyl Cations with Phenylsilane. *Organometallics* **2005,** *24*, 2688-2697.

63. Song, F.; Lancaster, S. J.; Cannon, R. D.; Schormann, M.; Humphrey, S. M.; Zuccaccia, C.; Macchioni, A.; Bochmann, M., Synthesis, Ion Aggregation, Alkyl Bonding Modes, and Dynamics of 14-Electron Metallocenium Ion Pairs [(SBI)MCH2SiMe3+···X-] (M = Zr, Hf): Inner-Sphere (X = MeB(C6F5)3) versus Outer-Sphere (X = B(C6F5)4) Structures and the Implications for "Continuous" or "Intermittent" Alkene Polymerization Mechanisms. *Organometallics* **2005,** *24*, 1315-1328.

64. Kilgore, U. J.; Basuli, F.; Huffman, J. C.; Mindiola, D. J., Aryl Isocyanate, Carbodiimide, and Isocyanide Prepared from Carbon Dioxide. A Metathetical Group-Transfer Tale Involving a Titanium–Imide Zwitterion. *Inorg. Chem.* **2005,** *45*, 487-489.

65. Steffen, W.; Blomker, T.; Kleigrewe, N.; Kehr, G.; Frohlich, R.; Erker, G., Generation of bis(iminoalkyl)pyridine cobalt(i) cations under metal alkyl free conditions that polymerize ethene. *Chem. Commun.* **2004,** (10), 1188-1189.

66. Chen, M.-C.; Roberts, J. A. S.; Marks, T. J., Marked Counteranion Effects on Single-Site Olefin Polymerization Processes. Correlations of Ion Pair Structure and Dynamics with Polymerization Activity, Chain Transfer, and Syndioselectivity. *J. Am. Chem. Soc.* **2004,** *126*, 4605-4625.

67. Al-Humydi, A.; Garrison, J. C.; Youngs, W. J.; Collins, S., Propene Polymerization Using ansa-Metallocenium Ions: Excess Activator Effects on Polymerization Activity and Polymer Microstructure. *Organometallics* **2004,** *24*, 193-196.

68. Nielsen, L. P. C.; Stevenson, C. P.; Blackmond, D. G.; Jacobsen, E. N., Mechanistic Investigation Leads to a Synthetic Improvement in the Hydrolytic Kinetic Resolution of Terminal Epoxides. *J. Am. Chem. Soc.* **2004,** *126*, 1360-1362.

69. Ma, K.; Piers, W. E.; Gao, Y.; Parvez, M., Isolation and Characterization of a Monomeric Cationic Titanium Hydride. *J. Am. Chem. Soc.* **2004,** *126*, 5668-5669.

70. Zhang, Y.; Reeder, E. K.; Keaton, R. J.; Sita, L. R., Goldilocks Effect of a Distal Substituent on Living Ziegler–Natta Polymerization Activity and Stereoselectivity within a Class of Zirconium Amidinate-Based Initiators. *Organometallics* **2004,** *23*, 3512-3520.

71. Zuccaccia, C.; Stahl, N. G.; Macchioni, A.; Chen, M.-C.; Roberts, J. A.; Marks, T. J., NOE and PGSE NMR Spectroscopic Studies of Solution Structure and Aggregation in Metallocenium Ion-Pairs. *J. Am. Chem. Soc.* **2004,** *126*, 1448-1464.

72. Schrock, R. R.; Casado, A. L.; Goodman, J. T.; Liang, L.-C.; Bonitatebus, P. J.; Davis, W. M., Preparation and Activation of Complexes of the Type [((mesityl)NCH2CH2)2NX]ZrMe2 (X = H, Me) with [Ph3C][B(C6F5)4] or [PhNMe2H][B(C6F5)4]. *Organometallics* **2000,** *19*, 5325-5341.

73. Baumann, R.; Davis, W. M.; Schrock, R. R., Synthesis of Titanium and Zirconium Complexes That Contain the Tridentate Diamido Ligand, [((t-Bu-d6)N-o-C6H4)2O]2- ([NON]2) and the Living Polymerization of 1-Hexene by Activated [NON]ZrMe2. *J. Am. Chem. Soc.* **1997,** *119*, 3830-3831.

74. McKnight, A. L.; Waymouth, R. M., Ethylene/Norbornene Copolymerizations with Titanium CpA Catalysts. *Macromolecules* **1999,** *32*, 2816-2825.

75. LaPointe, R. E.; Stevens, J. C.; Nickias, P. N.; McAdon, M. H. Homogeneous Olefin Polymerization Catalyst By Abstraction with Lewis Acids. US005721185A, February 24, 1998.

76. Nifant'ev, I. E.; Yarnykh, V. L.; Borzov, M. V.; Mazurchik, B. A.; Mstislavskii, V. I.; Roznyatovskii, V. A.; Ustynyuk, Y. A., Synthesis, structure, and fluxional behavior of 4-sila-, 4-germa-, and 4-stanna-3a,4,4a,8-tetrahydro-4,4,8,8-tetramethyl-s-indacenes. *Organometallics* **1991,** *10*, 3739-3745.

77. Braunschweig, H.; Breitling, F. M., Constrained geometry complexes - Synthesis and applications. *Coord. Chem. Rev.* **2006,** *250*, 2691-2720.

78. Christopher, J. N.; Jordan, R. F.; Petersen, J. L.; Young, V. G., Synthesis and Structures of rac-Me2Si(η 5-1-indenyl)2Hf(NMe2)2 and {Me2Si(η 5-1-indenyl)(η 3-2-indenyl)}Hf(NMe2)2. *Organometallics* **1997,** *16*, 3044-3050.

79. Diamond, G. M.; Jordan, R. F.; Petersen, J. L., Efficient Synthesis of Chiral ansa-Metallocenes by Amine Elimination. Synthesis, Structure, and Reactivity of rac-(EBI)Zr(NMe2)2. *J. Am. Chem. Soc.* **1996,** *118*, 8024-8033.

80. Diamond, G. M.; Jordan, R. F.; Petersen, J. L., Synthesis of Me2Si-Bridged ansa-Zirconocenes by Amine Elimination. *Organometallics* **1996,** *15*, 4045-4053.

81. Diamond, G. M.; Jordan, R. F.; Petersen, J. L., Synthesis of Group 4 Metal rac-(EBI)M(NR2)2 Complexes by Amine Elimination. Scope and Limitations. *Organometallics* **1996,** *15*, 4030-4037.

82. Christopher, J. N.; Diamond, G. M.; Jordan, R. F.; Petersen, J. L., Synthesis, Structure, and Reactivity of rac-Me2Si(indenyl)2Zr(NMe2)2. *Organometallics* **1996,** *15*, 4038-4044.

83. Carpenetti, D. W.; Kloppenburg, L.; Kupec, J. T.; Petersen, J. L., Application of Amine Elimination for the Efficient Preparation of Electrophilic ansa-Monocyclopentadienyl Group 4 Complexes Containing an Appended Amido Functionality. Structural Characterization of [(C5H4)SiMe2(N-t-Bu)]ZrCl2(NMe2H). *Organometallics* **1996,** *15*, 1572-1581.

84. Sun, W.-H.; Liu, S.; Zhang, W.; Zeng, Y.; Wang, D.; Liang, T., Syntheses, Characterization, and the Ethylene (Co-)Polymerization Screening of 2-Benzimidazolyl-N-phenylquinoline-8-carboxamide Half-Titanocene Chlorides. *Organometallics* **2010,** *29*, 732-741.

85. Liu, S.; Sun, W.-H.; Zeng, Y.; Wang, D.; Zhang, W.; Li, Y., Syntheses, Characterization, and Ethylene (Co-)Polymerization Screening of Amidate Half-Titanocene Dichlorides. *Organometallics* **2010,** *29*, 2459-2464.

86. Liu, S.; Yi, J.; Zuo, W.; Wang, K.; Wang, D.; Sun, W.-H., N-(2-Benzimidazolylquinolin-8-yl)benzamidate Half-Titanocene Chlorides: Synthesis, Characterization and Their Catalytic Behavior Toward Ethylene Polymerization. *J. Polym. Sci., Part A: Polym. Chem.* **2009,** *47*, 3154-3169.

87. Scoles, L.; Minhas, R.; Duchateau, R.; Jubb, J.; Gambarotta, S., Synthesis and Characterization of Novel Titanium(III) and -(IV) Alkyls and Carbenes Supported by Amide Ligands. Crystal Structure of [(Cy2N)2Ti(.mu.-CH2)]2. *Organometallics* **1994,** *13*, 4978-4983.

88. Searles, K.; Smith, K. T.; Kurogi, T.; Chen, C.-H.; Carroll, P. J.; Mindiola, D. J., Formation and Redox Interconversion of Niobium Methylidene and Methylidyne Complexes. *Angew. Chem. Intl. Ed.* **2016,** *55*, 6642-6645.

89. Dietrich, H. M.; Toernroos, K. W.; Anwander, R., "Ionic Carbenes": Synthesis, Structural Characterization, and Reactivity of Rare-Earth Metal Methylidene Complexes. *J. Am. Chem. Soc.* **2006,** *128*, 9298-9299.

90. Flores, J. A.; Cavaliere, V. N.; Buck, D.; Pinter, B.; Chen, G.; Crestani, M. G.; Baik, M.-H.; Mindiola, D. J., Methane activation and exchange by titanium-carbon multiple bonds. *Chem. Sci.* **2011,** *2*, 1457-1462.

91. Mackenzie, P. B.; Coots, R. J.; Grubbs, R. H., Synthesis, structure, and reactions of heterobinuclear μ -methylene complexes. *Organometallics* **1989,** *8*, 8-14.

92. Kurogi, T.; Carroll, P. J.; Mindiola, D. J., A radical coupled pathway to a stable and terminally bound titanium methylidene. *Chem. Commun.* **2017,** *53*, 3412-3414.

93. Grant, L. N.; Ahn, S.; Manor, B. C.; Baik, M.-H.; Mindiola, D. J., Structural elucidation of a mononuclear titanium methylidene. *Chem. Commun.* **2017,** *53*, 3415-3417.

94. Kurogi, T.; Kamitani, M.; Manor, B. C.; Carroll, P. J.; Mindiola, D. J., Reactivity Studies of a Zirconium Methylidene Complex: Group Transfer and Methylenation Reactions. *Organometallics* **2017**, *36*, 74-79.

95. Kamitani, M.; Pinter, B.; Searles, K.; Crestani, M. G.; Hickey, A.; Manor, B. C.; Carroll, P. J.; Mindiola, D. J., Phosphinoalkylidene and -alkylidyne Complexes of Titanium: Intermolecular C–H Bond Activation and Dehydrogenation Reactions. *J. Am. Chem. Soc.* **2015,** *137*, 11872-11875.

96. Crestani, M. G.; Hickey, A. K.; Gao, X.; Pinter, B.; Cavaliere, V. N.; Ito, J.-I.; Chen, C.-H.; Mindiola, D. J., Room Temperature Dehydrogenation of Ethane, Propane, Linear Alkanes C4–C8, and Some Cyclic Alkanes by Titanium–Carbon Multiple Bonds. *J. Am. Chem. Soc.* **2013,** *135*, 14754-14767.

97. Scott, J.; Mindiola, D. J., A tribute to Frederick Nye Tebbe. Lewis acid stabilized alkylidyne, alkylidene, and imides of 3d early transition metals. *Dalton Trans*. **2009,** (40), 8463-8472.

98. Due to the instability/decomposition of ***rac*-6** in methylene chloride and its low solubility in toluene, low temperature NMR study was not possible

99. Thorn, M. G.; Etheridge, Z. C.; Fanwick, P. E.; Rothwell, I. P., Cationic group 4 metal alkyl compounds containing o-arylphenoxide ligation. *Organometallics* **1998,** *17*, 3636-3638.

100. Bochmann, M.; Cuenca, T.; Hardy, D. T., Facile alpha-H Elimination in Cationic Zirconium Alkyl Complexes - Formation of mu-CH2 Complexes as a Possible Deactivation Pathway in Polymerization Catalysis. *J. Organomet. Chem*. **1994,** *484*, C10-C12.

101. Zhang, S. B.; Piers, W. E., Methane loss from cationic mu-methyl dimers formed via trityl borate activation of monocyclopentadienyl ketimide complexes Cp (Bu-t)(2)C=N Ti(CH3)(2) (Cp = C5H5, C5Me5, C5Me4SiMe3). *Organometallics* **2001,** *20*, 2088-2092.

102. Ghisolfi, A.; Condello, F.; Fliedel, C.; Rosa, V.; Braunstein, P., Facile and Room-Temperature Activation of Csp3-Cl Bonds by Cheap and Air-Stable Nickel(II) Complexes of (N-Thioether) DPPA-Type Ligands. *Organometallics* **2015,** *34*, 2255-2260.

103. Vivancos, A.; Paneque, M.; Poveda, M. L.; Alvarez, E., Building a parent iridabenzene structure from acetylene and dichloromethane on an iridium center. *Angew. Chem., Int. Ed*. **2013,** *52*, 10068-10071.

104. Pattacini, R.; Jie, S.; Braunstein, P., Facile dichloromethane activation and phosphine methylation. Isolation of unprecedented zwitterionic organozinc and organocobalt intermediates. *Chem. Commun*. **2009,** (8), 890-892.

105. Gomez-Benitez, V.; Toscano, R. A.; Morales-Morales, D., Synthesis and characterization of [Pd{PhP(C6H4-2-SCH2Cl)(C6H4-2-S)}(Ph2PCH2CH2PPh2)]Cl: An example of hemilability and dichloromethane activation. *Inorg. Chem. Commun*. **2007,** *10*, 1-6.

106. Yan, T.-H.; Tsai, C.-C.; Chien, C.-T.; Cho, C.-C.; Huang, P.-C., Dichloromethane Activation. Direct Methylenation of Ketones and Aldehydes with CH2Cl2 Promoted by Mg/TiCl4/THF. *Org. Lett*. **2004,** *6*, 4961-4963.

107. Sugawara, K.-I.; Hikichi, S.; Akita, M., Dichloromethane activation by chlorochromium(II) complexes with TpiPr2: generation of an electrophilic Cr-methylene

species without the action of an external Cl-abstraction reagent. *Chem. Lett.* **2001,** (11), 1094-1095.

108. Varga, V.; Pinkas, J.; Císařová, I.; Horáček, M.; Mach, K., Pentamethylcyclopentadienylmethyltitanium Silsesquioxanes and Their Zwitterionic Complexes with Tris(pentafluorophenyl)borane. *Organometallics* **2009,** *28*, 6944-6956.

109. Kilgore, U. J.; Basuli, F.; Huffman, J. C.; Mindiola, D. J., Aryl Isocyanate, Carbodiimide, and Isocyanide Prepared from Carbon Dioxide. A Metathetical Group-Transfer Tale Involving a Titanium–Imide Zwitterion. *Inorg. Chem.* **2006,** *45*, 487-489.

110. Basuli, F.; Clark, R. L.; Bailey, B. C.; Brown, D.; Huffman, J. C.; Mindiola, D. J., Latent low-coordinate titanium imides supported by a sterically encumbering [small beta]-diketiminate ligand. *Chem. Commun.* **2005,** (17), 2250-2252.

111. Shafir, A.; Arnold, J., Stabilization of a Cationic Ti Center by a Ferrocene Moiety: A Remarkably Short Ti–Fe Interaction in the Diamide {[(η 5-C5H4NSiMe3)2Fe]TiCl}22+. *J. Am. Chem. Soc.* **2001,** *123*, 9212-9213.

112. Guerin, F.; Stephan, D. W., Synthesis and structure of the dicationic bisborate adduct [(tBu3PN)2Ti{ μ -MeB(C6F5)3}2]. *Angew. Chem., Int. Ed.* **2000,** *39*, 1298-1300.

113. Stephan, D. W.; Stewart, J. C.; Guérin, F.; Spence, R. E. v. H.; Xu, W.; Harrison, D. G., Phosphinimides as a Steric Equivalent to Cyclopentadienyl: An Approach to Ethylene Polymerization Catalyst Design. *Organometallics* **1999,** *18*, 1116-1118.

114. Stephenson, C. J.; McInnis, J. P.; Chen, C.; Weberski, M. P.; Motta, A.; Delferro, M.; Marks, T. J., Ni(II) Phenoxyiminato Olefin Polymerization Catalysis: Striking Coordinative Modulation of Hyperbranched Polymer Microstructure and Stability by a Proximate Sulfonyl Group. *ACS Catal.* **2014,** *4*, 999-1003.

115. Weberski, M. P., Jr.; Chen, C.; Delferro, M.; Marks, T. J., Ligand Steric and Fluoroalkyl Substituent Effects on Enchainment Cooperativity and Stability in Bimetallic Nickel(II) Polymerization Catalysts. *Chem.-Eur. J.* **2012,** *18*, 10715-10732.

116. Kaminsky, W., Discovery of Methylaluminoxane as Cocatalyst for Olefin Polymerization. *Macromolecules* **2012,** *45*, 3289-3297.

117. Bochmann, M., The Chemistry of Catalyst Activation: The Case of Group 4 Polymerization Catalysts†. *Organometallics* **2010,** *29*, 4711-4740.

118. Chen, E. Y. X.; Marks, T. J., Cocatalysts for metal-catalyzed olefin polymerization: Activators, activation processes, and structure-activity relationships. *Chem. Rev.* **2000,** *100*, 1391-1434.

119. Möhring, P. C.; Coville, N. J., Group 4 metallocene polymerisation catalysts: quantification of ring substituent steric effects. *Coord. Chem. Rev.* **2006,** *250*, 18-35.

120. Klet, R. C.; VanderVelde, D. G.; Labinger, J. A.; Bercaw, J. E., Highly regioirregular polypropylene from asymmetric group 4 anilide(pyridine)phenoxide complexes. *Chem. Commun.* **2012,** *48*, 6657-6659.

121. McKnight, A. L.; Masood, M. A.; Waymouth, R. M.; Straus, D. A., Selectivity in Propylene Polymerization with Group 4 Cp–Amido Catalysts. *Organometallics* **1997,** *16*, 2879-2885.

122. Asakura, T.; Kakayama, N.; Demura, M.; Asano, A., Carbon-13 NMR Spectral Assignments of Regioirregular Polypropylene Determined from Two-Dimensional INADEQUATE Spectra and Chemical Shift Calculations. *Macromolecules* **1992,** *25*, 4876-4881.

123. Kaur, S.; Naik, D. G.; Singh, G.; Patil, H. R.; Kothari, A. V.; Gupta, V. K., Poly(1-octene) Synthesis Using High Performance Supported Titanium Catalysts. *J. Appl. Polym. Sci.* **2010,** *115*, 229-236.

124. Resconi, L.; Jones, R. L.; Rheingold, A. L.; Yap, G. P. A., High-molecular-weight atactic polypropylene from metallocene catalysts .1. Me(2)Si(9-flu)(2)ZrX(2) (X=Cl, Me). *Organometallics* **1996,** *15*, 998-1005.

125. Caporaso, L.; Loria, M.; Mazzeo, M.; Michiue, K.; Nakano, T.; Fujita, T.; Cavallo, L., Mechanism of Isotactic Styrene Polymerization with a C6F5-Substituted Bis(phenoxyimine) Titanium System. *Macromolecules* **2012,** *45*, 8588-8597.

126. ^{13}C NMR spectra of polypropylene products indicate that all contain trace levels of regioerrors as compared to standard literature spectra (see ref. 31). It is therefore possible that solubility properties are affected by both stereo- and trace regioerrors.

127. For propylene homopolymerization, ***rac*-3** and ***meso*-3** acivated with $B(C_6F_5)_3$ produce only trace amounts of polymer.

128. Lanza, G.; Fragalà, I. L.; Marks, T. J., Ligand Substituent, Anion, and Solvation Effects on Ion Pair Structure, Thermodynamic Stability, and Structural Mobility in "Constrained Geometry" Olefin Polymerization Catalysts: an Ab Initio Quantum Chemical Investigation. *J. Am. Chem. Soc.* **2000,** *122*, 12764-12777.

129. McDaniel, M. P.; Schwerdtfeger, E. D.; Jensen, M. D., The "comonomer effect" on chromium polymerization catalysts. *J. Catal.* **2014,** *314* (0), 109-116.

130. Awudza, J. A. M.; Tait, P. J. T., The "comonomer effect" in ethylene/ α -olefin copolymerization using homogeneous and silica-supported Cp2ZrCl2/MAO catalyst

systems: some insights from the kinetics of polymerization, active center studies, and polymerization temperature. *J. Polym. Sci., Part A: Polym. Chem.* **2007,** *46*, 267-277.

131. Nomura, K.; Komatsu, T.; Imanishi, Y., Polymerization of 1-hexene, 1-octene catalyzed by Cp′ TiCl2(O-2,6-iPr2C6H3)-MAO system. Unexpected increase of the catalytic activity for ethylene/1-hexene copolymerization by (1,3-tBu2C5H3)TiCl2(O-2,6-iPr2C6H3)-MAO catalyst system. *J. Mol. Catal. A: Chem.* **2000,** *152*, 249-252.

132. Chien, J. C. W.; Nozaki, T., Ethylene Hexene Copolymerization by Heterogeneous and Homogeneous Ziegler-Natta Catalysts and the Comonomer Effect. *J. Polym. Sci., Part A: Polym. Chem.* **1993,** *31*, 227-237.

133. Caporaso, L.; Izzo, L.; Sisti, I.; Oliva, L., Stereospecific Ethylene–Styrene Block Copolymerization with ansa-Zirconocene-Based Catalyst†. *Macromolecules* **2002,** *35*, 4866-4870.

134. Stephan, D. W.; Guérin, F.; Spence, R. E. v. H.; Koch, L.; Gao, X.; Brown, S. J.; Swabey, J. W.; Wang, Q.; Xu, W.; Zoricak, P.; Harrison, D. G., Remarkably Active Non-Metallocene Ethylene Polymerization Catalysts. *Organometallics* **1999,** *18*, 2046-2048.

135. Randall, J. C., A Review of High Resolution Liquid C-13 Nuclear Magnetic Resonance Characterization of Ethylene Based Polymers. *J. Macromol. Sci., Rev. Macromol. Chem. Phy.* **1989,** *C29*, 201-317.

136. Tanaka, R.; Viehmann, P.; Hecht, S., Bis(phenoxy-azo)titanium(IV) Complexes: Synthesis, Structure, and Catalytic Activity in Styrene Polymerization. *Organometallics* **2012,** *31*, 4216-4220.

137. Jian, Z.; Cui, D.; Hou, Z., Rare-Earth-Metal-Hydrocarbyl Complexes Bearing Linked Cyclopentadienyl or Fluorenyl Ligands: Synthesis, Catalyzed Styrene Polymerization, and Structure-Reactivity Relationship. *Chem. - Eur. J.* **2012,** *18*, 2674-2684.

138. Zhang, H.; Nomura, K., Living Copolymerization of Ethylene with Styrene Catalyzed by (Cyclopentadienyl)(ketimide)titanium(IV) Complex–MAO Catalyst System: Effect of Anionic Ancillary Donor Ligand. *Macromolecules* **2006,** *39*, 5266-5274.

139. Zhang, H.; Nomura, K., Living Copolymerization of Ethylene with Styrene Catalyzed by (Cyclopentadienyl)(ketimide)titanium(IV) Complex–MAO Catalyst System. *J. Am. Chem. Soc.* **2005,** *127*, 9364-9365.

140. Xu, G.; Lin, S., Titanocene–Methylaluminoxane Catalysts for Copolymerization of Styrene and Ethylene: Synthesis and Characterization of Styrene–Ethylene Copolymers. *Macromolecules* **1997,** *30*, 685-693.

141. Cho, W.; Cho, H.; Lee, C. S.; Lee, B. Y.; Moon, B.; Kang, J., Synthesis of new bis(amidine)-cobalt catalysts and their application to styrene polymerization. *Organometallics* **2014,** *33*, 1617-1622.

142. Dariva, C.; Lovisi, H.; Mariac, L. C. S.; Coutinho, F. M. B.; Oliveira, J. V.; Pinto, J. C., Propylene Solubility in Toluene and Isododecane. *Can. J. Chem. Eng.* **2003,** *81*, 147-152.

143. Homopolymerizations performed with ***meso*-3** and 2.4 equiv. $[Ph_3C][B(C_6F_5)_4]$ under 5 atm ethylene pressure and otherwise identical conditions to those presented in Table 1.1 yielded polyethylene with M_n = 473 kg/mol, $Đ$ = 4.7. In contrast to the CGC^2-M_2 catalysts (Chart 1, C), chain-transfer to monomer is not operative here, due to the observed increase in M_n with increasing monomer concentration (see ref 4h).

144. Coates, G. W., Precise Control of Polyolefin Stereochemistry Using Single-Site Metal Catalysts. *Chem. Rev.* **2000,** *100*, 1223-1252.

145. Miyake, G. M.; Chen, E. Y. X., Synthesis of highly syndiotactic polymers by discrete catalysts or initiators. *Polym. Chem.* **2011,** *2*, 2462-2480.

146. Veghini, D.; Henling, L. M.; Burkhardt, T. J.; Bercaw, J. E., Mechanisms of Stereocontrol for Doubly Silylene-Bridged Cs- and C1-Symmetric Zirconocene Catalysts for Propylene Polymerization. Synthesis and Molecular Structure of Li2[(1,2-Me2Si)2{C5H2-4-(1R,2S,5R-menthyl)}{C5H-3,5-(CHMe2)2)}]· 3THF and [(1,2-Me2Si)2{ η 5-C5H2-4-(1R,2S,5R-menthyl)}{ η 5-C5H-3,5-(CHMe2)2}]ZrCl2. *J. Am. Chem. Soc.* **1999,** *121*, 564-573.

147. Herzog, T. A.; Zubris, D. L.; Bercaw, J. E., A New Class of Zirconocene Catalysts for the Syndiospecific Polymerization of Propylene and Its Modification for Varying Polypropylene from Isotactic to Syndiotactic. *J. Am. Chem. Soc.* **1996,** *118*, 11988-11989.

148. Razavi, A.; Ferrara, J., Preparation and crystal structures of the complexes (η 5-C5H4CMe2 η 5-C13H8) MCl2 (M = Zr, Hf) and their role in the catalytic formation of syndiotactic polypropylene. *J. Organomet. Chem.* **1992,** *435*, 299-310.

149. Ewen, J. A.; Jones, R. L.; Razavi, A.; Ferrara, J. D., Syndiospecific Propylene Polymerizations with Group 4 Metallocenes. *J. Am. Chem. Soc.* **1988,** *110*, 6255-6256.

150. Brintzinger, H. H.; Fischer, D.; Mülhaupt, R.; Rieger, B.; Waymouth, R. M., Stereospecific Olefin Polymerization with Chiral Metallocene Catalysts. *Angew. Chem. Intl. Ed.* **1995,** *34*, 1143-1170.

151. Yasumoto, T.; Yamamoto, K.; Tsurugi, H.; Mashima, K., Isospecific polymerization of 1-hexene by C1-symmetric half-metallocene dimethyl complexes of

group 4 metals with bidentate N-substituted iminomethylpyrrolyl ligands. *Dalton Trans*. **2013,** *42*, 9120-9128.

152. Press, K.; Cohen, A.; Goldberg, I.; Venditto, V.; Mazzeo, M.; Kol, M., Salalen Titanium Complexes in the Highly Isospecific Polymerization of 1-Hexene and Propylene. *Angew. Chem. Intl. Ed.* **2011,** *50*, 3529-3532.

153. Kirillov, E.; Marquet, N.; Razavi, A.; Belia, V.; Hampel, F.; Roisnel, T.; Gladysz, J. A.; Carpentier, J.-F., New C1-Symmetric Ph2C-Bridged Multisubstituted ansa-Zirconocenes for Highly Isospecific Propylene Polymerization: Synthetic Approach via Activated Fulvenes. *Organometallics* **2010,** *29*, 5073-5082.

154. Li, G.; Lamberti, M.; D'Amora, S.; Pellecchia, C., C1-Symmetric Pentacoordinate Anilidopyridylpyrrolide Zirconium(IV) Complexes as Highly Isospecific Olefin Polymerization Catalysts. *Macromolecules* **2010,** *43*, 8887-8891.

155. Cohen, A.; Kopilov, J.; Goldberg, I.; Moshe, K., C1-Symmetric Zirconium Complexes of [ONNO']-Type Salan Ligands: Accurate Control of Catalyst Activity, Isospecificity, and Molecular Weight in 1-Hexene Polymerization. *Organometallics* **2009,** *28*, 1391-1405.

156. Miller, S. A.; Bercaw, J. E., Mechanism of Isotactic Polypropylene Formation with C1-Symmetric Metallocene Catalysts. *Organometallics* **2006,** *25*, 3576-3592.

157. Lee, M. H.; Han, Y.; Kim, D.-h.; Hwang, J.-W.; Do, Y., Isospecific Propylene Polymerization by C1-Symmetric Me2Si(C5Me4)(2-R-Ind)MCl2 (M = Ti, Zr) Complexes. *Organometallics* **2003,** *22*, 2790-2796.

158. Obora, Y.; Stern, C. L.; Marks, T. J.; Nickias, P. N., Ancillary Ligand Effects in Chiral C1-Symmetric ansa-Metallocene Catalysts for Stereoregular a-Olefin Polymerization. "Wingspan" Modification with Octahydrofluorene. *Organometallics* **1997,** *16*, 2503-2505.

159. Giardello, M. A.; Eisen, M. S.; Stern, C. L.; Marks, T. J., Chiral C1-Symmetric Group 4 Metallocenes as Catalysts for Stereogregular a-Olefin Polymerization. Metal, Ancillary Ligand, and Counteranion Effects. *J. Am. Chem. Soc.* **1995,** *117*, 12114-12129.

160. Giardello, M. A.; Eisen, M. S.; Stern, C. L.; Marks, T. J., Chiral, Non-C2 Symmetric Zirconocene Complexes as Catalysts for Stereoregular a-Olefin Polymerization. *J. Am. Chem. Soc.* **1993,** *115*, 3326-3327.

161. Roberts, J. A. S.; Chen, M.-C.; Seyam, A. M.; Li, L.; Zuccaccia, C.; Stahl, N. G.; Marks, T. J., Diverse Stereocontrol Effects Induced by Weakly Coordinating Anions. Stereospecific Olefin Polymerization Pathways at Archetypal Cs- and C1-Symmetric

Metallocenium Catalysts Using Mono- and Polynuclear Halo-perfluoroarylmetalates as Cocatalysts. *J. Am. Chem. Soc.* **2007,** *129*, 12713-12733.

162. Alt, H. G.; Köppl, A., Effect of the Nature of Metallocene Complexes of Group IV Metals on Their Performance in Catalytic Ethylene and Propylene Polymerization. *Chem. Rev.* **2000,** *100*, 1205-1222.

163. Kaminsky, W., Highly active metallocene catalysts for olefin polymerization. *J. Chem. Soc., Dalton Trans.* **1998,** (9), 1413-1418.

164. Bochmann, M., Cationic Group 4 metallocene complexes and their role in polymerisation catalysis: the chemistry of well defined Ziegler catalysts. *J. Chem. Soc., Dalton Trans.* **1996,** (3), 255-270.

165. De Rosa, C.; Di Girolamo, R.; Talarico, G., Expanding the Origin of Stereocontrol in Propene Polymerization Catalysis. *ACS Catal.* **2016,** *6*, 3767-3770.

166. Wang, X.-Y.; Wang, Y.-X.; Li, Y.-S.; Pan, L., Convenient Syntheses and Versatile Functionalizations of Isotactic Polypropylene Containing Plentiful Pendant Styrene Groups with High Efficiency. *Macromolecules* **2015,** *48*, 1991-1998.

167. Boussie, T. R.; Diamond, G. M.; Goh, C.; Hall, K. A.; LaPointe, A. M.; Leclerc, M. K.; Murphy, V.; Shoemaker, J. A. W.; Turner, H.; Rosen, R. K.; Stevens, J. C.; Alfano, F.; Busico, V.; Cipullo, R.; Talarico, G., Nonconventional Catalysts for Isotactic Propene Polymerization in Solution Developed by Using High-Throughput-Screening Technologies. *Angew. Chem. Intl. Ed.* **2006,** *45*, 3278-3283.

168. Homopolymerization of 1-hexene with ***meso*-7** (***meso*-3** + 2 equiv. $B(C_6F_5)_3$) utilizing 1.0 M 1-hexene in toluene and otherwise identical conditions to the 1-octene homopolymerizations yielded polymer with 91.8% mmmm (M_n = 21.4 kg/mol, $Đ$ = 2.9). Due to the inactivity of ***meso*-7** towards propylene homopolymerization, we cannot conclude that there is an obvious relationship between olefin length and isotacticity of the resulting polymer.

169. Deck, P. A.; Beswick, C. L.; Marks, T. J., Highly Electrophilic Olefin Polymerization Catalysts. Quantitative Reaction Coordinates for Fluoroarylborane/Alumoxane Methide Abstraction and Ion-Pair Reorganization in Group 4 Metallocene and "Constrained Geometry" Catalysts. *J. Am. Chem. Soc.* **1998,** *120*, 1772-1784.

170. Deck, P. A.; Marks, T. J., Cationic Metallocene Olefin Polymerization Catalysts. Thermodynamic and Kinetic Parameters for Ion Pair Formation, Dissociation, and Reorganization. *J. Am. Chem. Soc.* **1995,** *117*, 6128-6129.

171. Talarico, G.; Budzelaar, P. H. M., Ligand Coordination Driven by Monomer and Polymer Chain: The Intriguing Case of Salalen–Ti Catalyst for Propene Polymerization. *Macromolecules* **2017,** *50*, 5332-5336.

172. Zhang, Y.; Ning, Y.; Caporaso, L.; Cavallo, L.; Chen, E. Y. X., Catalyst-Site-Controlled Coordination Polymerization of Polar Vinyl Monomers to Highly Syndiotactic Polymers. *J. Am. Chem. Soc.* **2010,** *132*, 2695-2709.

173. Min, E. Y. J.; Byers, J. A.; Bercaw, J. E., Catalyst Site Epimerization during the Kinetic Resolution of Chiral α-Olefins by Polymerization. *Organometallics* **2008,** *27*, 2179-2188.

174. Alonso-Moreno, C.; Lancaster, S. J.; Zuccaccia, C.; Macchioni, A.; Bochmann, M., Evidence for Mixed-Ion Clusters in Metallocene Catalysts: Influence on Ligand Exchange Dynamics and Catalyst Activity. *J. Am. Chem. Soc.* **2007,** *129*, 9282-9283.

175. Talarico, G.; Budzelaar, P. H. M., Analysis of Stereochemistry Control in Homogeneous Olefin Polymerization Catalysis. *Organometallics* **2014,** *33*, 5974-5982.

176. Fan, W.; Leclerc, M. K.; Waymouth, R. M., Alternating Stereospecific Copolymerization of Ethylene and Propylene with Metallocene Catalysts. *J. Am. Chem. Soc.* **2001,** *123*, 9555-9563.

177. Michiue, K.; Onda, M.; Tanaka, H.; Makio, H.; Mitani, M.; Fujita, T., Styrene Polymerization Behavior of Phenoxy-Imine Ligated Ti Complexes/MAO: Formation of Highly Isotactic and Syndiotactic PS. *Macromolecules* **2008,** *41*, 6289-6291.

178. Chum, P. S.; Kruper, W. J.; Guest, M. J., Materials properties derived from INSITE metallocene catalysts. *Adv. Mater.* **2000,** *12*, 1759-1767.

179. Arriola, D. J.; Bokota, M.; Campbell, R. E.; Klosin, J.; LaPointe, R. E.; Redwine, O. D.; Shankar, R. B.; Timmers, F. J.; Abboud, K. A., Penultimate Effect in Ethylene–Styrene Copolymerization and the Discovery of Highly Active Ethylene–Styrene Catalysts with Increased Styrene Reactivity. *J. Am. Chem. Soc.* **2007,** *129*, 7065-7076.

180. Luo, Y.; Baldamus, J.; Hou, Z., Scandium Half-Metallocene-Catalyzed Syndiospecific Styrene Polymerization and Styrene–Ethylene Copolymerization: Unprecedented Incorporation of Syndiotactic Styrene–Styrene Sequences in Styrene–Ethylene Copolymers. *J. Am. Chem. Soc.* **2004,** *126*, 13910-13911.

181. Izzo, L.; Napoli, M.; Oliva, L., Regiochemistry of the Styrene Insertion with CH2-Bridged ansa-Zirconocene-Based Catalysts. *Macromolecules* **2003,** *36*, 9340-9345.

182. Capacchione, C.; Proto, A.; Ebeling, H.; Mülhaupt, R.; Möller, K.; Spaniol, T. P.; Okuda, J., Ancillary Ligand Effect on Single-Site Styrene Polymerization: Isospecificity of Group 4 Metal Bis(phenolate) Catalysts. *J. Am. Chem. Soc.* **2003,** *125*, 4964-4965.

183. Pellecchia, C.; Pappalardo, D.; Oliva, L.; Zambelli, A., .eta.5-C5Me5TiMe3-B(C6F5)3: A true Ziegler-Natta catalyst for the syndiotactic-specific polymerization of styrene. *J. Am. Chem. Soc.* **1995,** *117*, 6593-6594.

184. Motta, A.; Fragalà, I. L.; Marks, T. J., Stereochemical Control Mechanisms in Propylene Polymerization Mediated by C1-Symmetric CGC Titanium Catalyst Centers. *J. Am. Chem. Soc.* **2007,** *129*, 7327-7338.

185. Xu, Z.; Vanka, K.; Ziegler, T., Influence of the Counterion MeB(C6F5)3- and Solvent Effects on Ethylene Polymerization Catalyzed by [(CpSiMe2NR)TiMe]+: A Combined Density Functional Theory and Molecular Mechanism Study. *Organometallics* **2004,** *23*, 104-116.

186. Nifant'ev, I. E.; Ustynyuk, L. Y.; Laikov, D. N., DFT Study of Ethylene Polymerization by Zirconocene–Boron Catalytic Systems. Effect of Counterion on the Kinetics and Mechanism of the Process. *Organometallics* **2001,** *20*, 5375-5393.

187. Yang, S. H.; Huh, J.; Yang, J. S.; Jo, W. H., A Density Functional Study on the Stereoselectivity of Styrene Polymerization with ansa-Metallocene Catalyst. *Macromolecules* **2004,** *37*, 5741-5751.

188. Ramos, J.; Munoz-Escalona, A.; Martinez, S.; Martinez-Salazar, J.; Cruz, V., Ethylene-styrene copolymerization with constrained geometry catalysts: A density functional study. *J. Chem. Phys.* **2005,** *122*, 074901/1-07490/4.

189. Martinez, S.; Exposito, M. T.; Ramos, J.; Cruz, V.; Martinez, M. C.; Lopez, M.; Munoz-Escalona, A.; Martinez-Salazar, J., An experimental and computational evaluation of ethylene/styrene copolymerization with a homogeneous single-site titanium (IV)-constrained geometry catalyst. *J. Polym. Sci., Part A: Polym. Chem.* **2005,** *43*, 711-725.

190. Yang, S. H.; Jo, W. H.; Noh, S. K., Density functional study of the insertion mechanism for ethylene-styrene copolymerization with constrained geometry catalysts. *J. Chem. Phy.* **2003,** *119*, 1824-1837.

191. Oliva, L.; Longo, P.; Izzo, L.; Di Serio, M., Zirconocene-Based Catalysts for the Ethylene–Styrene Copolymerization: Reactivity Ratios and Reaction Mechanism. *Macromolecules* **1997,** *30*, 5616-5619.

192. Cotton, F. A.; Murillo, C. A.; Petrukhina, M. A., Novel η 3-allyl complexes of titanium. *J. Organomet. Chem.* **2000,** *593–594*, 1-6.

193. Wilke, G.; Bogdanović, B.; Hardt, P.; Heimbach, P.; Keim, W.; Kröner, M.; Oberkirch, W.; Tanaka, K.; Steinrücke, E.; Walter, D.; Zimmermann, H., Allyl-Transition Metal Systems. *Angew. Chem. Int. Ed. Engl.* **1966,** *5*, 151-164.

194. Any attempts to induce the olefin insertion by forcing the approach of ethylene into the Ti1-CH3 leads to the release of methane and the formation of the polymerization inactive structure ***rac*-4**.

195. Royo, E.; Royo, P.; Cuenca, T.; Galakhov, M., Insertion of Terminal and Internal Acetylenes into the Zr– μ -Methylene Bond of the Dinuclear Cationic Zirconium Complex [{Zr(η 5-C5H5)}2(μ -CH2)(μ -Cl)(μ - η 5-C5H4- η 5-C5H4)][BMe(C6F5)3]. Synthetic Aspects, NMR Spectroscopic Study, and Dynamic Behavior in Solution. *Organometallics* **2000,** *19*, 5559-5567.

196. Song, F. Q.; Cannon, R. D.; Lancaster, S. J.; Bochmann, M., Activator effects in metallocene-based alkene polymerisations: unexpectedly strong dependence of catalyst activity on trityl concentration. *J. Mol. Catal. A: Chem.* **2004,** *218*, 21-28.

197. Pangborn, A. B.; Giardello, M. A.; Grubbs, R. H.; Rosen, R. K.; Timmers, F. J., Safe and Convenient Procedure for Solvent Purification. *Organometallics* **1996,** *15*, 1518-1520.

198. Dolomanov, O. V.; Bourhis, L. J.; Gildea, R. J.; Howard, J. A. K.; Puschmann, H., OLEX2: a complete structure solution, refinement, and analysis program. *J. Appl. Cryst.* **2009**, *42*, 339-341

199. Sheldrick, G. M., A short history of SHELX. *Acta Cryst.* **2008**, *A64*, 112-122.

200. Perdew, J. P.; Burke, K.; Ernzerhof, M., Generalized gradient approximation made simple. *Phys. Rev. Lett.* **1996**, *77*, 3865-3868.

201. Yang, S. H.; Huh, J.; Jo, W. H., *Organometallics*, Density Functional Theory on the Regioselectivity of Styrene Polymerization with an ansa-Metallocene Catalyst. **2006**, *25*, 1144-1150.

202. Rassolov, V. A.; Pople, J. A.; Ratner, M. A.; Windus, T. L., 6-316* basis set for atoms K through Zn. *J. Chem. Phys.* **1998**, *109*, 1223-1229.

203. Valiev, M.; Bylaska, E. J.; Govind, N.; Kowalski, K.; Straatsma, T. P.; Van Dam, H. J. J.; Wang, D.; Nieplocha, J.; Apra, E.; Windus, T. L.; de Jong, W.,NWChem: A comprehensive and scalable open-source solution for large scale molecular simulations. *Comput. Phys. Commun.* **2010**, *181*, 1477-1489.

204. NBO Version 3.1, E. D. Glendening, A. E. Reed, J. E. Carpenter, and F. Weinhold

205. Gaussian 09, Revision D.01, Frisch, M. J.; Trucks, G. W.; Schlegel, H. B.; Scuseria, G. E.; Robb, M. A.; Cheeseman, J. R.; Scalmani, G.; Barone, V.; Mennucci, B.; Petersson, G. A.; Nakatsuji, H.; Caricato, M.; Li, X.; Hratchian, H. P.; Izmaylov, A. F.; Bloino, J.; Zheng, G.; Sonnenberg, J. L.; Hada, M.; Ehara, M.; Toyota, K.; Fukuda, R.; Hasegawa, J.; Ishida, M.; Nakajima, T.; Honda, Y.; Kitao, O.; Nakai, H.; Vreven, T.; Montgomery, Jr., J. A.; Peralta, J. E.; Ogliaro, F.; Bearpark, M.; Heyd, J. J.; Brothers, E.; Kudin, K. N.; Staroverov, V. N.; Kobayashi, R.; Normand, J.; Raghavachari, K.; Rendell, A.; Burant, J. C.; Iyengar, S. S.; Tomasi, J.; Cossi, M.; Rega, N.; Millam, J. M.; Klene, M.; Knox, J. E.; Cross, J. B.; Bakken, V.; Adamo, C.; Jaramillo, J.; Gomperts, R.; Stratmann, R. E.; Yazyev, O.; Austin, A. J.; Cammi, R.; Pomelli, C.; Ochterski, J. W.; Martin, R. L.; Morokuma, K.; Zakrzewski, V. G.; Voth, G. A.; Salvador, P.; Dannenberg, J. J.; Dapprich, S.; Daniels, A. D.; Farkas, Ö.; Foresman, J. B.; Ortiz, J. V.; Cioslowski, J.; Fox, D. J. Gaussian, Inc., Wallingford, CT, 2009.

Chapter 2.

1. Ginsbach, J. W.; Kieber-Emmons, M. T.; Nomoto, R.; Noguchi, A.; Ohnishi, Y.; Solomon, E. I. Structure/function correlations among coupled binuclear copper proteins through spectroscopic and reactivity studies of NspF. *Proc. Natl. Acad. Sci. U. S. A.* **2012**, *109*, 10793-10797.

2. Schenk, G.; Mitic, N.; Gahan, L. R.; Ollis, D. L.; McGeary, R. P.; Guddat, L. W. Binuclear Metallohydrolases: Complex Mechanistic Strategies for a Simple Chemical Reaction. *Acc. Chem. Res.* **2012**, *45*, 1593-1603.

3. Chen, S.-L.; Marino, T.; Fang, W.-H.; Russo, N.; Himo, F. Peptide Hydrolysis by the Binuclear Zinc Enzyme Aminopeptidase from Aeromonas proteolytica: A Density Functional Theory Study. *J. Phys. Chem. B* **2008**, *112*, 2494-2500.

4. Hadler, K. S.; Tanifum, E. A.; Yip, S. H.-C.; Mitic, N.; Guddat, L. W.; Jackson, C. J.; Gahan, L. R.; Nguyen, K.; Carr, P. D.; Ollis, D. L.; Hengge, A. C.; Larrabee, J. A.; Schenk, G. Substrate-Promoted Formation of a Catalytically Competent Binuclear Center and Regulation of Reactivity in a Glycerophosphodiesterase from Enterobacter aerogenes. *J. Am. Chem. Soc.* **2008**, *130*, 14129-14138.

5. Schwartz, J. K.; Liu, X. S.; Tosha, T.; Theil, E. C.; Solomon, E. I. Spectroscopic Definition of the Ferroxidase Site in M Ferritin: Comparison of Binuclear Substrate vs. Cofactor Active Sites. *J. Am. Chem. Soc.* **2008**, *130*, 9441-9450.

6. Mitić, N.; Smith, S. J.; Neves, A.; Guddat, L. W.; Gahan, L. R.; Schenk, G. The catalytic mechanisms of binuclear metallohydrolases. *Chem. Rev.* **2006**, *106*, 3338-3363.

7. Haak, R. M.; Wezenberg, S. J.; Kleij, A. W. Cooperative multimetallic catalysis using metallosalens. *Chem. Commun.* **2010**, *46*, 2713-2723.

8. Belle, C.; Pierre, J. L. Asymmetry in bridged binuclear metalloenzymes: Lessons for the chemist. *Eur. J. Inorg. Chem.* **2003**, 4137-4146.

9. Berry, J. F.; Thomas, C. M. Multimetallic complexes: synthesis and applications. *Dalton Trans.* **2017**, *46*, 5472-5473.

10. Hollingsworth, T. S.; Hollingsworth, R. L.; Rosen, T.; Groysman, S. Zinc bimetallics supported by a xanthene-bridged dinucleating ligand: synthesis, characterization, and lactide polymerization studies. *RSC Adv.* **2017**, *7*, 41819-41829.

11. Gnanamani, M. K.; Jacobs, G.; Hamdeh, H. H.; Shafer, W. D.; Liu, F.; Hopps, S. D.; Thomas, G. A.; Davis, B. H. Hydrogenation of Carbon Dioxide over Co–Fe Bimetallic Catalysts. *ACS Catal.* **2016**, *6*, 913-927.

12. Goulas, K. A.; Sreekumar, S.; Song, Y.; Kharidehal, P.; Gunbas, G.; Dietrich, P. J.; Johnson, G. R.; Wang, Y. C.; Grippo, A. M.; Grabow, L. C.; Gokhale, A. A.; Toste, F. D. Synergistic Effects in Bimetallic Palladium–Copper Catalysts Improve Selectivity in Oxygenate Coupling Reactions. *J. Am. Chem. Soc.* **2016**, *138*, 6805-6812.

13. Buchwalter, P.; Rosé, J.; Braunstein, P. Multimetallic Catalysis Based on Heterometallic Complexes and Clusters. *Chem. Rev.* **2015**, *115*, 28-126.

14. Edwards, J. K.; Freakley, S. J.; Carley, A. F.; Kiely, C. J.; Hutchings, G. J. Strategies for Designing Supported Gold–Palladium Bimetallic Catalysts for the Direct Synthesis of Hydrogen Peroxide. *Acc. Chem. Res.* **2014**, *47*, 845-854.

15. Matsunaga, S.; Shibasaki, M. Recent advances in cooperative bimetallic asymmetric catalysis: dinuclear Schiff base complexes. *Chem. Commun.* **2014**, *50*, 1044-1057.

16. Ahmed, S. M.; Poater, A.; Childers, M. I.; Widger, P. C. B.; LaPointe, A. M.; Lobkovsky, E. B.; Coates, G. W.; Cavallo, L. Enantioselective Polymerization of Epoxides Using Biaryl-Linked Bimetallic Cobalt Catalysts: A Mechanistic Study. *J. Am. Chem. Soc.* **2013**, *135*, 18901-18911.

17. Hetterscheid, D. G. H.; Chikkali, S. H.; de Bruin, B.; Reek, J. N. H. Binuclear Cooperative Catalysts for the Hydrogenation and Hydroformylation of Olefins. *ChemCatChem* **2013**, *5*, 2785-2793.

18. Tsui, E. Y.; Tran, R.; Yano, J.; Agapie, T. Redox-inactive metals modulate the reduction potential in heterometallic manganese-oxido clusters. *Nat. Chem.* **2013**, *5*, 293-299.

19. Thomas, R. M.; Widger, P. C. B.; Ahmed, S. M.; Jeske, R. C.; Hirahata, W.; Lobkovsky, E. B.; Coates, G. W. Enantioselective Epoxide Polymerization Using a Bimetallic Cobalt Catalyst. *J. Am. Chem. Soc.* **2010**, *132*, 16520-16525.

20. *Homo- and Heterobimetallic Complexes in Catalysis: Cooperative Catalysis*; Springer International Publishing: Switzerland, 2016.

21. McInnis, J. P.; Delferro, M.; Marks, T. J. Multinuclear Group 4 Catalysis: Olefin Polymerization Pathways Modified by Strong Metal–Metal Cooperative Effects. *Acc. Chem. Res.* **2014**, *47*, 2545-2557.

22. Delferro, M.; Marks, T. J. Multinuclear Olefin Polymerization Catalysts. *Chem. Rev.* **2011**, *111*, 2450-2485.

23. Li, H.; Marks, T. J. Nuclearity and cooperativity effects in binuclear catalysts and cocatalysts for olefin polymerization. *Proc. Natl. Acad. Sci. U.S.A.* **2006**, *103*, 15295-15302.

24. Liu, S.; Invergo, A. M.; McInnis, J. P.; Mouat, A. R.; Motta, A.; Lohr, T. L.; Delferro, M.; Marks, T. J. Distinctive Stereochemically Linked Cooperative Effects in Bimetallic Titanium Olefin Polymerization Catalysts. *Organometallics* **2017**, *36*, 4403-4421.

25. Guo, N.; Stern, C. L.; Marks, T. J. Bimetallic effects in homopolymerization of styrene and copolymerization of ethylene and styrenic comonomers: Scope, kinetics, and mechanism. *J. Am. Chem. Soc.* **2008**, *130*, 2246-2261.

26. Li, H.; Li, L.; Schwartz, D. J.; Metz, M. V.; Marks, T. J.; Liable-Sands, L.; Rheingold, A. L. Coordination Copolymerization of Severely Encumbered Isoalkenes with Ethylene: Enhanced Enchainment Mediated by Binuclear Catalysts and Cocatalysts. *J. Am. Chem. Soc.* **2005**, *127*, 14756-14768.

27. Wang, J.; Li, H.; Guo, N.; Li, L.; Stern, C. L.; Marks, T. J. Covalently linked heterobimetallic catalysis for olefin polymerization. *Organometallics* **2004**, *23*, 5112-5114.

28. Li, H.; Li, L.; Marks, T. J.; Liable-Sands, L.; Rheingold, A. L. Catalyst/cocatalyst nuclearity effects in single-site olefin polymerization. Significantly enhanced 1-octene and isobutene comonomer enchainment in ethylene polymerizations mediated by binuclear catalysts and cocatalysts. *J. Am. Chem. Soc.* **2003**, *125*, 10788-10789.

29. Li, L.; Metz, M. V.; Li, H.; Chen, M.-C.; Marks, T. J.; Liable-Sands, L.; Rheingold, A. L. Catalyst/Cocatalyst Nuclearity Effects in Single-Site Polymerization. Enhanced Polyethylene Branching and α-Olefin Comonomer Enchainment in Polymerizations Mediated by Binuclear Catalysts and Cocatalysts via a New Enchainment Pathway. *J. Am. Chem. Soc.* **2002**, *124*, 12725-12741.

30. Salata, M. R.; Marks, T. J. Catalyst Nuclearity Effects in Olefin Polymerization. Enhanced Activity and Comonomer Enchainment in Ethylene + Olefin Copolymerizations Mediated by Bimetallic Group 4 Phenoxyiminato Catalysts. *Macromolecules* **2009**, *42*, 1920-1933.

31. Salata, M. R.; Marks, T. J. Synthesis, Characterization, and Marked Polymerization Selectivity Characteristics of Binuclear Phenoxyiminato Organozirconium Catalysts. *J. Am. Chem. Soc.* **2008**, *130*, 12-13.

32. Gao, Y.; Chen, X.; Zhang, J.; Chen, J.; Lohr, T. L.; Marks, T. J. Catalyst Nuclearity Effects on Stereo- and Regioinduction in Pyridylamidohafnium-Catalyzed Propylene and 1-Octene Polymerizations. *Macromolecules* **2018**, *51*, 2401-2410.

33. Gao, Y.; Mouat, A. R.; Motta, A.; Macchioni, A.; Zuccaccia, C.; Delferro, M.; Marks, T. J. Pyridylamido Bi-Hafnium Olefin Polymerization Catalysis: Conformationally Supported Hf···Hf Enchainment Cooperativity. *ACS Catal.* **2015**, *5*, 5272-5282.

34. Liu, S.; Motta, A.; Mouat, A. R.; Delferro, M.; Marks, T. J. Very Large Cooperative Effects in Heterobimetallic Titanium-Chromium Catalysts for Ethylene Polymerization/Copolymerization. *J. Am. Chem. Soc.* **2014**, *136*, 10460-10469.

35. Liu, S.; Motta, A.; Delferro, M.; Marks, T. J. Synthesis, Characterization, and Heterobimetallic Cooperation in a Titanium–Chromium Catalyst for Highly Branched Polyethylenes. *J. Am. Chem. Soc.* **2013**, *135*, 8830-8833.

36. Sampson, J.; Choi, G.; Akhtar, M. N.; Jaseer, E. A.; Theravalappil, R.; Al-Muallem, H. A.; Agapie, T. Olefin Polymerization by Dinuclear Zirconium Catalysts Based on Rigid Teraryl Frameworks: Effects on Tacticity and Copolymerization Behavior. *Organometallics* **2017**, *36*, 1915-1928.

37. Radlauer, M. R.; Agapie, T. Bimetallic Zirconium Amine Bis(phenolate) Polymerization Catalysts: Enhanced Activity and Tacticity Control for Polyolefin Synthesis. *Organometallics* **2014**, *33*, 3247-3250.

38. Radlauer, M. R.; Buckley, A. K.; Henling, L. M.; Agapie, T. Bimetallic Coordination Insertion Polymerization of Unprotected Polar Monomers: Copolymerization of Amino Olefins and Ethylene by Dinickel Bisphenoxyiminato Catalysts. *J. Am. Chem. Soc.* **2013**, *135*, 3784-3787.

39. Wei, J.; Hwang, W.; Zhang, W.; Sita, L. R. Dinuclear Bis-Propagators for the Stereoselective Living Coordinative Chain Transfer Polymerization of Propene. *J. Am. Chem. Soc.* **2013**, *135*, 2132-2135.

40. Makio, H.; Terao, H.; Iwashita, A.; Fujita, T. FI Catalysts for Olefin Polymerization—A Comprehensive Treatment. *Chem. Rev.* **2011**, *111*, 2363-2449.

41. Zhong, L.; Cui, K.; Xie, P.; Chen, J.-Z.; Ma, Z. A New Titanium (IV) Complex Bearing Phenoxyimine-Fluorene Ligand and Its Use as Catalyst for Ethylene Homo- and Copolymerization. *J. Polym. Sci. Part A: Polym. Chem.* **2010**, *48*, 1617-1621.

42. Zhang, H.; Katao, S.; Nomura, K.; Huang, J. Synthesis of Half-Titanocenes Containing Phenoxy-imine Ligands and Their Use as Catalysts for Olefin Polymerization. *Organometallics* **2007**, *26*, 5967-5977.

43. Bott, R. K. J.; Hughes, D. L.; Schormann, M.; Bochmann, M.; Lancaster, S. J. Monocyclopentadienyl phenoxy-imine and phenoxy-amine complexes of titanium and zirconium and their application as catalysts for 1-alkene polymerisation. *J. Organomet. Chem.* **2003**, *665*, 135-149.

44. Huang, J.; Lian, B.; Qian, Y.; Zhou, W.; Chen, W.; Zheng, G. Syntheses of Titanium(IV) Complexes with Mono-Cp and Schiff Base Ligands and Their Catalytic Activities for

Ethylene Polymerization and Ethylene/1-Hexene Copolymerization. *Macromolecules* **2002**, *35*, 4871-4874.

45. Chang, S.; Jones, L.; Wang, C.; Henling, L. M.; Grubbs, R. H. Synthesis and Characterization of New Ruthenium-Based Olefin Metathesis Catalysts Coordinated with Bidentate Schiff-Base Ligands. *Organometallics* **1998**, *17*, 3460-3465.

46. Mena, M.; Royo, P.; Serrano, R. Electron-Deficient (Pentamethylcyclopentadienyl)titanium Trialkyls: Evidence of Ti-H-C and Ti-C-C Interactions. Crystal and Molecular Structure of μ-[o-(CH2)2C6H4]{(η5-C5Me5)Ti[o-(CH2)2C6H4]}2. *Organometallics* **1989**, *8*, 476-482.

47. Sanz, M.; Cuenca, T.; Galakhov, M.; Grassi, A.; Bott, R. K. J.; Hughes, D. L.; Lancaster, S. J.; Bochmann, M. Monocyclopentadienyl Bis(phenoxo-imino) Zirconium Complexes as Precatalyst Species for Olefin Polymerization. Stereospecific Methylation of an Imino Group with Formation of a Zirconium–amido Bond. *Organometallics* **2004**, *23*, 5324-5331.

48. Cariou, R.; Gibson, V. C.; Tomov, A. K.; White, A. J. P. Group 4 metal complexes bearing new tridentate (NNO) ligands: Benzyl migration and formation of unusual C-C coupled products. *J. Organomet. Chem.* **2009**, *694*, 703-716.

49. Woodman, P. R.; Alcock, N. W.; Munslow, I. J.; Sanders, C. J.; Scott, P. Chiral N2O2 Schiff-base complexes of titanium with a biaryl backbone: highly diastereoselective migratory insertion of alkyl at imine. *J. Chem. Soc., Dalton Trans.* **2000**, 3340-3346.

50. Razuvaev, G. A.; Mar'in, V. P.; Andrianov, Y. A. Migration of hydrogen atoms from cyclopentadienyl rings to metal and hydrogen exchange reactions upon thermal decomposition of dicyclopentadienyl compounds of titanium and zirconium. *J. Organomet. Chem.* **1979**, *174*, 67-75.

51. Ewart, S. W.; Sarsfield, M. J.; Williams, E. F.; Baird, M. C. Ethylene and propylene polymerization by cationic monocyclopentadienyl titanium catalysts containing the weakly coordinating anion [B(C6F5)4]. *J. Organomet. Chem.* **1999**, *579*, 106-113.

52. Klet, R. C.; Theriault, C. N.; Klosin, J.; Labinger, J. A.; Bercaw, J. E. Investigations into Asymmetric Post-Metallocene Group 4 Complexes for the Synthesis of Highly Regioirregular Polypropylene. *Macromolecules* **2014**, *47*, 3317-3324.

53. Luconi, L.; Rossin, A.; Tuci, G.; Tritto, I.; Boggioni, L.; Klosin, J. J.; Theriault, C. N.; Giambastiani, G. Facing Unexpected Reactivity Paths with ZrIV–Pyridylamido Polymerization Catalysts. *Chem. - Eur. J.* **2012**, *18*, 671-687.

54. Stephenson, C. J.; McInnis, J. P.; Chen, C.; Weberski, M. P.; Motta, A.; Delferro, M.; Marks, T. J. Ni(II) Phenoxyiminato Olefin Polymerization Catalysis: Striking Coordinative

Modulation of Hyperbranched Polymer Microstructure and Stability by a Proximate Sulfonyl Group. *ACS Catal*. **2014**, *4*, 999-1003.

55. Byers, J. A.; Bercaw, J. E. Kinetic resolution of racemic α-olefins with ansa-zirconocene polymerization catalysts: Enantiomorphic site vs. chain end control. *Proc. Natl. Acad. Sci. U.S.A.* **2006**, *103*, 15303-15308.

56. Seger, M. R.; Maciel, G. E. Quantitative 13C NMR Analysis of Sequence Distributions in Poly(ethylene-co-1-hexene). *Anal. Chem.* **2004**, *76*, 5734-5747.

57. Randall, J. C. A Review Of High-Resolution Liquid C-13 Nuclear Magnetic Resonance Characterizations of Ethylene Based Polymers. *J. Macromol. Sci., Rev. Macromol. Chem. Phy.* **1989**, *C29*, 201-317.

58. Breitmaier, E.; Voelter, W.: *Carbon-13 NMR Spectroscopy*; VCH Publishers: Weinheim, Germany, 1987.

59. Cohen, A.; Kopilov, J.; Goldberg, I.; Moshe, K. C1-Symmetric Zirconium Complexes of [ONNO']-Type Salan Ligands: Accurate Control of Catalyst Activity, Isospecificity, and Molecular Weight in 1-Hexene Polymerization. *Organometallics* **2009**, *28*, 1391-1405.

60. Asakura, T.; Demura, M.; Nishiyama, Y. Carbon-13 NMR Spectral Assignment of Five Polyolefins Determined from the Chemical Shift Calculation and the Polymerization Mechanism. *Macromolecules* **1991**, *24*, 2334-2340.

61. Tohi, Y.; Makio, H.; Matsui, S.; Onda, M.; Fujita, T. Polyethylenes with Uni-, Bi-, and Trimodal Molecular Weight Distributions Produced with a Single Bis(phenoxy−imine)zirconium Complex. *Macromolecules* **2003**, *36*, 523-525.

62. Görl, C.; Alt, H. G. The combination of mononuclear metallocene and phenoxyimine complexes to give trinuclear catalysts for the polymerization of ethylene. *J. Organomet. Chem.* **2007**, *692*, 5727-5753.

63. Bhaduri, S.; Mukesh, D.: Polymerization and Selective Oligomerization of Alkenes. In *Homogeneous Catalysis*; John Wiley & Sons, Inc, 2014; pp 167-200.

64. Bochmann, M. The Chemistry of Catalyst Activation: The Case of Group 4 Polymerization Catalysts†. *Organometallics* **2010**, *29*, 4711-4740.

65. Motta, A.; Fragala, I. L.; Marks, T. J. Proximity and Cooperativity Effects in Binuclear d(0) Olefin Polymerization Catalysis. Theoretical Analysis of Structure and Reaction Mechanism. *J. Am. Chem. Soc.* **2009**, *131*, 3974-3984.

66. Kaminsky, W. Discovery of Methylaluminoxane as Cocatalyst for Olefin Polymerization. *Macromolecules* **2012**, *45*, 3289-3297.

67. Bianchini, C.; Giambastiani, G.; Luconi, L.; Meli, A. Olefin oligomerization, homopolymerization and copolymerization by late transition metals supported by (imino)pyridine ligands. *Coord. Chem. Rev.* **2010**, *254*, 431-455.

68. Chen, E. Y. X. Coordination Polymerization of Polar Vinyl Monomers by Single-Site Metal Catalysts. *Chem. Rev.* **2009**, *109*, 5157-5214.

69. McDaniel, M. P.; Schwerdtfeger, E. D.; Jensen, M. D. The "comonomer effect" on chromium polymerization catalysts. *J. Catal.* **2014**, *314*, 109-116.

70. Awudza, J. A. M.; Tait, P. J. T. The "comonomer effect" in ethylene/α-olefin copolymerization using homogeneous and silica-supported Cp2ZrCl2/MAO catalyst systems: some insights from the kinetics of polymerization, active center studies, and polymerization temperature. *J. Polym. Sci., Part A: Polym. Chem.* **2007**, *46*, 267-277.

71. Nomura, K.; Komatsu, T.; Imanishi, Y. Polymerization of 1-hexene, 1-octene catalyzed by Cp′TiCl2(O-2,6-iPr2C6H3)–MAO system. Unexpected increase of the catalytic activity for ethylene/1-hexene copolymerization by (1,3-tBu2C5H3)TiCl2(O-2,6-iPr2C6H3)–MAO catalyst system. *J. Mol. Catal. A: Chem.* **2000**, *152*, 249-252.

72. Chien, J. C. W.; Nozaki, T. Ethylene Hexene Copolymerization by Heterogeneous and Homogeneous Ziegler-Natta Catalysts and the Comonomer Effect. *J. Polym. Sci., Part A: Polym. Chem.* **1993**, *31*, 227-237.

73. Pangborn, A. B.; Giardello, M. A.; Grubbs, R. H.; Rosen, R. K.; Timmers, F. J., Safe and Convenient Procedure for Solvent Purification. *Organometallics* **1996,** *15*, 1518-1520.

74. Galland, G. B.; de Souza, R. F.; Mauler, R. S.; Nunes, F. F., 13C NMR Determination of the Composition of Linear Low-Density Polyethylene Obtained with [η3-Methallyl-nickel-diimine]PF6 Complex. *Macromolecules*, **1999**, *32*, 1620-1625

75. Sheldrick, G. M.; SADABS; Bruker Analytical X-ray Systems, Madison, WI, 1999.

76. Dolomanov, O. V.; Bourhis, L. J.; Gildea, R. J.; Howard, J. A. K.; Puschmann, H., OLEX2: a complete structure solution, refinement, and analysis program. *J. Appl. Cryst.* **2009**, *42*, 339-341

77. Sheldrick, G. M., A short history of SHELX. *Acta Cryst.* **2009**, *A64*, 112-122

78. Sheldrick, G. M., Shelxtl Pc: An Integrated System for Solving, Refining, and Displaying Crystal Structures from Diffraction Data. Version 6.014 ed.; Bruker AXS: Madison, WI, 2000.

Original Research Proposal: Design of a Catalytic Surface as a Fully Immobilized Frustrated Lewis Pair for Organic Transformations

Anna M. Invergo

Abstract: Frustrated Lewis pairs consist of a Lewis acid and Lewis base pair, where each component is severely sterically hindered to the point that the two are unable to form an adduct. Frustrated Lewis pairs have demonstrated good activity in a variety of catalytic areas, however, heterogeneous analogs of these compounds, particularly fully immobilized iterations thereof, have been not well explored. Heterogeneous catalysts are commonly utilized in industry due to their higher thermal stability, recyclability, and ease of removal from products. While only a few examples are currently known, a proposed heterogeneous frustrated Lewis pair could provide access to a robust, transition metal-free catalyst capable of catalyzing a wide variety of reactions, and thus begin to explore questions about the commercial viability of these materials, as well as explore reactivity from a surface chemistry perspective.

Introduction

Heterogeneous catalysis comprises a field of work central to many industrial processes, including biomass conversion, olefin polymerization, petroleum refining, ammonia synthesis, and CO_2 reduction, to name a few.[1] Heterogeneous catalysts provide many advantages over their solution-phase counterparts, including higher thermal stability, recyclability, and ease of removal from catalytic products.[2] Many industrial processes utilize transition metal-based heterogeneous catalysts, but for small molecule transformations, especially for the production of pharmaceuticals and hair and skincare goods, trace metals are highly detrimental.[3]

Frustrated Lewis pairs (FLPs) are materials comprised of a severely sterically congested Lewis acid and Lewis base pair, and are frequently free of transition metals. The steric hindrance of each component prevents the Lewis pair from forming an adduct, resulting in "unquenched reactivity".[4] FLPs have demonstrated powerful catalytic abilities, most notably in the cleavage and activation of H_2 and the hydrogenation of a variety of compounds, including polar N-containing substrates,[5-7] as well as ketones and aldehydes,[8,9] olefins,[10-12] alkynes,[13] and aromatic compounds (including some selectivity for pyridine and aniline-type compounds).[14,15] Beyond hydrogenation, FLP chemistry is also used in a variety of other reactions, such as the capture[16] and hydroboration/reduction of CO_2,[17] N_2O capture[18] and subsequent C-H bond activation,[19] NO[20] and SO_2 capture,[21] and polymerization of polar monomers.[22-24]

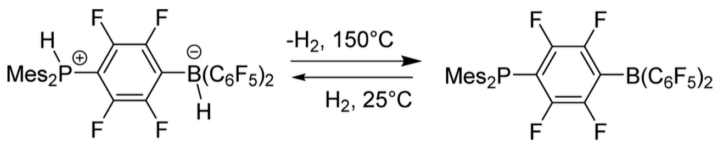

Scheme A1. Example of a well-known FLP activating H_2.

With the exception of polymerizations, most of the products formed by FLP catalysis are small molecules that are either liquid, or that are readily soluble in the reaction medium. In principle, a heterogeneous FLP catalyst should impart the benefit of facile removal from the reaction mixture. The synthesis of such a compound could provide new insights into surface reactivity, namely, whether there is an inherent reactivity in the support that could be exploited for the production of new catalytic materials. Catalytic reactions with the new compound can then begin to explore whether the known benefits of heterogeneous catalysis (superior thermal stability, recyclability) could be realized in the area of small-molecule FLP catalysis.

Scientific Objectives

The objective of this research project is, in a large sense, to study the effects of the utilization of a support on the catalytic activity of frustrated Lewis pairs. The first specific part of this objective aims to synthesize a heterogeneous FLP through careful selection of surface precursors, to determine appropriate characterization methods, and to perform comprehensive characterization of the resulting material. The second specific aim of this objective focuses on determining the efficacy of the heterogeneous FLP in a variety of catalytic probe reactions, and elucidate the effect of the support on the catalysis.

Previous Work

Homogeneous FLP-based catalysis is well known and, although a relatively young field, has been extensively studied since the first published FLP-catalyzed reaction in 2006. Very recently, the benefits of FLP chemistry have begun to permeate into heterogeneous catalysis, prompting the study of various new solid/semi-solid catalysts that have demonstrated good reactivity for cleavage and activation of H_2, along with the hydrogenation of unsaturated substrates.[3,25-27] These four currently known heterogeneous FLPs will be discussed below.

The first known heterogeneous FLP catalysts were reported by Szeto *et al*. in 2016.[3] The supported FLPs were prepared by treating dehydroxylated silica with tris(*iso*-butyl)aluminum, in order to consume free surface silanols, followed by the grafting of an organophosphine via a hydroquinone linker. Introduction of perflouoroaryl boranes in the form of either $B(C_6F_5)_3$ or Piers' reagent[28] results in the formation of an adduct. The complexes are active for *Z*-selective alkyne reduction, albeit under fairly forcing conditions (for example: 80° C, 40 bars of hydrogen pressure), to achieve either 98% or 9% reduction of 3-hexyne with the two different catalysts, with either the tris borane or the Piers' borane adduct, respectively); however, the compounds suffer from activity loss following one catalytic cycle. Activity was able to be restored, but only upon the addition of supplemental borane.

In the same year, Xing *et al*. reported a similar heterogeneous FLP compound in which tris(pentafluorophenyl) borane was supported on a pre-dried silica-500 surface. To this supported borane was then added tri-*t*-butyl phosphine to form the solid FLP. This supported compound was found to be proficient for the heterolytic cleavage of H_2 through NMR scale reactions, under fairly mild conditions (for example: 65° C, 2 bars of H_2/D_2 pressure). Preliminary results indicate that the compound is also active for the hydrogenation of alkenes.[27]

In 2017, Trunk *et al*. reported the synthesis and catalytic proficiencies of a semi-immobilized FLP material. This process began with the synthesis of a microporous polymer network that was based on triarylphosphine building blocks, resulting in Lewis basic polyphosphines. The two polymer networks created used phosphines of differing levels of steric bulk in order to prevent adduct formation. The polymer networks demonstrated significant swelling in a multitude of solvents, so tris(pentafluorophenyl) borane was then dissolved in DCM and added to the polyphosphines, thus absorbing the Lewis acid into the pores of the polymer. The

borane remained in the polymer network following a drying period, and solid state ^{31}P MAS NMR revealed coordination of the polymer phosphines to an acidic species. This catalyst was shown to be effective at H_2/D_2 activation as well as H/D exchange, as monitored by ^{1}H NMR.[25]

Most recently, in 2018, Willms *et al*. reported a semi-solid FLP that was similarly based on a polymeric material. The Lewis basic component was a polyamine organic framework based on a *p*-xylylenediamine/1,4-bis(bromomethyl)benzene backbone. The polymer was then swollen in solvent and tris(pentafluorophenyl) borane was impregnated into the polymeric framework, which was then monitored closely by ATR IR spectroscopy. The compound was studied catalytically for the hydrogenation of diethyl benzylidenemalonate. The reaction was found to go to completion and required somewhat forcing conditions (i.e. 20 bars of hydrogen pressure at 80° C), although less forcing than that required by a molecular FLP control made by combining tris(pentafluorophenyl borane) with DABCO (i.e. 60 bars of hydrogen pressure at 80° C). The H_2 activating nature of the compound was tracked by and found to be successful through ^{11}B NMR.[26]

Proposed Research

This project will begin with the synthesis of a novel heterogeneous FLP. What sets this compound apart from the previously made solid state FLPs is that one component of the Lewis pair will be integrated into the surface, while the other component will be directly tethered to the surface, resulting in a FLP-type catalyst that is *fully immobilized*. This should, in principle, largely help to increase catalytic recyclability while reducing the need to continually re-introduce one of the Lewis pair components.

Surface selection is critical in this phase. The ideal situation would favor the use of a Lewis basic surface to which a Lewis acid component could then be tethered. The most well-known Lewis basic surface is MgO, although it may not provide an ideal platform for attaching additional

components, due to a lack of reactive surface hydroxyl groups. However, this problem may be alleviated by utilizing MgO supported on a SiO_2 surface. This MgO on SiO_2 surface will initially be synthesized through incipient wetness impregnation following the protocols established by Sushkevich *et al*. and shown in Scheme A2. This procedure involves forming a slurry of silica gel in an aqueous solution of $Mg(NO_3)_2$. Following an extensive drying period at both room temperature and at 100° C, the sample is then calcined in air at 500° C for 4 hours. If this proves unsuccessful, a multitude of other protocols (including wet kneading and mechanical mixing) exist for this process that will allow for tailoring of the amount of MgO supported. This is critical for two reasons: 1) there will still need to be surface silanols remaining after supporting MgO to allow for the tethering of the Lewis acid component, and 2) tuning the amount of MgO supported will help to vary the Lewis basicity of the support as a whole. Production of multiple surfaces with varying degrees of Lewis basicity will ideally help to establish a pattern of reactivity during catalytic testing.

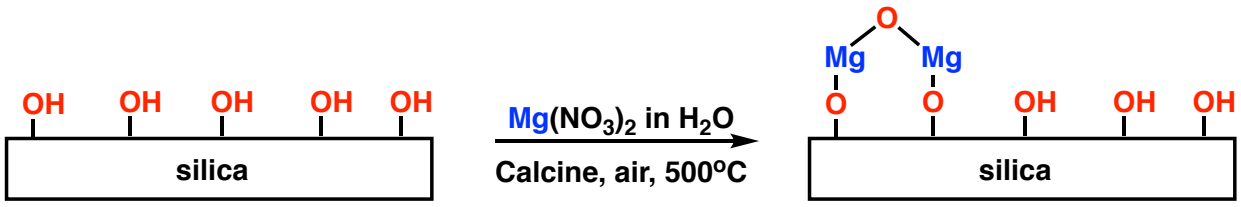

Scheme A2. Sample preparation of MgO on SiO_2 by incipient wetness impregnation.

High levels of characterization are required for a heterogeneous catalyst, as reliable and commonly used bulk measurements, such as solution NMR, are not available. Additionally, there are multiple aspects of the surface that must be characterized. The surface area can be determined by utilizing the technique of N_2 adsorption, which will have further implications on the catalytic performance of the final compound. Further characterization of the surface can be achieved through powder x-ray diffraction, ICP-AES, and IR spectroscopy. Perhaps most important in terms

of catalysis is the level of surface acidity and basicity. Surface acidity can be probed utilizing temperature programmed desorption (TPD) of ammonia or pyridine, or titration using amines, while titration with benzoic acid can determine the surface basicity.

The next step in the synthesis of the heterogeneous FLP will be the production of a Lewis acid that has the ability to be tethered to the surface, ideally through reaction with the remaining surface silanol groups. The target Lewis acid is a perfluorophenyl borane, based on Piers' borane, which can be synthesized via the route shown in Scheme A3 (A). There are several known synthetic routes to form Piers' reagent, most of which involve either toxic tin reagents or multiple, low-yielding steps. Scheme A3, B, shows a potential alternate, Sn-free route to Piers' borane requiring fewer steps, based partially on previous work in the synthesis of hetero-tri(aryl)boranes.[29] This compound can be characterized by solution NMR, specifically ^{11}B, ^{1}H, ^{13}C, and potentially ^{19}F. Further characterization would involve x-ray crystallography (if suitable crystals can be produced) and combustion-based CHN elemental analysis.

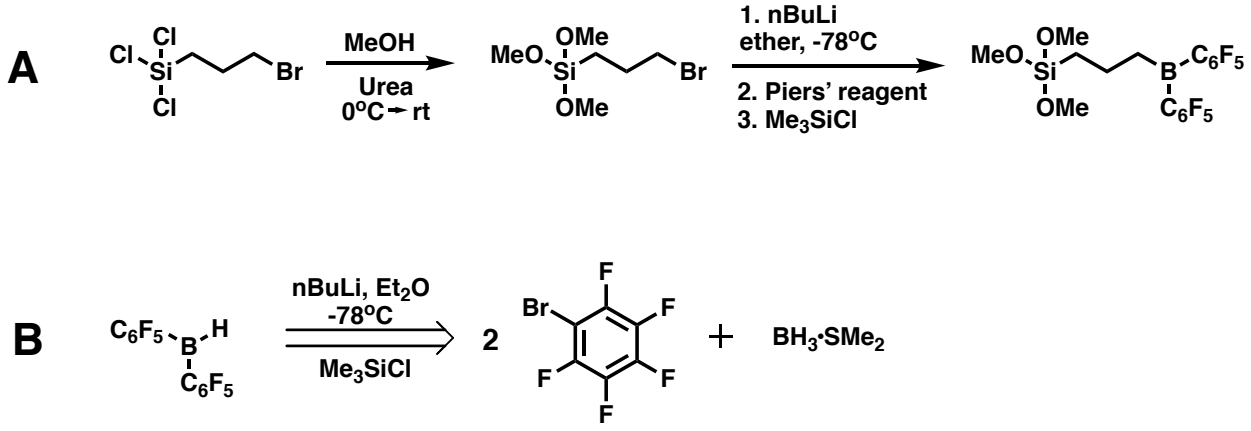

Scheme A3. A) Proposed synthetic route for siloxyborane to be used in the supporting reaction. B) Retrosynthetic analysis of Piers' reagent.

The final step of synthesis will involve the tethering of the Lewis acid by reaction of the borane with the remaining surface silanol groups through solution phase grafting, with a general

synthetic scheme shown in Scheme A4. Characterization of the heterogeneous FLP will be more challenging than the Lewis acid precursor, and will necessarily involve the use of solid state NMR techniques, specifically ^{13}C cross-polarization magic angle spinning (CP/MAS), ^{11}B MAS, ^{19}F MAS, and potentially ^{25}Mg MAS NMR,[30] as well as DRIFTS, in order to characterize presence of or change in functional groups. Elemental analysis will also be required, but the traditional combustion-based process will likely not provide much useful information. In this case, alternative techniques exist in order to quantify elemental composition of a solid-state compound. Extended x-ray absorption fine structure (EXAFS) or x-ray photoelectron spectroscopy (XPS), which can serve to determine the elemental composition as well as confirm the levels of different atoms on the surface, which is needed in order to determine the number of potentially active sites and which cannot be determined through NMR in this case. Energy dispersive x-ray spectroscopy (EDXS) is another method that can be used to confirm elemental composition.

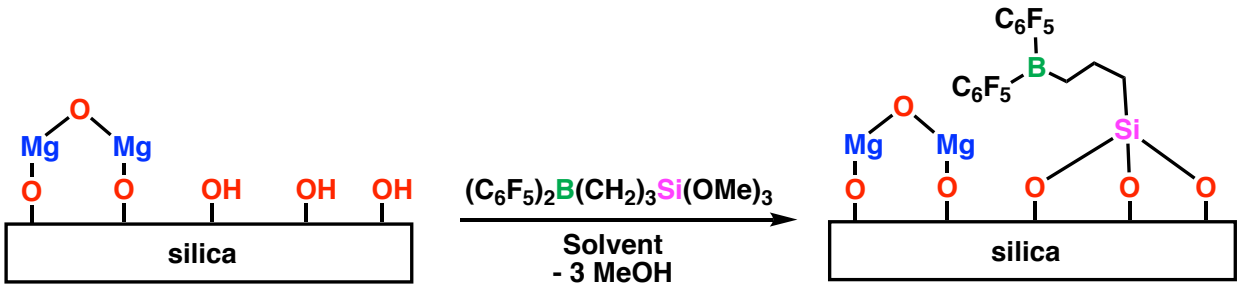

Scheme A4. General procedure for tethering of the siloxyborane to MgO/SiO_2 via reaction with remaining surface silanols through solution phase grafting.

Following successful synthesis and characterization of the heterogeneous FLP, the second aim of this project will involve performing catalytic probe reactions to examine the catalyst's ability to perform a variety of small molecule transformations, and potentially investigate activity towards polymerizations as well. In general, in order to determine whether the proposed compound

will indeed demonstrate the H_2 activating nature that is characteristic of FLP catalysts, the first reaction to be performed with this compound will be H/D scrambling, which can be performed on the NMR scale under ambient H_2/D_2 pressures and can therefore be easily monitored.[31] This will also help to establish a baseline of reactivity relative to more well-known H_2-activating FLP-systems.

The previously studied heterogeneous FLP most similar in structure to the proposed FLP, that developed by Szeto *et al*., had demonstrated activity towards the hydrogenation of alkynes.[3] Therefore, the first probe reaction will focus on a similar hydrogenation of alkynes, in order to establish a baseline reactivity to compare with existing supported FLP.

These catalytic runs will focus first on determining the ideal reaction conditions in terms of duration, temperature, catalyst loading, and solvent (with some special attention paid to minimizing the use of halogenated solvents in an effort to develop a more environmentally friendly process),[32] and then more specifically on the activity and stereoselectivity of the proposed heterogeneous FLP, especially as compared to the existing heterogeneous FLP. Analysis of any stereochemical effects can be quickly analyzed by GC. Another important metric will be the determination of recyclability. These experiments should be fairly straightforward to carry out, and can be accomplished by filtering the reaction mixture, washing the recovered catalyst with the reaction solvent, drying the catalyst, and utilizing it in another reaction. This process can be repeated until the level of recyclability is determined. Furthermore, it would also prove highly instructive to perform post-catalytic characterization of the FLP to determine any structural change and to ensure that leaching of any of the surface components does not occur. This characterization of used catalyst will be performed after both one and multiple catalytic runs. Finally, control

reactions will be run under identical conditions to those established for the proposed heterogeneous FLP, but using either MgO/SiO_2 or the borane precursor as a catalyst.

While it is useful to determine how the proposed catalyst performs to similar existing compounds, it is even more important to determine the efficacy of heterogeneous catalyst versus the homogeneous FLPs that we aim to replace. Regardless of whether alkyne reduction is successful, a variety of other reactions will then be attempted. Since solution-phase FLP chemistry has focused most heavily on hydrogenations, this will be the next series of catalytic probe reactions to be explored with the proposed compound. As the field of heterogeneous FLP catalysis is still in its infancy, any catalysis able to be performed by the proposed compound will be instructive towards further iterations of this class of catalyst. Focusing on hydrogenations will provide the key benefit of allowing for comparisons between heterogeneous and solution-phase FLPs, determining whether similar reactions can be performed with a catalyst that is ideally more thermally robust and catalytically recyclable, and, also importantly, by a transition-metal free catalyst. However, any other reactions previously catalyzed by FLPs, as well as other catalytic reactions, can be explored in the future as well.

The synthesis of the proposed heterogeneous FLP will, admittedly, prove to be challenging at best. Initially, much efforts will need to be focused on producing a support (MgO on SiO_2) with the correct level of Lewis basicity. In the event that appropriate basicity cannot be achieved by supporting MgO on SiO_2, an attempt will be made to support the borane reagent directly on MgO.

The synthesis and supporting of the borane will pose some additional challenges. As was presented before, the ideal borane reagent would have a hydrocarbon linker with siloxy end groups to aid in reaction with silanols on the MgO/SiO_2 surface. If the proposed synthesis of the siloxyborane reagent proves to be too challenging, there are multiple alternate routes that could be

attempted. For example, the lithiation step (Scheme A3, A) could potentially be replaced by a Grignard-style preparation. If there are difficulties using an alkyl linker between the siloxy group and the borane, an aryl linker could be utilized instead. If the siloxyborane synthesis is successful but the supporting reaction does not work, direct supporting of tris(perfluorophenyl)borane will be attempted, following the protocols set by Wanglee *et al*.[33]

Finally, in terms of synthesis of the new compound, if the current route of utilizing a Lewis basic surface and supporting a Lewis acidic compound is unsuccessful, the reverse of this (i.e. supporting a Lewis basic reagent on a Lewis acidic surface) could potentially be viable. This is due to the fact that there is an abundance of Lewis acidic surfaces. This leaves the main focus on synthesizing an appropriate Lewis basic reagent to be supported, but there should be a number of these to be explored, particularly N-containing compounds.

In terms of the catalytic reactions, homogeneous FLPs have been shown to catalyze a wide variety of reactions. In the event that the aforementioned focus on hydrogenations proves to be unsuccessful, there are many other reactions that can be tested instead. As was mentioned previously, since heterogeneous FLP catalysts are rare and not well studied yet, any catalytic activity would be a major contribution towards the field.

Finally, it is possible that if the proposed heterogeneous FLP is successfully synthesized, it will demonstrate no catalytic activity. In this case, the catalyst can then be modified in some other ways (different Lewis acid precursor, for example), to both improve activity and to begin to provide insight into structure-activity relationships in heterogeneous catalytic reactivity.

Summary and Conclusions

Although frustrated Lewis pair catalysis is still a young and developing technology, it has managed to make a large impact on the field overall, particularly in area of hydrogenation catalysis,

due to the fact that very effective catalysts can be produced using main group elements. This fact has large implications for a multitude of applications, but it has especially high potential for use in fine chemical industries, where trace amounts of metals can be highly detrimental to the resulting products. Meanwhile, heterogeneous catalysts are commonly utilized in industry due to their higher thermal stability, recyclability, and ease of removal from products relative to their molecular analogs. Keeping this in mind, proposed here is a catalyst that seeks to apply the benefits of heterogeneous catalysis to FLP technology, to ideally produce a new class of catalysts to be used for a variety of organic transformations. By synthesizing a fully immobilized compound, this project seeks to impart the benefits of heterogeneous catalysts into reactions easily accessible by frustrated Lewis pairs. In doing so, materials like the proposed compound will be among the first of many compounds on a new path towards better catalysts.

References

1. Friend, C. M.; Xu, B. Heterogeneous Catalysis: A Central Science for a Sustainable Future. *Acc. Chem. Res.* **2017**, *50*, 517-521.

2. Stalzer, M. M.; Delferro, M.; Marks, T. J. Supported Single-Site Organometallic Catalysts for the Synthesis of High-Performance Polyolefins. *Catal Lett* **2015**, *145*, 3-14.

3. Szeto, K. C.; Sahyoun, W.; Merle, N.; Castelbou, J. L.; Popoff, N.; Lefebvre, F.; Raynaud, J.; Godard, C.; Claver, C.; Delevoye, L.; Gauvin, R. M.; Taoufik, M. Development of silica-supported frustrated Lewis pairs: highly active transition metal-free catalysts for the Z-selective reduction of alkynes. *Catal. Sci. Tech.* **2016**, *6*, 882-889.

4. Stephan, D. W. Frustrated Lewis Pairs. *J. Am. Chem. Soc.* **2015**, *137*, 10018-10032.

5. Chase, P. A.; Welch, G. C.; Jurca, T.; Stephan, D. W. Metal-Free Catalytic Hydrogenation. *Angew. Chem. Intl. Ed.* **2007**, *46*, 8050-8053.

6. Greb, L.; Daniliuc, C.-G.; Bergander, K.; Paradies, J. Functional-Group Tolerance in Frustrated Lewis Pairs: Hydrogenation of Nitroolefins and Acrylates. *Angew. Chem. Intl. Ed.* **2013**, *52*, 5876-5879.

7. Spies, P.; Schwendemann, S.; Lange, S.; Kehr, G.; Fröhlich, R.; Erker, G. Metal-Free Catalytic Hydrogenation of Enamines, Imines, and Conjugated Phosphinoalkenylboranes. *Angew. Chem. Intl. Ed.* **2008**, *47*, 7543-7546.

8. Mahdi, T.; Stephan, D. W. Enabling Catalytic Ketone Hydrogenation by Frustrated Lewis Pairs. *J. Am. Chem. Soc.* **2014**, *136*, 15809-15812.

9. Scott, D. J.; Fuchter, M. J.; Ashley, A. E. Nonmetal Catalyzed Hydrogenation of Carbonyl Compounds. *J. Am. Chem. Soc.* **2014**, *136*, 15813-15816.

10. Greb, L.; Oña-Burgos, P.; Schirmer, B.; Grimme, S.; Stephan, D. W.; Paradies, J. Metal-free Catalytic Olefin Hydrogenation: Low-Temperature H2 Activation by Frustrated Lewis Pairs. *Angew. Chem. Intl. Ed.* **2012**, *51*, 10164-10168.

11. Inés, B.; Palomas, D.; Holle, S.; Steinberg, S.; Nicasio, J. A.; Alcarazo, M. Metal-Free Hydrogenation of Electron-Poor Allenes and Alkenes. *Angew. Chem. Intl. Ed.* **2012**, *51*, 12367-12369.

12. Paradies, J. Metal-Free Hydrogenation of Unsaturated Hydrocarbons Employing Molecular Hydrogen. *Angew. Chem. Intl. Ed.* **2014**, *53*, 3552-3557.

13. Chernichenko, K.; Madarász, Á.; Pápai, I.; Nieger, M.; Leskelä, M.; Repo, T. A frustrated-Lewis-pair approach to catalytic reduction of alkynes to cis-alkenes. *Nature Chemistry* **2013**, *5*, 718-723.

14. Mahdi, T.; del Castillo, J. N.; Stephan, D. W. Metal-Free Hydrogenation of N-Based Heterocycles. *Organometallics* **2013**, *32*, 1971-1978.

15. Segawa, Y.; Stephan, D. W. Metal-free hydrogenation catalysis of polycyclic aromatic hydrocarbons. *Chem. Commun.* **2012**, *48*, 11963-11965.

16. Mömming, C. M.; Otten, E.; Kehr, G.; Fröhlich, R.; Grimme, S.; Stephan, D. W.; Erker, G. Reversible Metal-Free Carbon Dioxide Binding by Frustrated Lewis Pairs. *Angew. Chem. Intl. Ed.* **2009**, *48*, 6643-6646.

17. Sgro, M. J.; Stephan, D. W. Synthesis and reactivity of ruthenium tridentate bis-phosphinite ligand complexes. *Dalton Trans.* **2013**, *42*, 10460-10472.

18. Otten, E.; Neu, R. C.; Stephan, D. W. Complexation of Nitrous Oxide by Frustrated Lewis Pairs. *J. Am. Chem. Soc.* **2009**, *131*, 9918-9919.

19. Ménard, G.; Hatnean, J. A.; Cowley, H. J.; Lough, A. J.; Rawson, J. M.; Stephan, D. W. C–H Bond Activation by Radical Ion Pairs Derived from R3P/Al(C6F5)3 Frustrated Lewis Pairs and N2O. *J. Am. Chem. Soc.* **2013**, *135*, 6446-6449.

20. Cardenas, A. J. P.; Culotta, B. J.; Warren, T. H.; Grimme, S.; Stute, A.; Fröhlich, R.; Kehr, G.; Erker, G. Capture of NO by a Frustrated Lewis Pair: A New Type of Persistent N-Oxyl Radical. *Angew. Chem. Intl. Ed.* **2011**, *50*, 7567-7571.

21. Sajid, M.; Klose, A.; Birkmann, B.; Liang, L.; Schirmer, B.; Wiegand, T.; Eckert, H.; Lough, A. J.; Frohlich, R.; Daniliuc, C. G.; Grimme, S.; Stephan, D. W.; Kehr, G.; Erker,

G. Reactions of phosphorus/boron frustrated Lewis pairs with SO2. *Chem. Sci.* **2013**, *4*, 213-219.

22. Knaus, M. G. M.; Giuman, M. M.; Pöthig, A.; Rieger, B. End of Frustration: Catalytic Precision Polymerization with Highly Interacting Lewis Pairs. *J. Am. Chem. Soc.* **2016**, *138*, 7776-7781.

23. He, J.; Zhang, Y.; Falivene, L.; Caporaso, L.; Cavallo, L.; Chen, E. Y. X. Chain Propagation and Termination Mechanisms for Polymerization of Conjugated Polar Alkenes by [Al]-Based Frustrated Lewis Pairs. *Macromolecules* **2014**, *47*, 7765-7774.

24. Zhang, Y.; Miyake, G. M.; John, M. G.; Falivene, L.; Caporaso, L.; Cavallo, L.; Chen, E. Y. X. Lewis pair polymerization by classical and frustrated Lewis pairs: acid, base and monomer scope and polymerization mechanism. *Dalton Trans.* **2012**, *41*, 9119-9134.

25. Trunk, M.; Teichert, J. F.; Thomas, A. Room-Temperature Activation of Hydrogen by Semi-immobilized Frustrated Lewis Pairs in Microporous Polymer Networks. *J. Am. Chem. Soc.* **2017**, *139*, 3615-3618.

26. Willms, A.; Schumacher, H.; Tabassum, T.; Qi, L.; Scott, S. L.; Hausoul, P. J. C.; Rose, M. Solid Molecular Frustrated Lewis Pairs in a Polyamine Organic Framework for the Catalytic Metal-free Hydrogenation of Alkenes. *ChemCatChem* **2018**, *10*, 1835-1843.

27. Xing, J.-Y.; Buffet, J.-C.; Rees, N. H.; Norby, P.; O'Hare, D. Hydrogen Cleavage by Solid-Phase Frustrated Lewis Pairs. *Chem. Commun.* **2016**, *52*, 10478-10481.

28. Parks, D. J.; Spence, R. E. v. H.; Piers, W. E. Bis(pentafluorophenyl)borane: Synthesis, Properties, and Hydroboration Chemistry of a Highly Electrophilic Borane Reagent. *Angew. Chem. Intl. Ed.* **1995**, *34*, 809-811.

29. Blagg, R. J.; Wildgoose, G. G. H2 Activation Using the First 1 : 1: 1 Hetero-tri(aryl) Borane. *RSC Adv.* **2016**, *6*, 42421-42427.

30. Liu, Z.; Lee, J.; Xiang, G.; Glass, H. F. J.; Keyzer, E. N.; Dutton, S. E.; Grey, C. P. Insights into the electrochemical performances of Bi anodes for Mg ion batteries using 25Mg solid state NMR spectroscopy. *Chem. Commun.* **2017**, *53*, 743-746.

31. vom Stein, T.; Perez, M.; Dobrovetsky, R.; Winkelhaus, D.; Caputo, C. B.; Stephan, D. W. Electrophilic Fluorophosphonium Cations in Frustrated Lewis Pair Hydrogen Activation and Catalytic Hydrogenation of Olefins. *Angew. Chem. Intl. Ed.* **2015**, *54*, 10178-10182.

32. Jessop, P. G. Searching for Green Solvents. *Green Chem.* **2011**, *13*, 1391-1398.

33. Wanglee, Y.-J.; Hu, J.; White, R. E.; Lee, M.-Y.; Stewart, S. M.; Perrotin, P.; Scott, S. L. Borane-Induced Dehydration of Silica and the Ensuing Water-Catalyzed Grafting of B(C6F5)3 To Give a Supported, Single-Site Lewis Acid, ≡ SiOB(C6F5)2. *J. Am. Chem. Soc.* **2012**, *134*, 355-366.

Anna M. Invergo
invergo@u.northwestern.edu

SCIENTIFIC SKILLS AND PROFICIENCIES

▪ **Synthesis and characterization of organic and organometallic compounds**
Extensive experience in synthesis, isolation and purification of air-, light-, water- and temperature-sensitive compounds, utilizing inert atmosphere synthetic techniques including Schlenk and high vacuum technique, inert atmosphere box use, handling and manipulation of highly pyrophoric chemicals, characterization techniques including NMR (^{1}H, ^{11}B, ^{13}C, ^{19}F, COSY, HSQC, one- and two-dimensional NOESY, DEPT, VT-NMR), IR and x-ray crystallography.

▪ **Polymer synthesis and characterization**
Extensive experience in the preparation of polyethylene and other specialty polymers. Expertise in of chemical, structural and mechanical properties of various polymers using techniques such as high temperature polymer NMR, TGA, DSC and several modes of GPC.

▪ **Catalysis**
Expertise in various methods of polymerization catalysis, including use of high pressure/high vacuum lines for olefin polymerization, as well as catalytic methodologies for atom-transfer radical polymerization of methacrylates and ring-opening polymerization of lactides.

▪ **Chemistry of lubricants**
Development of processes for preparing specialty polymer additives that have potential applications in improving lubrication and tribological properties of motor oils.

EDUCATION

Northwestern University, The Graduate School, Evanston, IL
June 2018
Ph.D., Chemistry, Advised by Tobin J. Marks (GPA: 3.60/4.00)

Northwestern University, Kellogg School of Management, Evanston, IL
Aug 2017
Certificate, Management for Scientists and Engineers

University of Louisville, Louisville, KY
May 2013
B.S. in Chemistry, *Cum Laude* (GPA: 3.73/4.00)

RESEARCH EXPERIENCE

Graduate Researcher **Sep 2013-Present**
Advisor: Prof. Tobin J. Marks

- Worked as part of a highly collaborative, multidisciplinary team of chemists, materials scientists, mechanical engineers, and tribologists at Northwestern University and Argonne National Laboratory to design and develop novel lubricant additives aimed at improving fuel efficiency in motor vehicles.
- Synthesized, characterized, and catalytically evaluated multiple series of binuclear organotitanium catalysts, as well as mononuclear control catalysts, for homogeneous ethylene and α-olefin polymerization, and performed full characterization of resulting polymers.
- Cooperatively developed a synthetic method for the production of a diblock copolymer for use as a viscosity-modifying additive for motor oil, and performed full characterization of resulting copolymers.
- Initiated a collaborative effort to methodologically study the performance of novel organomanganese complexes in catalyzing ring-opening polymerization of a series of lactides for the production of "green" polymers.
- Maintained research group's TGA-DSC and high temperature GPC. Duties involved training new users, performing routine annual and as-needed maintenance, and extensive troubleshooting/repairing. Additionally, created and implemented a standard operating procedure and collaboratively developed a method/apparatus for solvent recycling/purification for GPC.

Undergraduate Researcher **Aug 2011-Jun 2013**

Advisor: Prof. Christopher T. Burns

- Synthesized novel arene phosphinimine sulfonamide ligands and pyridyl-imine-amine pincer ligands for palladium and zinc complexation, respectively, for use as olefin polymerization catalysts.
- Mentored multiple junior undergraduate students. Responsible for teaching and assisting with use of gloveboxes, Schlenk lines, related synthetic techniques, and general laboratory procedures and safety.

PUBLICATIONS AND PRESENTATIONS

Shu, D., Mouat, A. R., Stephenson, C. J., **Invergo, A. M.**, Delferro, M., Marks, T. J., Ligand-Unsymmetrical Phenoxyiminato Dinickel Catalyst for High Molecular Weight Long-Chain Branched Polyethylenes, *ACS Macro Lett*. **2015**, *4*, 1297-1301

Invergo, A. M.,* Liu, S.,* McInnis, J. P.,* Mouat, A. R., Motta, A., Lohr, T. L., Delferro, M., Marks, T. J., Distinctive Stereochemically-Linked Cooperative Effects in Bimetallic Titanium Olefin Polymerization Catalysts, *Organometallics*, **2017**, *36*, 4403-4421. (*Co-first author)

Invergo, A. M.,* Liu, S.,* Dicken, R. D.; Mouat, A. R., Lohr, T. L., Delferro, M., Marks, T. J., How Close is Too Close? Polymerization Behavior and Monomer Dependent Reorganization of a Bimetallic Salphen Organotitanium Catalyst, *Organometallics*, **2018**, *Submitted*. (*Co-first author)

Invergo, A. M., Liu, S., McInnis, J. P., Mouat, A. R., Motta, A., Lohr, T. L., Delferro, M., Marks, T. J. Stereochemically-Linked Cooperative Effects in Bimetallic Organotitanium Catalysts for

Olefin Polymerization, *Spring Symposium of the Catalysis Club of Chicago*, *Naperville*, *IL*, May 16, 2017

Invergo, A. M., Liu, S., McInnis, J. P., Mouat, A. R., Motta, A., Lohr, T. L., Delferro, M., Marks, T. J. Stereochemically-Linked Cooperative Effects in Bimetallic Organotitanium Catalysts for Olefin Polymerization, *Vladimir Nikolayevich Ipatieff Sesquicentennial Celebration Symposium*, *Evanston*, *IL*, Sept. 7, 2017

LEADERSHIP AND TEACHING EXPERIENCE

▪ **Lincolnwood Science Partnership Mentor (Northwestern University, 2014-2017)**
Conducted scientific experiment demonstrations for 4th grade students on a weekly basis throughout the Fall Semester to introduce them to scientific methods and principles. Judged science fair projects at the end of the Fall Semester.

▪ **Science Club Mentor (Northwestern University, Science in Society, 2015-2016)**
Mentored a group of middle school students on a weekly basis throughout the school year as part of the Pederson-McCormick Boys & Girls Club of Chicago's Science Club outreach program. Assisted students in designing science fair projects and led weekly activities allowing students to explore different scientific topics. Additionally, attended quarterly professional development seminars and trainings to develop mentorship skills.

▪ **Searle Center New TA Conference Workshop Leader (Northwestern University, 2015)**
Designed and led two peer-reviewed workshops for incoming graduate students from multiple disciplines to introduce them to teaching strategies and the responsibilities of a graduate teaching assistant. Attended multiple workshops/trainings to further explore topics in developing engaging workshops for the interdisciplinary audience and strategies for leading effective discussions.

▪ **Graduate teaching assistant (Northwestern University, 2013-2014)**
Taught weekly sophomore level organic chemistry laboratory sessions at Northwestern University, as well as a 2-week intensive senior level NMR spectroscopy course. Other duties included grading and holding weekly tutoring sessions and office hours.

▪ **Undergraduate teaching assistant (University of Louisville, 2011-2013)**
Taught weekly honors organic chemistry laboratory sessions. Other duties included grading reports and holding weekly office hours. Periodically attended supplemental workshops and seminars focused on improving teaching skills and introducing teaching strategies.

▪ **Resources for Academic Achievement tutor (University of Louisville, 2010-2011)**
Held weekly remedial tutoring sessions for general chemistry undergraduates. Selection of qualified candidates was partially based on performance in the course as a student.

- **Resources for Academic Achievement Student Ambassador (University of Louisville, 2010-2011)**

Mentored a group of new freshmen students to facilitate their transition into college. Periodically attended mentorship development workshops and seminars, and was named runner-up Mentor of the Year.

HONORS AND AFFILIATIONS

- American Chemical Society 2009-Present
- Phi Lambda Upsilon Honors Chemistry Society, *Northwestern University* 2015-Present
- ACS Award in Inorganic Chemistry 2013
- Hypercube Scholar Award 2013
- CRC General Chemistry Award 2010
- Society of Undergraduate Chemistry Students (Secretary), *University of Louisville* 2011-2013
- University of Louisville Honors Scholar 2011-2013
- National Merit Scholar 2009
- University of Louisville Trustee's Scholarship 2009-2013